UC Berkeley
UC Berkeley Electronic Theses and Dissertations

Title
Roles of the plant cell wall in powdery mildew disease resistance in Arabidopsis thaliana: PMR5 (POWDERY MILDEW RESISTANT 5) affects the acetylation of cell wall pectin

Permalink
https://escholarship.org/uc/item/1t02j7v1

Author
Lim, Candice Cherk

Publication Date
2013

Peer reviewed|Thesis/dissertation

eScholarship.org Powered by the California Digital Library
University of California

Roles of the plant cell wall in powdery mildew disease resistance in *Arabidopsis thaliana*: PMR5 (POWDERY MILDEW RESISTANT 5) affects the acetylation of cell wall pectin

By

Candice Cherk Lim

A dissertation submitted in partial satisfaction of the

requirements for the degree of

Doctor of Philosophy

in

Plant Biology

in the

Graduate Division

of the

University of California, Berkeley

Committee in charge:

Professor Shauna Somerville, Chair
Professor Patricia Zambryski
Associate Professor Mary Wildermuth
Professor James Berger

Spring 2013

Abstract

Roles of the plant cell wall in powdery mildew disease resistance in *Arabidopsis thaliana*: PMR5 (POWDERY MILDEW RESISTANT 5) affects the acetylation of cell wall pectin

by

Candice Cherk Lim

Doctor of Philosophy in Plant Biology

University of California, Berkeley

Professor Shauna Somerville, Chair

The *pmr5* (*powdery mildew resistant 5*) mutant was found in a screen for genes involved in susceptibility to *Golovinomyces cichoracearum*, a biotrophic pathogen that infects Arabidopsis. PMR5 is a member of the TBL (TRICHOME BIREFRINGENCE LIKE) family, which is composed of 46 functionally uncharacterized plant-specific proteins. Initial characterization of this mutant showed that *pmr5*-mediated disease resistance acts independently of the salicylic acid, jasmonic acid, and ethylene signal transduction pathways, and that there are changes in the *pmr5* cell wall that may be linked to the gain of resistance in the mutant. Specifically, PMR5 may be affecting cell wall pectin by acetylation. Characterization of the *pmr5* cell wall has revealed changes in pectin composition and a decrease in acetylation. This is corroborated by the ability of heterologously expressed PMR5 protein to bind to pectin, with decreased binding affinity to acetylated pectin. The cell wall and disease phenotypes of the *pmr5* mutant may be revealing a potential role of PMR5 in the elusive plant cell wall integrity-signaling pathway. This work summarizes the continuing efforts in both determining the biochemical function of PMR5 and investigating the mechanism behind *pmr5*-mediated disease resistance.

Dedication

To A.Y.L. and T.Y.L.

Table of Contents

Abstract 1
Dedication i
Table of Contents ii
List of Figures iii
List of Tables v
Acknowledgements vi
CHAPTER 1: Defense at the plant cell wall 1
Preface 2
Part I: Host pathogen warfare at the plant cell wall 2
Part II: An update on trends in plant cell wall defense: the cell wall integrity (CWI) pathway 9
Figures 16
CHAPTER 2: Investigating the function of PMR5 (POWDERY MILDEW RESISTANT 5) 18
Introduction 19
Materials and Methods 20
Results 28
Discussion 42
Figures 45
Tables 82
Appendix 93
CHAPTER 3: Identifying potential *pmr5*-mediated disease resistance pathway partners 95
Introduction 96
Materials and Methods 96
Results 97
Discussion 99
Tables 101
CHAPTER 4: Suppressors of *pmr5*-mediated disease resistance 107
Introduction 108
Materials and Methods 108
Results 109
Discussion 112
Figures 114
Tables 120
CHAPTER 5: A hypothetical model for *pmr5*-mediated disease resistance 131
References Cited 134

List of Figures

Figure 1.1. Electron micrographs of different pathogens infecting plant cells 16

Figure 1.2. Overview of the plant cell signaling components mediating responses upon pathogen attack 17

Figure 2.1. Modified TBL protein family tree with *G. cichoracearum* phenotypes 45

Figure 2.2. Schematic of pectin structure 46

Figure 2.3. Secondary structure alignments of PMR5, putative alpha-galactosidase, and rhamnogalacturonan acetylesterase 47

Figure 2.4. *PMR5* gene expression generated by the eFP browser.....48

Figure 2.5. Schematic of *PMR5* gene structure 49

Figure 2.6. Virus induced gene silencing of *PMR5* in Arabidopsis.....50

Figure 2.7. Complementation after site-directed mutagenesis of catalytic residues 52

Figure 2.8. Principle component analysis of Fourier transform infrared spectroscopy spectra from wild-type and *pmr5* cell walls 53

Figure 2.9. Oligosaccharide mass profiling analysis of xyloglucan composition 54

Figure 2.10. Acetic acid assay comparing acetylation of cell walls 55

Figure 2.11. Saccharification assay comparing cell wall digestability.....56

Figure 2.12. Cell wall immunolabeling of stem sections.....57

Figure 2.13. Example of immunolabeling of spotted extracts with LM6 anti-arabinan antibody.58

Figure 2.14. Glycome profiling of rosette leaves 59

Figure 2.15. Arabidopsis seed mucilage is rich in rhamnogalacturonan I 60

Figure 2.16. Morphology and phenotypes of transgenic lines used in localization study.....61

Figure 2.17. FTIR spectrum of cell walls from plants expressing *35S:PMR5-GFP* 62

Figure 2.18. Localization of PMR5 in plants expressing *pPMR5:PMR5:GFP*.....63

Figure 2.19. PMR5 is more highly expressed in root cortical cells in plants expressing *pPMR5:PMR5:GFP*.....64

Figure 2.20. Detection of PMR5 in leaves from plants expressing *pPMR5:PMR5-GFP* 65

Figure 2.21. Fractionation and western blot of PMR5 from plants expressing *pPMR5:PMR5-GFP*.....66

Figure 2.22. Localization of PMR5 after brefeldin A treatment.....67

Figure 2.23. Localization of PMR5 in plants expressing *35S:PMR5-GFP* 68

Figure 2.24. Co-localization of PMR5 with Golgi in plants expressing *35S:PMR5-GFP* 69

Figure 2.25. Fractionation and western blot of PMR5 from plants expressing *35S:PMR5-GFP* .70

Figure 2.26. Localization of PMR5 at fungal penetration sites 24 hpi with *G. cichoracearum*....71

Figure 2.27. Unsuccessful detection of PMR5-Myc-His 72
Figure 2.28. Heterologous expression of MBP-PMR5-His 73
Figure 2.29. Purification of MBP-PMR5-His after bacterial protein extraction reagent lysis 74
Figure 2.30. Optimized purification of MBP-PMR5-His 75
Figure 2.31. MBP-PMR5-His binds to chemically extracted Arabidopsis pectin 76
Figure 2.32. MBP-PMR5-His binds to enzymatically extracted Arabidopsis pectin 77
Figure 2.33. MBP-PMR5-His does not bind Arabidopsis rhamnogalacturonan I 78
Figure 2.34. MBP-PMR5-His binding affinity to galactanase-digested pectin 79
Figure 2.35. MBP-PMR5-His binds to oligogalacturonides.....80
Figure 2.36. MBP-PMR5 binds more weakly to Ac-PGA 81
Figure 4.1. Growth phenotypes of the suppressors of *pmr5*-mediated disease resistance.....114
Figure 4.2. Gene schematic of *PMR5* and *TBR1* with annotated suppressor mutations.....115
Figure 4.3. Morphological characterization of lines used in the TBR suppressor study 116
Figure 4.4. Allelism test between P5S20 and P5S3 118
Figure 4.5. Principle component analysis of FTIR spectra from P5S6 and P5S20 cell walls 119
Figure 5.1. Hypothetical model of *pmr5*-mediated disease resistance 133

List of Tables

Table 2.1. List of plasmids used in this study 82
Table 2.2. List of primers used in this study 84
Table 2.3. Transgenic plant lines generated and used in this study 85
Table 2.4. *PMR5* TILLING lines screened for powdery mildew disease resistance 86
Table 2.5. Bioinformatics prediction tools used in this study 87
Table 2.6. *PMR5* gene expression in wild-type versus *pmr5* plants by qPCR analysis 88
Table 2.7. Arabidopsis accessions containing non-conservative polymorphisms in *PMR5*.....89
Table 2.8. PMR5 signal peptide BLAST results of proteins with similar N-terminal sequences 90
Table 2.9. Phenotypes and genotypes of plant lines used in this study 91
Table 2.10. MBP-PMR5-His binding affinity to commercially available polysaccharides 92
Table 3.1. Differentially expressed genes between uninfected Col-0 and *pmr5* plants.....101
Table 3.2. Mapman analysis of differentially expressed genes between Col-0 and *pmr5*.....102
Table 3.3. Differentially expressed genes between Col-0 and *pmr5* plants after inoculation with *Golovinomyces cichoracearum*.....103
Table 3.4. *MIOX4* gene expression in uninfected and infected plants by qPCR analysis 104
Table 3.5. Overrepresented *cis* elements within gene list from Table 3.3 105
Table 3.6. Common genes between microarray experiments using infected and uninfected plant tissue 106
Table 4.1. P5S6 mapping data 120
Table 4.2. Test crosses for genetic complementation of P5S6, P5S14, and *tbr1/pmr5* 121
Table 4.3. Transgenic lines for molecular complementation of P5S6 and P5S14 with *TBR1* ...122
Table 4.4. Genes involved in *pmr5*-mediated disease resistance 123
Table 4.5. Mapman analysis of differentially expressed genes between P5S6 and *pmr5* 124
Table 4.6. Mapman analysis of differentially expressed genes between *tbr1-1/pmr5* and *pmr5* 125
Table 4.7. Mapman analysis of shared genes: P5S6 v *pmr5* and *tbr1-1/pmr5* v *pmr5* 126
Table 4.8. Virtual Plant analysis of shared genes: P5S6 v *pmr5* and *tbr1-1/pmr5* v *pmr5* 127
Table 4.9. P5S20 mapping data 128
Table 4.10. Nonsynonymous changes on chromosome 3 from P5S20 129

Acknowledgements

I want to thank my advisor, Shauna Somerville, for guiding me through my PhD with abundant support and enthusiasm. Her support in my scientific decisions enabled me to become a more confident person in and out of the lab. I admire her honest curiosity in the fundamental questions in biology and how she asserts herself even when she is in the minority. She has been incredibly understanding of my goals in life, which has fueled a lot of my motivation to produce good data in the lab. I have been extremely fortunate to have Shauna as my advisor.

The members of my thesis and qualifying exam committees were invaluable for their suggestions on experiments and how to improve them. Their expertise in other fields really complemented my research. I thank Mary Wildermuth for her wealth of knowledge of current literature related to powdery mildew disease. Her energy and enthusiasm was contagious and helped me during the last push to the end. I thank James Berger for his expertise in protein expression and purification; if not for him, I would have had many more dead ends. I thank Henrik Scheller who met with me for two hours in preparation for my qualifying exam, and displayed continued interest in my project for the next few years. I thank Pat Zambryski for asking the basic questions to remind us all to communicate less esoterically so that we can all be more grounded scientists.

Members of the Somerville labs were instrumental for my development as a scientist, especially Kian Hematy, Clarisa Bejar, Nadav Sorek, Philipp Benz, Clarice Souza, and Heidi Szemenyei. They were all mentors in some form or another during the last couple of years, and have taught me most of the bench skills I've acquired, as well as life lessons that I will take with me moving forward.

I had a lot of help and many fruitful collaborations, which I hope to have acknowledged throughout the thesis. Being a part of these collaborations has made me hopeful about what can come out of academic research. In particular, I want to thank Amancio Souza for some great discussion about cell wall science and parenting as graduate students, Jake Brunkard for his humor and help with a late, but key, experiment, Brad Dotson for always being available to talk about TBLs, and Dawn Chiniquy for happily discussing PMR5-related matters. I also want to acknowledge my undergraduate researcher, Frazier Phillips, who I had great brainstorming sessions with, and who kept me on my toes and taught me how to articulate science at the bench.

I want to thank my classmates who were very supportive in the early years when I was playing catch up, and in the last year during our scramble to the finish line.

I thank the professors in my life that believed I could succeed in a graduate program: Amy Cheng Vollmer and Nick Kaplinsky for teaching biology at Swarthmore College, and Devaki Bhaya at the Carnegie for hosting me during a summer so that I could gain research experience.

I thank my family for their support, despite not knowing what I was actually doing, as well as my friends from middle and high school, who have kept me grounded and given me breaks from the science world.

Finally, I thank Andrew and Tobin for their love and support. The last couple of years have been incredibly stressful at times, but with them by my side, these years have also been filled with joy, humor, and love. I thank Tobin for the unconditional love he shows me, when he wants to, and I thank Andrew for taking care of our family and reminding me that I'm worth it everyday. They have given me the courage to achieve a dream, and for that, I am so grateful.

CHAPTER 1: Defense at the plant cell wall

Preface

The first part of this introduction is taken in its entirety from a review, "Host pathogen warfare at the plant cell wall", which was published in 2009 in *Current Opinion in Plant Biology* (Hematy et al., 2009). This review was co-authored by Kian Hematy, Shauna Somerville, and myself. Kian Hematy drafted the initial outline, and I contributed to the sections on pathogen invasion strategies, host recognition of intact and damaged self, and cellular responses. I also created Figure 2 based on an original figure by Kian Hematy. All authors of this review worked together to edit the manuscript to produce the final published version.

In the second part of this introduction, I add to this with recent trends in plant cell wall defense that have surfaced in the last few years, focusing on the existence of a cell wall integrity-signaling pathway.

Part I: Host pathogen warfare at the plant cell wall

Hematy K, Cherk C, and Somerville S. 2009. Host-pathogen warfare at the plant cell wall. *Current Opinion in Plant Biology*. 12(4):406-13.

Introduction

The plant cell wall is an exoskeleton surrounding the cell protoplast, and is composed of a highly integrated and structurally complex network of polysaccharides, including cellulose, hemicelluloses and pectin (for comprehensive reviews of the cell wall structure see (Cosgrove, 2005)). In brief, cell wall synthesis begins when a pectin rich middle lamella is deposited at the cell plate during cytokinesis. Then, the primary cell wall is synthesized and remodelled following cell growth. Finally, a thicker secondary cell wall is deposited once the cell has reached its final size. Growth and cell shape are largely determined by the balance between expansion driven by turgor and constraint provided by the plant cell wall. The cell wall is also a highly dynamic structure that is constantly remodelled during growth and development and in response to environmental cues. For example, upon pathogen attack, plants often deposit callose rich cell wall appositions (i.e. papillae) at sites of attempted pathogen penetration, accumulate phenolic compounds and various toxins in the wall and synthesize lignin-like polymers to reinforce the wall (Huckelhoven, 2007). Thus, much like the ramparts or fortress walls of ancient cities, the plant cell wall can be an important defensive structure that many pathogens encounter first before confronting intracellular plant defences (Lipka et al., 2008; Underwood and Somerville, 2008). Pathogens use mechanical force or release cell wall degrading enzymes to break down this barrier. At the cell wall, they also release pathogen-associated molecular patterns (PAMPs) either inadvertently or as a consequence of plant degradative enzymes (e.g. the release of chitin oligomers by plant chitinases). Plants, in turn, appear to sense these PAMPs and damage to their cell walls and activate a variety of defences, including the production of reactive oxygen species (ROS), the production and export of anti-microbial compounds and fortification of their cell walls. In addition, sensing PAMPs may activate intracellular defences like the salicylic acid pathway, perhaps priming the plant for the next stage of warfare.

In this commentary, we suggest that in addition to its structural role, the plant cell wall also relays information about the environment to the cell cytoplasm via signal transduction pathway(s) that are patterned after PAMP signalling pathways. In the case of microbe attack, cell wall fragments generated by either the plant or the microbe activate plant defences, reinforcing

the protection provided by plant cell wall. Experimental results supporting this model are discussed in detail below. Roles for the plant cuticle in defence are not addressed in this article.

Pathogens use different invasion strategies but similar weapons

There are a variety of pathogen lifestyles from biotrophs to necrotrophs, which influence the kinds of interactions that occur at the plant cell wall. Necrotrophs release copious amounts of cell wall degrading enzymes, presumably in an attempt to lyse plant cells before they can mount an effective defence. Biotrophs, however, appear to operate by stealth, minimizing damage to the host cell wall. This difference in lifestyle is partially reflected in the repertoire of cell wall degrading enzymes encoded by the genomes of the two types of pathogens. The biotroph *Ustilago maydis* encodes relatively few cell wall degrading enzymes (Kamper et al., 2006); while a necrotroph like *Erwinia* spp., which causes soft rot diseases, produces a broad spectrum of lipases and cutinases to degrade the host cuticle, pectinases to increase accessibility for other enzymes like cellulases and xylanases and several other hydrolases to break down the hemicellulose chains (Toth and Birch, 2005). Interestingly, the nematode roundworm, *Globodera rostochiensis*, produces expansin proteins to loosen the cell wall (Qin et al., 2004).

Although this review is focused mainly on those pathogens that must damage the host cell wall to gain access to the protoplast, similar observations have been made for a number of bacterial pathogens that reside in the apoplast and do not invade the plant cell protoplast (see Fig. 1.1). These bacterial pathogens release PAMPs into the cell wall space that not only can be detected by specialized PAMP receptors in the plant plasma membrane, the pattern recognition receptors (PRR) (see article in this issue by Zipfel) but also may be detected indirectly by their impact on the plant cell wall. A number of bacterial pathogens release cell wall degrading enzymes (Toth and Birch, 2005) and electron micrographs show minor amounts of plant cell wall degradation adjacent to populations of bacteria (Plotnikova et al., 2000).

Plant surveillance of pathogen invasion: elicitors inform about enemies

Plants possess different mechanisms to detect pathogen invasion. They can directly detect pathogen presence by non-self recognition of PAMPs or they can monitor the integrity of their own cell wall (i.e. ‘intact self’ or ‘degraded self’). The cellular responses to PAMPs such as flg22 or chitin and cell wall perturbation are very similar (e.g. induction of ROS, overproduction of callose and lignin). Thus, PAMP signalling can be used to study the less characterized cell wall integrity signalling. Below we focus on what is known about cell wall integrity signalling. Cell wall integrity signalling is best characterised in yeast, in which cell wall damage is sensed by the plasma membrane-resident WSC1, WSC2, WSC3 and MID2 receptors (Levin, 2005). Precisely how the cell wall damage is sensed by these receptors is unknown. The sensors recruit Rom1/2 GEFs (guanyl-nucleotide exchange factors) to the plasma membrane and then stimulate nucleotide exchange on the Ras-like G-protein RHO1. Activation of RHO1 directly regulates a β-1,3-glucan synthase (Fks1), which synthesizes one of the major polysaccharide components of the yeast cell wall. Activated RHO1 also initiates a MAP-kinase cascade that activates the transcription factors RLM1 and the SBF complex (Swi4/Swi6) to regulate the expression of genes required for cell wall repair and cell cycle transitions. Actin cytoskeleton rearrangements and post-translational activation of the Fks1 glucan synthase are also triggered. Thus, cell wall integrity in yeast is focused on sensing cell wall damage and the activation of genes and enzymes needed to repair the cell wall.

In cell wall integrity sensing in plants, neither the signalling molecule nor the signal transduction event is known, although there are hints that damage to polysaccharides triggers responses in plants. No homologues of WSC1 or MID2 receptors have been found; however, plant genomes encode several potential receptor-like kinases (RLK) that could act as cell wall integrity sensors. Cell wall damage (e.g. in cell wall mutants or following treatment with cell wall damaging agents) can be associated with elevated levels of plant defence hormones like salicylic acid (SA), ethylene (ET) or jasmonic acid (JA) suggesting that one outcome of cell wall integrity signalling is the activation of plant defences to limit pathogen ingress at sites of pathogen attack and, pre-emptively, at wound sites. An overview of what is known about sensing each of the plant cell wall components is given below.

Sensing cell wall damage

We speculate that in plants, cell damage may be sensed by one or more of the following: detection of damage to polysaccharides, release of oligosaccharides, inhibition of cell wall synthesis or assembly, or deformation of the plasma membrane adjacent to damaged and weakened cell walls.

As cellulose is the most abundant and strongest component of the plant cell wall, pathogens target it for degradation to facilitate penetration and to generate glucose units as a food source. Mutations in *CESA*s (encoding subunits of the cellulose synthase complex) for either the primary or secondary cell wall induce a number of stress and defence-like responses and enhance resistance to certain pathogens. Cellulose deficiency in the primary cell wall (e.g. in mutant *cesa3* (=*cev1*)) elicits ET and JA signalling and enhances resistance to bacteria, fungi and aphids (Ellis et al., 2002; Ellis et al., 2002). Similarly, inhibition of cellulose synthesis with the herbicide isoxaben induces JA and SA synthesis as well as some defence-associated genes (Hamann et al., 2009). However, SA, ET and JA-independent resistance to the soil-borne bacterium *Ralstonia solanacearum* and the necrotrophic fungus *Plectosphaerella cucumerina* is observed in mutants deficient in cellulose in secondary cell walls (Hernandez-Blanco et al., 2007). By contrast, some *Streptomyces* species release toxins (e.g. thaxtomin A) that inhibit cellulose synthesis and facilitate virulence (Loria et al., 2008). How the plant cell detects a defect in cellulose synthesis is unknown; it may monitor the plasma membrane-localized cellulose synthase complex, the crystallinity or content of cellulose produced or the generation of degraded cellulose fragments (Hematy et al., 2007).

Plant hemicelluloses include xyloglucans, xylans, glucuronoarabinoxylan, glucomannans and, in grasses, mixed-linkage glucans (Cosgrove, 2005). Cellulose microfibrils are interconnected by hemicelluloses to form the network that is actively remodelled by plant enzymes (e.g. xyloglucan endotransglycosylase) during cell expansion (Vissenberg et al., 2000). Interestingly the mutant, *resistant to Agrobacterium transformation 4* (*rat4*), is deficient in the cellulose synthase-like A9 (*CSLA9*) (Zhu et al., 2003). CSLA proteins have mannan/glucomannan synthase activity *in vitro* (Liepman et al., 2005). Additionally, *mur3* mutants, which are affected in a xyloglucan galactosyltransferase, have increased SA levels in their petioles and are resistant to *Hyaloperonospora parasitica* (Tedman-Jones et al., 2008).

Pectins are the most complex polysaccharides in plants, composed of eleven different monosaccharides and requiring a minimum of 67 enzymes for biosynthesis (Mohnen, 2008). The mutants, *pmr5* (*powdery mildew resistant5*) and *pmr6*, have changes in cell wall pectin composition (Vogel et al., 2002; Vogel et al., 2004). The penetration success of the powdery mildew pathogen on these two mutants resembles wild type suggesting that a change in cell wall

digestibility by this fungal pathogen *per se* was not responsible for the disease resistance phenotype (Humphry and Somerville, unpublished data). Thus, it is possible that the changed cell wall or altered pectic fragments released during fungal attack stimulate plant defences in these two mutants.

Cell wall elicitors

Pathogens secrete numerous glycosyl hydrolases and lyases (e.g. β-1,4-and β-1,3-glucanases, pectinases, xylosidases, arabinosidases and glucosidases with diverse specificities) that degrade the plant cell wall and release potential cell wall elicitors (Huckelhoven, 2007). For instance, degradation of cellulose by β-1,4-glucanases generates cellodextrin and degradation of the homogalacturonic domain of pectins generates oligogalacturonic acid (OGA). Oligosaccharides generated by cell wall degrading enzymes can act as elicitors to trigger plant defences (Aziz et al., 2007). OGA are the best characterized plant cell wall derived elicitors. Their ability to elicit a response depends on length (degree of polymerization (dp) > 9) and degree of methyl-esterification (Osorio et al., 2008). Treatment of plants with OGA can trigger calcium influx, ROS production, changes in gene expression and the ET and JA pathways (Aziz et al., 2004; Moscatiello et al., 2006). In addition, plant genomes encode a wide range of plant cell wall degrading enzymes, which probably play roles in cell expansion but may also generate oligosaccharide elicitors under stress conditions.

In addition to degradative enzymes, pathogens secrete proteins with carbohydrate binding modules (CBM) but lacking in enzymatic activity. The cellulose binding elicitor lectin (CBEL) from *Phytophthora parasitica nicotianae* possesses two CBM1, which elicit a hypersensitive response (Gaulin et al., 2006). The role of these proteins is not completely understood. As has been proposed for the pectate lyase domain of the bacterial HrpW effector, the CBM1 domains could serve to help anchor the pathogen to the plant cell wall (Charkowski et al., 1998). Alternately, the CBM1 domains could disrupt associations between polysaccharides, such as between glucan chains within cellulose microfibrils or between cellulose and hemicelluloses. While the CBEL protein may be a PAMP, it is also possible that the induced defence responses result from disruption of associations among glucan-containing polysaccharides by the CBM. In some cases, the hydrolytic enzyme, not its product, is recognized. A fungal ethylene-inducing xylanase (EIX) protein is recognized by the tandem tomato resistance genes, *LeEix1* and *LeEix2* (Ron and Avni, 2004). Interestingly, some pathogens appear to modify the host cell wall to benefit infection. A secreted cellulose-binding protein from the parasitic nematode *Heterodera schachtii* was shown to bind a host cell wall localized pectin methylesterase (AtPME3) (Hewezi et al., 2008). Arabidopsis *pme3* mutants were more resistant to nematode penetration, suggesting that interaction between the nematode protein and host pectin methylesterase facilitates infections. Nematode infection also stimulates production of plant cellulases and expansins, which are necessary for cell wall relaxation during the formation of root syncytia (Wieczorek et al., 2008).

Mechano-sensing of cell wall damage

The plant cell wall is physically linked to the plasma membrane at discrete sites that form Hechtian strands upon plasmolysis (Mellersh and Heath, 2001). In mammalian cells, plasma membrane-localized integrins bind to extracellular proteins containing Arg-Gly-Asp (RGD) motifs, thus providing a physical link between the plasma membrane and the extracellular matrix (Kadler et al., 2008). Although no integrin-like proteins have been found in plants, RGD-binding

sites at the plant plasma membrane have been detected (Canut et al., 1998). These RGD-binding sites may link to the cell wall, as treatment of plasmolyzed cells with RGD peptides disrupts Hechtian strand formation (Mellersh and Heath, 2001). Interestingly, treatment with RGD peptides also decreases defence responses during penetration and increases fungal penetration success and intracellular growth (Mellersh and Heath, 2001). Consistent with this observation, pathogen effector proteins with an RGD motif (e.g. the IPI-O protein from *P. infestans*) have a similar effect on cell wall plasma membrane connections (Senchou et al., 2004). Although there is no evidence supporting the idea that binding to RGD-containing proteins (or other cell wall components) in the extracellular matrix by plasma membrane receptors transduces changes in the mechanical properties of the plant cell wall, this is an attractive idea.

Damage of the cell wall probably weakens the mechanical strength of the wall and reduces the ability of the cell wall to constrain turgor-driven expansion of the protoplast. Mutants with reduced cellulose levels commonly develop swollen cells (Hamann et al., 2009). This effect may be perceived as a signal of pathogen invasion or wounding. Interestingly, providing osmotic support to seedlings treated with a cellulose synthase inhibitor reduced the cell swelling phenotype and other cellular responses like lignin deposition or the oxidative burst (Hamann et al., 2009). Plasma membrane protuberance upon cell wall perforation or invagination to accommodate haustorium formation have both been observed (Xu and Mendgen, 1997). Such mechanical stress on the plasma membrane could potentially activate mechano-sensing ion channels (MscS-like channels (Haswell et al., 2008)) or the Ca^{2+}-permeable, stretch-activated channel mid1-complementing activity 1 (Mca1), and then trigger changes in intracellular Ca^{2+} levels, initiating signalling events (Nakagawa et al., 2007).

Plasma membrane-anchored receptors: the embrasures of the fortress battlements

One can assume that perception of plant cell wall damage involves plasma membrane-anchored proteins, like the RLK (Fig. 1.2). These RLKs may sense damage to the plant cell wall directly via their extracellular domain or may interact with a cell wall based receptor to form a complex.

Wall-associated kinases (WAK) were the first cell wall binding receptor kinases to be described (He et al., 1996). WAK1 possesses an extracellular domain containing an epidermal growth factor (EGF)-like motif and appears to be covalently bound to the cell wall (He et al., 1996). The WAK1 protein is released from the cell wall fraction by polygalacturonase treatment, suggesting it is bound to a pectin ligand (Wagner and Kohorn, 2001). The association between WAK1 and pectin is likely to be covalent since it survives boiling in SDS and DTT but the exact nature of the bond is unknown. Furthermore, $WAK1_{67–254aa}$, produced in yeast, binds to polygalacturonic acid (PGA) and OGA (dp > 9) in a Ca^{2+}-dependent manner (Decreux and Messiaen, 2005).

Some WAK family members are involved in responses to biotic stress (He et al., 1998). The WAK1 transcript accumulates to elevated levels upon pathogen infection or following treatment with SA (He et al., 1998). A more direct role in pathogen resistance has been shown for *WAKL22/RFO1* (*RESISTANCE TO FUSARIUM OXYSPORUM 1*), which confers broad spectrum resistance against *Fusarium* species (Diener and Ausubel, 2005). Taken together, the evidence cited above suggests that WAKLs are good candidates for receptors that monitor pectin integrity during pathogen attack and trigger defence responses. The predicted WAKL proteins are highly similar in their cytoplasmic region but are more divergent in their extracellular ligand-

binding region, suggesting that they could recognize different pectin or, in some cases, glycine-rich protein ligands (Verica et al., 2003).

The *Catharanthus roseus* receptor-like kinase1-like (CrRLK1-like) family members appear to perceive extracellular signals and, in response, regulate various aspects of development (Hematy and Hofte, 2008). A member of this family, *THESEUS1 (THE1)* from Arabidopsis, was identified in a mutant screen for suppressors of the cellulose-deficient mutant *procuste1* (*prc1* (=*cesa6*)). Mutation of *THE1* partially restores normal stature, and suppresses gene mis-regulation and ectopic lignification in *prc1* (Hematy et al., 2007). THE1 is an attractive candidate for a cellulose integrity sensor, although it is unknown whether THE1 acts directly by binding to cellulose or indirectly by detecting the pleiotropic changes found in *pcr1* mutants. No direct role in pathogen resistance has been described for any *CrRLK1L* family member. However, a few hints suggest these RLKs might play such a role: (i) genes regulated by THE1 in a *prc1* background are stress-related, (ii) another CrRLK1L member (At2g23200) has been shown, like the PRRs FLS2 and EFR, to interact *in vitro* with the bacterial effector AvrPto (Xiang et al., 2008) and (iii) At5g39000 encodes a protein with an RGD-binding motif (Gouget et al., 2006).

Some RLKs have lectin-like extracellular domains (Shiu and Bleecker, 2001). Lectins appear to play a role in plant defence against pathogens (Peumans and Van Damme, 1995). For instance, wheat-germ agglutinin binds chitin and exhibits antifungal activity (Broekaert et al., 1989). Additionally, lectin-containing RLK may bind polysaccharides in the plant cell wall and, as proposed for WAK and WAKL, sense changes in host cell walls upon pathogen intrusion (Gouget et al., 2006).

Cellular responses to changes in the cell wall

Signalling

As noted above, cell wall damage is sensed by plants and leads to the activation of various kinds of signalling pathways. Deficiencies in cellulose, whether found in mutants or in plants treated with cellulose synthesis inhibitors, lead to the activation of the ET and JA signalling pathways (Ellis et al., 2002; Ellis et al., 2002; Hamann et al., 2009), and in some cases, to the activation of the SA or ABA pathways (Hernandez-Blanco et al., 2007; Hamann et al., 2009). A deficiency in wound and pathogen-induced callose deposition is associated with hyper-activation of the SA signalling pathway and resistance to some pathogens (Nishimura et al., 2003). Similarly, SA levels were elevated in petioles with a deficiency of xyloglucan galactosyltransferase (Tedman-Jones et al., 2008). The release of OGA, like other PAMPs, leads to the production of secondary signalling events, such as ROS production, JA synthesis and changes in intracellular Ca^{2+} (Aziz et al., 2004; Moscatiello et al., 2006). Changes in the resistance or susceptibility of some plant cell wall mutants also suggest that other uncharacterized defence signalling pathways are activated, although this has not been established directly (Vogel et al., 2002; Zhu et al., 2003; Vogel et al., 2004).

Plant cell wall strengthening

The plant cell is reinforced with several polymers in regions of pathogen attack and at damaged sites. Most commonly observed is the deposition of papillae containing callose, lignin-like polymers, structural proteins such as extensins and in some cases antimicrobial proteins like thionins and defensins (Huckelhoven, 2007). Callose is also deposited along the edges of wounds and, on occasion, completely encases attacked cells. This polysaccharide is thought to act as a

physical reinforcement at sites of damage. Both the rapidity and the universality of the callose deposition at sites of pathogen attack and wounding, and its role is sealing breaks in the cell wall suggests that callose is potentially an important downstream response in cell wall integrity signalling in plants.

In addition to callose deposition, damaged cell walls can be reinforced by the deposition of lignin or extensins. Lignin is a rigid and hydrophobic polymer usually present in the secondary cell wall of the vasculature. Hyper-lignification is often seen in cellulose-deficient mutants (Hematy et al., 2007) or in response to pathogen attack (Huckelhoven, 2007), presumably to reinforce the cell wall. This lignin deposition has an active role in blocking powdery mildew penetration in wheat (Bhuiyan et al., 2008). Extensins are hydroxyproline-rich proteins present in the plant cell wall, which can crosslink forming a rigid network (Cannon et al., 2008). Overexpression of extensins in Arabidopsis reduces susceptibility to *P. syringae* pv tomato DC3000 (Wei, 2006).

Neutralization of the enemies' artillery

One plant response to pathogen attack is the neutralization of their weapons. Plants produce peptide inhibitors to neutralize the cell wall degrading enzymes secreted by pathogens. Microbial pectinases are inhibited by polygalacturonase-inihibitor proteins (PGIP) and xylanases by xylanase inhibitor proteins (XIP) (Misas-Villamil and van der Hoorn, 2008). These plant inhibitor proteins are thought to fulfil two roles; one is to minimize cell wall damage and the other to maximize the production of cell wall derived elicitors of defined degree of polymerization, like OGA (Misas-Villamil and van der Hoorn, 2008).

Counter-attack from the host

Much as ancient fortresses were defended by archers, plants secrete antimicrobial metabolites, either constitutively or induced upon infection, into the cell wall (Field et al., 2006). Plant cells also secrete anti-microbial proteins like the defensins and pathogenesis-related (PR) proteins into the cell wall space. Some PR proteins are hydrolases able to degrade pathogen cell walls. Pathogen-derived cell wall fragments (e.g. chito-oligomer fragments from fungi and insects) would then be released and trigger PAMP responses, reinforcing host defences (Huckelhoven, 2007). An additional feature of this counter-attack is that the plant focuses its resources subcellularly just at sites of pathogen attack. Plant organelles and cytoplasm become concentrated at these sites (Koh and Somerville, 2006). Plasma membrane-resident proteins implicated in penetration resistance (e.g. the PEN1 (=SYP121) syntaxin, the PEN3 (=PDR8) ABC transporter and MLO, a negative regulator of penetration resistance) accumulate in round patches at pathogen attack sites (Underwood and Somerville, 2008). The complexity of the interactions between defence responses originating in the cell wall and those arising intracellularly is illustrated by the observation that both ET and glucosinolate degradation were required for callose production elicited by the PAMP, flg22 (Clay et al., 2009).

Conclusions

The induction of defence-related pathways by plant cell wall damage or change supports the role of the cell wall as not only a physical barrier but also as an important sensory component for downstream signalling pathways. As the cell wall is an important barrier or shield for plant cells, monitoring its integrity allows plants to quickly activate pathways to minimize pathogen entry and reduce the spread of disease. Although a number of plant responses to cell wall

damage have been described, a detailed path from cell wall damage via a signal and receptor to a specific output has not been determined. Future research will aim at identifying more of these plant cell wall derived elicitors with particular interest in discovering their plant receptors that induce the defence responses.

Part II: An update on trends in plant cell wall defense: the cell wall integrity (CWI) pathway

Introduction

In the last few years, there has been increased interest in elucidating a cell wall integrity (CWI) pathway for plants (reviews from (Humphrey et al., 2007; Ringli, 2010; Seifert and Blaukopf, 2010; Hamann, 2012; Nuhse, 2012; Underwood, 2012; Wolf et al., 2012)). Most of the literature focuses the existence of a mechanism by which the plant can constantly remodel and modify its cell wall during normal growth and development. Interestingly, many of the cell wall mutants used in research on a CWI pathway have altered disease resistance, hinting at a link between cell wall integrity during growth and development and plant immunity. The largest leap forward in this field is in the identification of new potential cell wall sensors that could act in detecting cell wall perturbations. New insights on signaling components are also presented in this section.

The complexity of the dynamic cell wall

Our current understanding of cell wall architecture remains rather simplistic and more research is needed to fully determine the structure and composition of the cell wall. We know that the cell wall is composed of a complex network of cellulose, hemicellulose, pectin, lignin, and proteins (Somerville et al., 2004), but how exactly these components form the intricate network is largely unknown. Recent advances in technology have allowed researchers to better determine the fine structure of the cell wall.

In 2011, Dick-Perez *et al*. used magic-angle-spinning solid-state NMR to analyze the structure and relationship of the polysaccharides that compose the complex cell wall. Unlike previous models showing hemicellulose-coated cellulose as the main framework for the cell wall, Dick-Perez *et al*. found few peaks supporting this model. They instead found that there were extensive pectin-cellulose interactions, suggesting that pectin may be more important in structure and function of the cell wall than previously thought (Dick-Perez et al., 2011). The structure of pectic rhamnogalacturonan I has also been further characterized, showing longer repeats of galacturonic acid interspersed with rhamnose residues, instead of the previously thought 1:1 alternating ratio composing the RGI backbone (Yapo, 2011).

After laying the initial network of polysaccharides, plants need to remodel and maintain their cell walls throughout development, such as during expansion and secondary cell wall formation, while also needing to adapt to environmental stresses, such as wounding or pathogen attack. The importance of the cell wall in defense can be illustrated by noting the extensive number of mechanisms that pathogens have evolved to breach the wall. There are biotrophs that require stealth to survive undetected by the plant host, likely by mediating suppression of host defenses and signaling (Panstruga, 2003; Wildermuth, 2010). There are also necrotrophs like *Erwinia* and *Botrytis* that completely macerate host tissue (Laluk and Mengiste, 2010). A parasitic nematode can inject effector proteins that dissolve and even rearrange the cell wall (Gheysen and Mitchum, 2011). The plant thus needs to actively adjust and reorganize its walls

during normal cell growth, while also defending against a wide range of pathogen attack strategies.

Indeed, cell walls can adjust their composition and structure in response to pathogen infection (Dong et al., 2008). To protect other cell wall polysaccharides from degradation, lignin precursors can be secreted and cross-linked into the cell wall (Vanholme et al., 2010). *CAD-C* and *CAD-D*, primary genes in the lignin biosynthetic pathway encoding cinnamyl alcohol dehydrogenases have been shown to be essential for defense against *Pseudomonas syringae* pv. *tomato* (Tronchet et al., 2010). Pathogen infection has also been shown to trigger covalent binding of phytochemicals to the cell wall (Bednarek, 2012). This highly dynamic process at the cell wall in response to pathogen attack resembles the changes needed for normal cell wall growth and expansion, leading many to believe in the existence of a CWI signaling pathway and the convergence with defense signaling against pathogens that break through the cell wall.

Altered wall, altered susceptibility to pathogens

More cell wall-related mutants have been found to have altered susceptibility to pathogens. In rice, the Cellulose synthase-like F6 protein was found to be important in synthesizing mixed-linkage glucan, and when mutated, the mutant plants developed a lesion mimic phenotype with enhanced defense-related gene expression and enhanced disease resistance to *Xanthomonas oryzae* pv. *oryzae* (Vega-Sanchez et al., 2012). Mutations in *COBRA*, involved in cellulose deposition and orientation, led to an induction of defense and stress-related genes (Ko et al., 2006). Acetylation of cell wall polysaccharides has been implicated in immunity. In a screen for genes containing the Cas1p sequence from *Cryptococcus neoformans*, Manabe *et al.* found that a mutation in *REDUCED WALL ACETYLATION 2* resulted in increased resistance to *Botrytis* (Manabe et al., 2011). Interestingly, *AXY4* (*ALTERED XYLOGLUCAN 4/TBL27*) and *RWA2* seem to work in the same pathway, where RWA2 may be transporting an acetyl group to AXY4 for xyloglucan acetylation (Gille et al., 2011). Although the *axy4* mutant did not show any resistance phenotypes, it is part of the same protein family as PMR5 (POWDERY MILDEW RESISTANT 5/TBL44). A mutation in *PMR5* confers resistance to *Golovinomyces cichoracearum* and leads to altered cell wall pectin (Vogel et al., 2004). Like RWA2, the TBL family of proteins also contains some weak homology to the Cas1p sequence, possibly implicating this family of proteins in polysaccharide acetylation (Anantharaman and Aravind, 2010). The enhanced resistance phenotypes of these cell wall-related mutants support the hypothesis that there may be a CWI-sensing mechanism that triggers defense responses when the cell wall is altered.

Pharmacological drugs have been used successfully in studying the cell wall, especially in cases where cell wall mutants are lethal. When Arabidopsis seedlings were treated with thaxtomin A, genes involved in cellulose synthesis, pectin metabolism, and cell wall remodeling were altered, and defense-related genes leading to callose deposition were induced (Bischoff et al., 2009). Hamann *et al.* used a similar approach and found that chemically inhibiting cellulose biosynthesis resulted in expression changes in genes involved in mechanoperception, lignin and cell wall biosynthesis, as well as activation of pathogen response genes dependent on jasmonic acid signaling (Hamann et al., 2009). By using a pharmacological approach, researchers can now detect the primary effects of cell wall perturbation before the cell wall adapts to the change.

There could be several reasons why mutations in cell wall-related genes could lead to enhanced disease resistance. Changes in cell wall composition may prevent pathogens from breaching the wall and successfully extracting nutrients for reproduction. A more intriguing

hypothesis is that cell wall mutants simulate a break-in, causing activation of a CWI maintenance pathway that may be priming the plant's immunity against disease (Hamann, 2012).

A case for a CWI signaling pathway in plants

As explained in the review (section 1, this chapter), yeast have a well-characterized CWI pathway (Levin, 2005), whereas a plant CWI pathway remains elusive. Due to the complex and dynamic changes in plant cells, Hamann and Denness assert that a dedicated plant CWI maintenance mechanism is likely disguised among the multitude of other cell-related signaling events during development and interaction with the environment (Hamann and Denness, 2011). However, it is well known that there is an intimate relationship between cell wall architecture and growth (Benatti et al., 2012). Although there are no homologues in plants that resemble members of the yeast pathway, there are still several similarities that are shared (Hamann and Denness, 2011). Sensors in plant cell walls, such as receptor-like kinases (RLKs) may be functional analogs to yeast sensors that monitor the functional integrity of the wall (Ringli, 2010; Hamann and Denness, 2011). The best example of this is THE1 (THESEUS1), which is a plasma membrane-localized kinase capable of detecting cellulose perturbations and affecting the growth response (Hematy et al., 2007). Interestingly, plant *MCA1* and *MCA2* (*MID1-COMPLEMENTING ACTIVITY1* and *2*) can rescue the mutant phenotype of a MID1 deficient yeast strain (Nakagawa et al., 2007; Yamanaka et al., 2010). MID1 in yeast is used in mechano-perception via calcineurin, a calcium-dependent serine-threonine phosphatase. Complementation with *MCA1* and *MCA2*, along with calcium influx defects in the *mca1/2* mutant, suggests that MCA1 and 2 may be putative stretch-activated calcium channels involved in detecting CWI in plants (Nakagawa et al., 2007; Yamanaka et al., 2010).

Evidence of the signaling events downstream of cell wall damage perception has also arisen in recent years. Cell wall damage has been uncoupled from growth by blocking a signaling pathway, showing that the stunted growth phenotypes seen in cell wall mutants were not due to a weakened cell wall, but rather involvement of a 1-aminocyclopropane-1-carboxylic acid-dependent pathway (Tsang et al., 2011). Brassinosteroid (BR) signaling has been implicated in CWI, as the BR signaling pathway was activated upon interference with pectin methylesterase activity (Wolf et al., 2012). Downstream of signaling events, cell wall mutants have drastic changes in expression of cell wall biosynthesis and remodeling genes, highlighting the perception of the cell wall alteration and responding accordingly to adjust the cell wall (Seifert and Blaukopf, 2010). Slowly, new players in the once elusive plant CWI pathway are emerging.

New potential receptors for CWI

The CrRLK1L family contains several membrane-localized RLKs that have carbohydrate-binding domains and may be functioning in CWI sensing (review, (Boisson-Dernier et al., 2011)). One of the star members of this family is THE1, and it has been implicated in being a sensor in a CWI mechanism (Hematy et al., 2007). THE1 was shown to be required for signaling via calcium, reactive oxygen species (ROS), and jasmonic acid signaling cascades, leading to cell wall damage-induced lignin deposition (Denness et al., 2011). A mutation in *FER* (*FERONIA*), encoding a RLK characterized in pollen tube reception, was found to also confer resistance to *Golovinomyces orontii* (Kessler et al., 2010). HERK1 (HERKULES1), another CrRLK1L family member, THE1, and FER have all been implicated in BR-induced cell elongation based on their transcriptional induction after BR application (Guo et al., 2009). The

roles of these CrRLK1L family members all point to cell wall sensors involved in signaling leading to cell wall maintenance.

Additional work has been done to further characterize wall-associated kinases (WAKs), supporting their role as pectin sensors in a CWI-sensing pathway (Kohorn and Kohorn, 2012). WAK2 was found to influence the expression and activity of a vacuolar invertase, suggesting that WAK2 may be sensing the cell wall by pectin attachment and then transducing a signal to trigger changes in solute concentration and turgor pressure necessary for cell expansion (Kohorn et al., 2006). Signaling downstream of WAK2 involves MPK6, but not MPK3, which highlights a potential switch point in signaling (Kohorn et al., 2012). A chimera between the WAK1 receptor domain and the EFR (a pattern recognition receptor that triggers defenses) kinase domain showed that WAK1 domain can bind oligogalacturonides (OGAs) and trigger the downstream responses of a typical EFR receptor upon pathogen-associated molecular pattern (PAMP) detection (Brutus et al., 2010). A reverse chimera with the EFR receptor domain and the WAK1 kinase domain WAK1 resulted in defense responses characteristic of those activated by OGAs, including increased resistance to fungal and bacterial pathogens (Brutus et al., 2010). Additionally, Kohorn *et al.* found that both WAK1 and WAK2 can bind pectin *in vitro* and activate cell wall related transcriptional changes (Kohorn et al., 2009). These combined experiments suggest that in addition to WAKs binding to endogenous cell wall pectin and signaling during normal cell wall maintenance, WAKs can also bind OGAs and trigger a pathogen response. Thus WAKs provide a prime example of a receptor where the CWI pathway intersects with plant immunity. It will be interesting to determine the mechanism by which WAKs respond differently to short OGA fragments generated by pathogens and to longer pectins existing in the cell wall during growth and development.

As cell wall pectin is highly diverse and complex, there are probably several other pectin receptors in addition to the WAKs. Other cell wall sensor candidates may be found in the proline-rich extensin-like receptor kinase (PERK) family (Nakhamchik et al., 2004). PERK4 was found to localize in the plasma membrane, and the protein was extracted more easily with pectinase treatment (Bai et al., 2009). This resembles the WAKs, in which a domain anchors the receptor in the cell wall, making PERK4 a potential CWI sensor. Ectopic expression of BnPERK was shown to cause aberrant deposits of callose and cellulose (Haffani et al., 2006). The cell wall changes indicate that PERK is capable of signaling to result in cell wall modifications, an ability that a CWI sensor would have.

An interesting addition to potential CWI receptors lies in the legume-like lectin receptor kinases. These receptors contain extracellular lectin motifs that can bind various carbohydrates, and are considered important in cell wall-plasma membrane contact (Bouwmeester et al., 2011). Interestingly, several members of this family are induced upon treatment with elicitors and pathogen infection (Kanzaki et al., 2008; Xin et al., 2009). It was known that RGD sequences from *Phytophthora infestans* were needed for attachment to the host and were able to disrupt cell wall-plasma membrane connections (Senchou et al., 2004; Gouget et al., 2006). From this information, the lectin receptor kinase family was identified, including LecRK79, which mediates cell wall-plasma membrane adhesions and is induced upon pathogen infection (Gouget et al., 2006; Bouwmeester and Govers, 2009). Recently, Bouwmeester *et al*. were able to identify LecRK-I.9, and found similar compromised cell wall-plasma membrane adhesion in the mutant, as well as increased susceptibility to *Phytophthora brassicae* and a lack of callose deposition after *Pseudomonas syringae* infection or flg22 treatment (Bouwmeester et al., 2011).

Understanding the components necessary for pathogen attack like the RGD sequence could be instrumental at identifying more sensors.

Another recently discovered player in cell wall-plasma membrane adhesion is NDR1 (NON-RACE SPECIFIC DISEASE RESISTANCE-1) (Knepper et al., 2011). NDR1 has been implicated in PAMP-triggered immunity (Coppinger et al., 2004; Day et al., 2006), but has only recently been shown to share homology with mammalian integrins important in adhesion and signaling (Knepper et al., 2011). Reminiscent of the RGD motif recognized by the L-like lectin receptor kinases, Knepper *et al*. found that the NGD motif was critical for proper cell wall-plasma membrane adhesion as well as defense against *Pseudomonas syringae* pv *tomato* DC3000 (Knepper et al., 2011). These results suggest that cell wall-plasma membrane adhesion is important for plant defense responses, possibly because the RLKs that mediate the cell wall-plasma membrane adhesion are responsible for triggering a signaling cascade. Thus, RLKs involved in cell wall-plasma membrane adhesion could be prime candidates for CWI sensors.

Alongside the plasma membrane, the cytoskeleton may also be involved in CWI sensing, as the cytoskeleton is known to play a role in innate immunity (Hardham et al., 2007). Formins are membrane-anchored proteins that bind actin, and have been shown to be induced after infection with *Meloidogyne incognita* (Favery et al., 2004). Martiniere *et al.* have shown that Formin1 is actually anchored to the cell wall by a sequence with homology to extensins (Martiniere et al., 2011). This is exciting because formins are activated by Rho-GTPases, the central regulator in the yeast CWI pathway (Levin, 2011). Association with the cell wall and potential signaling partners make the formins an attractive CWI sensor in plants.

The RLK subfamily XIII consists of those containing LRR (leucine-rich-repeat) domains, such as ERECTA (Shiu and Bleecker, 2001). ERECTA has been associated with processes involving development and immunity against *Ralstonia solanacearum, Plectosphaerella cucumerina,* and *Phythium irregulare* (Llorente et al., 2005). Using a suppressor screen to find resistant plants against *P. cucumerina* in the *er-1* background, Sanchez-Rodriguez *et al.* identified suppressors that rescued the disease phenotype, but not the *er*-associated developmental phenotypes (Sanchez-Rodriguez et al., 2009). Analysis of the cell walls showed a positive correlation between uronic acids content and resistance, suggesting some form of cell wall-mediated disease resistance (Sanchez-Rodriguez et al., 2009). In the same family, FEI1 and FEI2 have been characterized to play a role in anisotropic expansion and cell wall biogenesis (Xu et al., 2008). Although this family of RLKs have not been directly linked to CWI sensing, their roles in cell wall modification and immunity make them intriguing sensor candidates.

The CWI signal for damage or danger

The term DAMPs (danger- or damage-associated molecular patterns) has arisen to describe endogenous elicitors that induce similar responses as PAMPs (Boller and Felix, 2009; Zipfel, 2009). The best-studied DAMP is that of OGAs, which are small fragments of homogalacturonic acid generated during pathogen infection. In wheat, OGAs trigger ROS and oxylipin activity, along with improved resistance to *Blumeria graminis* f. sp. *tritici* (Randoux et al., 2010). In addition, acetylation of OGAs increased papilla and reduced the formation of fungal haustoria (Randoux et al., 2010). This mirrors the importance of methylation in OGAs to immunity against *Botrytis cinerea* in strawberry (Osorio et al., 2008).

In addition to modified signals and elicitors, structural conformation of these signals is also important in determining a response. By circular dichroism spectrometry, Cabrera *et al.* found that OGAs mature to form an egg-box structure (calcium-associated multimer chains of

OGA) and that the formation of egg boxes increased their binding to WAK1 (Cabrera et al., 2008). Interestingly, altering the reducing end of the egg box reduced WAK1 triggered activity (Cabrera et al., 2008). From previous work (Kohorn et al., 2012), it is known that WAKs differentially bind to various lengths of OGA for either CWI or immunity. Taking these results together with differential activity of OGA egg-box ends, we may be seeing how the plant is recognizing and differentiating between the various pectin fragments to indicate self or non-self generated elicitors. Perhaps during pathogen infection, unaltered OGAs are generated and perceived by the plant to lead to a defense response, whereas altered OGAs are generated during normal pectin remodeling.

It seems that modifications to endogenous signals may be a common theme in differentiating two overlapping and similar pathways. Whether DAMP signaling or normal cell wall maintenance is occurring depends on modifications to signals such as OGAs. It will be interesting to see whether these modifications in conformation or conjugations are shared among all DAMPs. This hypothesis would suggest that fewer receptors are needed to transmit signals or elicitors generated from the complex plant cell wall. Technology that will elucidate the structure of the cell wall will be important to have a better grasp of potential cell wall-generated signaling molecules.

Signaling and responses of the CWI pathway

More supporting evidence for ROS signaling in CWI pathway has emerged in the last few years (review, (O'Brien et al., 2012)). A signaling cascade involving calcium and ROS production, and the accumulation of jasmonic acid, has been shown to be important in a feedback loop for cell wall damage-induced lignin deposition (Hamann et al., 2009; Denness et al., 2011). Lignin deposition was enhanced in jasmonic acid mutants, but decreased in cell wall damage perception (MCA1, THE1) and ROS mutants (Denness et al., 2011). ROS signaling has also been implicated in defense responses, where it triggers phytoalexin production and callose deposition at the cell wall (Daudi et al., 2012; O'Brien et al., 2012). However, how the ROS signal would be differentiated between a CWI and defense pathway is unknown.

ROP-GEFs, guanine nucleotide exchange factors that mediate RHO GTPases (ROPs) may be involved in the signaling cascade with ROS. Duan *et al*. found that ROP-GEFs exist in a pathway between ROS-regulated root hair development, and FER, a potential cell wall damage perception sensor (Duan et al., 2010). Moreover, it was found that a dominant negative allele of AtROP6 had constitutively active SA-related expression changes, increased resistance to *Golovinomyces orontii*, and impaired pre-invasive resistance to the non-adapted powdery mildew, *Blumeria graminis f. sp. hordei* (Poraty-Gavra et al., 2013). Thus the ROPs and ROPGEFs show phenotypes consistent with other potential CWI players, and may be functioning as intermediate signaling players in the pathway.

ROS can be made by NADPH oxidases or Class III peroxidases (Daudi et al., 2012; O'Brien et al., 2012), and both generate ROS involved in signaling downstream of cell wall damage. There are 10 *AtRBOH* (Arabidopsis respiratory burst oxidase (RBO) homolog) genes, and *RBOHD* and *RBOHF* are needed for defense against Pseudom*onas syringae* pv. *tomato DC 3000* and *Peronospora parasitica* (Torres et al., 2002; Chaouch et al., 2012; Daudi et al., 2012). Denness *et al.* also found that cell wall-induced lignin deposition depends on RBOHD-dependent ROS burst (Denness et al., 2011). Peroxidase-dependent oxidative burst was found to be important in basal resistance and pattern triggered immunity-mediated PAMP recognition (Daudi

et al., 2012). Thus it is not unreasonable to speculate that peroxidases may also be important in cell wall damage-induced ROS formation.

The heterotrimeric G-proteins form a complex and are involved in many signaling events for proper development (Temple and Jones, 2007). The *agb1* mutant (impaired in the G-beta subunit), as well as the *agg1* and *agg2* mutants (encoding the G-gamma subunits and forms an obligate dimer with G-beta), were all susceptible to *Plectosphaerella cucumerina*. Interestingly, the G-protein-mediated resistance was independent of salicylic acid, jasmonic acid, ethylene and abscisic acid signaling pathways, and the mutants had altered cell wall composition and altered expression in cell wall-related genes (Delgado-Cerezo et al., 2012). Although not direct evidence that the G-proteins function in a CWI pathway, the cell wall theme of resistance remarkably resembles that of other potential CWI mutants such as *pmr5* and *pmr6.*

A common response seen with cell wall-related mutants and studies on cell wall perturbation is the deposition of callose, which is also a major component of papillae structures formed after pathogen attack. Studies on papillae and their role in defense have been plentiful in the past few years (review, (Underwood, 2012)). Papillae are now known to not only act as a physical barrier against pathogens, but are also sites of accumulation of antimicrobial secondary metabolites (Bednarek et al., 2009; Clay et al., 2009). For example, phenolic polymers have been known to be incorporated into papillae, and mutants impaired in cinnamyl alcohol dehydrogenase (catalyzing the final step of mono-lignol biosynthesis) are affected in defense against *Pseudomonas syringae pv. tomato* (Tronchet et al., 2010). Several studies on mutants impaired in papillae formation and callose deposition have shown the importance of these structures in defense, and its importance is highlighted by the fact that these localized reinforcements at the cell wall appear to be a shared response of pattern triggered immunity (Nomura et al., 2006; Nicaise et al., 2009; Bohlenius et al., 2010; Enrique et al., 2011).

As the CWI pathway is likely responsible for proper cell wall formation and cell growth, a potential end response is the alteration of cell cycle regulation. Several candidate CWI signaling players, such as the brassinosteroids and ethylene, have been shown to be important in cell wall remodeling during cell division and elongation (Sanchez-Rodriguez et al., 2010). Changes in cell cycle regulation are particularly important for plant symbionts that initiate host endoreduplication, a process where host cell ploidy is increased without mitotic division (Wildermuth, 2010). An example of this is the *pmr5* cell wall mutant, which has been shown to be affected in powdery mildew-induced endoreduplication (Chandran et al., 2013). Thus the CWI-signaling pathway is not only affecting changes in cell wall composition, but is also likely affecting basic processes in growth and development as an end response.

Conclusions

The last few years have seen a proliferation of evidence in support of the existence of a CWI-sensing pathway. Determining the fine structure of the cell wall will be important in identifying potential CWI signals derived from the cell wall. Pharmacological methods will be invaluable in dissecting signaling components in this interconnected pathway. New roles in cell wall maintenance for ERECTA and NDR1 will be interesting to characterize in reference to their known functions in normal development and innate immunity. Moreover, binding partners to ERECTA, NDR1, as well as other potential cell wall sensors can now be studied (Roux et al., 2011). Now with several potential cell wall sensor candidates, it will be important to determine other CWI signals to decipher the downstream signaling pathways that lead to the changes and responses we see.

Figures

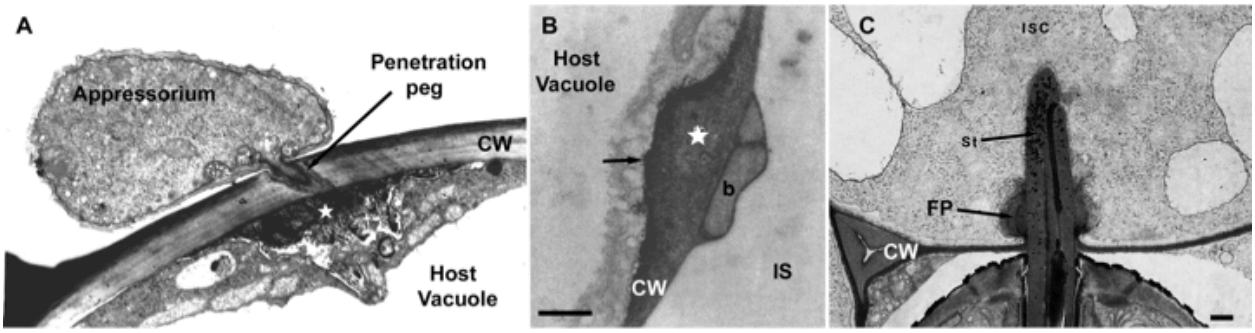

Figure 1.1. Electron micrographs of different pathogens infecting plant cells. Figure taken from (Hematy et al., 2009).
(a) *Blumeria graminis* f. sp. *hordei* fungal appressorium penetrating the cell wall of a barley leaf epidermal cell. One can observe the degradation of the plant cell wall (CW) by the penetration peg and the host cellular responses involving cytoplasm polarization and deposition of an electron dense cell wall apposition beneath the penetration site. Adapted from (Zeyen and Bushnell, 1979).
(b) A *Pseudomonas syringae* pv *phaseolicola* bacterium (b) infecting in the intercellular space (IS) of lettuce cells. The arrow points to a H_2O_2 deposition at the papilla plant cell membrane interface. Adapted from (Bestwick et al., 1997). Bar = 0.5 mm
(c) Penetration of root cells by the Soybean Cyst Nematode *Heterodera glycines*. Image courtesy of David Chitwood, Nematology Laboratory, USDA.
isc: initial syncitial cell; St: stylet; FP: feeding plug; Bar = 1 mm. White star in (a) and (b) represent the papilla deposited at the plant cell.

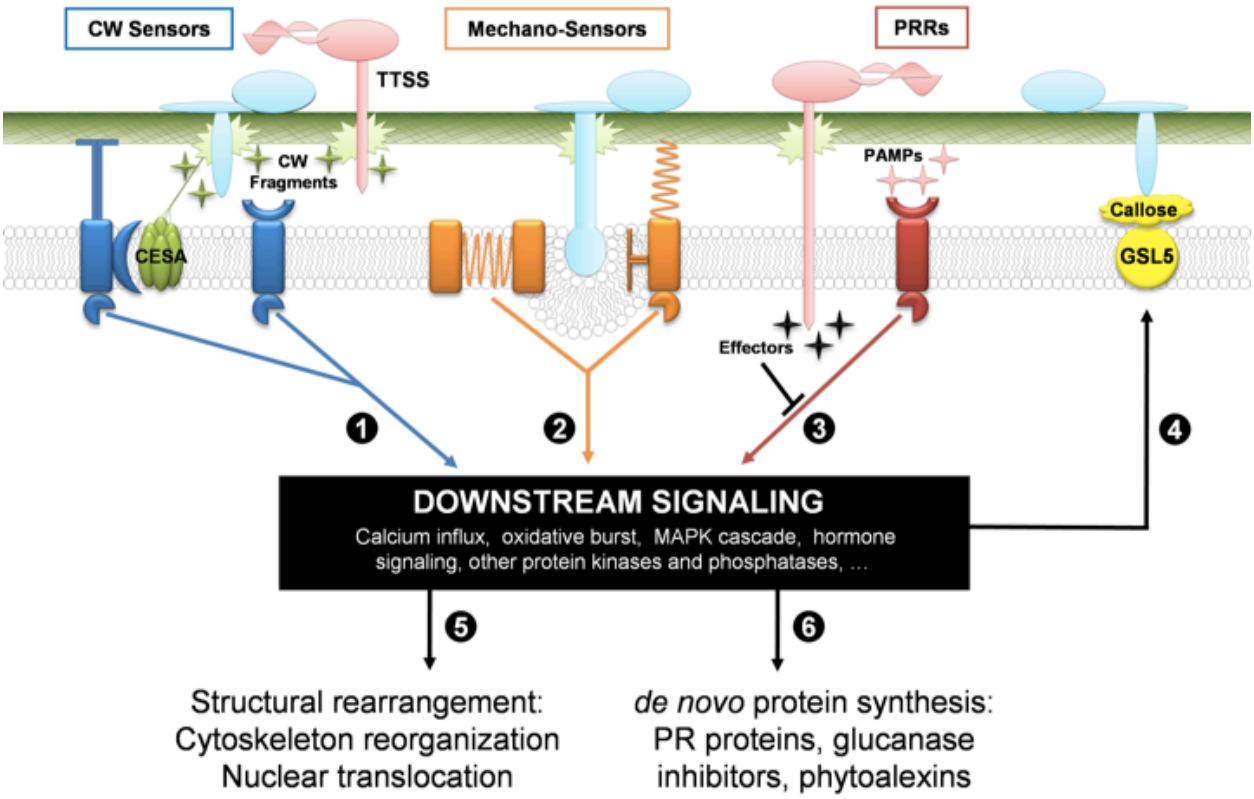

Figure 1.2. Overview of the plant cell signalling components mediating responses upon pathogen attack. Plant cells possess a variety of membranes receptors that perceive endogenous (e.g. plant cell wall (CW)-derived fragments = green stars) or exogenous (e.g. PAMP = pink stars) signals, which can be either peptides or oligosaccharides (or both in the case of proteoglycans). A given ligand activates a specific receptor, which initiates downstream signalling events. (1) Plant cells monitor their own cell wall through sensors like THE1. Inhibition of cellulose synthesis by the Streptomyces toxin thaxtomin A or disruption of cellulose structure by a pathogen cellulose-binding protein could activate this pathway. (2) Additionally, host cells may perceive pathogen intrusion through mechano-sensors. Stretching of the plasma membrane by invasive growth of a fungal haustorium could potentially disrupt cell wall plasma membrane links via WAKs and other RLK, or act on stretch-activated Ca2+ channels like Mca1. (3) Pathogen invasion can also be detected by the presence of PAMPs (pathogen-derived peptides or cell wall fragments) and by plant derived cell wall fragments generated by enzymes secreted by pathogens to aid penetration. Pathogens sometimes possess effectors (black stars) that can block defence responses. The three types of sensors seem to converge on common signalling pathways. Responses involve rapid events such as post-protein phosphorylation and activation (4), and slower events, like structural rearrangements of the cellular components (5) and induction of *de novo* protein synthesis (6) to produce defensive compounds like phytoalexins, glucanases inhibitors and glucanases. Figure taken from (Hematy et al., 2009).

CHAPTER 2: Investigating the function of PMR5 (POWDERY MILDEW RESISTANT 5)

Introduction

Powdery mildew disease affects over 9000 species of plants and is caused by several related species of fungi. The biotrophic lifestyle of these fungal pathogens requires them to maintain healthy hosts in order to colonize and reproduce without activating host defense mechanisms. A white powdery layer covering leaves and stems of susceptible plants characterizes the disease. This white layer is composed of an array of hyphal growth at the surface of the leaf, implantations of membranous sacs called haustoria below the leaf surface, and towers of conidiophore stalks that are capable of releasing the next generation of spores.

Several Arabidopsis mutants that are resistant to the compatible powdery mildew pathogen, *Golovinomyces cichoracearum,* have been isolated and characterized as the *pmr* (*powdery mildew resistant*) mutants (Vogel and Somerville, 2000). *PMR2* encodes an ortholog to *MLO* (*MILDEW RESISTANT LOCUS*) in barley (Consonni et al., 2006). *PMR4/GSL5* encodes callose synthase, which was found to be salicylic acid dependent in its defense response (Nishimura et al., 2003). *PMR6* was cloned and found to have sequence similarities to a pectate lyase like protein (Vogel et al., 2002). Like the *pmr6* mutant, the *pmr5* mutant also had altered cell wall composition, but had no sequence similarity to other genes of known function (Vogel et al., 2004). Interestingly, both *pmr5*- and *pmr6*-mediated disease resistance act independently of salicylic acid, jasmonic acid, and ethylene pathways (Vogel et al., 2002; Vogel et al., 2004). Both *pmr5* and *pmr6* mutants share similar morphological phenotypes, including flatter and more rounded leaves. When crossed to generate the double mutant *pmr5/pmr6*, there was an increase in uronic acids, indicating an additive effect by the two mutations on cell wall pectin levels (Vogel et al., 2004).

PMR5/TBL44 is part of the TBL family of proteins, which contains 46 plant specific members (Fig. 2.1). The family is named after TBR (TRICHOME BIREFRINGENCE), a protein involved in cellulose biosynthesis (Bischoff et al., 2010). Other members of this family include ESK1/TBL29 (ESKIMO1) and AXY4/TBL3 (ALTERED XYLOGLUCAN 4). A mutation in *ESK1* resulted in increased freezing tolerance, and was hypothesized to be involved in secondary cell wall biosynthesis and modification of xylem cells (Lefebvre et al., 2011). The *axy4* mutant was deficient in xyloglucan acetylation (Gille et al., 2011). Although none of the proteins in this family have been functionally characterized for biochemical activity, the trend seems to imply that TBL proteins are involved in cell wall biosynthesis and modification. Moreover, PMR5 seems to be unique in its disease resistance phenotype when mutated. Mutants from the TBL family were isolated and tested for disease resistance to *G. cichoracearum*. Several were isolated previously from the Somerville group, and two additional insertional mutants of At3g30900 and At3g14850 were also isolated. Of those tested, only the *pmr5* mutant was resistant (Fig. 2.1). This suggests that disease resistance in the *pmr5* mutant is likely a secondary effect, and that the primary function of PMR5 is in cell wall modification.

Although an altered cell wall could affect the penetration efficiency of the pathogen, this is not the case for the *pmr5* mutant as the fungus can penetrate through the wall to form haustoria at numbers comparable to wild-type (Vogel et al., 2004). There is building evidence that an additional pathway that senses cell wall integrity (CWI) is responsible for a response against pathogen attack (see Chapter 1). PMR5 could potentially act in this novel CWI-sensing pathway. Based on initial analyses of the *pmr5* cell wall and its similarities to *pmr6*, we hypothesize that PMR5 functions as a pectin modifier. Pectin is a complex group of polysaccharides composed of homogalacturonan, rhamnogalacturonan I, rhamnogalacturonan II, and xylogalacturonan, and

many of the enzymes that are involved in pectin biosynthesis and modification are unknown (pectin review: (Caffall and Mohnen, 2009); Fig. 2.2 from (Liepman et al., 2010)). We hypothesize that when *PMR5* is mutated, pectin composition in the cell wall is altered and new polysaccharide fragments could be generated during normal cell wall maintenance or pathogen attack. These fragments could then elicit responses that could alter morphology and disease resistance.

Materials and Methods

Molecular biology techniques

Polymerase chain reaction (PCR)
Standard *Taq* polymerase (New England Biolabs, NEB) was used for genotyping purposes, along with 10x Standard *Taq* buffer, 2.5µM dNTPs, and 10µM of each primer. Phusion polymerase (NEB) was used for cloning purposes, along with 5x HF buffer, 2.5µM dNTPs, and 10µM of each primer. Followed manufacturer's instructions for reaction conditions. PCR samples were mixed with 6x OrangeG loading dye and run on 1% agarose gels with ethidium bromide.

Plasmid DNA purification
Overnight cultures containing the plasmid were purified using the Miniprep kit (Qiagen) according to manufacturer's instructions.

Site directed mutagenesis
Agilent/Stratagene Quikchange XL II kit was used following manufacturer's protocol to mutate single residues from plasmid DNA.

Plant RNA isolation and cDNA synthesis
Plant RNeasy kit (Qiagen) was used to isolate plant RNA following manufacturer's instructions with on column DNaseI treatment. cDNA was synthesized from 0.5-1µg of total RNA using the M-MuLV kit (NEB) following manufacturer's instructions. Standard PCR methods were used to amplify transcripts from the cDNA

Cloning strategies

Standard cloning methods were used according to (Ausubel et al., 1995). All constructs were sequenced to verify that they did not contain unwanted mutations and that they were in frame with any N-terminal or C-terminal tags. Plasmids and oligonucleotide primers used in this study are listed in Tables 2.1 and 2.2, respectively.

Construction of VIGS plasmids
610 bp and 721 bp of the N-terminal region of *PMR5,* including the 5'UTR, was amplified from SP/pUC57 with additional restriction sites and subcloned into pCR8. Along with pYL156 (pTRV2), the insert was digested using EcoRI and KpnI restriction enzymes. The digested inserts and plasmid were separately ligated with T4 ligase to form pTRV2-610 and pTRV2-721 and transformed into chemically competent cells.

Synthesis of pPMR5:PMR5-mCherry-Myc-His

Construct was synthesized by DNA2.0 (https://www.dna20.com/) and cloned into pUC57 to create plasmid SL/pUC57 (See Appendix 2.1 for full sequence). EcoRI, HindIII, XhoI, and SacII sites were designed to clone out *PMR5* for other genes of interest to be tagged with mCherry, myc, or 6xHis tags. Factor Xa and enterokinase are both proteases that cleave at specific peptide sequences, which have been designed into the construct so that the purification tags can be removed. *pPMR5:PMR5-mCherry-Myc-His*, derived from plasmid SL/pUC57 was cloned into pCR8 (Invitrogen), a TOPO Gateway entry vector, and used in a LR reaction with pMDC99, a promoterless and tagless destination vector, to form SL/pMDC99.

Construction of pPMR5:PMR5-Myc-His
Plasmid SL/pUC57 was digested with XhoI and SalI restriction enzymes and religated to remove *mCherry* to form the plasmid, SP/pUC57. *pPMR5-PMR5-Myc-His* was cloned from SP/pUC57 into pENTR-D-TOPO (Invitrogen) to create SP/pENTR, which was then used in a LR reaction with pMDC99 to form SP/pMDC99.

Construction of pPMR5:PMR5-GFP (pGWB4)
Primers specific to 1kb upstream of the start codon (promoter of *PMR5*) and the end of *PMR5* with stop codon omitted were designed to amplify the insert from SP/pUC57 using Phusion polymerase. The PCR fragment was cloned into pCR8 after TA extension with standard *Taq* to create the plasmid, pP5:P5/pCR8. An LR Gateway reaction was performed with pGWB4, a Gateway-compatible vector with a C-terminal green fluorescent protein (GFP) tag (Nakagawa et al., 2007), to form pP5:P5-GFP/pGWB4.

Construction of pPMR5:PMR5-Strep
Primers specific to 1kb upstream of the start codon (promoter of *PMR5*) and the end of *PMR5* with stop codon omitted plus strep tag sequence (TGGAGCCACCCGCAGTTCGAAAAA) were designed to amplify the insert from SP/pUC57 using Phusion polymerase. The PCR fragment was cloned into pCR8 after TA extension with standard *Taq* to form pP5:P5-Strep/pCR8.

Construction of putative catalytic mutants: S142A, D379A, H382A
SP/pENTR and pP5:P5-Strep/pCR8 were used as templates for site directed mutagenesis of putative catalytic residues in *PMR5* using the QuikChange II XL site directed mutagenesis kit (Agilent/Strategene). Mutations were generated to create the mutants, S142A (TCA to GCA), D379A (CAT to GCT), and H382A (GAT to GCT) either with or without a strep tag. An LR reaction between each tagless catalytic mutant (S142A/pENTR, D379A/pENTR, or H382A/pENTR) and pGWB16 was done to form S142A/pGWB16, D379A/pGWB16, and H382A/pGWB16 for floral dipping.

Construction of Pichia pastoris *expression plasmids*
PMR5 without its 29aa N-terminal signal peptide and the PMR5 DUF231 domain were cloned from Arabidopsis cDNA with primers containing EcoRI and KpnI ends with Phusion polymerase. PCR products and pPICZaC and pGAPZaC plasmids (Invitrogen) were digested with EcoRI and KpnI, gel purified, then ligated with T4 ligase to form P5c/pPICZaC, DUF/pPICZaC, P5c/pGAPZaC, and DUF/pGAPZaC. The ligation products were transformed into chemically competent TOP10 cells (Invitrogen) and plated on LB with 25µg/ml zeocin for selection. Colonies were prescreened for insertions using 5'AOX and 3'AOX primers, and

sequenced. Constructs were then transformed into freshly prepared Pichia competent cells, strain X-33 (Invitrogen).

Construction of E.coli *expression plasmids*
PMR5 truncations were cloned using the *PMR5* CDS with P5cF, C-GDSL F, and DUF231 forward primers and the P5-his-Sbf1 reverse primer (Table 2.2) from SP/pUC57 using Phusion polymerase to create fusions with 3x glycine linker, a 6x histidine tag, and a SbfI restriction enzyme site. Blunt-end PCR fragments were digested with SbfI to create one SbfI-overhang, while pMALc and pMALp plasmids (NEB) were digested with XmnI and SbfI to create an SbfI-overhang and a blunt end. Digested products gel purified and ligated with T4 ligase to form P5c/pMALc, P5c/pMALp, and CG/pMALp. Plasmids were transformed into chemically competent cells before plating on LB with carbanicillin. Colonies were sequenced with DUF231, P5Seq2-2 primers. Plasmids were then transformed into NEB express (NEB) or Origami B(DE3) (Novagen) cells for expression.

Plant techniques

Plant growth conditions
Columbia-0 (Col-0) and Landsberg *erecta* (Ler) ecotypes of *Arabidopsis thaliana* seed were surface sterilized with 30% bleach and 0.5% SDS for 15 m prior to copious water washes and then resuspended in 0.15% agar solution. Seeds were stratified at 4ºC for at least 2 days. Sterilized seeds were germinated on ½ Murashige Skoog 0.8% agarose plates with 1% sucrose in 24 h light. Plates of seedlings to be etiolated were wrapped in two layers of foil. 5-6-day-old seedlings were transplanted to soil and grown in Percival (12 h, 14 h) or Conviron (16 h) growth chambers at 70% relative humidity, with 12 h, 14 h, or 16 h light with photosynthetically active radiation of 100µE m^{-2} s^{-1}, at temperatures of 22°C during the day and 20°C at night. Pots were fertilized with Miracle Gro at the first watering, and then bottom tray watered thereafter.

Arabidopsis powdery mildew growth and infections
Golovinomyces cichoracearum UCSC1 was maintained on cucumber (*Cucumis sativus*) var Bush Champion (Burpee). Plants were grown for 3 weeks in growth chambers at 22°C with a 16 h photoperiod. Plants were inoculated by placing a 1.3-m-tall settling tower over the flat and using compressed air to disperse the spores from two to three cucumber leaves infected 7-9 days prior to inoculation. After 5 m, the plants were returned to a Conviron growth chamber with 16 h light with photosynthetically active radiation of 100µE m^{-2} s^{-1}, 22ºC day and 20ºC night, and 75% relative humidity.

Generation of transgenic Arabidopsis
Plasmids were transformed into Agrobacteria GV3101 by electroporation, and clones were selected on plates containing 25µg/ml rifampicin, 25µg/ml gentamycin, and 60µg/ml kanamycin. Positive clones were grown in LB with antibiotics overnight, and the cells were pelleted and resuspended in infiltration media for floral dipping (Clough and Bent, 1998). Plants were covered with a plastic dome for 24 h, then grown in growth chambers to set seed. Seeds were screened for resistance to hygromycin, methionine sulfoximine, or BASTA, then genotyped to confirm the presence of the transgene. A list of all transgenic lines generated in this study can be found in Table 2.3.

Arabidopsis genomic DNA isolation
Genomic DNA was isolated according to (Edwards et al., 1991). Briefly, plant tissue was ground in DNA extraction buffer (200mM Tris pH 7.5, 250mM NaCl, 25mM EDTA pH8, 0.5% SDS), vortexed, and then spun down to separate gDNA in the supernatant and larger cell debris in the pellet. The supernatant was resuspended in an equal volume of isopropanol to precipitate the DNA, centrifuged, and the pellet was washed with two volumes of 70% ethanol. Genomic DNA was left to dry at room temperature, and then resuspended in water.

TILLING lines
The sequence in Appendix 2.2 was submitted to a TILLING service (http://tilling.ucdavis.edu/index.php/Arabidopsis_TILLING) (McCallum et al., 2000). TILLING lines were planted and inoculated with *G. cichoracearum*. Those that showed lack of susceptibility were backcrossed to Col-0, and were allowed to self-pollinate. A list of the TILLING mutants with their annotated mutations and current status of the TILLING lines can be found in Table 2.4.

T-DNA insertion lines
Insertional lines were ordered from the Arabidopsis Biological Resource Center (http://abrc.osu.edu/) (Table 2.3). Primers specific to the T-DNA border (LBb1.3) and an internal gene primer were used to genotype the lines to identify homozygous mutations (Alonso et al., 2003).

Virus induced gene silencing in Arabidopsis
Virus induced gene silencing of *PMR5* in Arabidopsis was done following a modified protocol by (Burch-Smith et al., 2006). Col-0 plants were grown to 9 d at 16 h light growth conditions, when the first true leaves were fully expanded. Agrobacteria containing modified Tobacco Rattle Virus (TRV) expressing 610bp or 721bp of the N-terminus of PMR5 sequence, including the 5'UTR, was grown overnight in LB with 25µg/ml rifampycin, 25µg/ml gentamycin, and 60µg/ml kanamycin. pTRV1 (pYL192), pTRV2-GUS (negative control) and pTRV2-PDS (phytoene desaturase, positive control) were grown alongside. Overnight cells were pelleted and resuspended in infiltration media (10mM $MgCl_2$, 10mM MES, and 200 µM acetosyringone) to OD_{600} of 1.5. pTRV1 and pTRV2 were combined 1:1 and mixed for at least 2 h prior to syringe-infiltration in the first true leaves. 13 days after Agrobacteria infiltration, plants were inoculated with *G. cichoracearum*. At 24 hpi, 5 dpi, 7 dpi, and 9 dpi, plants were photographed to document phenotypic changes after silencing. A duplicate set of silenced plants was left uninfected. Leaf tissue from infected and uninfected silenced plants corresponding to PDS-silenced leaves was harvested at 24 hpi and 5 dpi for qPCR analysis of transcription silencing. Separate pots of silenced plants were used at each time point to prevent nonspecific effects from tissue harvesting.

Biochemical techniques

SDS-PAGE and Western blot
SDS-PAGE was run according to (Laemmli, 1970). Proteins were run on 4-15% Tris HCl pre-cast SDS-PAGE gels (Criterion) at 180V for 1 h. Gels were either stained with GelCode Blue

(Thermo Pierce) for 1 h with a water destain following manufacturer's protocol, or transferred to a nitrocellulose membrane when used for western blotting. Transfers were run at 100V for 1 h at 4ºC. Blots were blocked with 5% milk in Tris-buffered saline solution (TBS) for at least 1 h at room temperature prior to incubation with primary and secondary antibodies with three washes of TBS with 0.05% Tween 20 (TBST) in between. Blots were visualized with chemilluminescent substrate (Pierce) and using the LAS4000 image reader (GE Healthcare Life Sciences).

Expression of MBP-PMR5-His in E. coli

Protein was expressed following the manufacturer's suggested protocol from the pMAL Protein Fusion and Purification system manual (NEB). P5c/pMALc was transformed into Origami B(DE3) cells and grown in LB with glucose and carbanicillin (ampicillin) at 37ºC overnight to inoculate a 1L culture to obtain an OD_{600} of 0.5. The culture was induced with 0.3mM IPTG and grown at 16ºC for 16 h. Cells were centrifuged at 10,000xg for 15 m, washed with cold TBS buffer, and the pellet was stored at -20ºC until needed.

Purification of MBP-PMR5-His protein

Protein was purified following a modified protocol from (Sorek et al., 2007). Pellets from 1L of culture were resuspended and homogenized in 50ml lysis buffer (50mM NaH_2PO_4 pH 7.6, 150mM NaCl, 5mM imidazole, 5% glycerol, 1mM beta-mercaptoethanol) using the Avestin E3 Emulsiflex Homogenizer. The homogenate was centrifuged at 20,000 rpm in a JA-20 Beckman-Coulter floor centrifuge at 4ºC for 1.5 h. The PMR5 protein was purified from the supernatant first by batch binding using Ni-NTA (Qiagen) resin before eluting on column with 200mM imidazole. Protein elutions from the His-tag purification were subsequently column-purified using amylose resin (NEB) and eluted with 10mM maltose.

Protein sequencing

80kDa bands generated from MBP-PMR5-His purification were cut out from a SDS-PAGE gel and digested following the UC Berkeley QB3 proteomics/mass spectrometry protocol (http://qb3.berkeley.edu/pmsl/pdfs/ezymatic%20digestion%20of%20protein%20samples.pdf). Briefly, gel fragments were washed with a 100mM ammonium bicarbonate wash, reduced with 45mM DTT, incubated with 100mM iodoacetamide for irreversible alkylation, then washed with 50:50 mix of acetonitrile and ammonium bicarbonate. Gel pieces were dehydrated with acetonitrile and then dried by a vacuum centrifuge. Gel pieces were rehydrated with 25mM ammonium bicarbonate containing Promega modified trypsin to digest overnight at room temperature. Peptides were recovered in the supernatant from the overnight digest and then further extracted with 60% acetonitrile/0.1% formic acid and 100% acetonitrile. Samples were analyzed by one-dimensional LC/MS-MS by the UC Berkeley QB3 proteomics/mass spectrometry lab (http://qb3.berkeley.edu/pmsl/home.htm).

Nitrocellulose binding dot blot assay

Polysaccharides were spotted on pre-wetted nitrocellulose membrane using the Biodot apparatus (Bio-Rad). TBS buffer was used to clear the wells by vacuum before application of sugars in 100µl of TBS buffer, which were then vacuumed to apply to the membrane. Wells were washed once with TBS buffer and vacuumed through. The membrane was dried at 80ºC for 1 h and then blocked in 5%milk/TBS for at least 3 h at room temperature. Binding proteins (i.e., MBP-PMR5-His, 3 h-boiled MBP-PMR5-His, MBP) were incubated with the blot for 1 h at room temperature

(about 100µg per 96-spotted membrane) then washed thrice with TBST. Blots were incubated with primary antibody (1:10000 anti-MBP, NEB) in blocking solution overnight, washed thrice with TBST, then incubated with secondary antibody (1:3000 anti-mouse HRP, Promega) in blocking solution for at least 1 h room temperature. Blot was washed thrice with TBST and then chemilluminscent substrate (Pierce) was applied prior to visualization using the LAS4000 image reader.

Purification of PMR5-Myc-His from Arabidopsis thaliana
Proteins were isolated as described in (Sorek et al., 2010). 7-day-old light-grown seedlings (300mg) were frozen in liquid nitrogen and stored at -80ºC until used. Samples were ground with liquid nitrogen in a mortar and pestle until a fine powder formed. 600µl of HEPES based protein extraction buffer (+PMSF and other protease inhibitor) was added to mortar and the slurry was transferred to 11mm x 34mm ultracentrifuge tubes (Beckman). Samples were left on ice for 20 m. Tubes were centrifuged at 100,000xg in MLA-130 tabletop ultracentrifuge for 1 h at 4ºC. Supernatant was kept as the soluble fraction (S). Protein extraction buffer with 1% SDS and 1% Triton100 was added to pellet and resuspended, and then left on ice for 20 m. Tubes were centrifuged again at 100,000xg in MLA-130 tabletop ultracentrifuge for 1 h at 4ºC, and the supernatant was kept as microsomal fraction (M). Pellet was kept as insoluble/cell wall fraction (I).

Purification of PMR5-GFP from Arabidopsis thaliana
Proteins were isolated as described in (Sorek et al., 2010). 4-day-old light-grown seedlings (100mg) were frozen in liquid nitrogen and stored at -80ºC until used. Samples were ground with liquid nitrogen in a mortar and pestle until a fine powder formed. 300µl of HEPES based protein extraction buffer (+PMSF and other protease inhibitor) was added to mortar and the slurry was transferred to 11mm x 34mm ultracentrifuge tubes (Beckman). Samples were left on ice for 20 m. Tubes were centrifuged at 100,000xg in MLA-130 tabletop ultracentrifuge for 1 h at 4ºC. Supernatant was kept as the soluble fraction (S). Protein extraction buffer with 1% SDS and 1% Triton100 was added to pellet and resuspended, and then left on ice for 20 m. Tubes were centrifuged again at 100,000xg in MLA-130 tabletop ultracentrifuge for 1 h at 4ºC, and the supernatant was kept as microsomal fraction (M). Pellet was kept as insoluble/cell wall fraction (I).

Protein quantification
Proteins were quantified using a modified Bradford assay for 96-well plates following the manufacturer's protocol from the Bio-Rad Protein Assay manual. A standard curve was made using 0.5, 1, 2, 4µg of BSA in a total volume of 15µl. 5µl of sample was loaded. All samples were loaded in triplicate on 96-well plate. 200µl of diluted Bio-Rad protein assay reagent was added and absorbance at 595nm was read to calculate the concentration of samples from the standard curve.

Acetyltransferase activity assay for NMR analysis
100 µg of MBP-PMR5-His in water was buffer exchanged into deuterium oxide (D_2O) using a Vivaspin 20 10,000 MWCO centrifugal concentrator to a ratio of 1:50 H_2O:D_2O. 50 µg of MBP-PMR5-His in D_2O was mixed with 1 mg acetyl-coA (Sigma A2056) and 5 mg polygalacturonic acid (Megazyme Lot 30402) in 0.8 ml total volume of D_2O. The sample was mixed at 500 rpm

for 24 h at room temperature, then stored at -20ºC until analysis by NMR.

Cell wall analyses

Sample preparation for Fourier Transform InfraRed (FTIR) spectrometry and principle component analysis (PCA)
Samples were prepared and analyzed by FTIR spectroscopy as in (Persson et al., 2005). 3-week-old plants were destarched overnight in the dark and then immersed in 80% ethanol overnight at room temperature. Tissue was centrifuged at 3200xg for 5 m at room temperature, and the ethanol was decanted. Samples were then washed with 80% ethanol again, and then tissue was treated three times with a mix of 1:1 (v:v) chloroform:methanol and rocked at room temperature for 10 m with decanting in between. Samples were then treated with 100% acetone twice for 30 m at room temperature. The cell wall material was air dried for 1 h in a fume hood, then vacuum centrifuged overnight. Dried cell wall material was stored at room temperature for future use. Cell walls material was ground to a powder prior to analysis with the Thermo Nicolet 6700 FTIR with Smart Diamond ATR accessory. OMNIC software was used to perform the PCA as well as a spectral subtraction, both of which gave similar results.

Sample preparation for Raman spectroscopy
5mm sections of the second internode of 6-week-old plants were dehydrated using an ethanol gradient (25%, 50%, 70%, 100%) for one hour at a time, then kept at 100% ethanol for 2 days, before decreasing the gradient (70%, 50%, 25%) back to 100% water. The samples were then embedded in 1:1 (v:v) PEG4000:water for 3 days at 60ºC, then kept at room temperature to solidify. 50-100µM sections were made using a Leica microtome. The PEG was solubilized with copious water and then D_2O was used to cover the remaining tissue on the slide with a 0.17mm coverslip and nail polish around the edges. Raman imaging was performed as described in (Schmidt et al., 2010).

Preparation of alcohol insoluble residue (AIR)
AIR was prepared as described in (Gunl et al., 2011). Tissue was flash frozen in liquid nitrogen and lyophilized with Labconco freeze dryer for 48 h. Lyophilized material was stored at room temperature until needed. Dried material was flash frozen and ground using a Retsch MM 400 ball mill at 30 Hz for 3 m, then flash frozen again before repeating a second grinding. The powdered samples were treated with 70% ethanol twice, then 1:1 methanol:chloroform thrice, centrifuging for 10 m at 14000 rpm and decanting after each wash. The cell wall pellet was dried in a vacuum centrifuge at 60ºC for 15 m. Samples were destarched with solution containing sodium azide, amylase (Sigma A6380), and pullulanase M2 (Megazyme) in 0.5X McIlvaines buffer pH5 overnight at 37ºC. Samples were heated at 99ºC and then pellet washed with water 3 times, and then once with 70% ethanol. Destarched pellet was dried in a vacuum centrifuge at 60ºC for 45 m.

Cell wall fractionation and immunodetection
Cell wall fractions were isolated following a modified protocol from (Melton and Smith, 2001). Fresh weight tissue (50mg) flash frozen and ground to a powder or destarched AIR (1mg) were sequentially extracted with 50mM CDTA pH 6.5, then 50mM Na_2CO_3 20mM $NaBH_4$ pH 11, then 4M KOH 20mM $NaBH_4$ pH 14. Samples were incubated in each solvent twice for 1 h each

and spun 2500xg for 5 m before collection. Supernatants from the sequential extractions were spotted on nitrocellulose, dried at 80ºC for 1 h, blocked for 3 h, then probed with cell wall antibodies as described above.

Cell wall immunolabeling
Col-0 and *pmr5* plant stems were harvested when Col-0 stems were about 20-25cm tall and fixed and prepared as in (Verhertbruggen et al., 2009). Briefly, 1.5cm long stems were harvested 10cm distal from the rosette, and fixed in paraformaldehyde. Stems were then gradually exchanged into Steedman's wax embedding media, and sequentially sectioned at 60µm thick with a vibrotome. Sections were placed on polysine-coated glass slides and the embedding media was washed away with ethanol. The stem sections were then probed with cell wall antibodies and Alexa-fluor 488 conjugated secondary antibodies for visualization using an epifluorescence microscope.

Oligosaccharide Mass Profiling (OLIMP):
Samples were prepared and analyzed as described in (Gunl et al., 2011). Briefly, AIR was isolated from 5-10 light-grown seedlings per sample in triplicate, then digested with a xyloglucan endoglucanase and analyzed using an Axima matrix-assisted laser desorption/ionization time-of-flight (Shimadzu) set to linear positive mode with an acceleration voltage of 20,000 V.

Acetic acid Assay
AIR was resuspended in water to a concentration of 10mg/ml. 100µl of AIR slurry (1mg) was used for the Megazyme KACET acetic acid assay modified from (Manabe et al., 2011). 1mg of AIR was saponified with 1M sodium hydroxide at room temperature overnight, then neutralized with 1M hydrochloric acid. Samples were spun down at 14,000rpm for 10 m, and supernatant (released acetyl groups) was used for acetic acid assay modified for 96-well format. Absorption at 340nm using UV-transparent plates (Costar) was read using the Paradigm plate reader to obtain 3 values after the addition of each kit solution, and the acetate release was calculated based on manufacturer's instructions.

Pectinase digests of AIR
3mg of AIR was incubated with endopolygalacturonase M2 (Megazyme) and pectin methyl esterase (gift from Pauly lab) overnight in ammonium formate buffer pH 4.5. The supernatant containing pectin was collected after centrifuging at 14,000rpm for 10 m. Samples were washed thrice with water and washes saved. Supernatant plus washes and pellet were lyophilized overnight, then resuspended in water.

RGI side chain digests
Pectin (Sigma P9135) or polygalacturonic acid (Megazyme 30402) was digested with arabinanase (Megazyme 91001) or galactanase (Megazyme 101001b) in sodium acetate buffer pH 4 for 30 m according to manufacturer's recommended instructions. Reactions were stopped by heating to 99ºC for 20 m. Antibodies specific to arabinan and galactan were used to determine the digestion efficiency.

Saccharification assay

Saccharification was assayed using a modified protocol from (Pryor and Nahar, 2010). AIR (1mg) was incubated with Accellerase 1500 (Genencor) in 50mM citrate buffer pH 4.5 overnight at 50ºC with constant mixing with biological and technical triplicates. The reaction was stopped by heating to 100ºC for 10 m, then centrifuged for 10 m. The supernatant containing released glucose was measured using the YSI 2700 Select Biochemistry Analyzer.

Seed mucilage production and labeling
Mucilage was produced as described in (Willats et al., 2001). ~5000 seeds (0.1g) were imbibed in 1ml of water or 50mM CDTA pH 7 overnight with shaking. Supernatant containing the seed mucilage was collected after centrifugation at 8000xg for 3 m. Seeds were stained with 0.05% ruthenium red (w/v) for 10 m before visualization using the epifluorescence microscope under bright field. Mucilage was used for spotting and probing with antibodies as in (Willats et al., 2001). *in situ* labeling of seed mucilage was done as described in (Macquet et al., 2007). Briefly, seeds were imbibed and demasked with heat and citric acid. The seeds were then incubated with LM5 or LM6 antibodies and the corresponding Alexa Fluor 488-conjugated secondary antibody before mounting in anti-fade agent (Citifluor) and visualization with the confocal microscope. The 488 nm laser was used to visualize the rhamnogalacturonan I epitopes, while the 561 nm laser was used to visualize autofluorescence. Images were merged and analyzed in ImageJ.

Microscopy techniques

Confocal microscopy
Imaging was performed on a Leica SD6000 microscope with a 63x 1.2W water-immersion objective or a 100x 1.4NA oil-immersion objective equipped with a Yokogawa CSU-X1 spinning disk system and 488 nm and 561 nm lasers controlled by Metamorph software. Z series were collected with a 200-300 nm step size and reassembled in ImageJ as in (Anderson et al., 2010).

Epifluorescence microscopy
Images of stained seed mucilage were collected on a Leica DMI 5000 B microscope equipped with a 5x objective under bright field.

Microscopy image analysis
ImageJ (http://rsb.info.nih.gov/ij/) was used to analyze microscopy images. Confocal images were assembled into Z-stacks to create maximum intensity Z-projections, and were merged to generate colored images for co-localization studies. A Z-axis profile was used to calculate the mean pixel intensity at each Z stack to generate a graph mapping the changes in fluorescence across a Z stack.

Results

Gene studies of PMR5

Bioinformatics analysis
The exponential accumulation of sequencing data has led to the developmental of many computational tools that quickly align and compare sequences, and can categorize them into

functional and structural groups. Bioinformatics techniques were used to reveal structural motifs that may be useful in characterizing PMR5. A list of the prediction tools used in this study can be found in Table 2.5.

The TBL proteins all have a conserved putative catalytic triad composed of a serine, an aspartic acid, and a histidine. The serine sits within a conserved GDS motif, which is part of a larger conserved domain called the TBL domain (Bischoff et al., 2010), while the other two residues sit in a conserved DxxH arrangement at the C-terminus of the DUF231 domain. The GDS motif is conserved in some esterases and lipases (Akoh et al., 2004). The serine from the TBL motif and the aspartic acid and histidine in the DUF231 domain have been hypothesized to encode a catalytic triad important for esterase function based on sequence homology with a capsular protein, Cas1p, of *Cryptococcus neoformans* (Anantharaman and Aravind, 2010). The Cas1p protein is important for proper O-acetylation of glucuronoxylomannans and virulence of the fungal pathogen in animal hosts (Janbon et al., 2001). Cas1p orthologs also fit into the SGNH/GDSL superfamily, which contains acyltransferases and esterases (Anantharaman and Aravind, 2010). Like members of the SGNH/GDSL superfamily, TBL members contain the catalytic triad of SDH; however, TBL members lack the conserved G and N. This modified SGNH/GDSL family was termed the PC-esterase family after its inclusion of PMR5-related proteins and homology to the Cas1p proteins (Anantharaman and Aravind, 2010).

TBR was modeled to a structure of rhamnogalacturonan acetylesterase (RGAE) from *Aspergillus aculeatus*, a fungal protein also containing the aforementioned catalytic triad (Bischoff et al., 2010). However, despite the similarity in structure, esterase activity could not be demonstrated (Bischoff et al., 2010). The secondary structure prediction tool, PHYRE was used to compare the secondary structures of the fungal RGAE with PMR5 (Fig. 2.3). The C-terminal domains both share a similar pattern of helices bookmarking the ends, with one helix-sheet-helix in the middle, and a helix after the conserved DxxH motif in the DUF231 region of PMR5. However, overall there is poor secondary structure similarity.

A thorough computational analysis on PMR5 was run in collaboration with Kimmen Sjolander (University of California, Berkeley). Several iterations of PSI-BLAST revealed non-plant proteins that shared some sequence homology. The focus was primarily on the N-terminal domain of PMR5 since it has the least homology with the TBL family of proteins. This would hypothetically point to the unique functions, such as substrate specificity, of PMR5 distinct from the TBL family. Although Cas1p was identified as a shared motif with the *PMR5* sequence, there were only a few residues that overlapped between the two. In addition, a fungal ortholog from *Coprinopsis cinerea okayama* was identified, which matched 29 amino acids at the C-terminal end of PMR5 and contained the conserved DxxH motif, with 51% identity and 62% similarity. PSI-BLAST with the *C. cinerea okayama* sequence replicated PMR5, but did not provide other leads.

The PMR5 sequence was submitted into the Phylofacts suite, which outputs a conservation analysis to predict critical residues, as well as an alignment with homologous proteins (Krishnamurthy et al., 2006). One annotated protein was a putative alpha-galactosidase from *Coffea arabica*. This protein has no homology to other known alpha-galactosidases. The putative coffee alpha-galactosidase was annotated after it was purified from a fraction retaining alpha-galactosidase activity and sequenced (Pierre Marraccini, personal communication). An antibody against an alpha-galactosidase from guar was able to detect the putative coffee alpha-galactosidase and was used to show localization in the cell wall and the cytoplasm (Marcos Buckeridge, personal communication). However, the activity of the putative alpha-galactosdiase

has yet to be shown (Marcos Buckeridge, personal communication). The secondary structure of the putative coffee alpha-galactosidase was compared with PMR5, and revealed remarkable similarities in the number and ordering of helices and beta sheets based on PHYRE prediction (Fig. 2.3). In addition, the putative coffee alpha-galactosidase contains the conserved catalytic triad shared in the TBL family of proteins. Based on the similarities between the secondary structures of PMR5 and the putative coffee alpha-galactosidase, it is possible that they share similar functions.

PMR5 gene expression in the pmr5 mutant

The *pmr5* mutation is a recessive loss of function mutation, as the full-length native gene can rescue the mutant. The mutation is a single point mutation that causes tryptophan 265 to convert to an early stop codon. Gene expression data from the eFP browser indicates that *PMR5* is weakly expressed throughout development, with 10-fold increases in meristematic root cortical cells and two-fold increases upon cold treatment (Fig. 2.4). *pmr5* plants have a two-fold decrease in *PMR5* transcript compared to wild-type Col-0 (Table 2.6). Interestingly, 4-day old etiolated seedlings were found to have a 170-fold increase in *PMR5* gene expression in wild-type plants, whereas in the *pmr5* mutant, this induction was nonexistent and the expression levels stayed constant. Additionally, upon infection with powdery mildew, *PMR5* transcription is induced in wild-type rosette leaves, whereas this induction in transcription is not seen in the *pmr5* mutant (Table 2.6).

Generation of additional mutant alleles of PMR5

There is currently only one mutant allele of *PMR5* from the original EMS mutagenesis screen for *pmr* mutants (Vogel and Somerville, 2000). To identify other alleles of *pmr5*, a search through Arabidopsis accessions for natural variation within the *PMR5* gene revealed two accessions, Tsu-1 and Bur-0 that contained nonconservative polymorphisms (Table 2.7, Fig. 2.5). However, neither ecotypes were resistant to the host powdery mildew despite these polymorphic differences ((Adam and Somerville, 1996); Yongqing Li, unpublished data).

Two available T-DNA insertional lines were available for the *PMR5* locus, SALK_034969 and SALK_131057. Both of these lines were determined to be misannotated in the TAIR database after sequencing the lines to determine the location of the T-DNA insertion (Fig. 2.5). SALK_034969 contains an insertion in the promoter region, about 250 bp upstream of the start codon. SALK_130157 has an insertion in the 3'UTR, and not in the last exon as annotated. Neither of these lines were resistant to *G. cichoracearum* like the original *pmr5* allele.

TILLING (Targeting Induced Local Lesions IN Genomes) lines were generated that contained mutations within *PMR5* along with other background mutations (McCallum et al., 2000). Several lines that have nonconservative polymorphisms were obtained (Table 2.4). These lines have been screened for powdery mildew disease resistance (Table 2.4) and some have been backcrossed to Col-0 to remove background mutations. The first backcross was left to self fertilize to provide a segregating population. The current status of all the TILLING lines can be found in Table 2.4. In the future, a fragment containing the mutation in *PMR5* can be amplified and sequenced. Alternatively, PCR markers can be designed to specifically genotype the new mutation. Once backcrossed, these TILLING lines will be useful second alleles for future studies of *PMR5*.

Virus induced gene silencing of PMR5 in Arabidopsis

To confirm that powdery mildew disease resistance and altered morphology is due to the loss of functional PMR5 protein, *PMR5* was transiently silenced in Arabidopsis using a tobacco-rattle virus (TRV)-induced gene silencing system (Burch-Smith et al., 2006). Silencing *PMR5* allows the monitoring of powdery mildew disease susceptibility in newly forming leaves that have not yet established an adapted cell wall. 610 bp and 721 bp of the N-terminal region of *PMR5*, including the 5'UTR, was chosen for cloning into the pTRV2 vector based on their unique sequences distinct from other TBL family members. A construct with GUS, a gene not endogenous in plants, was used as a negative control, and a construct with phytoene desaturase (PDS), important for leaf pigmentation, was used as a positive control.

Plants were inoculated with *G. cichoracearum* 13 days post Agrobacteria infiltration, as plants infiltrated with pTRV1 and pTRV2-PDS showed symptoms of silencing in new leaf tissue (leaves 5-8) at that time (Fig. 2.6a). Silenced plants were photographed 24 hpi, 5 dpi, 7 dpi, and 9 dpi, along with a corresponding duplicate set of silenced plants that were left uninfected. Although plants infiltrated with TRV were smaller than wild-type plants that were not infiltrated, TRV-induced gene silencing did not affect powdery mildew susceptibility, as all GUS-silenced plants showed signs of infection in at least one of the silenced leaves (Fig. 2.6a). New leaves from plants infiltrated with pTRV1 and pTRV2-PMR5 were smaller and leaf curling was seen. As the *PMR5*-silenced plants grew, the leaves became more similar to *pmr5* plants, showing flatter, rounder leaves, as well as extended petioles (Fig. 2.6a). By 9 dpi, *PMR5*-silenced leaves were clearly more resistant than the negative control (Fig 2.6b).

Leaf tissue from uninfected and infected plants corresponding to *PDS*-silenced leaves was collected at 24 hpi and 5 dpi for RNA extraction and qPCR analysis to confirm silencing of *PMR5*. *PMR5* silenced plants had a 1.3- to 4-fold decrease in *PMR5* expression compared to *GUS*-silenced plants (Fig. 2.6c). The decrease in *PMR5* expression of *PMR5*-silenced plants is comparable to that between *pmr5* and wild-type (Table 2.6). Increased resistance in *PMR5*-silenced leaves confirms the phenotype seen in the *pmr5* mutant plant, indicating that a mutation in *PMR5* is responsible for powdery mildew disease resistance.

Catalytic inactivation of TBL family conserved residues in PMR5

To determine whether PMR5 function was dependent on the putative catalytic residues described previously (Anantharaman and Aravind, 2010), site-directed mutagenesis was used to target S142, D379, and H382. The fully complementing construct, *pPMR5:PMR5-Myc-His*, was used as a template to create three separate mutations: S142A, D379A, and H382A (Fig. 2.5). Plants were genotyped for the presence of the transgene by amplifying from the C-terminal Myc-tag sequence and an internal *PMR5* specific primer. Whereas PMR5-Myc-His complements the *pmr5* mutant, none of the mutated catalytic constructs complemented (Fig. 2.7). This suggests that S142, D379, and H382 are all required for *pmr5*-mediated disease resistance. Unfortunately, because the PMR5-Myc-His protein in the wild-type control could not be detected by western blot, the presence of the mutated protein in the catalytic mutants could not be confirmed (see localization section). Thus, no definitive conclusions could be made about the lack of complementation in the lines containing mutated catalytic residues.

There are several potential reasons for why the protein cannot be detected *in planta*. First, the protein may be produced in low abundance, especially since *PMR5* expression is generally low (Fig. 2.4). Increasing the starting plant material for protein purification may address this issue. Second, it is possible that mutations at the conserved putative catalytic residues are causing protein instability and degradation. Alternatively, detection with the Myc and His tags

may be insufficient at detecting the presence of protein *in planta*. Thus, a new construct with a C-terminal strep tag has been cloned. The catalytic mutations were reconstructed with an introduced strep sequence. These constructs are currently available in a Gateway compatible entry vector (Table 2.1). They will need to be modified for in frame cloning into the destination vector of choice.

Cell wall characterization of the *pmr5* mutant

Cell wall fingerprints by FTIR and Raman spectroscopy

Pectin changes were found in *pmr5* by FTIR microscopy (Vogel et al., 2004). Using microscopy methods, the researchers could pinpoint specific regions on the leaf with altered cell wall fingerprints. To determine whether the results could be reproduced by analyzing whole tissues to better represent the variation within the leaf, an ATR (attenuated total reflectance) accessory with ground cell walls and larger sample size was used. Grinding the samples instead of analyzing intact leaf discs, as was done previously, allows for the analysis of the cell wall beyond the cuticle, and the ATR accessory allows for more scans to provide a more accurate reading. Cell walls isolated from *pmr5* from Col-0 were reliably separated based on principle component analysis; however, the pectin peaks generated by Vogel *et al.* could not be reproduced (Fig. 2.8). FTIR spectroscopy is highly influenced by the environment; analysis of similarly grown Col-0 plants on separate days clustered distinctly from one another (Yongqing Li, unpublished). In summary, the results from FTIR spectroscopy suggest that the cell wall profiles between *pmr5* and wild-type are different, however, this technique cannot be used to determine what cell wall components are contributing to this difference.

In collaboration with Martin Schmidt and Pradeep Perera from the Adams lab, the technique of Raman spectroscopy to analyze the cell wall was explored to complement FTIR spectroscopy methods. Raman spectroscopy has potential to provide support for the pectin changes found by FTIR, since clear peaks for pectin can be distinguished from other cell wall material (Gierlinger et al., 2008). Senescent Arabidopsis tissue has been successfully analyzed by Raman spectroscopy (Schmidt et al., 2010). However, since pectin composition changes upon senescence, senescent tissue could not be used to study the pectin changes in the *pmr5* mutant cell wall. Imaging live tissue by Raman spectroscopy has been a challenge due to the autofluorescent compounds found in green plant tissues. Thus, a sample preparation protocol for Raman imaging of green Arabidopsis tissue was developed.

An attempt to remove lipid compounds from the cell walls by treatment with ethanol, methanol:chloroform, and acetone was insufficient at removing autofluorescence. Next, a step ethanol gradient was tested, with increasing ethanol concentrations to 100% ethanol before decreasing concentrations back to water. The ethanol was sufficient to remove the autofluorescence so that there was a strong Raman signal of the cell wall. However, most of the sections were shredded during sectioning, suggesting that 25-50uM sections were too thin. 100uM sections may be the optimal section thickness for Raman imaging of ethanol treated PEG embedded Arabidopsis. This project was discontinued after determining that more optimization would be required.

Oligosaccharide mass profiling of xyloglucan

As PMR5 exists in the same protein family as AXY4, which is important for proper xyloglucan acetylation, it was possible that the proteins were modifying similar cell wall

substrates. Oligosaccharide mass profiling (OLIMP) was done to test whether PMR5 affected xyloglucan composition. Following previous methods, cell wall samples were digested by xyloglucan endoglucanase and then analyzed by MALDI-TOF mass spectrometry (Gunl et al., 2011). There were no differences in xyloglucan composition of *pmr5* cell walls compared to wild type (Fig. 2.9).

pmr5 cell walls have less acetylation

The acetylation of *pmr5* cell walls was tested based on the lack of acetylation in the *axy4* mutant. Destarched cell walls (alcohol insoluble residue, AIR) were saponified to cleave acetyl esters from cell wall polysaccharides and the solubilized acetic acid was measured (Manabe et al., 2011). Although there was some variability in the assay (see caption in Fig. 2.10), cell walls from 3-week-old *pmr5* plants consistently had less acetylation compared to wild-type cell walls (Fig. 2.10). To determine in which fraction the acetylation defect occurred, AIR was digested with a combination of endopolygalacturonase and a pectin methyl esterase to release pectin into the supernatant. The supernatant containing the solubilized pectin, as well as the residue, was tested for acetylation. Released acetic acid from total cell walls isolated from *pmr5* plants was about 77% that of wild-type. Whereas *pmr5* had 87% of wild-type acetic acid in the residue fraction, it only had 60% of acetic acid in the pectin supernatant fraction, suggesting that the decrease in total AIR was likely due to a decrease in pectin acetylation (Fig. 2.10). Non-destarched AIR was also tested in case the destarching process had pectin-extracting effects. *pmr5* samples from non-destarched AIR also had less acetylation than wild type (Fig. 2.10). There were no differences in acetylation when comparing AIR isolated from etiolated 4-day-old seedlings (Fig 2.10).

Cell wall acetylation may affect the digestability, or saccharification, of the cell wall, as fewer acetyl groups would mean a more open backbone for cell wall degrading enzymes. Cell walls from 6-week-old plants were treated with Accellerase, a commercial cocktail of enzymes, and released glucose was measured to determine the digestibility of the cell wall. *pmr5* cell walls are less digestable than wild-type (Fig. 2.11). Additionally, *rwa2*, a mutant with 70% of wild-type acetylation, showed no change in digestability (Fig. 2.11). Although it is possible that less acetylation would improve digestability of cell wall polymers, cell wall mutants likely have other secondary changes to reinforce the cell wall. The decrease in arabinan seen in our immunolabeling data may be causing the cell walls to be stiffer, as enzymatically removed arabinan increased calcium crosslinking in the cell walls (Caffall and Mohnen, 2009). Thus, the saccharification result corroborates existing data that there is a difference in cell wall composition in the *pmr5* mutant, but it cannot be used to directly infer the cell wall acetylation profile.

Antibody labeling reveals pectic RGI differences in the pmr5 cell wall

The plant cell wall community has a collection of cell wall antibodies to probe the cell wall (Knox, 1997). These antibodies were used to further characterize changes in the cell wall that might not be detectable by spectroscopic methods. Stem tissue was chosen for the ease of making sections and more consistent labeling. Immunolabeling studies were done in collaboration with Yves Verhertbruggen from Henrik Scheller's laboratory at the Joint BioEnergy Institute.

Compared to Col-0, transverse stem sections of *pmr5* showed an increase and a decrease of galactan and arabinan epitopes respectively (Fig. 2.12). Both galactan and arabinan are side

chains of pectic rhamnogalacturonan I (RGI), which along with its neutral side chains, is composed of alternating galacturonic acid and rhamnose residues (Fig. 2.2). LM5, which recognizes galactan, showed an increase of labeling at the epidermis and pith parenchyma (Fig. 2.12). LM6, which recognizes arabinan, showed a decrease of binding at the epidermis and the cortical parenchyma (Fig. 2.12). LM13, which recognizes longer chain arabinans, also lacked binding to the *pmr5* epidermis, whereas it bound to the wild-type epidermis (Fig. 2.12). There were no differences when using homogalacturonan antibodies, LM18, LM19, or LM20. In addition, *pmr5* stems also had a wavy and irregular epidermal phenotype not seen in wild-type stems, which correlated with the ratio of even and intact sections that could be produced (data not shown).

Cell wall extracts were also labeled with the LM5 and LM6 antibodies to determine if differences could be detected from whole tissues. Col-0 and *pmr5* cell walls were treated with CDTA to extract pectin, and sodium carbonate and potassium hydroxide to extract hemicellulose (Melton and Smith, 2001). After spotting the extracts on nitrocellulose, the extracts were probed with cell wall antibodies and the respective conjugated secondary antibodies. The results were variable within each line, possibly due to environmental variation (Fig. 2.13 – LM6 example). Although there were no significant differences in labeling of cell wall extractions from Col-0 and *pmr5*, this is expected considering the specificity of cell types showing differences in the stem sections.

To correlate the cell wall changes in the stems to leaf tissue, cell walls isolated from rosette leaf samples were prepared for glycome profiling in collaboration with Siva Kumar from Michael Hahn's lab at the Complex Carbohydrate Research Center (University of Georgia). The Hahn group has successfully used a large collection of cell wall antibodies to characterize several fractions of the cell wall after sequential treatment with solvents (Kong et al., 2011). Preliminary analysis of the differences in the 3-week-old rosette leaf glycome profiles between Col-0 and *pmr5* reveal changes in pectin epitopes, and not in xylan epitopes (Fig. 2.14). These differences are especially apparent in the oxalate fraction, which is enriched in pectins with high galacturonic acid content. Like the stem immunolabeling results, the greatest changes are seen with RGI antibody labeling of pectin. However, although the samples were treated equally and the profiles are comparable, the wild-type profile is atypical for rosette leaf tissue. This experiment is being redone by Siva Kumar.

RGI phenotypes in seed mucilage

The RGI side chain phenotypes were further investigated using seed mucilage in collaboration with Bradley Dotson from Chris Somerville's lab. Arabidopsis seeds produce seed mucilage enriched in RGI, making it a convenient purified source of RGI for further analyses. Arabidopsis seed mucilage exists in two layers ((Macquet et al., 2007); Fig. 2.15). The outer water-soluble layer is rich in unsubstituted RGI, and also contains epitopes detectable by homogalacturonan-specific antibodies (Willats et al., 2001). It was recently found that the RGI backbone in Arabidopsis is less regular in its rhamnose and galacturonic acid repeats, and that there may be longer stretches of galacturonic acid residues between rhamnose residues (Dick-Perez et al., 2011). This would be consistent with the homogalacturonan-specific antibody binding to this layer of mucilage. This outer water-soluble layer can be easily removed by agitation (Western et al., 2000). The inner adherent layer of seed mucilage contains RGI side chain epitopes detectable by confocal microscopy (Macquet et al., 2007). Both layers were analyzed to compare differences in RGI labeling between wild-type and *pmr5* seed mucilage.

Seed mucilage can be stained with ruthenium red and imaged. *pmr5* seed mucilage was more deeply stained with ruthenium red compared to wild-type Col-0 seed mucilage (Fig. 2.15). However, this did not correlate with the disease phenotype, since complementing lines, *pPMR5:PMR5-Myc-His* and *35S:PMR5-GFP,* both have similar levels of staining as *pmr5* (Fig. 2.15). In addition, *pmr5* seeds, along with the complemented transgenic lines in the *pmr5* background, all settled in the tube more compactly compared to Col-0, which may suggest less overall seed mucilage production of seeds in the *pmr5* background.

To analyze the inner layer, two approaches were taken. Imbibed seeds coated in seed mucilage were treated with CDTA to test the solvent's effectiveness at exposing the inner layer containing arabinan and galactan. CDTA did not remove the inner layer, but did change the binding properties of ruthenium red. Seed mucilage from wild-type, *pmr5*, and the complementing lines, *35S:PMR5-GFP* and *pPMR5:PMR5-Myc-His* showed much paler staining after CDTA treatment, but no differences among the lines (Fig. 2.15). The next approach was *in situ* labeling of the seed mucilage using LM5 and LM6 antibodies (Macquet et al., 2007). Fluorescent spots in the mucilage indicated the presence of galactan and arabinan epitopes in both wild type and *pmr5* (data not shown). The number and intensity of the spots varied within a genotype, and even within a seed. Thus, *in situ* labeling of seed mucilage could not be used to differentiate between the wild-type and mutant cell wall composition. In summary, the variation of mucilage phenotypes from seed to seed within each genotype has made it difficult to make any conclusions about any pectin differences that *pmr5* may have compared to wild-type.

Imaging RGI by metabolic labeling with fucose analog

Anderson *et al.* (2012) characterized a new method to image RGI in cell walls by metabolic labeling with an alkynylated fucose analog. Based on our immunolabeling results showing differences in RGI composition, we were interested in whether the fucose distribution was also altered. Charlie Anderson tested *pmr5* for changes in fucose accumulation, but did not see any difference in RGI labeling compared to wild type (data not shown).

Localization of PMR5

Bioinformatics analysis of PMR5 localization

Based on the cell wall differences we observed between wild-type and *pmr5*, it was hypothesized that PMR5 would either act in the cell wall, directly modifying cell wall components, or would localize in the Golgi apparatus, where the pectins are assembled for the secretory pathway. The protein contains an N-terminal hydrophobic region and no other predicted transmembrane domains. The PMR5 amino acid sequence was submitted into several localization prediction tools, including SignalP 3.0, Phobius, Target P, and PSORT (Table 2.5). According to these prediction tools, PMR5 is predicted to have a signal peptide and is part of the secretory pathway. This suggests that the signal peptide is cleaved during its translocalization through the secretory pathway. Alternatively, the putative signal peptide may not be removed and could act to anchor the protein inside a membrane, as suggested for the localization of AXY4 in the Golgi (Gille et al., 2011). The anchor hypothesis has also been used to hypothesize the localization of PMR5 in the endoplasmic reticulum (Vogel et al., 2004).

The signal peptide sequence (MGSLLPLLGISVVSAIFFLVLQQPEQSSS) was submitted to NCBI BLAST to identify proteins already characterized for their subcellular localization. There were no annotated proteins when the parameters were restricted to plants.

When the parameters were expanded to all organisms, restricting alignments to N-terminal regions, there was still no clear group of proteins indicating a specific localization (Table 2.8). Several membrane bound proteins were retrieved, but further analysis of these sequences showed that they contained large transmembrane domains later in the sequence. Thus, by *in silica* methods, it still could not be determined whether the signal peptide is cleaved to result in a soluble protein in the secretory pathway, or whether the hydrophobic N-terminus is used to anchor PMR5 in a membrane.

Complementation of transgenic lines for localization studies

Two new fluorescent fusion lines using the native promoter were constructed. In addition to microscopic methods to determine subcellular localization, high-speed centrifugation was used to fractionate the cellular components and determine the localization. The first construct was designed and synthesized containing the *PMR5* native promoter driving the expression of the *PMR5* coding sequence with a fluorescent tag as well as other tags for purification. Two fully complementing lines were generated expressing PMR5-mCherry for determining localization by microscopy and PMR5-Myc-His for *in planta* protein purification (Fig. 2.16). A third construct was generated with the native promoter fused to PMR5 with a C-terminal GFP to improve the fluorescent signal intensity. The native promoter GFP line complements the acetylation phenotype (Fig. 2.10). Three individual lines were obtained and were susceptible to the host powdery mildew (Fig. 2.16), as well as the related *Golovinomyces orontii* (Divya Chandran, unpublished); however, the disease symptoms caused by both fungal pathogens lagged behind wild-type symptoms by two days and had fewer conidiophores detectable by eye, indicating that these GFP constructs are only partially complementing the *pmr5* mutant. Moreover, although these transgenic lines are wild-type in size and height, they look more similar to the *pmr5* mutant with rounder and flatter leaves. qPCR analysis of *PMR5* gene expression indicates that transcript abundance in the native promoter GFP lines is at least at wild-type levels or higher (Table 2.9). This line was also crossed with the XT-mCherry Golgi marker for co-localization studies.

The *35S:PMR5-GFP* line fully complements the *pmr5* mutant; its morphology, size, and disease susceptibility is rescued to wild-type phenotypes (Fig. 2.16). Moreover, the FTIR spectrum of *pmr5* plants expressing *35S:PMR5-GFP* indicates that the cell wall composition is rescued to wild-type (Fig. 2.17; Gregory Mouille, unpublished). The overexpression line was crossed with a Golgi marker fused with a red fluorescent protein (XT-mCherry). The dually fluorescent line had slower growth similar to the 35S:XT-mCherry marker line, but powdery mildew susceptibility was not affected (Fig. 2.16).

PMR5-GFP localizes to the endoplasmic reticulum

PMR5-GFP localizes to web-like structures characteristic of the endoplasmic reticulum (ER) in partially complemented *pmr5* plants expressing *pPMR5:PMR5-GFP* (Fig. 2.18) PMR5-GFP was seen best in young (4-5 day old) seedling roots, especially in cortical cells just below the epidermal cell layer in the elongation zone (Fig. 2.19). This correlates with the increase in *PMR5* gene expression in the quiescent center cells at the meristem based on the eFP browser (Fig. 2.4). Fluorescence in the elongation zone also correlates with the increase in PMR5 gene expression in rapidly expanding tissue seen by qPCR analysis of etiolated seedlings (Table 2.6). Despite the 170-fold increase in gene expression in etiolated seedlings, PMR5-GFP could not be detected in hypocotyls of dark grown seedlings. Moreover, PMR5-GFP could not be detected in mature leaf tissue. However, a western blot of protein extracted from 3-week-old rosette leaves

showed that PMR5-GFP protein is present and detectable by anti-GFP antibody (Fig. 2.20). Although cytosolic localization could not be seen with the native promoter lines by microscopic methods, PMR5-GFP was detected in both the soluble and microsomal fractions by western blot (Fig. 2.21).

Bright speckles were seen in the native promoter GFP line, but could not be identified. These speckles did not co-localize with the Golgi marker (Fig. 2.18). Moreover, PMR5 was not found in Golgi enrichments by density centrifugation and surface charge separation (Parsons et al., 2012). The speckles were slightly larger in size and were not mobile. 4-day-old seedlings were treated with brefeldin A (BFA) to determine whether the bodies were dependent on proper trafficking to the Golgi. BFA affects proteins in the secretory pathway by inhibiting transport from the ER to the Golgi (Ritzenthaler et al., 2002). Although the XT-mCherry Golgi marker aggregated into BFA bodies, this was not seen with PMR5-GFP (Fig. 2.22). This suggests that PMR5-GFP does not localize to the Golgi, and that the speckled bodies are not endosomal in nature. It is possible that the speckles are due to background autofluorescence, as occasionally bright speckles could be seen in untransformed Col-0 and *pmr5* plants.

As PMR5 is hypothesized to be modifying pectin and pectin modifying proteins are thought to be localized in the Golgi (Caffall and Mohnen, 2009), ER localization of PMR5 was unexpected. Because the native promoter lines are only partially complementing the *pmr5* mutant, it cannot be concluded whether the fusion protein is properly localized. Although the native promoter lines were only partially complementing the mutant, overexpression of PMR5-GFP fully complements the *pmr5* mutant (Fig. 2.16). Plants expressing *35S:PMR5-GFP* had strong detectable fluorescence signal at several stages of development, including seedling roots, hypocotyls of dark grown seedlings, and in the leaf epidermis. In all cases with the overexpression line, PMR5-GFP confirmed the ER localization seen in the native promoter lines (Fig. 2.23). ER localization was also seen previously with a 35S:PMR5-YFP line (Miguel Carvalho, unpublished). Additionally, cytosolic streaming was seen in the 488nm wavelength to visualize GFP. Occasionally, bright round spots were seen, and were later identified to be Golgi based on co-localization with the XT-mCherry Golgi marker (Fig. 2.24).

Western blot analysis using an anti-GFP antibody supported the localization based on microscopy. Protein was isolated and fractionated by high-speed centrifugation to separate the soluble and microsomal fractions. Bands corresponding to the size of PMR5-GFP were found in both soluble and microsomal fractions (Fig. 2.25). A second smaller band was also seen, as well as a band running the size of free GFP (Fig. 2.25). Boiling the samples prior to running SDS-PAGE affected the presence of the free GFP band, which has been seen previously (Jose Estevez, personal communication). When fractions were heated at various temperatures prior to loading SDS-PAGE gels, the amount of free GFP seen on the western blot positively correlated with temperature (Fig. 2.25). However, despite the presence of free GFP, the presence of the 70kDa band representing PMR5-GFP in the soluble fraction still supports the cytosolic localization determined by microscopic methods (Fig. 2.25).

PMR5-GFP localizes to penetration sites after powdery mildew infection

Other proteins that are involved in powdery mildew disease resistance have shown localization at penetration sites upon infection (PEN1: (Bhat et al., 2005); PEN2: (Lipka et al., 2005); PEN3: (Stein et al., 2006)). The localization of PMR5 at fungal penetration sites would provide a direct link between its role in cell wall modification to its role in powdery mildew disease resistance. PMR5-GFP can be seen focally localized at penetration sites 24 hours post

inoculation with *G. cichoracearum* (Fig. 2.26). Based on previously imaged marker proteins surrounding papillae and haustorial bodies (Koh et al., 2005), the penetration site localization of PMR5-GFP is not ER-like, suggesting that the localization of PMR5 in papillae-like structures is not passive localization with the ER.

PMR5-GFP may be re-localizing to the papillae from the ER, but this has yet to be confirmed. As only one 24 hpi time point was taken, it cannot be concluded whether the protein is re-localizing to the penetration site from the ER or the cytosol, or whether there is new synthesis and deposition. A time course is needed to monitor PMR5 protein movement from the ER to the penetration site in order to confirm re-localization. Co-localization with PEN1 or PEN3 and stable presence in papillae after plasmolysis would confirm that PMR5-GFP is localized at the papillae. As the syntaxin PEN1 is involved in deposition of callose and other cell wall material (Collins et al., 2003), it would be interesting to determine whether PEN1 is necessary for PMR5 localization. There is some evidence that the PMR5 localization at the penetration site is not PEN1-dependent based on the absence of PMR5 in the SYP61 (SYNTAXIN OF PLANTS 61) endosomal proteome, where PEN1 is present (Drakakaki et al., 2012), and based on the finding that PEN1 localization is BFA-dependent (Nielsen et al, 2012), and PMR5 localization is BFA-independent. More work will need to be done to characterize the localization of PMR5 at these sites of penetration.

Troubleshooting detection of pPMR5:PMR5-mCherry and pPMR5:PMR5-Myc-His

The *pPMR5:PMR5-mCherry* construct was created to determine the localization of PMR5 expressed under its native promoter. This line was specifically fused to mCherry so that it could later be crossed to other cytological markers that were GFP fusions. Despite full complementation of the *pmr5* mutant with this mCherry-fusion protein, the protein could not be detected by confocal microscopy despite multiple attempts to improve protein abundance.

According to the eFP browser's expression data, PMR5 is more highly expressed in the cortical cells in the meristematic region of the root, and may be induced by cold treatment (Fig. 2.4). 3-, 4-, 5-, and 6-day-old light-grown seedlings were examined at the cotyledons, leaves, meristems, and roots, but no temporally upregulated regions showing fluorescence were detected. The mCherry line was also exposed to cold treatment at 4ºC for 24 hours to determine if induction of the transcript level would improve abundance and detection of the fusion protein. This was also unsuccessful, as the fluorescent protein could still not be detected. Lastly, since *PMR5* gene expression is induced 20 fold in wild-type five days after infection (Table 2.6), plants were examined after infection, but again could not be detected above background.

One potential reason for the lack of fluorescence is improper folding of the fluorophore. Although PMR5 may be folded correctly, evident by complementation of the mutant phenotype, the mCherry fusion may not be. This could be due to a short linker region, which was composed of a four amino acid linker (TSPR) included primarily for the nucleotide restriction sites. Therefore, the *pPMR5:PMR5-mCherry* line cannot be used for localization. Homozygous seeds have been collected in case this line could be used for other purposes.

A separate line, *pPMR5:PMR5-Myc-His*, was generated from the mCherry construct after splicing out the mCherry gene, and was made for fractionation purposes. Like the mCherry line, the Myc-His line fully complemented the *pmr5* mutant. However, the expected sized band representing the Myc-His tagged protein could not be detected by western blot after high-speed centrifugation to fractionate the cellular components. Enrichment of the protein after purification with nickel resin was also unsuccessful at improving detection by western blot (Fig. 2.27).

Binding studies of MBP-PMR5-His

Protein expression and purification

Since *E. coli* was used in the past for expression of PMR5 unsuccessfully, the *Pichia pastoris* expression system was chosen because of its ability to process higher eukaryotic proteins with machinery for better protein processing, folding, and posttranslational modification (Invitrogen). Moreover, Pichia was successfully used previously in the lab (Christian Voigt, personal communication; (Bauer et al., 2006)). One caveat of Pichia expression is the possibility of over-glycosylation. The PMR5 protein sequence was submitted into bioinformatics tools, which predicted one potential N-glycosylation site (NetNGlyc, NetOGlyc). Thus, with only one potential site, PMR5 was a good candidate for protein expression in Pichia.

PMR5 was cloned with and without the signal peptide into vectors suitable for Pichia expression. Two vectors contain an alpha secretion signal for secretion of the protein into the supernatant, while the other two do not contain alpha secretion signals and express the proteins intracellularly. The pPICZ series contains a methanol inducible promoter, while the pGAPZ series is a constitutively active promoter. After confirming several clones by sequencing and growth on selection plates, multiple pilot expression experiments were tested, but all were unsuccessful. Several time points (24h, 48h, 72h, 96h) from both the supernatant and the pellet were tested, but the protein could not be seen by western blot, indicating low to no expression of PMR5 in Pichia.

In collaboration with Philipp Benz from Chris Somerville's group, PMR5 was expressed in *Neurospora crassa*, a rising model organism. *PMR5* was cloned without its putative signal peptide into a Neurospora expression vector. The final construct was dually tagged and expressed under a highly expressing CBH1 promoter. Neurospora cells transformed with *PMR5* grew poorly, similar to another TBL member that was also included in the pilot expression study (Philipp Benz, personal communication). This suggests that these plant TBL proteins may be toxic in Neurospora.

Other *E. coli* expression vectors were investigated, ultimately leading to the discovery of the pMAL system (NEB). With the pMAL system, very high levels of protein expression were achieved, possibly due to the N-terminal maltose binding protein (MBP) fusion that may have helped solubilize and stabilize PMR5. The coding sequence of *PMR5* was cloned without the signal peptide (amino acids 1-29) and with a hexahistidine C-terminal tag into the pMALc vector, which contains an IPTG inducible promoter and expresses proteins in the cytoplasm. This construct was also cloned into the pMALp vector, which results in periplasmic expression. A truncated version of PMR5, starting with the first conserved cysteine (C66) was also cloned. The two plasmids were transformed separately into Origami B(DE3) cells and NEB Express (BL21 derivative) cells, and both types of cells showed equally good induction of MBP-PMR5-His at the expected size after staining an SDS-PAGE gel (Fig. 2.28). Protein was thereafter purified from Origami cells expressing the full length PMR5 sequence without the signal peptide sequence cloned in the pMALc plasmid, a combination which gave higher yields of protein compared to periplasmic expression and a higher chance of proper disulfide bond formation.

MBP-PMR5 protein was isolated by a dual purification scheme. Crude lysate was first purified using the His-tagged end with nickel NTA resin (Qiagen), and then the elutions containing nickel purified proteins were purified over an amylose column (NEB), as done successfully in other labs (James Berger, personal communication). Purifying with two columns

and with N- and C-terminal tags allows for the purification of the full-length protein. B-PER, a detergent-based lysis buffer was first used to lyse the cells, but resulted in many degradation products (Fig. 2.29). The degradation products were likely due to the detergents found in B-PER. Detergents were omitted and cells were manually lysed using a homogenizer with a subsequent centrifugation to obtain a crude lysate for nickel and amylose purifications. This proved to be an optimized protocol for purification of MBP-PMR5-His. The elutions after two columns contained a ~80 kDa band after staining an SDS-PAGE gel and that was detectable with an anti-MBP antibody (Fig. 2.30). This band was confirmed to be MBP-PMR5-His by mass spectrometry sequencing.

Binding to Arabidopsis extractions

Based on the altered cell wall profile in the *pmr5* mutant, it is possible that PMR5 protein would differentially bind to cell wall extractions from *pmr5* compared to wild-type. Alkali solvents were used to extract three fractions sequentially: a high galacturonic acid pectin enriched fraction extracted with CDTA, and then two hemicellulose and neutral sugars rich fractions extracted with sodium carbonate and potassium hydroxide, respectively (Melton and Smith, 2001). Whole rosette leaves were used when preparing the samples to eliminate any variation within the proximal-distal areas of the leaf. Secondary cell wall contamination from the vasculature within each leaf would be eliminated based on the chemical extraction performed. Two sample preparations were tested. The first was simply frozen with liquid nitrogen, ground, and then treated with the solvents. The second was pretreated with a series of ethanol and chloroform:methanol (1:1 v:v) washes to constitute the alcohol insoluble residue (AIR) before the addition of extraction solvents.

MBP-PMR5-His binds Arabidopsis pectin fractions (Figs. 2.32, 2.33). In the untreated samples, MBP-PMR5-His bound all of the fractions, with strongest binding in the potassium hydroxide fraction. In the AIR samples, MBP-PMR5-His bound most strongly to the sodium carbonate fraction, then the CDTA fractions. Strong binding to the potassium hydroxide fraction from the untreated samples is probably due to contaminants in the cells, and not a reflection of cell wall material. Thus, for the purposes of comparing binding to cell wall components, the AIR samples are likely to provide more accurate binding data. Regardless of treatment, there was large variation in the binding of each fraction, and there was no significant difference in binding of MBP-PMR5-His to extractions from *pmr5* versus wild-type (Fig. 2.31). Binding to the pectin fractions isolated enzymatically that contained differences in acetylation was also tested. If *pmr5* is lacking in pectin acetylation, perhaps the PMR5 protein would bind more strongly to less acetylated substrates. However, this was not the case, and although MBP-PMR5-His bound to the pectin fractions, there was no difference in binding between mutant and wild-type (Fig. 2.32).

Since there were differences in galactose and arabinose epitopes in the immunolabeling data, binding of pectic RGI was specifically investigated. MBP-PMR5-His does not bind seed mucilage, enriched in unsubstituted RGI, from either *pmr5* or wild-type seed (data not shown). MBP-PMR5 also does not bind fractionated Arabidopsis RGI from leaves (Fig. 2.33). These results indicate that MBP-PMR5 binds to a non-RGI pectic polymer.

Binding commercial nonacetylated polysaccharides

Several commercially available polysaccharides were tested for binding by MBP-PMR5-His. These cell wall components have been fractionated and purified from plant sources that are enriched in these polysaccharides. A dilution series of the polysaccharides were spotted on

nitrocellulose, incubated with MBP-PMR5-His, and then subsequently probed with the appropriate antibodies for visualization using chemilluminescence. MBP alone was used as a negative binding control. LM5, LM6, and LM13 were used to detect the application of polysaccharides on nitrocellulose to ensure that any lack of binding by MBP-PMR5-His was not due to the lack of substrate on the membrane. MBP-PMR5-His binds strongly to pectin and polygalacturonic acid (PGA) from citrus peel, as well as various methyl esterified forms of pectin (Table 2.10). It binds weakly to potato RGI and larch arabinogalactan, but not to soybean RG, sugar beet arabinan, lupin galactan, wheat arabinoxylan, or tamarind xyloglucan. Probing with LM5, LM6, and LM13 antibodies shows that although MBP-PMR5-His does not bind the latter polysaccharides, epitopes recognizable by these antibodies showed the presence of the polysaccharide on the nitrocellulose membrane (Table 2.10).

Interestingly, MBP-PMR5 bound somewhat to potato RGI, but not soybean RG. A comparison of monosaccharide analyses (Megazyme) did not show any monosaccharide enriched in one type from the other. Polysaccharide structure was also compared to determine if the differential binding was due to structure, but both are branched with arabinan, galactan, and arabinogalactan (soybean: (Nakamura et al., 2001); potato: (Obro et al., 2004)). One possible reason for the differential binding may be in the accessibility of the epitopes. It was found that soybean RG elutes with much larger fragments, similar to Arabidopsis RGI, than potato RGI, which elutes with smaller fragments of oligogalacturonic acid (Amancio Souza, personal communication).

As PGA is a less heterogeneous mixture than pectin, subsequent studies focused on using PGA with the hypothesis that PMR5 may be binding homogalacturonan. Monosaccharide composition of PGA (Megazyme) showed some contamination with galactose and arabinose. To rule out RG side chains as the binding epitope for PMR5, PGA was digested with commercial galactanases and arabinanases to remove these RGI side chains prior to binding with MBP-PMR5. Galactanase treated PGA removed most of the galactan epitopes in PGA detectable by LM5. Despite the removal of galactan chains from PGA, MBP-PMR5 still bound strongly to the digested polysaccharide, indicating that galactose moieties are not necessary for PMR5 binding to PGA (Fig. 2.34). PGA was also treated with two arabinanases from *A. niger* and *C. japonicus* (Megazyme), but the digest was incomplete and arabinan epitopes still remained as detected by LM6. Thus, residual arabinose in the PGA could not be tested for importance in MBP-PMR5 binding to the commercial PGA source.

To determine the importance of the length of the polysaccharide, or degree of polymerization (dp), for binding, we obtained oligogalacturonides (OGAs), which are short fragments (dp 10-25) of homogalacturonan from digested PGA (gift from Clarice Souza). MBP-PMR5 binds just as well to OGAs, indicating that MBP-PMR5 can bind short stretches of homogalacturonan (Fig. 2.35). Shorter fragments could not be tested due to the limitations of the method, as smaller fragments do not bind well to nitrocellulose. Other methods would need to be employed to test whether MBP-PMR5 can bind galacturonic acid chains with a dp less than 10.

PMR5 binding to PGA is dependent on acetylation

To determine whether the acetylation profile of the polysaccharide was important for MBP-PMR5 binding, the acetylation of the panel of polysaccharides was determined. All but one of the polysaccharides was devoid of acetylation (Table 2.10). PGA had some detectable released acetate as measured by the acetic acid assay kit (Megazyme), results that are corroborated with NMR analysis of the PGA stock (Hagit Sorek, personal communication). This

indicates that MBP-PMR5 can bind non-acetylated polysaccharides, but since it is unclear the degree of which PGA is acetylated PGA, no conclusions could be made about the ability of MBP-PMR5 to bind to acetylated pectin.

To address this, acetylated PGA (Ac-PGA) was chemically synthesized in collaboration with Shu-Lun Tang from Chris Somerville's group. As *pmr5* cell walls are less acetylated, the hypothesis would be that PMR5 is acting as an acetyltransferase, transferring acetyl groups to an unacetylated polymer. Thus, if a polymer is already acetylated, PMR5 would bind more weakly to the polymer, which in this case would be Ac-PGA. Based on NMR, the acetylated PGA product had an additional acetyl group on every fourth galacturonic acid (Fig. 2.36a). This change was enough to alter the properties of the product. Ac-PGA was less water-soluble and yellower in color. Prolonged heating of a low concentration of Ac-PGA was sufficient to solubilize it, and the solubilized Ac-PGA could be bound and detected successfully on nitrocellulose. Interestingly, JIM5, which recognizes lowly methylated homogalacturonan, bound much more strongly to Ac-PGA than to PGA (Fig. 2.36b). The different physical properties, as well as the difference in antibody binding, indicate that Ac-PGA is indeed a different polymer than PGA.

MBP-PMR5-His binds more weakly to Ac-PGA than to PGA (Fig. 2.36c). De-esterification treatment of Ac-PGA with sodium hydroxide was sufficient at restoring LM5 and LM6 detection of galactan and arabinan contamination in the initial PGA starting material, but did not completely rescue MBP-PMR5-His binding (Fig. 2.36c). The lack of MBP-PMR5-His binding to the sodium hydroxide-treated Ac-PGA may be due to the altered nature of the pectic substrate in an alkali environment, in which the galacturonic acid becomes galacturonate (Shu-lun Tang, personal communication). The next step would be to neutralize the reaction with an acid to re-acidify the substrate to galacturonic acid; this could potentially improve MBP-PMR5-His binding after the acetyl groups are cleaved. Decreased binding to Ac-PGA compared to PGA indicates that PMR5 binding is dependent on the acetylation profile of the sugar substrate.

Preliminary acetyltransferase activity assays

We attempted to detect *in vitro* acetyltransferase activity using MBP-PMR5-His in a reaction with acetyl-coA and our putative sugar substrate, PGA. Acetyl-coA has been shown previously to be a suitable acetyl group donor for polysaccharide acetylation (Pauly and Scheller, 2000). A collaboration with Hagit Sorek from Dave Wemmer's group was formed to determine whether an incubation with these three components would be sufficient at producing acetylated PGA detectable by NMR. No clear peaks indicating newly acetylated PGA were identified (data not shown). An additional experiment was performed by Dawn Chiniquy, using ^{14}C-labeled acetyl-coA, to see if radioactivity could be found in precipitated polysaccharides after incubation with MBP-PMR5-His and PGA. The first trial was unsuccessful; no radioactivity could be detected in the precipitated polysaccharide product (data not shown).

Discussion

We now have more evidence supporting our hypothesis that PMR5 is a cell wall modifying protein. The decrease in acetylation in *pmr5* cell walls suggests that PMR5 has a role in cell wall acetylation. As AXY4 may also act as an acetyltransferase, the acetyltransferase function may be shared among the TBL family. One explanation for the large number of TBL proteins may be the necessity for acetylation of several different polysaccharide substrates. We

have shown by OLIMP analysis as well as binding studies to xyloglucan that PMR5 does not act on hemicellulose substrates like AXY4. Immunolabeling of stems and glycome profiling of leaves from the *pmr5* mutant have revealed differences in pectin composition. Along with the pectin binding data with MBP-PMR5-His and acetylation differences in pectin fractions, our data strongly suggest that PMR5 may be acetylating pectin.

Our initial immunolabeling data pointed us towards rhamnogalacturonan I, but we did not see PMR5 binding to Arabidopsis RGI sources. We saw binding to the sodium carbonate fraction isolated from AIR, which contains hemicellulose, along with some residual pectin from the CDTA fraction and pectin side chains with neutral charges like galactose and arabinose from RGI. Taking into consideration strong binding with pectin, PGA, and OGA, and that MBP-PMR5 does not bind Arabidopsis RGI isolated from leaves or from seed mucilage, it is likely that PMR5 is binding to PGA and not RGI in the sodium carbonate fraction. Although there was some contamination with other sugars in the commercial PGA, we know that PMR5 binding is not dependent on the galactose as digesting the galactose did not affect binding. Although we could not conclude whether arabinose is needed for PMR5 binding, the lack of binding to purified arabinan, arabinogalactan, and arabinogalactan proteins suggests that arabinan is probably not the substrate.

The cell wall analyses that suggest RGI as the substrate and the binding experiments that suggest homogalacturonan as the substrate may seem conflicting; however, this discrepancy can be explained by the occurrence of secondary changes in the cell wall to compensate for the lack of acetylation. Acetylation may be especially important early in cell wall development, as *PMR5* gene expression is induced in seedlings during rapid cell elongation. Early acetylation defects could affect the biosynthesis and final composition of the pectins in the cell wall. The lack of differentially expressed genes between wild-type and *pmr5* 3-week-old plants support this hypothesis. Despite the clear morphological differences in the mutant, it seems that the plants had adapted to the mutation, adjusted its cell walls, and returned to transcriptional homeostasis. Thus, we hypothesize that PMR5 is a homogalacturonan acetyltransferase, and that the RGI changes we see are compensatory effects.

PMR5 is unique in the TBL family of putative acetyltransferases because it is the only one that confers resistance to *G. cichoracearum* when mutated. If each TBL protein is specific to a polysaccharide in the cell wall, then the homogalacturonan that PMR5 is acetylating must be important in its role in powdery mildew disease resistance, in addition to normal cell growth and expansion. The differently acetylated homogalacturonan in the *pmr5* mutant could act as the novel fragment taking part of the CWI-signaling pathway, which alters cell wall composition and inhibits disease. Thus, we focused our efforts in determining the exact substrate and product of PMR5's putative acetyltransferase activity.

We know that PMR5 binding to PGA is dependent on its acetylation profile. When chemically acetylated, PMR5 binds the Ac-PGA more weakly. As a putative acetyltransferase, PMR5 should be able to bind non-acetylated galacturonic acid (putative substrate) just as well as mono-acetylated galacturonic acid (putative product); however, as galacturonic acid exists as a chain, neighboring acetylated residues are likely affecting PMR5 binding, resulting in the decrease in binding affinity to Ac-PGA. To further test the model that the acetylation profile of the galacturonic acid chain determines PMR5 binding affinity, we attempted to remove the acetyl groups by de-esterification treatment with sodium hydroxide. This treatment should remove neighboring acetyl groups and restore PMR5 binding to the de-esterified sugar. However, this was not the case; PMR5 binding to sodium hydroxide-treated Ac-PGA was not rescued to levels

comparable to PGA. This was unexpected, but could be explained by the de-esterification treatment and resulting product. Since the sodium hydroxide-treated Ac-PGA was not neutralized with an acid, the pectic backbone was likely altered into galacturonate. Thus, it is still possible that PMR5 binding is dependent on the acetylation profile of PGA.

We tested PGA as a candidate substrate for the putative acetyltransferase activity of PMR5. However, simply incubating the putative acetyl donor, acetyl-coA, along with PMR5 and PGA did not produce acetylated PGA. Although optimization of the reaction conditions are still needed, it is likely that other proteins are needed to complete the acetyltransferase reaction. Specifically, if mirroring the putative xyloglucan acetyltransferase, AXY4, an acetyl group transporter like RWA2 may be required for proper acetylation of cell wall polysaccharides (Gille et al., 2011). Thus a system that includes other cell wall proteins could prove to be more effective at detecting acetyltransferase activity if PMR5 is indeed an acetyltransferase.

PMR5 also binds OGAs, and OGAs have been well described in CWI-signaling or cell wall damage literature. Signaling downstream of OGA detection is usually characterized by calcium influx, ROS production, and activation of ET and JA pathways (Aziz et al., 2004; Moscatiello et al., 2006). As *pmr5*-mediated disease resistance is independent of JA and ET pathways, it is unlikely that PMR5 is acting though OGA signaling. Preliminary assays testing ROS by hydrogen peroxide detection in *pmr5* plants with diaminobenzidine tetrahydrochloride did not provide any leads. Thus, *pmr5*-mediated disease resistance is distinct from the pathway downstream of OGA detection.

Subcellular localization of PMR5 is still inconclusive. ER localization of PMR5-GFP was seen in both the partially complementing native promoter lines, as well as the fully complementing overexpression line. This is unexpected, as canonically it is has been thought that Golgi is the site where pectin is synthesized (Caffall and Mohnen, 2009). When overexpressed, we did see Golgi localization of PMR5-GFP. It may be possible that the GFP protein is interfering with Golgi localization in the native promoter construct, and that sufficient protein is entering the Golgi in the overexpression construct to fully complement the mutant. To determine whether some of the protein is localized in the Golgi, just undetectable by microscopic methods, we treated seedlings expressing *pPMR5:PMR5-GFP* with brefeldin A to inhibit proper protein transport to the Golgi. As no BFA bodies labeled with PMR5-GFP aggregated, we assume that PMR5 is not transported to the Golgi, and that ER localization is a real phenomenon. To corroborate the ER localization, a PMR5 fusion with an ER retention signal could be constructed to determine whether retention of PMR5 in the ER would complement the *pmr5* mutant. If PMR5 is indeed acetylating pectin in the ER, it would be a novel finding in our knowledge of how and where pectins are synthesized and modified.

Cytosolic PMR5-GFP was also detected by fractionation and western blotting methods, suggesting that PMR5 may additionally exist as a soluble protein. N-terminal sequencing of PMR5 protein isolated from plants could confirm whether the putative PMR5 signal peptide is cleaved. Cytosolic protein could explain how PMR5 can also localize to sites of fungal penetration. Alternatively PMR5 may also be passively re-localized with ER to the penetration site, as has been shown previously (Koh et al., 2005). These preliminary observations of PMR5 localization at penetration sites open the possibility of the protein working directly in disease resistance at the site of penetration. However, based on our cell wall analyses and binding assays, our hypothesis still remains that a pectin-derived fragment generated in the *pmr5* mutant is involved in a CWI-signaling pathway, causing changes to the cell wall and altering powdery mildew susceptibility as secondary effects.

Figures



Figure 2.1. Modified tree of 46 TBL family of proteins from (Bischoff et al., 2010). Blue dots indicate mutants that are susceptible to *G. cichoracearum*. Red dots indicate mutants that are resistant to *G. cichoracearum*

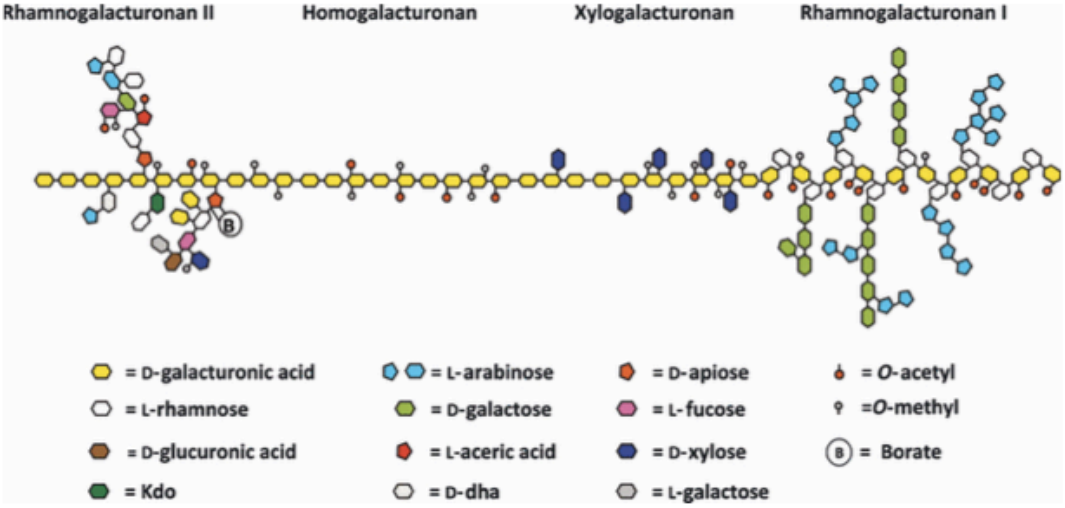

Figure 2.2. Schematic of an idealized pectin structure from (Liepman et al., 2005).

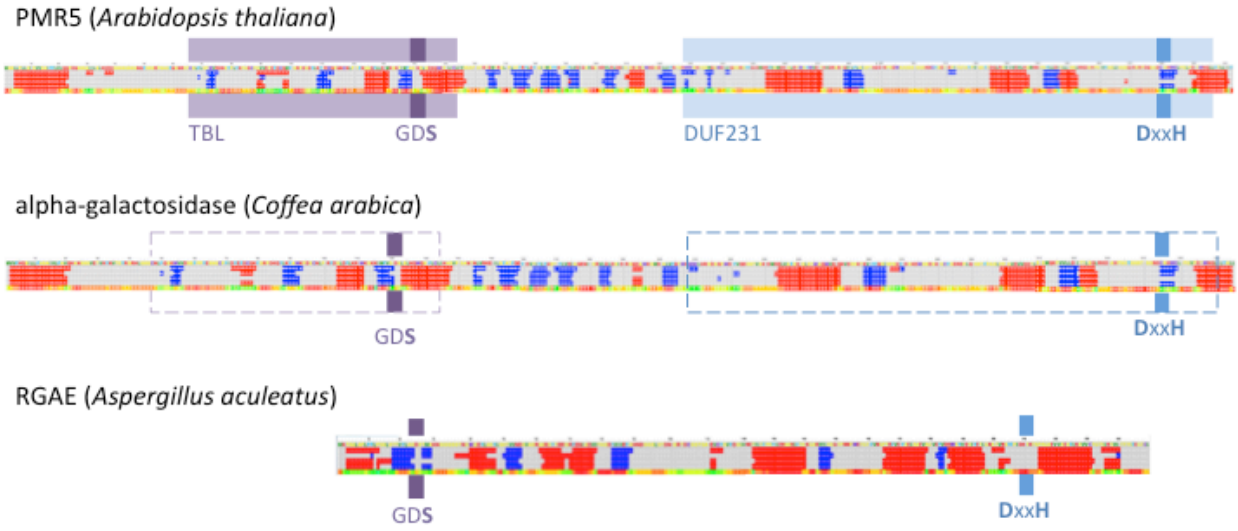

Figure 2.3. Secondary structure alignments of PMR5 from Arabidopsis (Uniprot ID: Q9LUZ6), putative alpha-galactosidase from *Coffea arabica* (Uniprot ID: Q42656), and rhamnogalacturonan acetylesterase (RGAE) from *Aspergillus aculeatus* (Uniprot ID: Q00017). Images stitched together from Phyre (Kelley and Sternberg, 2009). Within alignment, red indicates predicted alpha helices, and bright blue indicates predicted beta sheets. Purple (TBL domain) and light blue (DUF231, pfam03005) background bars indicate TBL family conserved regions. Dark purple (S from GDS) and dark blue (DxxH in DUF231 domain) bars indicate putative catalytic residues. Dashed boxes indicate shared TBL domains.

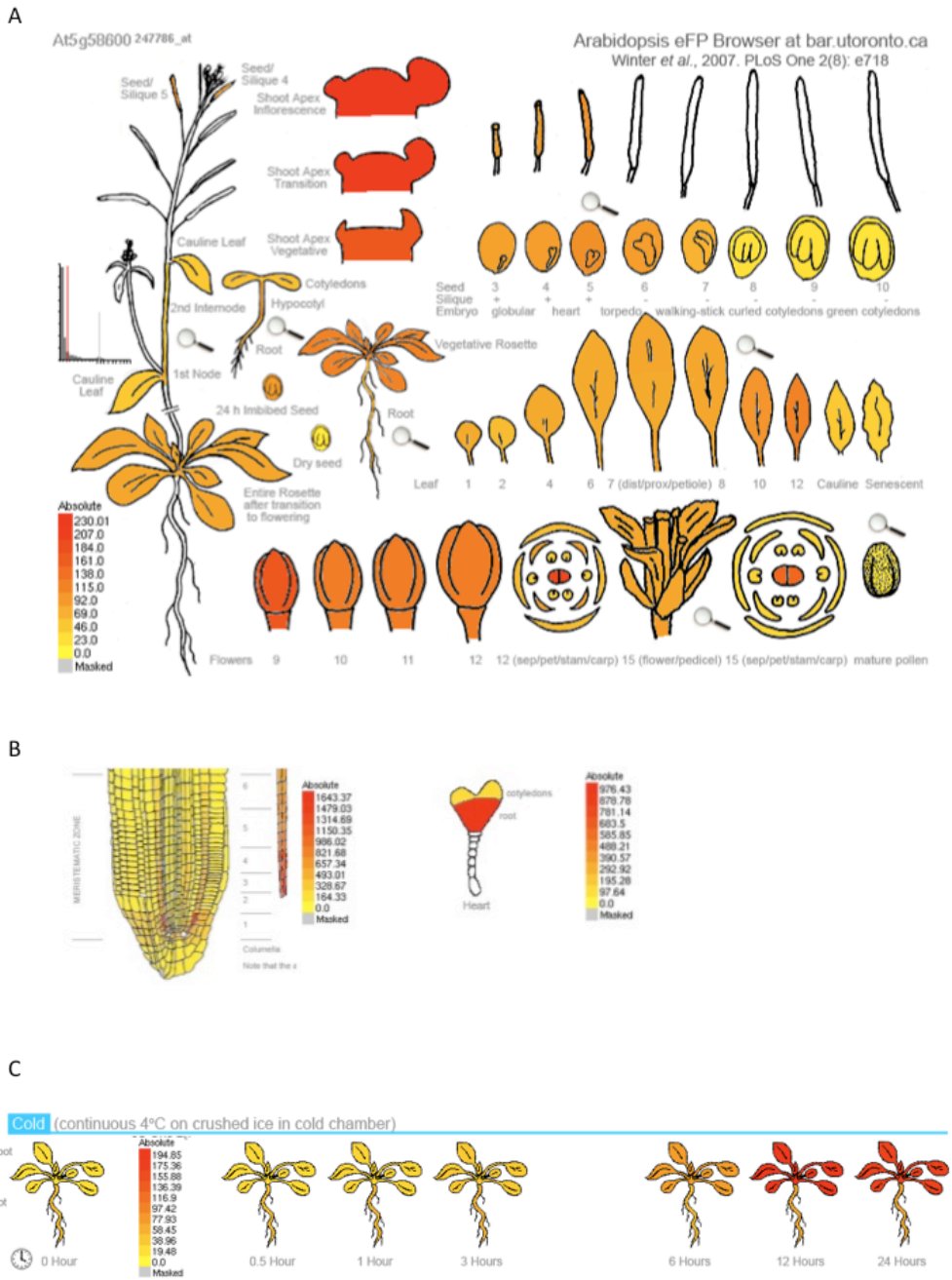

Figure 2.4. *PMR5* gene expression generated by the eFP browser (Winter et al., 2007)
(a) PMR5 gene expression across developmental stages (Schmid et al., 2005)
(b) Increased PMR5 expression in cortical cells of root meristems (left, (Brady et al., 2007)) and root cell of the heart stage embyro (right, (Casson et al., 2005))
(c) Increased PMR5 expression after cold treatment (Kilian et al., 2007)

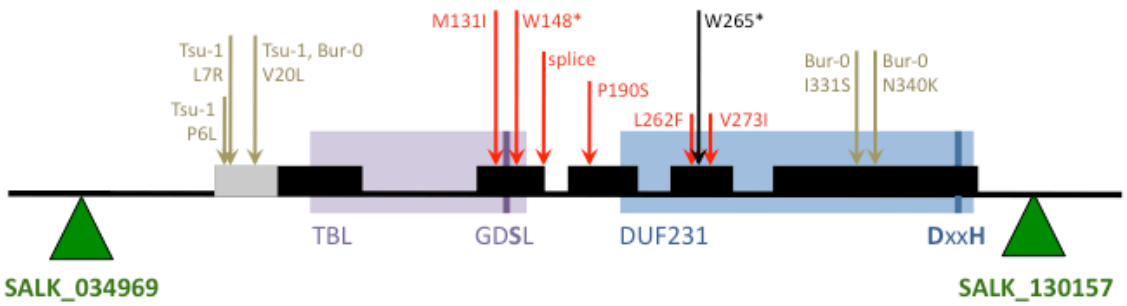

Figure 2.5. Gene schematic of *PMR5* indicating positions of alleles available for genetic studies. Gray bar indicates hydrophobic region, predicted to be a 29 aa signal peptide. Black arrow indicates *pmr5* mutation causing W265*. Purple (TBL domain) and light blue (DUF231, pfam03005) background bars indicate TBL family conserved regions. Dark purple (S from GDS) and dark blue (DxxH in DUF231 domain) bars indicate putative catalytic residues. Green triangles indicate positions of T-DNA insertions confirmed by sequencing. Red arrows indicate TILLING sites with amino acid changes annotated above. Brown arrows indicate polymorphisms in other Arabidopsis accessions.

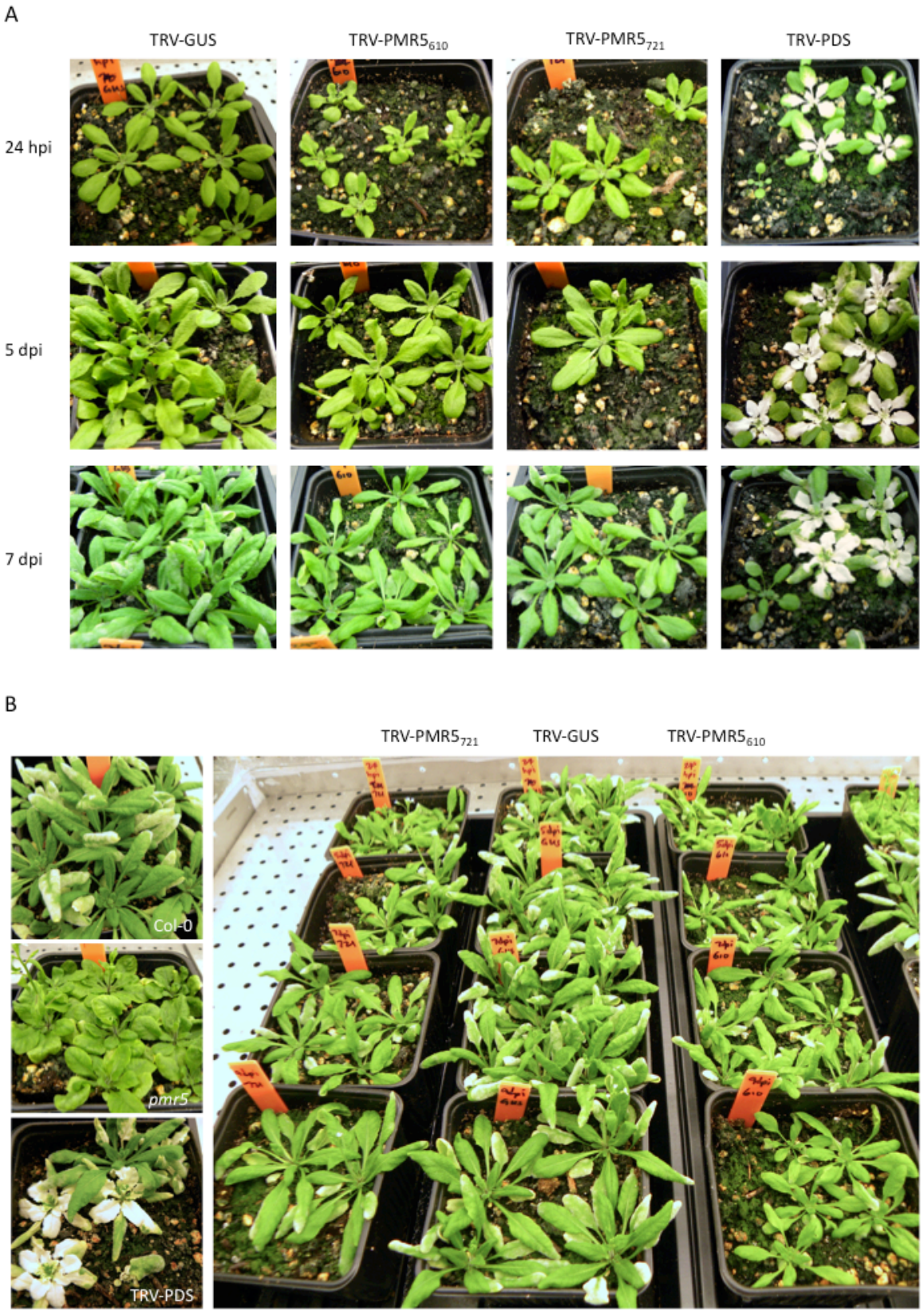
A
TRV-GUS
TRV-PMR5610
TRV-PMR5721
TRV-PDS
24 hpi
5 dpi
7 dpi
B
TRV-PMR5721
TRV-GUS
TRV-PMR5610
Col-0
pmr5
TRV-PDS

C *PMR5* gene expression fold change versus TRV-GUS

	TRV-PMR5$_{610}$	TRV-PMR5$_{721}$
24 h	-3.55	-2.32
24 hpi	-1.32	-2.19
5 d	-4.14	-4.97
5 dpi	-2.31	-1.37

Figure 2.6. Virus induced gene silencing of *PMR5* in Arabidopsis leads to increased powdery mildew disease resistance. Col-0 plants were Agrobacteria-infiltrated with pTRV1 and PTRV2 vectors at 9 days post stratification. Symptoms of positive control, phytoene desaturase (TRV-PDS), showed at 12 days post infiltration, and plants were inoculated with *G. cichoracearum* at 13 days post infiltration. TRV-GUS was used as a negative control.
(a) Comparison of 24 hpi, 5 dpi, and 7 dpi plants after inoculation with *G. cichoracearum.* Note the leaf curling and smaller stature of plants in those infiltrated with TRV-PMR5 at 24 hpi. Noticeable powdery mildew disease symptoms appear at 7 dpi in newly formed leaves of plants infiltrated with TRV-GUS, but not in plants infiltrated with either constructs of TRV-PMR5.
(b) Morphology and disease susceptibility of plants at 9 dpi with *G. cichoracearum*. TRV-GUS plants are susceptible like wild-type, while TRV-PMR5 plants are more resistant to *G. cichoracearum.*
(c) qPCR analysis to confirm *PMR5*-gene silencing compared to the *GUS*-silenced negative control at 14 days (24 hpi *G. cichoracearum*) and 18 days (5 dpi *G. cichoracearum*) post Agrobacteria-infiltration with TRV.

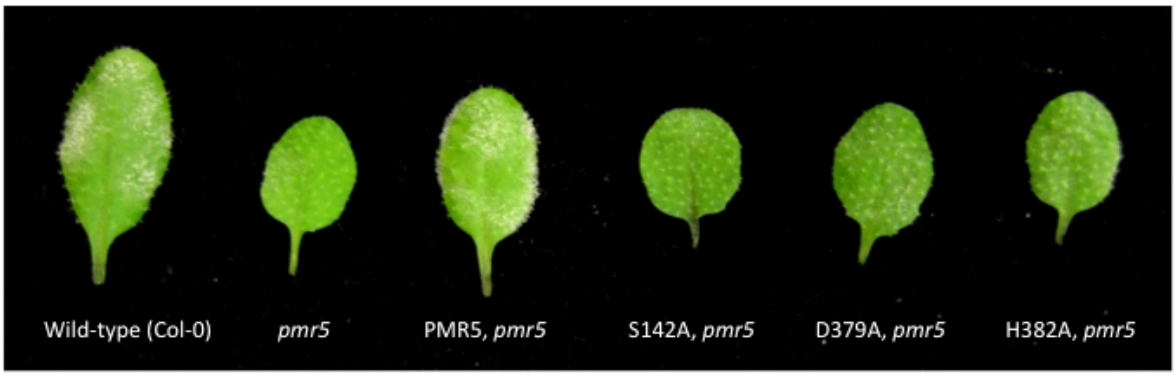

Figure 2.7. Complementation assay after site directed mutagenesis of catalytic residues. 3-week-old plants were inoculated with *G. cichoracearum*, and representative leaves were photographed 8 dpi. Five independent lines per catalytic mutation were obtained with similar results.

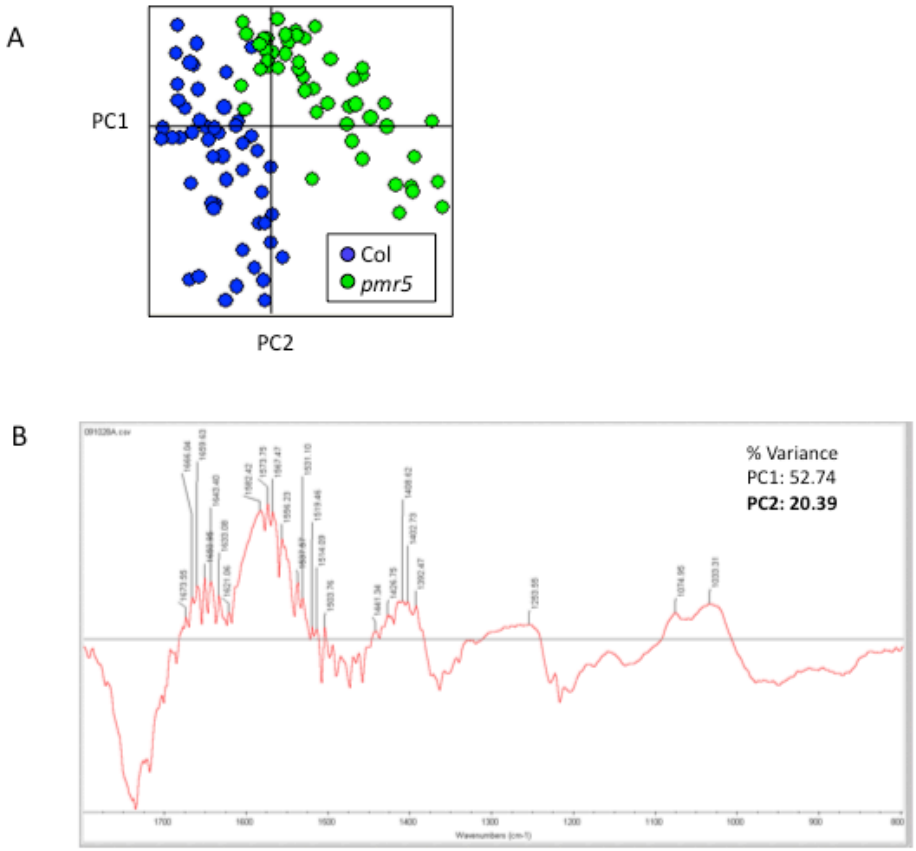

Figure 2.8. PCA analysis of FTIR spectra from wild-type and *pmr5* cell walls isolated from 3-week-old rosette leaves. Each data point in the PCA analysis represents 10 ATR scans (technical replicates) of 5 biological replicates per line.
(a) PCA analysis of FTIR spectra from Col-0 and *pmr5* cell walls, which show clear distinction by PC2
(b) PC2 eigenvector does not replicate pectin peaks seen previously by FTIR microscopy (Vogel et al., 2004). Peaks were not assigned.
.

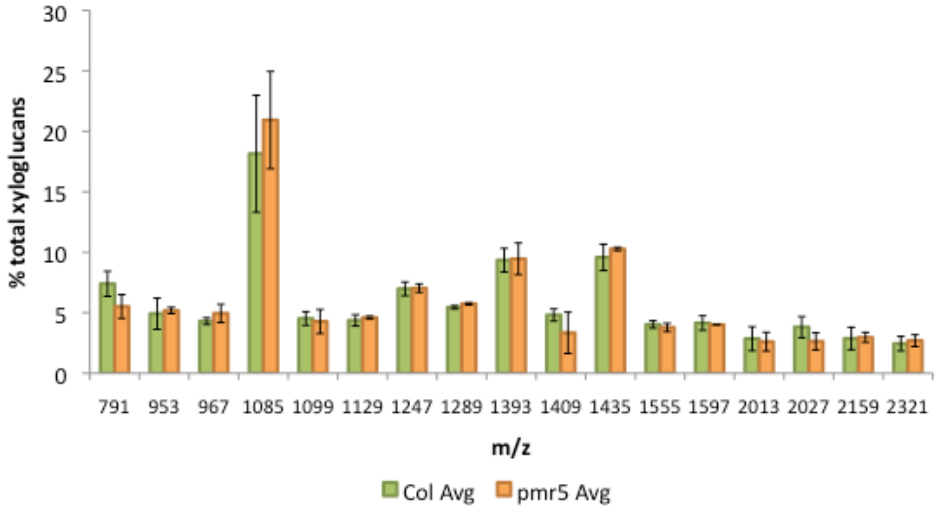

Figure 2.9. Oligosaccharide mass profiling of xyloglucan composition of Col-0 and *pmr5* cell walls isolated from 3-week-old rosette leaves. Values shown are means +/- standard deviation (n=3).

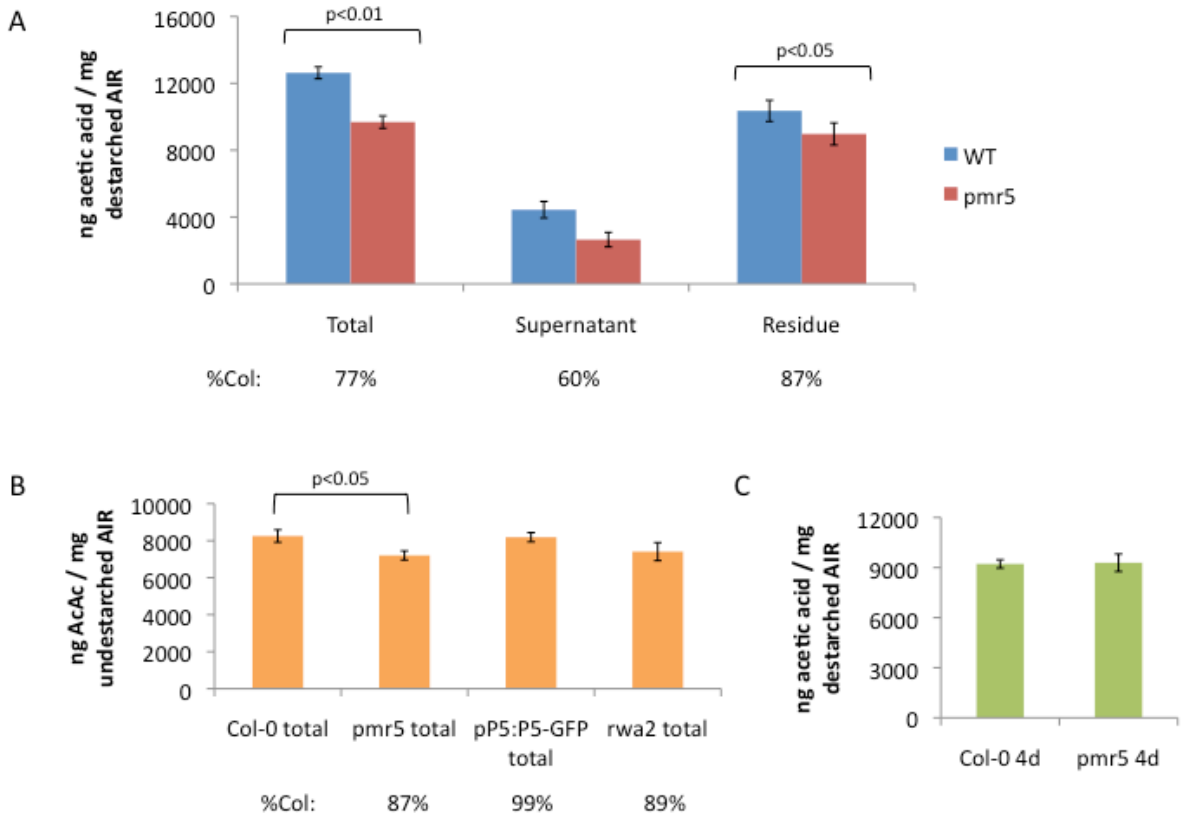

Figure 2.10. Acetic acid released after saponification from 3-week-old rosette leaf cell walls.
(a) Total de-starched cell walls were treated with endopolygalacturonase and pectin methyl esterase to fractionate pectins into the supernatant and non-pectin in the residue. Values shown are means +/- standard error (n=9). The experiment testing total AIR was repeated eight times; four experiments showed statistically significant decrease in the acetylation of *pmr5* leaves compared to Col-0 based on one-way ANOVA with Tukey Test ($p<0.01$), whereas the other four experiments showed a decrease in acetylation of *pmr5* leaves, but the difference was not statistically significant. The experiment testing the pectin fraction was only done once. Although there was a 40% decrease in pectin acetylation in the *pmr5* mutant, the difference is not statistically significant. However, there is a statistically significant decrease in the acetylation of the *pmr5* total (t-test, $p<0.01$) and residue fractions (t-test, $p<0.05$).
(b) Undestarched cell walls show decreased acetylation in *pmr5* compared to Col-0 (t-test, $p<0.05$). Acetylation abundance is restored in plants expressing *pPMR5:PMR5-GFP*. *rwa2-3* was used as a positive control for decreased acetylation (Manabe et al., 2011). Values shown are means +/- standard error (n=9). This experiment was done twice with similar results.
(c) Total destarched AIR from etiolated 4-day-old seedlings showed no difference in acetylation between Col-0 compared to *pmr5*. Values shown are means +/- standard error (n=9). This experiment was done once.

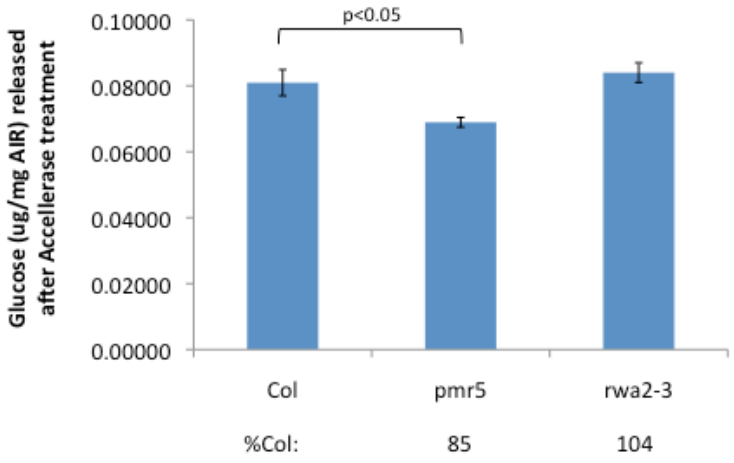

Figure 2.11. Saccharification of cell walls from 6-week-old rosette leaves with Accellerase cocktail as measured by glucose released. Values are means +/- standard error (n=9). *pmr5* cell walls are less digestable than Col-0 (one-way ANOVA, Tukey test $p<0.05$). This experiment was done once.

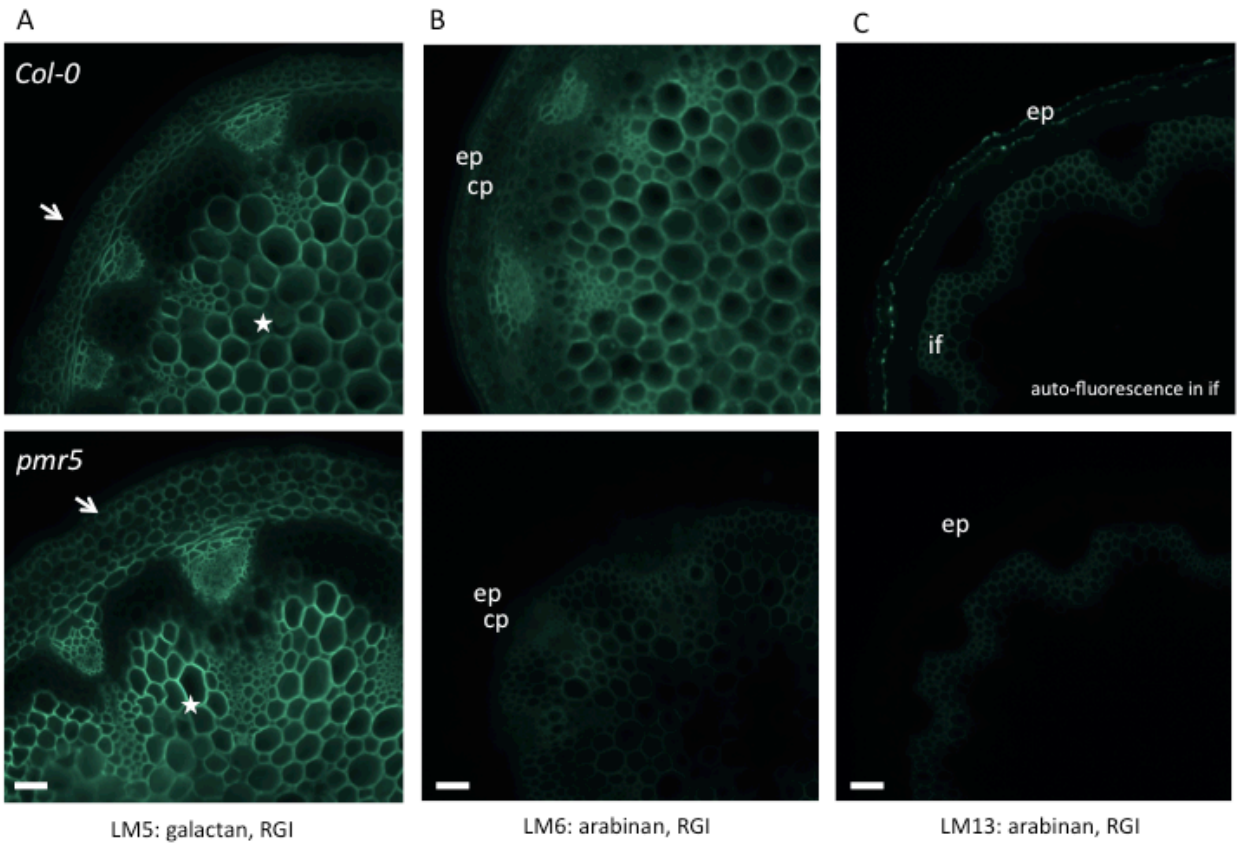

Figure 2.12. Cell wall immunolabeling of transverse stem sections. Arrows indicate the outer surface of the epidermis, ep = epidermis, cp= cortical parenchyma, if = interfascicular parenchyma. Scale bar = 50µm
(a) Increased LM5 galactan labeling in *pmr5*, especially in pith parenchyma (marked with asterisks)
(b) Decreased LM6 arabinan labeling in *pmr5*. Intensity of labeling in this image is not representative.
(c) Decreased LM13 arabinan labeling in *pmr5* in the epidermis

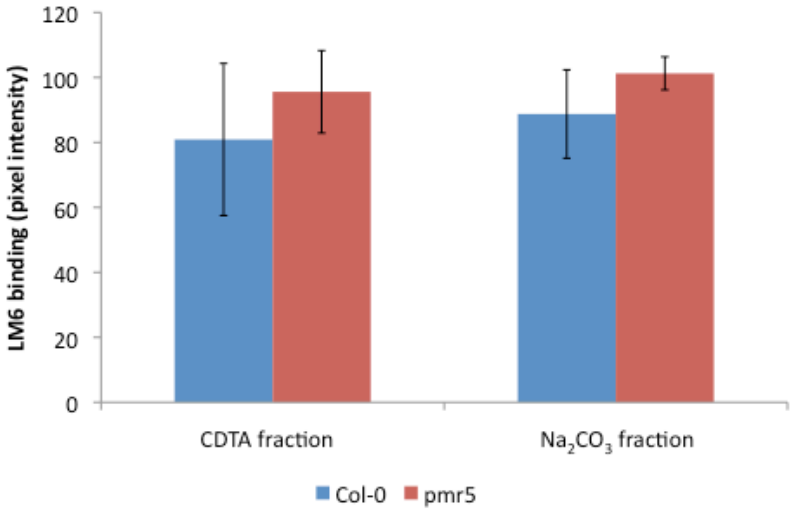

Figure 2.13. Example of immunolabeling of spotted extracts with LM6 arabinan antibody. Cell walls from Col-0 and *pmr5* 3-week-old rosette leaves were sequentially treated with increasingly alkali solvents (CDTA, sodium carbonate, potassium hydroxide). Extracts were spotted in a dilution series and probed with LM6, JIM5, and JIM7 antibodies. Binding is represented by chemilluminescent detection of antibodies bound to epitopes of spots, and measured using ImageJ. Values are means +/- standard deviation (n=6). No differences were seen in labeling of any fraction and with all antibodies between Col-0 and *pmr5* cell walls.

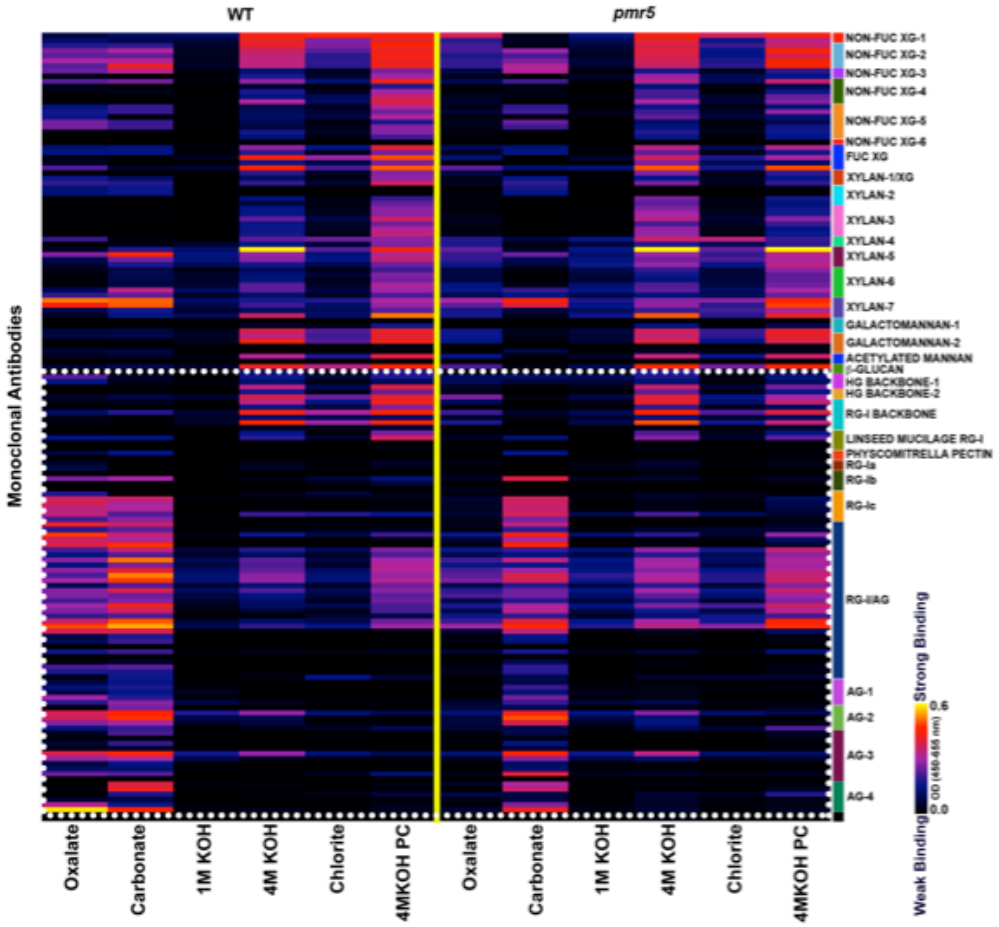

Figure 2.14. Glycome profiling of wild-type and *pmr5* cell walls isolated from 3-week-old rosette leaves. Greatest changes occur in oxalate fraction enriched in pectins. Dotted box highlights pectin antibodies. Figure from Siva Kumar.

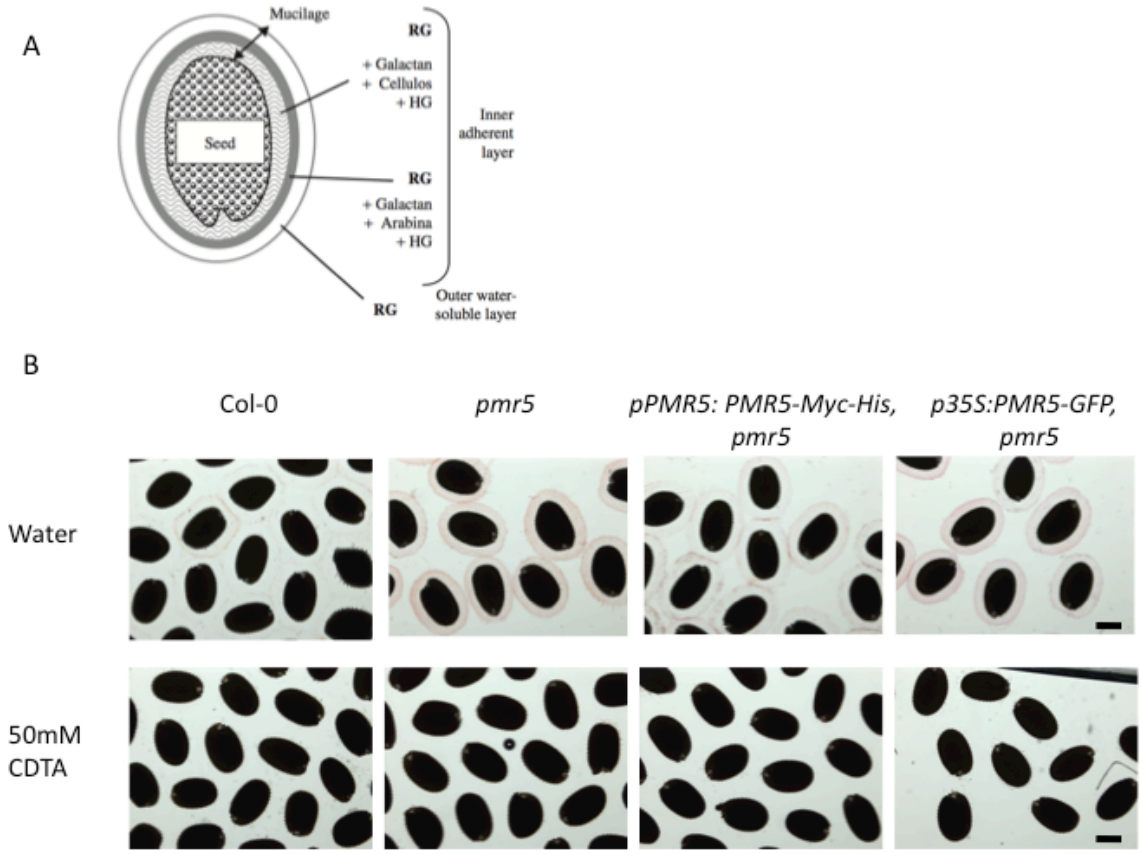

Figure 2.15. Arabidopsis seed mucilage is rich in rhamnogalacturonan I
(a) Image illustrating the layers of Arabidopsis seed mucilage taken from Figure 10 from (Macquet et al., 2007)
(b) Ruthenium red staining of seed mucilage after imbibing in water or 50mM CDTA. Scale bar = 300 μm

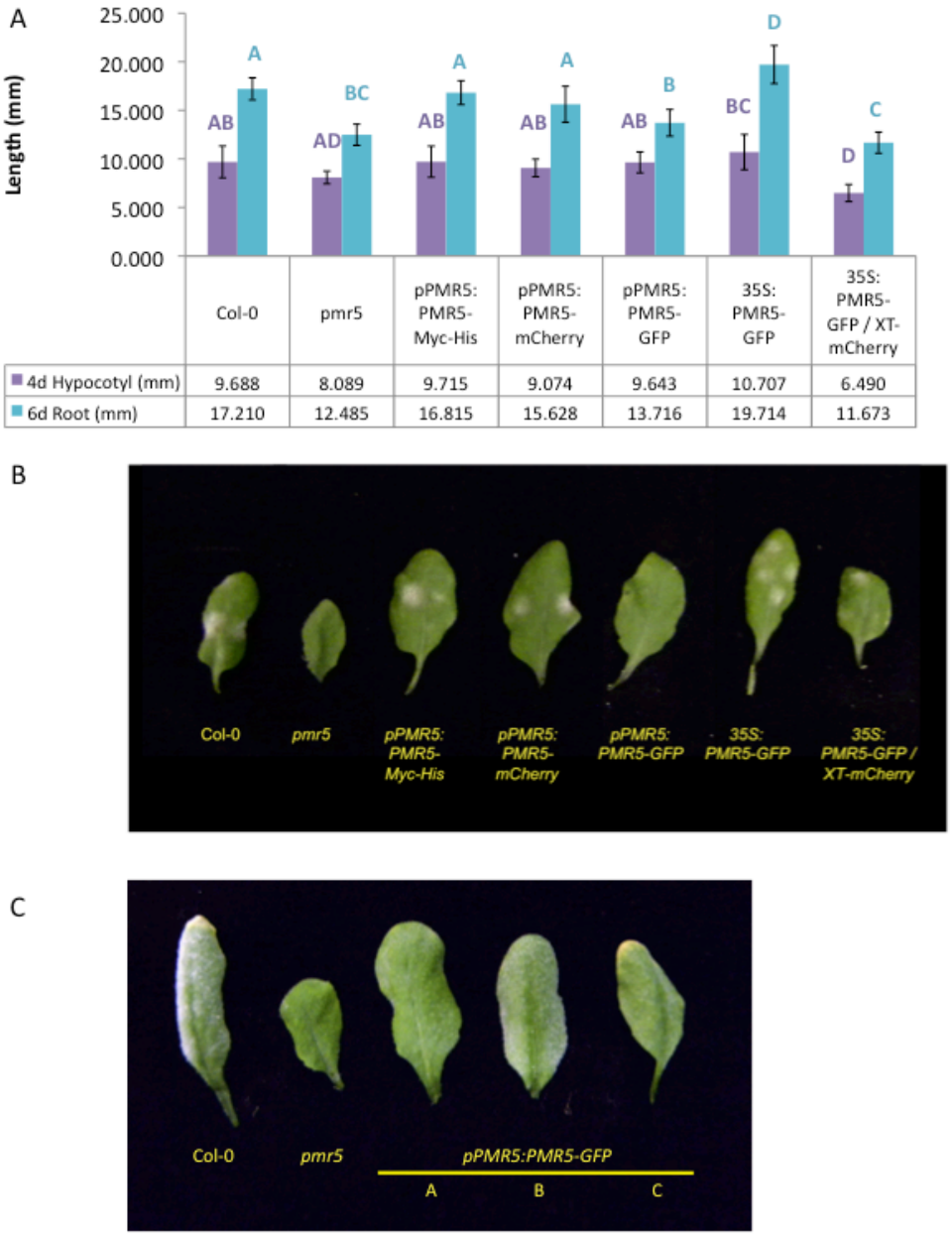

Figure 2.16. Morphology and phenotypes of transgenic lines used in the localization study
(a) 4-day-old etiolated seedling hypocotyl lengths and 6-day-old light grown seedling root lengths. Values are means +/- standard deviation (n>10). Statistical analysis of hypocotyl data is based on one-way ANOVA on Ranks test with Dunn's method for multiple comparison ($p<0.05$). Statistical analysis of root data is based on one-way ANOVA with Tukey test ($p<0.05$)
(b) Disease symptoms of 3-4-week-old rosette leaves after light inoculation with *G. cichoracearum*. Representative leaves were photographed 9 dpi.
(c) Disease symptoms of 3-4-week-old rosette leaves of three individual lines expressing *pPMR5:PMR5-GFP* (A-C) after heavy inoculation with *G. cichoracearum.* Representative leaves were photographed 9 dpi.

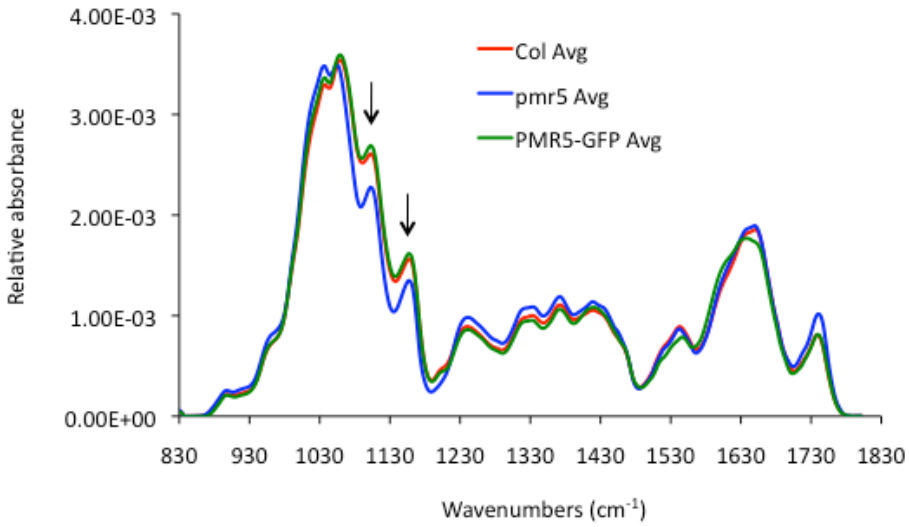

Figure 2.17. FTIR spectrum of 6-day-old etiolated seedlings of wild-type (Col-0), *pmr5*, and complementing line, *35S:PMR5-GFP*. Arrows indicate regions of considerable differences in *pmr5* cell wall composition compared to wild type. Cell walls isolated from *pmr5* plants expressing *35S:PMR5-GFP* show full complementation of cell wall composition back to wild type. Data from Gregory Mouille.

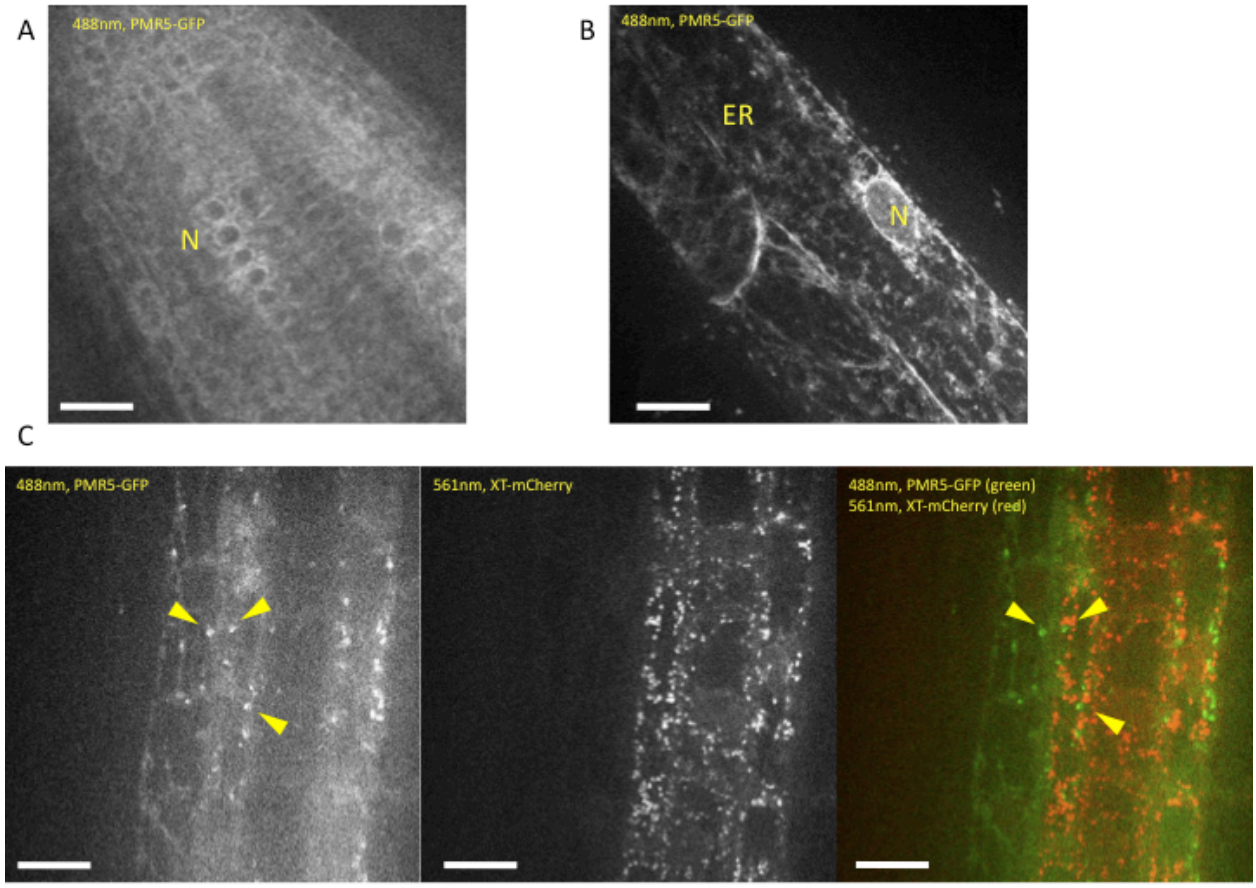

Figure 2.18. Localization of PMR5-GFP in 6-day-old seedling roots of plants expressing *pPMR5:PMR5-GFP and 35S:XT-mCherry* (Golgi marker). Web-like structures surrounding nuclei (N) are characteristic of endoplasmic reticulum (ER). Scale bar = 20 µm
(a) Single Z layer at root tip of 6-day-old seedling expressing *pPMR5:PMR5-GFP*
(b) Maximum Z projection of cortical root cells in elongation zone of 6-day-old seedlings
(c) Co-localization of PMR5-GFP with XT-mCherry. Yellow arrowheads point at bright GFP speckles that do not co-localize with XT-mCherry. Images are single Z slices, and merged with ImageJ

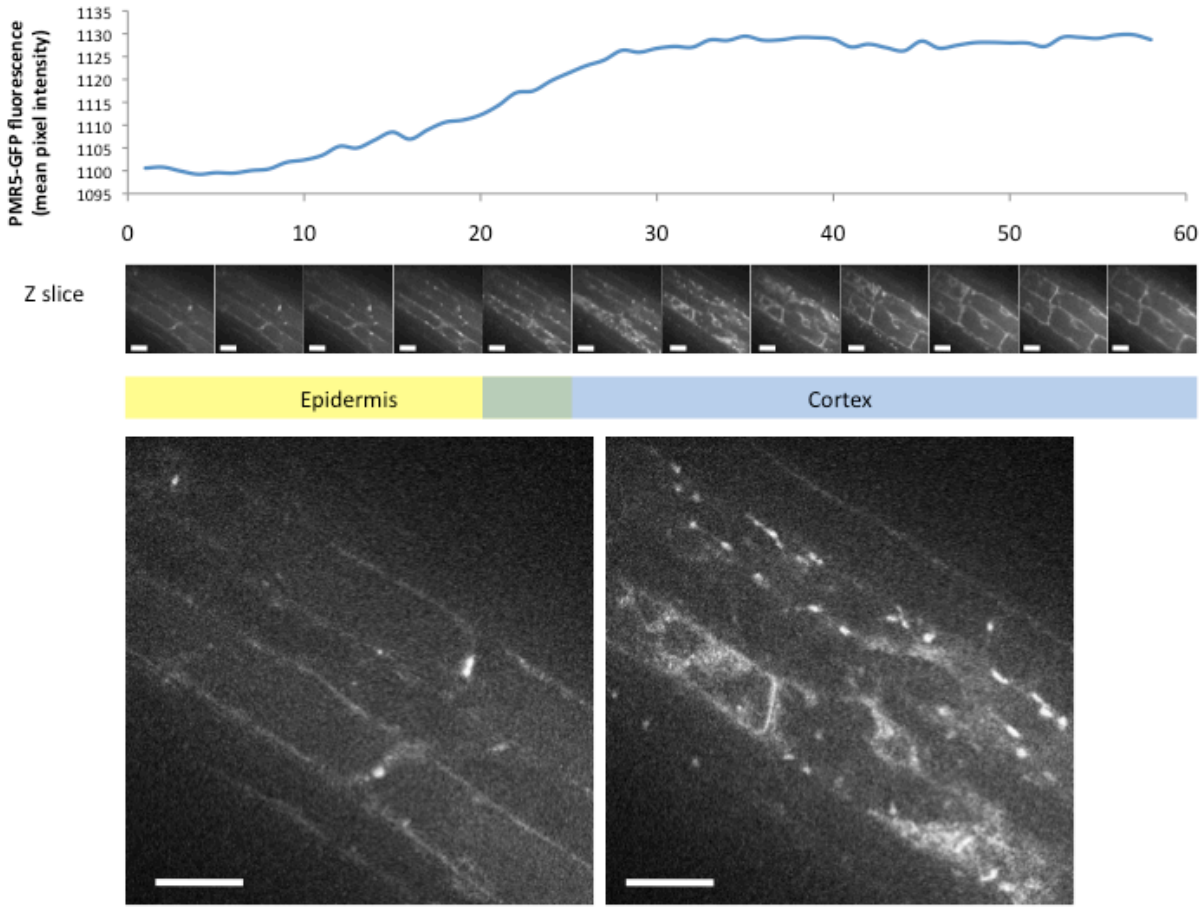

Figure 2.19. PMR5-GFP localizes in the ER, especially in the cortical root cells, of plants expressing *pPMR5:PMR5-GFP*. Z-axis profile tracks mean fluorescence across Z-projection from epidermal cells to cortical cells. Representative Z-slices are shown at every five slices. Larger images are at Z-slice 1 (left, epidermis) and Z-slice 30 (right, cortex). Scale bar = 20 μm

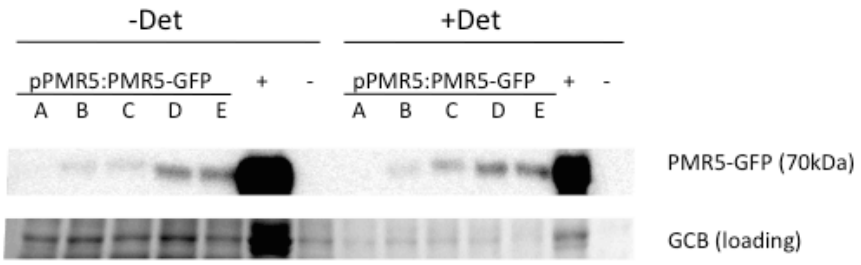

Figure 2.20. Detection of PMR5-GFP in leaves by western blotting with GFP antibody. PMR5-GFP can be detected in crude protein extracts of 2-week-old rosette leaves from T2 individuals from *pPMR5:PMR5-GFP*-transformed *pmr5* plants. *A* did not contain the transgene, whereas *B-E* contain the transgene. *E* was found to be homozygous after growing the T3 generation. *E* is annotated as "pPMR5:PMR5-GFP A" in Table 2.9. 6-day-old seedlings expressing *35S:PMR5-GFP* acted as positive control (+). 2-week-old rosette leaves from *pmr5* plants acted as negative control (-). Protein samples were isolated with and without detergent (+/- Det) in the lysis buffer. Gelcode Blue (GCB) is shown for protein loading.

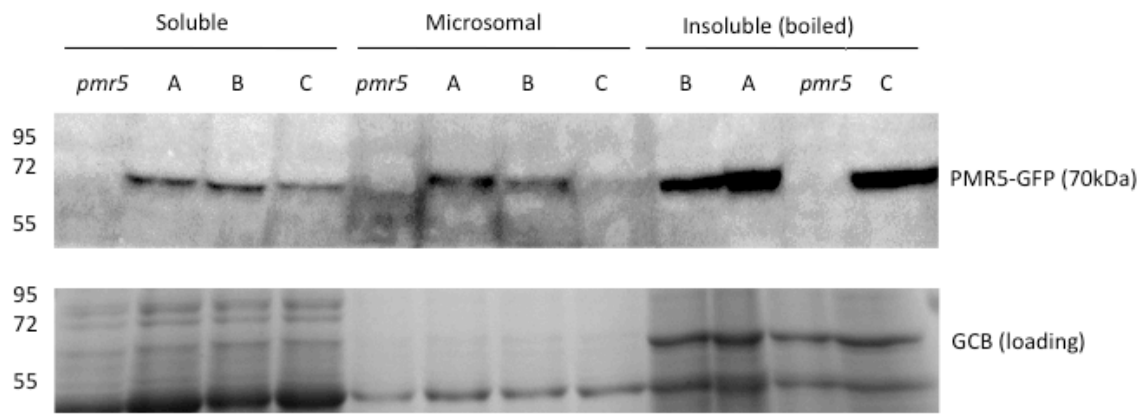

Figure 2.21. Fractionation of PMR5-GFP from 4-day-old seedlings expressing *pPMR5:PMR5-GFP* (A,B,C), and western blotting and detection of PMR5-GFP in soluble, microsomal, and insoluble fractions with anti-GFP antibody. Protein isolated from 4-day-old *pmr5* seedlings was included as a negative control. Gelcode Blue (GCB) is shown for protein loading.

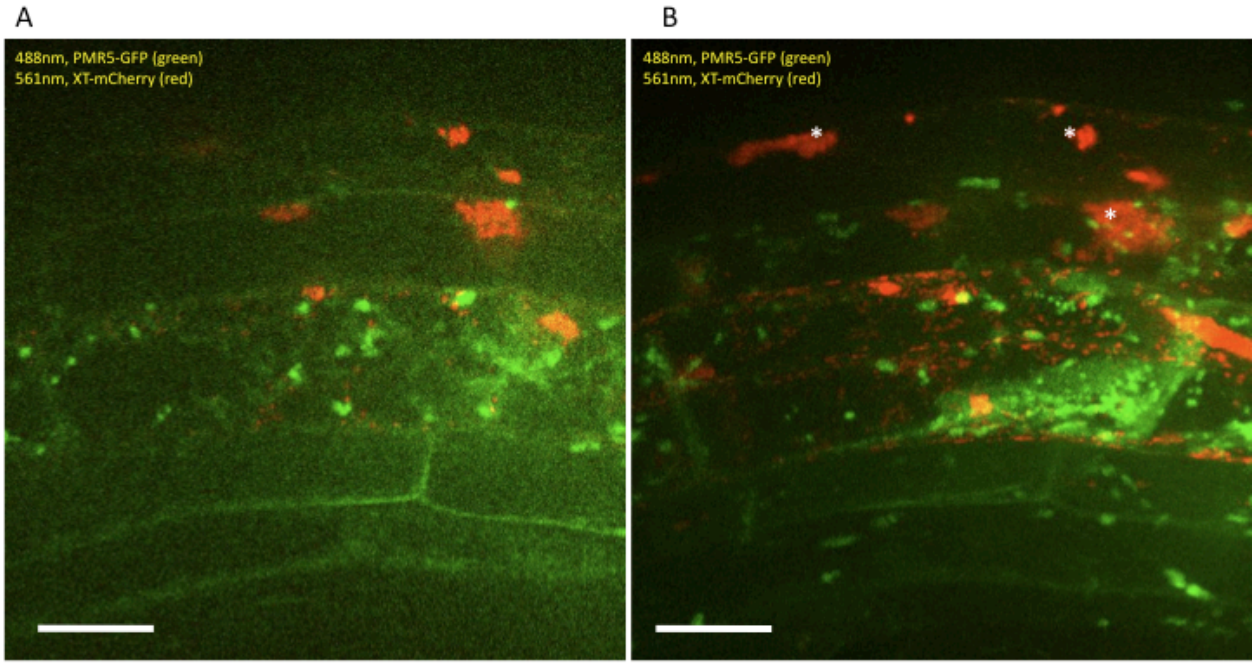

Figure 2.22. Localization of PMR5-GFP and XT-mCherry (Golgi marker) after brefeldin A (BFA) treatment of 4-day-old seedlings. PMR5-GFP is not sensitive to BFA treatment, whereas the red Golgi marker has aggregated into BFA bodies (white asterisks). Scale bar = 20 μm
(a) Single Z slices of PMR5-GFP and XT-mCherry from plants expressing *pPMR5:PMR5-GFP* and *35S:XT-mCherry* from Z stacks in (b).
(b) Maximum Z projection of merged images from plants expressing *pPMR5:PMR5-GFP* and *35S:XT-mCherry*

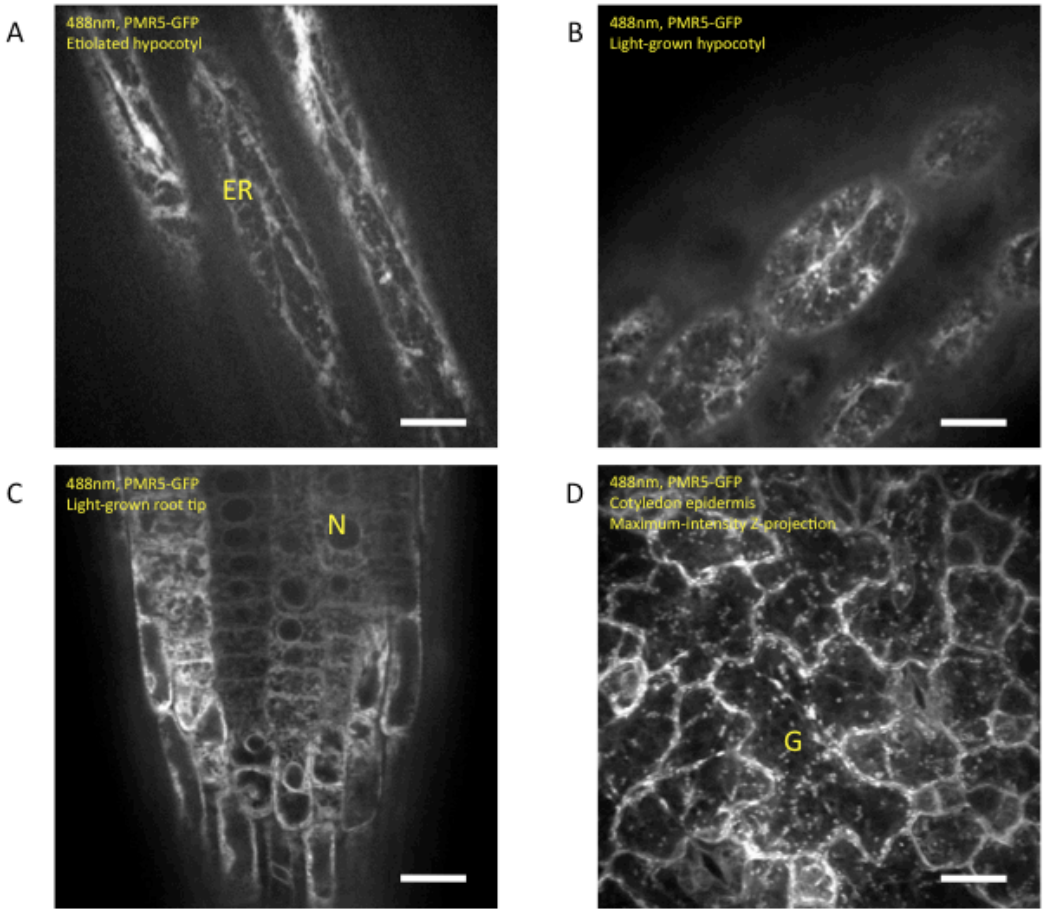

Figure 2.23. Localization of PMR5-GFP in 7-day-old seedlings expressing 35S:PMR5-GFP in the endoplasmic reticulum, cytosol, and Golgi (G, speckles) as seen in (a) dark grown seedling hypocotyls, (b) light grown seedling hypocotyls, (c) light grown seedling root tips, and (d) epidermal cotyledon tissue (maximum-intensity Z-projection). Web-like structures surrounding nuclei (N) are characteristic of endoplasmic reticulum (ER). Scale bar = 10 μm.

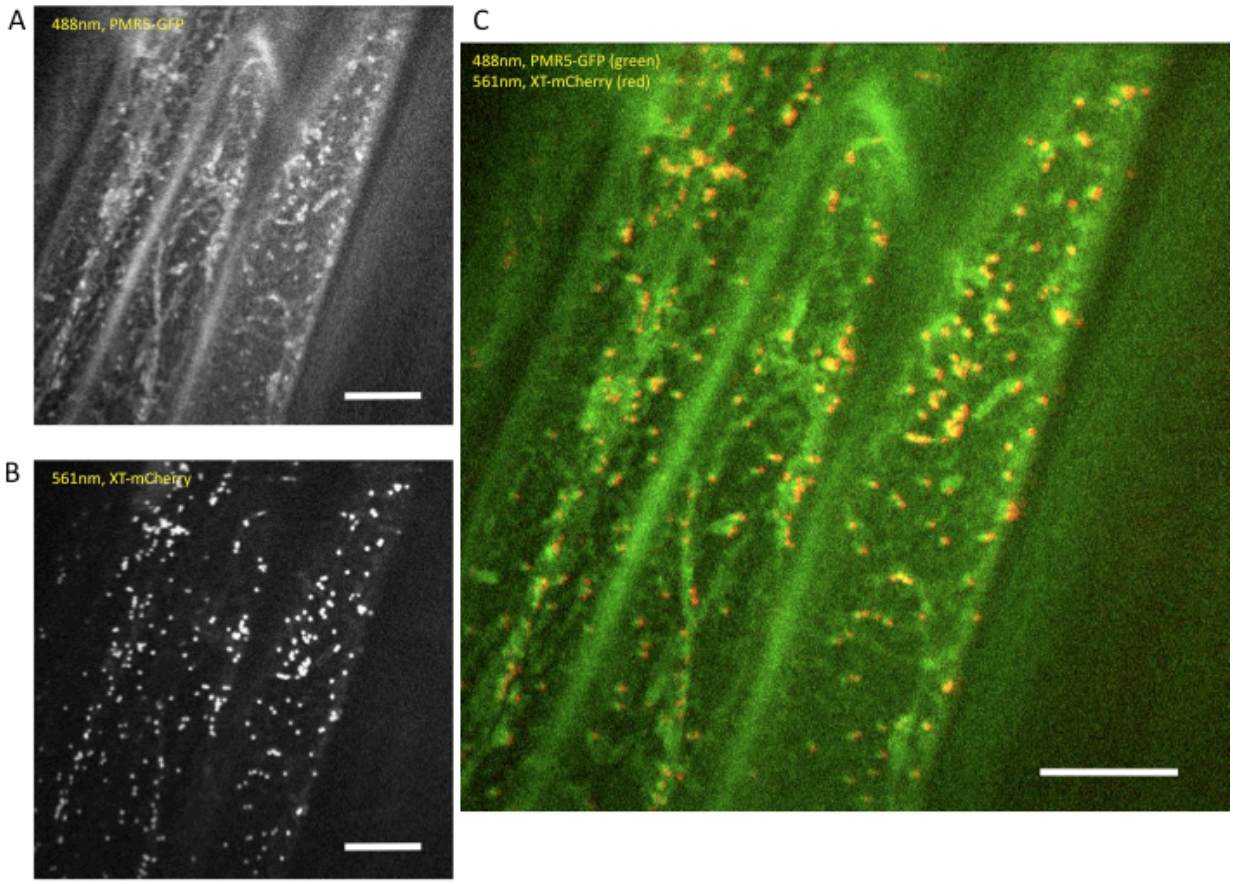

Figure 2.24. Co-localization of PMR5-GFP with Golgi marker (XT-mCherry) in 4-day-old light grown seedling roots of plants expressing both *35S:PMR5-GFP* and *35S:XT-mCherry*. Images are single Z slices. Scale bar = 20 μm
(a) PMR5-GFP visualized with 488nm laser
(b) XT-mCherry visualized with 561nm laser
(c) Merged images showing Golgi co-localization in yellow.

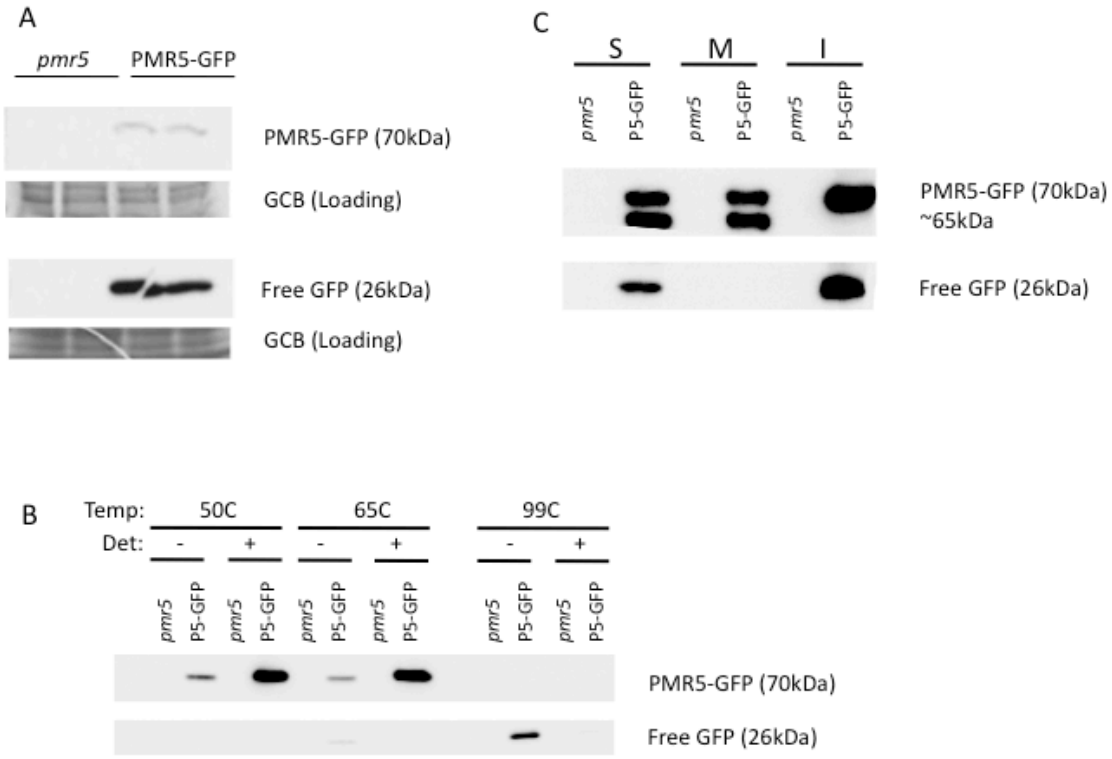

Figure 2.25. Fractionation of PMR5-GFP from plants expressing *35S:PMR5-GFP*
(a) PMR5-GFP (70kDa) and free GFP (26kDa) detected after crude protein extraction and western blotting and detection of GFP with GFP antibody. Gelcode Blue (GCB) is shown for protein loading.
(b) Heating the fusion proteins prior to SDS-PAGE loading cleaves the GFP. Protein samples were isolated with or without detergent (+/- Det) in the lysis buffer.
(c) PMR5-GFP is found in both the soluble (S) and microsomal (M) fractions after high-speed centrifugation. Other than the insoluble (I) fraction, samples were not boiled. Despite omitting boiling step prior to loading SDS-PAGE gel, some free GFP can be seen in the soluble fraction. An unidentified 65 kDa fragment was also detected in the soluble and microsomal fractions.

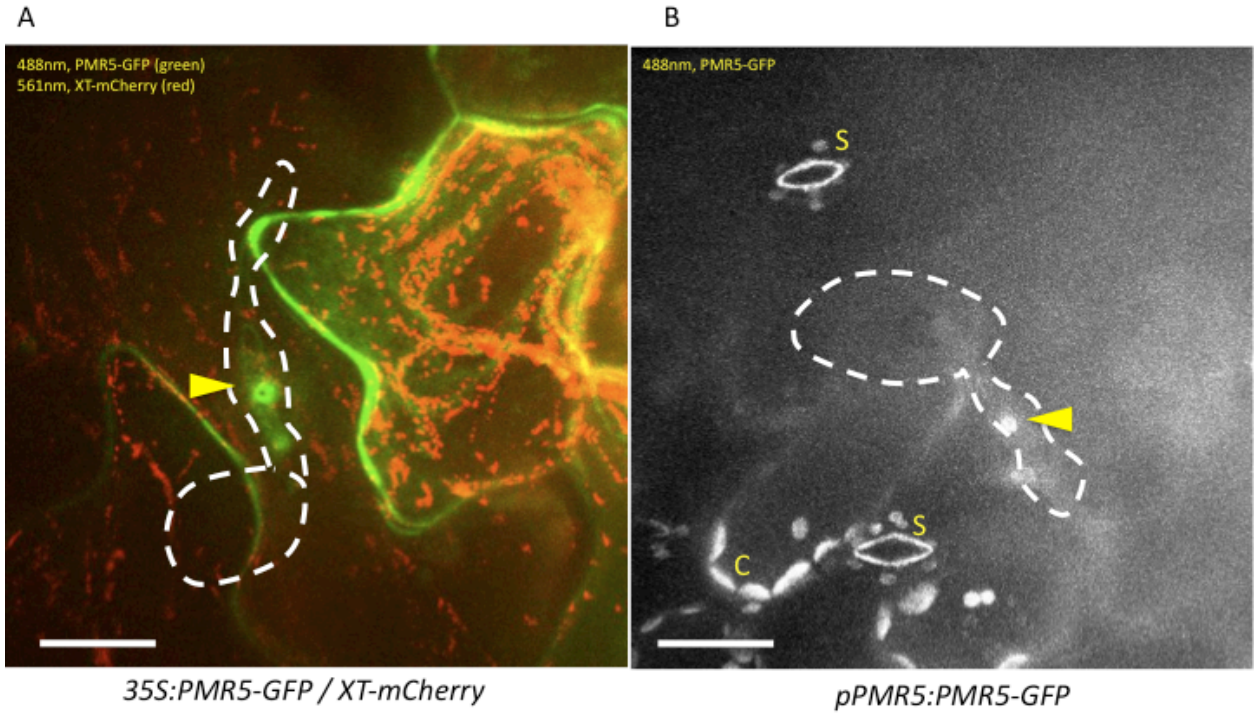

Figure 2.26. Localization of PMR5-GFP at fungal penetration sites 24 hpi with *G. cichoracearum.* XT-mCherry (Golgi marker, red) does not re-localize to or co-localize at penetration sites. White dashed lines outline fungal spore and appressorial germ tube. Yellow arrowheads point to penetration sites. Stomata (S) and chloroplasts (C) are labeled due to autofluorescence in the weakly fluorescing native promoter GFP line. Scale bar = 20 µm
(a) Maximum Z projection of PMR5-GFP and XT-mCherry from plants expressing *35S:PMR5-GFP* and *35S:XT-mCherry*
(b) Maximum Z projection of PMR5-GFP from plants expressing *pPMR5:PMR5-GFP*

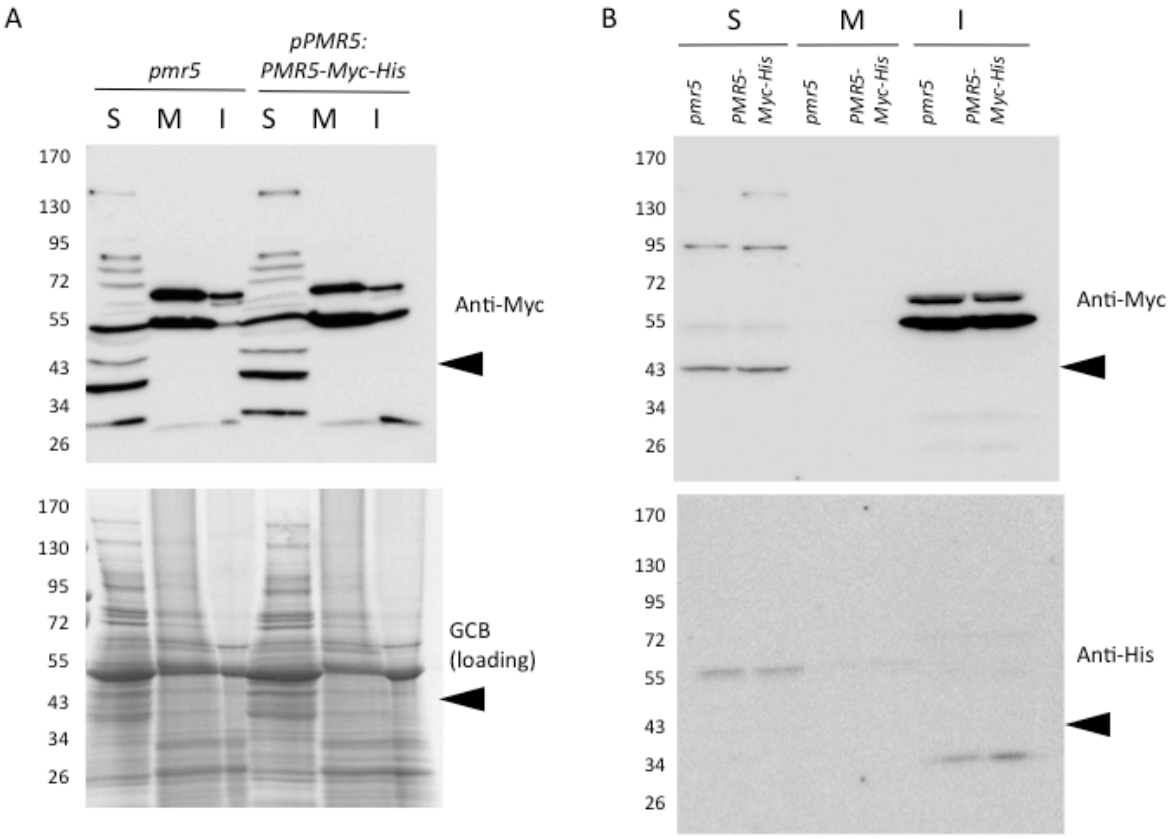

Figure 2.27. PMR5-Myc-His could not be detected in by western blot. Arrowheads indicate expected band size for PMR5-Myc-His at 44kDa
(a) Protein from 7-day-old light grown seedlings was fractionated into soluble (S), microsomal (M), and insoluble (I) fractions prior to SDS-PAGE and western blot analysis. Top: Anti-myc probed western blot. Bottom: Gel Code Blue-stained SDS-PAGE gel.
(b) His-tagged proteins from 7-day-old light grown seedlings were first enriched by nickel-NTA purification prior to fractionation. Top: Anti-myc probed western blot. Bottom: Anti-his probed western blot. Stained protein gel for loading was not run for this set of samples.

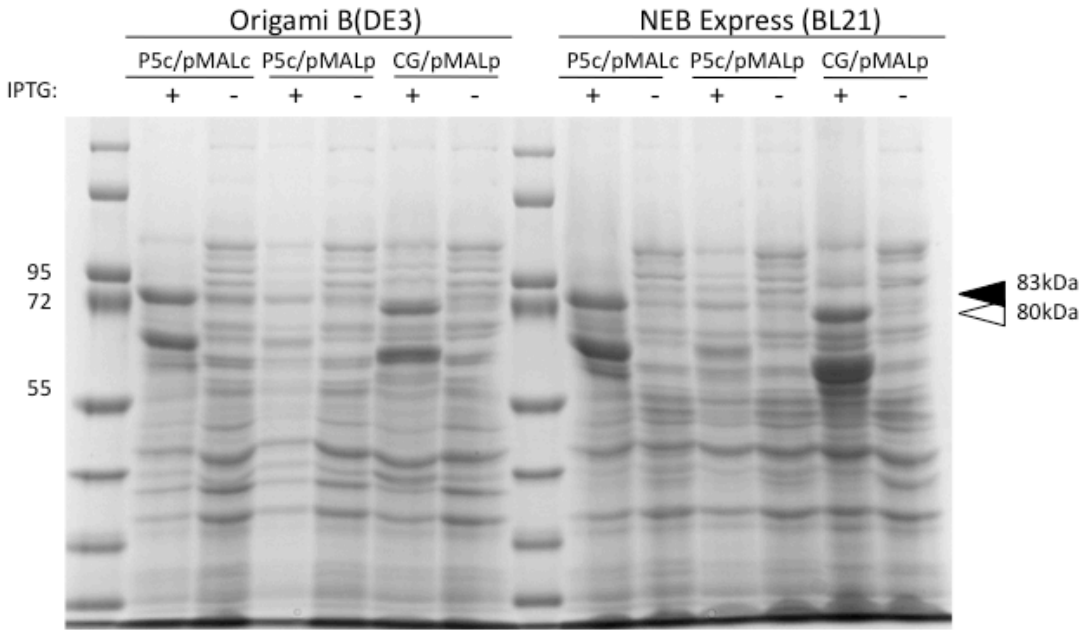

Figure 2.28. Stained SDS-PAGE gel of crude cell lysate from cells expressing MBP-PMR5-His after 0.3mM IPTG induction. Arrowheads indicate expected band size for MBP-PMR5-His at 83kDa (black) and MBP-PMR5$_{C66\text{-}end}$-His at 80kDa (white). P5c = PMR5 CDS without signal peptide; CG = PMR5 with N-terminal truncation, beginning at first conserved cysteine (C66); pMALc = pMAL vector with cytosolic expression; pMALp = pMAL vector with periplasmic expression.

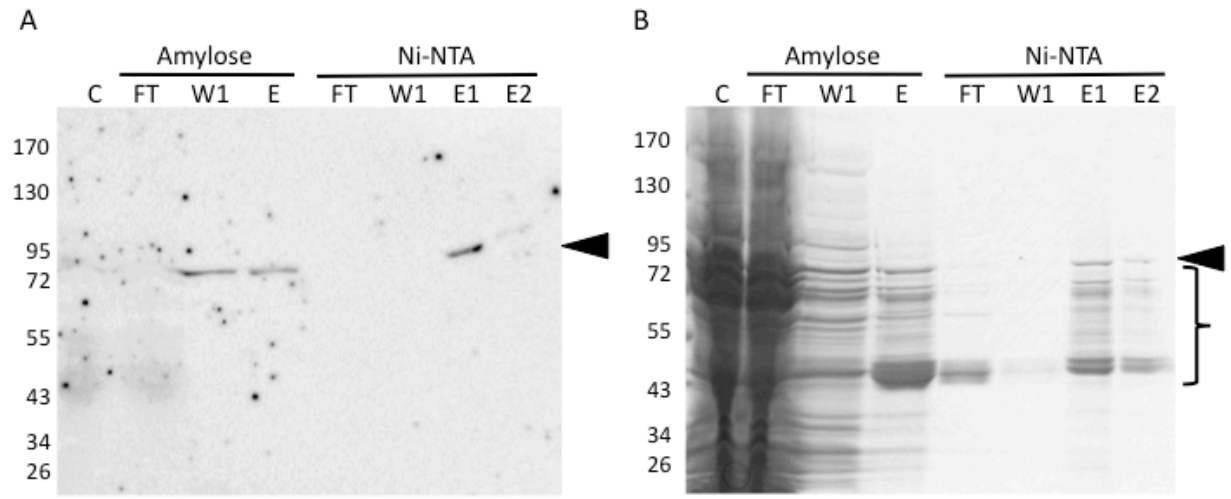

Figure 2.29. Purification of MBP-PMR5-His using B-PER lysis buffer. C, crude lysate; FT, flow-through; W, wash; E, elution.
(a) Detection of MBP-PMR5-His by western blot and anti-his antibody at expected band size of 83 kDa (arrowhead)
(b) GelCode blue stained SDS-PAGE gel showing smaller degradation products in elutions (bracket)

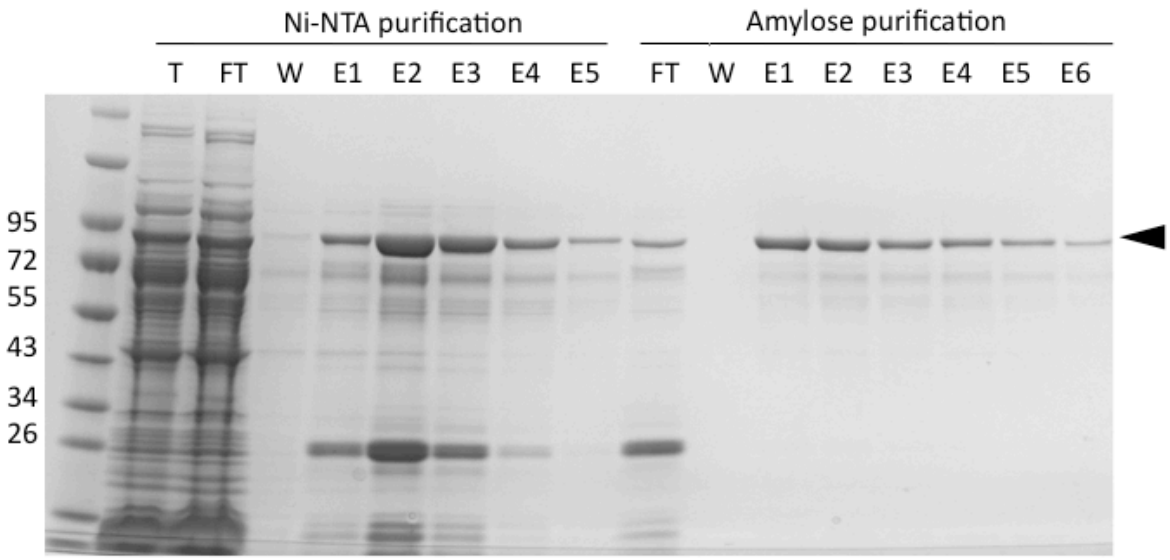

Figure 2.30. Optimized purification of MBP-PMR5-His. SDS-PAGE gel stained with GelCode Blue after dual purification with nickel-NTA followed by amylose resins. T, total crude lysate; FT, flow through; W, last column volume of wash; E, elutions. Arrowhead indicates expected band size of MBP-PMR5-His at 83 kDa

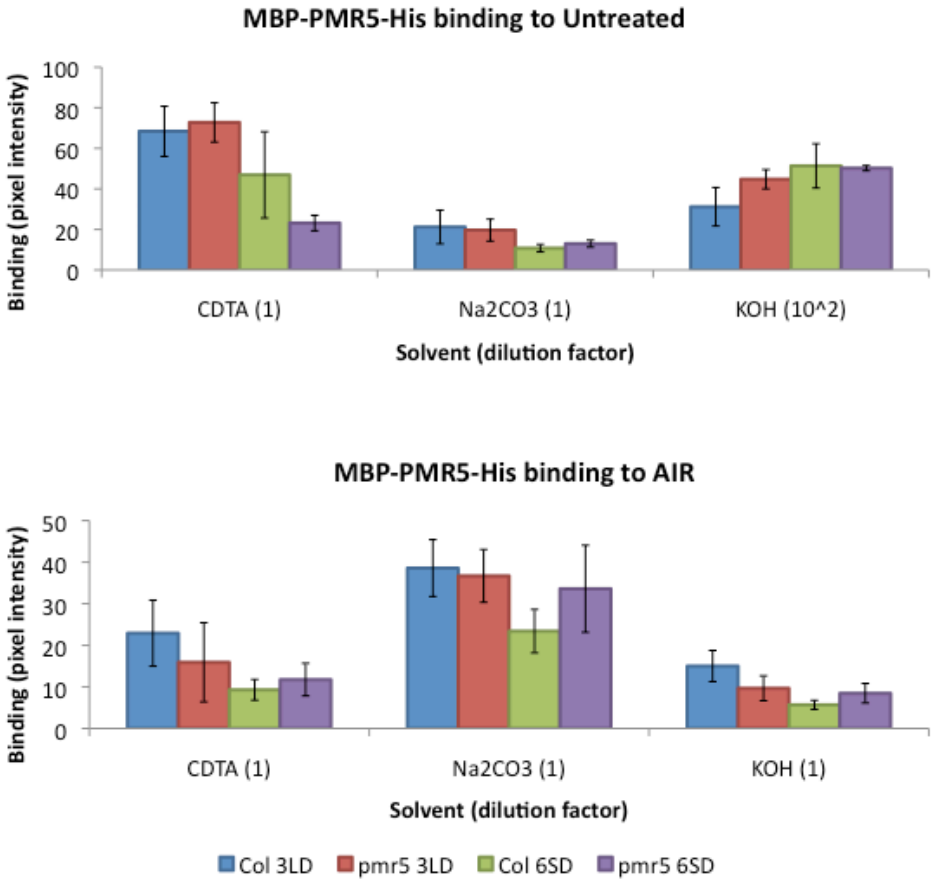

Figure 2.31. MBP-PMR5-His binds chemically extracted Arabidopsis pectin from untreated samples and AIR prepared from 3-week-old long day (LD) or 6-week-old short day (SD) plants. No binding above background was seen in blots probed with MBP only (negative control). Numbers in parentheses indicate dilution factor of extract used for spotting. Values shown are means +/- standard deviation (n=3)

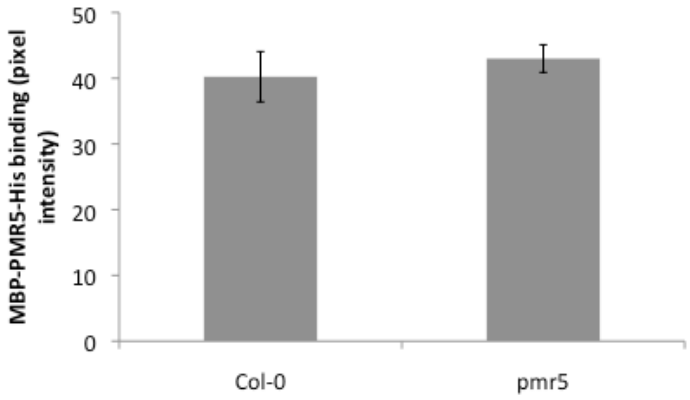

Figure 2.32. MBP-PMR5-His binds to enzymatically extracted Arabidopsis pectin similarly in wild-type Col-0 and *pmr5*. Acetylation was found to be decreased in pectin samples isolated from *pmr5* cell walls. No binding above background was seen in blots probed with MBP only (negative control). Values shown are means +/- standard deviation (n=3)

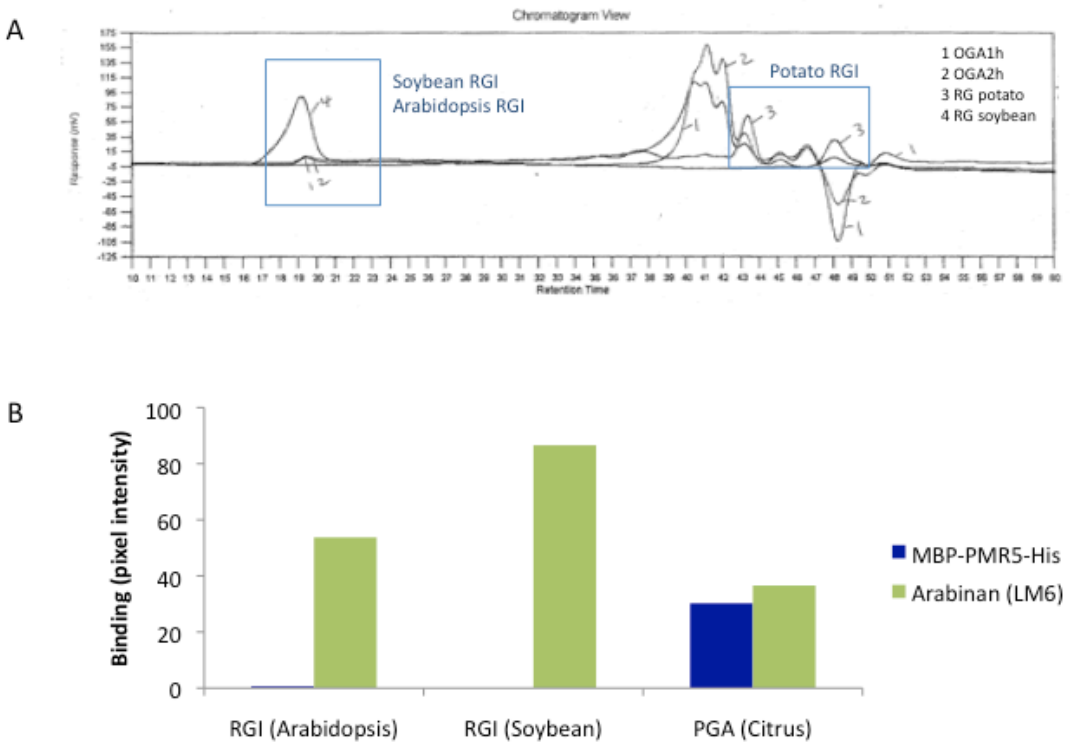

Figure 2.33. MBP-PMR5-His does not bind Arabidopsis RGI
(a) Spectral output of elutions from size exclusion chromatography of OGAs, soybean RGI, and potato RG. Figure modified from Amancio Souza.
(b) Lack of MBP-PMR5-His binding to Arabidopsis RGI. LM6 labeling acts as control for presence of arabinan epitopes in Arabidopsis RGI fraction. Soybean RGI and PGA used as positive LM6 binding control, and PGA used as positive MBP-PMR5-His control (see Table 2.10). No binding above background was seen in blots probed with MBP only (negative control). Values shown are means of two measurements and experiment was repeated twice with similar results.

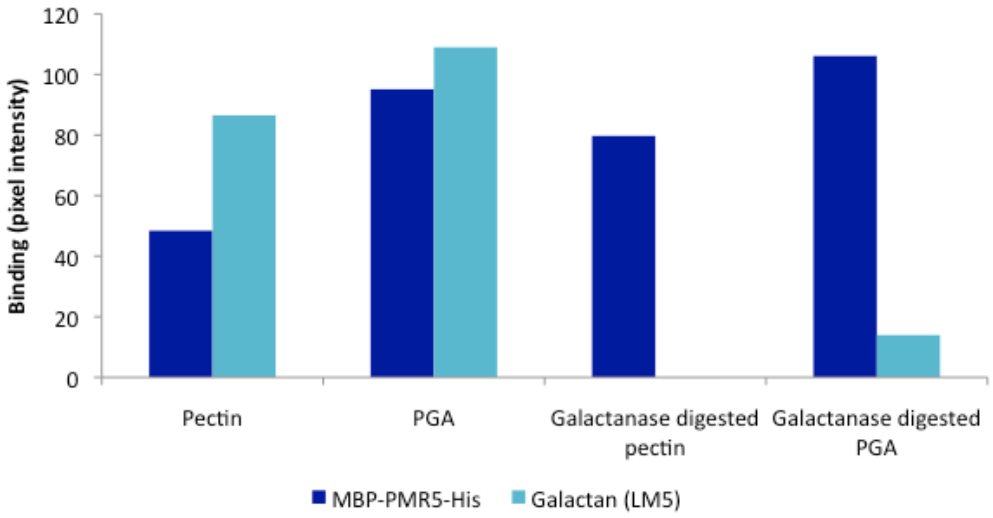

Figure 2.34. MBP-PMR5-His binding affinity to galactanase digested pectin. LM5 labeling acts as control for presence of galactan epitopes in samples. No binding above background was seen in blots probed with MBP only (negative control). Values shown are single measurements of binding (pixel intensity). Experiment was repeated twice with similar results.

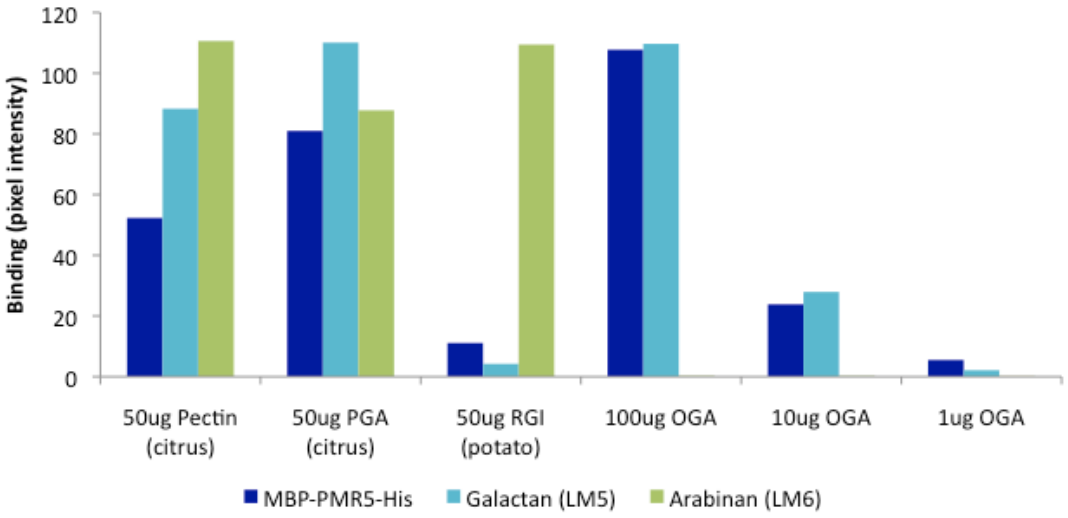

Figure 2.35. MBP-PMR5-His binds to oligogalacturonides, shorter chains of PGA with a degree of polymerization of 10-25 monomers. Pectin and PGA are positive controls for MBP-PMR5-His binding. RGI acts as negative control for MBP-PMR5-His binding. LM5 and LM6 labeling act as controls for presence of pectic epitopes in samples. No binding above background was seen in blots probed with MBP only (negative control). Values shown are single measurements, and experiment was repeated twice with similar results.

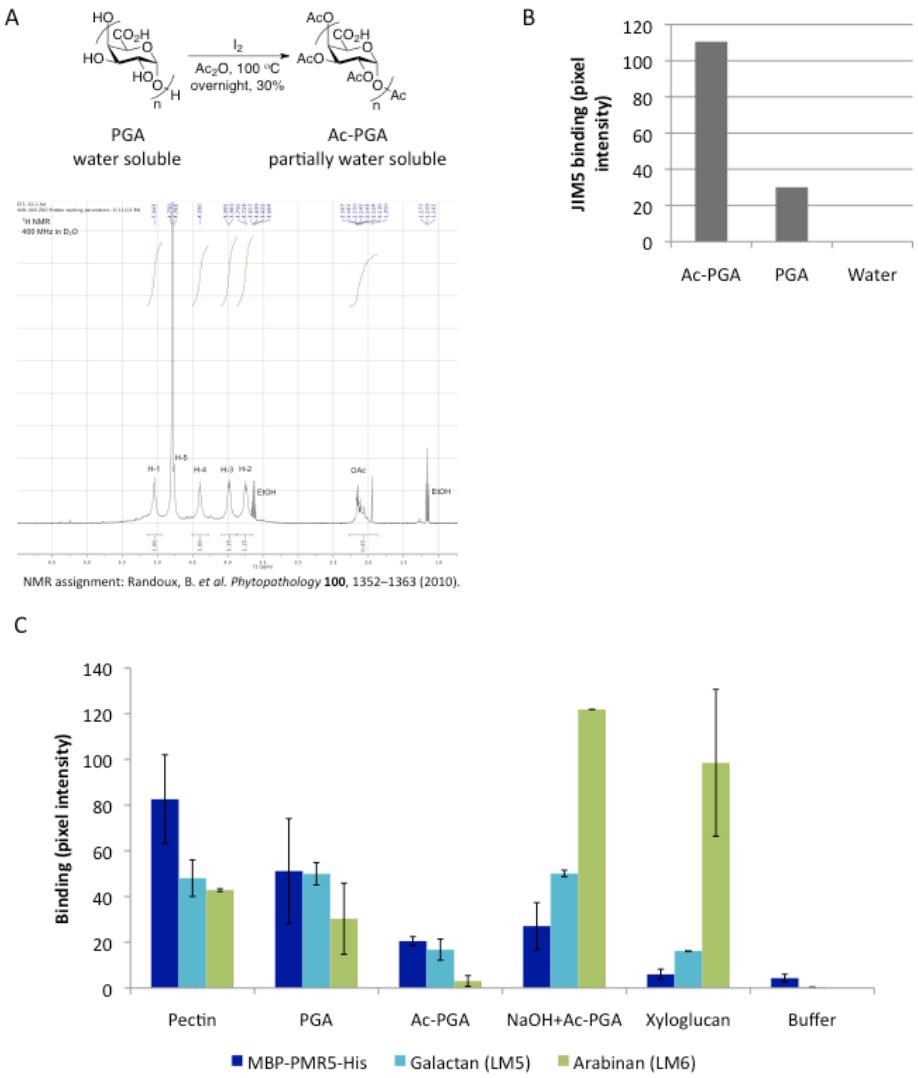

Figure 2.36. MBP-PMR5-His binds more weakly to acetylated PGA.
(a) Chemical reaction to synthesize Ac-PGA and NMR spectrum of product. NMR peaks were assigned as in (Randoux et al., 2010). Degree of substitution (DS) of acetylated PGA is 0.28 acetyl groups per monomer. DS was calculated by dividing the number of Ac groups (calculated by dividing the integration of Ac protons by 3) with the number of ring protons (calculated by dividing the integration of ring protons by 5). Data from Shu-lun Tang.
(b) JIM5 binding properties of Ac-PGA compared to PGA. Both polysaccharides were applied at equal amounts prior to detection with JIM5 antibody. Ac-PGA is labeled more with JIM5, which recognizes methylated homogalacturonan.
(c) MBP-PMR5-His binds more weakly to Ac-PGA. De-esterification treatment of Ac-PGA restores detection of galactan and arabinan eptiopes recognized by LM5 and LM6 antibodies, respectively. Xyloglucan and buffer act as negative MBP-PMR5-His binding controls. Boiled MBP-PMR5 and MBP were used as negative protein binding controls (data not shown). Values shown are means +/- standard deviation of four (MBP-PMR5-His) or two (LM5, LM6) measurements.

Tables

Table 2.1. List of plasmids used in this study

Plasmid name	Description	Source
pENTR-D-TOPO	TOPO entry vector for directional cloning with kanamycin resistance	Invitrogen
pCR8-TOPO	TOPO entry vector with spectomycin resistance	Invitrogen
pPICZa	Pichia expression vector with methanol inducible promoter; expresses proteins extracellularly; contains C-terminal Myc and 6xHis tags; zeocin resistance	Invitrogen
pGAPZa	Pichia expression vector with constitutively active promoter; expresses proteins intracellularly; contains C-terminal Myc and 6xHis tags; zeocin resistance	Invitrogen
pMALc5x	Expression vector with N-terminal maltose binding protein tag and Factor Xa cleavage site; expresses proteins in cytoplasm; ampicillin resistance	New England Biolabs
pMALp5x	Expression vector with N-terminal maltose binding protein tag and Factor Xa cleavage site; expresses proteins in periplasm; ampicillin resistance	New England Biolabs
pMDC99	Gateway compatible destination vector with no tags or promoters; kanamycin resistance	Somerville - 20C plasmid stock
pGWB4	Gateway compatible destination vector with C-terminal GFP tag and no promoter; kanamycin resistance	Somerville - 20C plasmid stock
pGWB16	Gateway compatible destination vector with C-terminal 3x Myc tag and no promoter; kanamycin resistance	Somerville -20 plasmid stock
pYL192 (pTRV1)	Tobacco rattle virus (TRV)-induced gene silencing vector containing TRV movement protein and replicase	Zambryski lab, UC Berkeley
pYL156 (pTRV2)	TRV-induced gene silencing vector containing TRV coat protein and multiple cloning site for restriction digest/ligation cloning strategy	Zambryski lab, UC Berkeley
TRV2-AtPDS	Positive control for TRV-induced gene silencing, silences of phytoene desaturase (PDS)	Zambryski lab, UC Berkeley
TRV2-GUS	Negative control for TRV-induced gene silencing, silences GUS	Zambryski lab, UC Berkeley
TRV2-empty	Negative control for TRV-induced gene silencing	Zambryski lab, UC Berkeley
pTRV2-610	TRV-induced gene silencing construct, silencing 610bp of the N-terminal region of PMR5, including the 5'UTR (up to TBL family conserved C66)	This study
pTRV2-721	TRV-induced gene silencing construct, silencing 721bp of the N-terminal region of PMR5, including the 5'UTR (up to the start of the DUF231 domain)	This study
pP5:P5/pCR8	pPMR5:PMR5 (pCR8-TOPO): 1kb upstream promoter and PMR5 CDS cloned into pCR8	This study
SL/pUC57	pPMR5:PMR5-mCherry-Myc-His (pUC57): 1kb upstream promoter and PMR5 CDS with C-terminal mCherry and Myc and His tags synthesized into pUC57	This study
SL/pMDC99	pPMR5:PMR5-mCherry-Myc-His (pUC57): 1kb upstream promoter and PMR5 CDS with C-terminal mCherry and Myc and His tags cloned into pMDC99	This study

SP/pUC57	pPMR5:PMR5-Myc-His (pUC57): 1kb upstream promoter and PMR5 CDS with C-terminal Myc and His tags (mCherry spliced out) into pUC57	This study
SP/pENTR	pPMR5:PMR5-Myc-His (pENTR-D-TOPO): 1kb upstream promoter and PMR5 CDS with C-terminal Myc and His tags cloned into pENTR-D-TOPO	This study
SP/pMDC99	pPMR5:PMR5-Myc-His (pMDC99): 1kb upstream promoter and PMR5 CDS with C-terminal Myc and His tags (mCherry spliced out) cloned into pMDC99	This study
S142A/pENTR	pPMR5:PMR5 with S142A (pENTR): 1kb upstream promoter and PMR5 CDS with mutated S142A cloned into pENTR	This study
D379A/pENTR	pPMR5:PMR5 with D379A (pENTR): 1kb upstream promoter and PMR5 CDS with mutated D379A cloned into pENTR	This study
H382A/pENTR	pPMR5:PMR5 with H382A (pENTR): 1kb upstream promoter and PMR5 CDS with mutated H382A cloned into pENTR	This study
S142A/pGWB16	pPMR5:PMR5-Myc-His with S142A (pGWB16): 1kb upstream promoter and PMR5 CDS with mutated S142A with C-terminal Myc and His tags; cloned with stop codon before pGWB16 internal C-terminal myc tag	This study
D379A/pGWB16	pPMR5:PMR5-Myc-His with D379A (pGWB16): 1kb upstream promoter and PMR5 CDS with mutated D379A with C-terminal Myc and His tags; cloned with stop codon before pGWB16 internal C-terminal myc tag	This study
H382A/pGWB16	pPMR5:PMR5-Myc-His with H382A (pGWB16): 1kb upstream promoter and PMR5 CDS with mutated H382A with C-terminal Myc and His tags; cloned with stop codon before pGWB16 internal C-terminal myc tag	This study
pP5:P5-Strep/pCR8	pPMR5:PMR5-Strep (pCR8): 1kb upstream promoter and PMR5 CDS with 6x glycine linker and C-terminal streptavidin tag cloned into pCR8	This study
S142A-Strep/pCR8	pPMR5:PMR5-Strep with S142A (pCR8): 1kb upstream promoter and PMR5 CDS with mutated S142A cloned into pCR8	This study
D379A-Strep/pCR8	pPMR5:PMR5-Strep with D379A (pCR8): 1kb upstream promoter and PMR5 CDS with mutated D379A cloned into pCR8	This study
H382A-Strep/pCR8	pPMR5:PMR5-Strep with H382A (pCR8): 1kb upstream promoter and PMR5 CDS with mutated H382A cloned into pCR8	This study
pP5:P5-GFP/ pGWB4	pPMR5:PMR5-GFP (pGWB4): 1kb upstream promoter and PMR5 CDS with C-terminal GFP tag in pGWB4	This study
P5c/pPICZaC	PMR5-Myc-His (pPICZa): PMR5 CDS cloned without signal peptide into pPICZa	This study
DUF/pPICZaC	PMR5DUF231-end(pPICZa): PMR5 CDS truncation from DUF231 to end cloned without signal peptide into pPICZa	This study
P5c/pGAPZaC	PMR5-Myc-His (pGAPZa): PMR5 CDS cloned without signal peptide into pGAPZa	This study
DUF/pGAPZaC	PMR5DUF231-end(pGAPZa): PMR5 CDS truncation from DUF231 to end cloned without signal peptide into pGAPZa	This study
P5c/pMALc	MBP-PMR5-His (pMALc): PMR5 CDS without signal peptide tagged with N-terminal maltose binding protein and C-terminal 6xHis tag in pMALc	This study
P5c/pMALp	MBP-PMR5-His (pMALp): PMR5 CDS without signal peptide tagged with N-terminal maltose binding protein and C-terminal 6xHis tag in pMALp	This study
CG/pMALp	MBP-PMR5C66-end-His (pMALp): N-terminal truncated PMR5 (C66-end) CDS with N-terminal maltose binding protein and C-terminal 6xHis tag in pMALp	This study

Table 2.2. List of primers used in this study

Primer name	Sequence (5' to 3')	Comments
LBb1-3 SALK	ATTTTGCCGATTTCGGAAC	T-DNA genotyping
900 LP	AAGAGCTGGTTCCAGCTATCC	For T-DNA genotyping of At2g30900. Designed with iSect
900 RP	CGGCTTAGATTTTCTGGGAAG	
850 LP	ACGAAGCAGCAGAAGGATGT	For T-DNA genotyping of At3g14850. Designed with Primer3Plus
850 RP	GGTACCCCAGAGAGACACCA	
PMR5 qPCR1 F	ACAATCCGGCGTTTCTTCTC	PMR5 qPCR, from Dawn Chiniquy
PMR5 qPCR1 R	AGGCAAACACCAATGGCTAC	
UBQ5F	GAAGACTTACACCAAGCCGAAG	qPCR housekeeping gene from Wildermuth lab
UBQR	TTCTGGTAAACGTAGGTGAGTCC	
MIOX4 QF	CCTGGTGGCTAAAGAAAACGGAAG	MIOX4 qPCR. Designed with AtRTPrimer
MIOX4 QR	TCCACCGAATTCACCACCTCAA	
TAA1 QF1	ACGGAGGATCGGTACATAGTGGTTG	TAA1 qPCR. Designed with AtRTPrimer
TAA1 QR1	TCCCAACCACTATGTACCGATCCTC	
pPMR5 F	CCTGGTGATATTGAATAG	1kb upstream of PMR5, before next gene
PMR5 no stop R	ATAGATGAGAAGCGTATAC	ends before stop codon in PMR5
P5c F	GCCATTATACTGAGCTTGAAG	PMR5 without 29aa putative signal peptide
C-GDSL F	TGCTCTCTCTTCCTCGG	NT truncated PMR5 starting at C66
P5 Seq 2-2 R	GAACGGAGCTTTGTAAAATG	Sequencing within PMR5
RP F	TCACGTTGATAGATCCCGAAC	Sequencing within PMR5
EcoRI-5UTR	AAGAATTCCAGCTTCCTTTTTTGTTTTC	EcoRI site upstream of 5UTR of PMR5 for VIGS cloning
NT610-KpnI	AAGGTACCGAACGGAGCTTTGTAAAATG	KpnI site downstream of NT region of PMR5 at P5Seq2-2 site. With EcoRI-5UTR, should produce 610bp fragment. For VIGS cloning
D379A	CCAGACCAGTCTGCAGCTTGTAGCCATTGGTG	PMR5 site directed mutagenesis, D379A
D379A Rev	CACCAATGGCTACAAGCTGCAGACTGGTCTGG	
H382A	TCTGCAGATTGTAGCGCTTGGTGTTTGCCTGG	PMR5 site directed mutagenesis, H382A
H382A Rev	CCAGGCAAACACCAAGCGCTACAATCTGCAGA	
S142A	ATGTTTGCGGGTGATGCATTGGGGAAGAATCAATGG	PMR5 site directed mutagenesis, S142A
S142A Rev	CCATTGATTCTTCCCCAATGCATCACCCGCAAACAT	
5' AOX1	GACTGGTTCCAATTGACAAGC	Genotyping insert within Pichia expression plasmids
3' AOX1	GCAAATGGCATTCTGACATCC	
P5c ZaC EcoRI F	AAGAATTCAGCCATTATACTGAGCTTGAAG	PMR5 without signal peptide, Includes EcoRI site for Pichia expression cloning
P5 ZaBC KpnI R	ACTGGTACCAAATAGATGAGAAGCGTATA	PMR5 with KpnI site for Pichia expression cloning
P5nsR strep2	TTATTTTTCGAACTGCGGGTGGCTCCAAGCGCTATAGATGAGAAGCGTATACAAC	Includes link (SA) then Strep tag (WSHPQFEK*). Additional GTT to improve stability
P5-His-SbfI R	TTTCCTGCAGGGTGATGATGATGATGGTGTCCTCCTCCATAGATGAGA	For pMAL E. coli expression cloning; adds 3xGly, 6xHis, and SbfI site (to make dual tagged protein with NT MBP and CT His

Table 2.3. Transgenic plant lines used in this study

Transgenic line	**Genotype**	**Resistance**	**Source**
SALK_147643	Mutation in exon of At2g30900	Kan	ABRC, (Alonso et al., 2003)
CS838817	Mutation in exon of At3g14850	Kan	ABRC, (Alonso et al., 2003)
SALK_130157	Mutation in 3'UTR of *PMR5*	Kan	ABRC, (Alonso et al., 2003)
SALK_034969	Mutation in promoter of *PMR5*	Kan	ABRC, (Alonso et al., 2003)
35S:PMR5-GFP	*pmr5*	unknown	Ginger Brininstool
pPMR5:PMR5-mCherry-Myc-His	*pmr5*	Hyg, Kan (pMDC99)	This study
pPMR5:PMR5-Myc-His	*pmr5*	Hyg, Kan (pMDC99)	This study
pPMR5:PMR5-Myc-His with S142A	*pmr5*	Hyg, Kan (pGWB16)	This study
pPMR5:PMR5-Myc-His with D379A	*pmr5*	Hyg, Kan (pGWB16)	This study
pPMR5:PMR5-Myc-His with H382A	*pmr5*	Hyg, Kan (pGWB16)	This study
pPMR5:PMR5-GFP	*pmr5*	Hyg, Kan (pGWB4)	This study
35S:TBR1-Myc-His-Flash	P5S6	Basta (pCAMBIA)	Bradley Dotson, Frazier Phillips
35S:TBR1-Myc-His-Flash	P5S14	Basta (pCAMBIA)	Bradley Dotson, Frazier Phillips
pTBR1:TBR1-Myc-His-Flash	*tbr1-1*	Basta (pCAMBIA)	Frazier Phillips
pTBR1:TBR1-Myc-His-Flash	*tbr1-1/pmr5*	Basta (pCAMBIA)	Frazier Phillips
pTBR1:TBR1-Myc-His-Flash	P5S6	Basta (pCAMBIA)	Frazier Phillips
pTBR1:TBR1-Myc-His-Flash	P5S14	Basta (pCAMBIA)	Frazier Phillips

Table 2.4. TILLING lines containing mutations in the *PMR5* gene. Stock = from ABRC; PM^R = line prescreened for powdery mildew resistance; BC1 = a PM^R line backcrossed once to Col-0; BC1 selfed = a segregating generation, which needs to be screened for ¼ resistant plants

Name	Mutation	ABRC Stock Name	Stock	PM^R	BC1	BC selfed	Comments
Ti3	M131I	CS92386		x		x	
Ti5	W148*	CS93987		x			Difficult to cross
Ti7	Splice	CS95073	x				Difficult to cross
Ti9	P190S	CS92118		x	x	x	
Ti10	L262F	CS93455	x				Low germination rate
Ti11	V273I	CS94070	x				Low germination rate

Table 2.5. Bioinformatics tools used in this study

Name	Purpose	Web Location	Reference
eFP browser	Arabidopsis gene expression	http://bar.utoronto.ca/efp/cgi-bin/efpWeb.cgi	(Winter et al., 2007)
TAIR	Arabidopsis polymorphisms	http://www.arabidopsis.org	
PHYRE	Secondary structure	http://www.sbg.bio.ic.ac.uk/~phyre/	(Kelley and Sternberg, 2009)
Phylofacts	Structural phylogenomics	http://phylogenomics.berkeley.edu/phylofacts/	(Krishnamurthy et al., 2006)
BLAST	Orthologous sequence alignments	http://blast.ncbi.nlm.nih.gov/Blast.cgi	(Altschul et al., 1997)
Phobius	Signal peptide	http://phobius.sbc.su.se/	(Kall et al., 2004)
PSORT	Subcellular localization	http://psort.hgc.jp/form.html	(Nakai and Horton, 1999)
SignalP 3.0	Subcellular localization	http://www.cbs.dtu.dk/services/SignalP-3.0/	(Bendtsen et al., 2004)
Target P	Subcellular localization	http://www.cbs.dtu.dk/services/TargetP/	(Emanuelsson et al., 2000)
NetOGlyc	O-glycosylation	http://www.cbs.dtu.dk/services/NetOGlyc/	(Julenius et al., 2005)
SUBA	Subcellular localization	http://suba.plantenergy.uwa.edu.au/	(Heazlewood et al., 2005)
ATHENA	Enrichment of *cis* elements	http://www.bioinformatics2.wsu.edu/cgi-bin/Athena/cgi/home.pl	(O'Connor et al., 2005)
AtRTPrimer	Primer design for qRT-PCR	http://atrtprimer.kaist.ac.kr/	(Han and Kim, 2006)

Table 2.6. Fold change of *PMR5* gene expression versus 3-week-old uninfected Col-0 rosette leaves as analyzed by qPCR. Values are means (n=3). Experiments with uninfected leaves and seedlings were repeated twice with similar results. Experiment with infected leaves was repeated once.

	3-week-old rosette leaves	**4-day-old etiolated seedlings**	**3-week-old rosette leaves 5 dpi with *G. cichoracearum***
Col-0	1.00	204.55	20.35
pmr5	0.67	0.68	0.54

Table 2.7. Nonconservative polymorphic differences within At5g58600 (*PMR5*) exons between Col-0 versus Bay-0, C24, Est-1, Ler-1, Tsu-1, Van-0, Goettingen-7, RRS-10, Lov-5, Bor-4, NGA-8, Tamm-2, Fei-0, Bur-0, Br-0, Cvi-0, Sha, Ts-1, RRS-7. Data on polymorphisms found in the Seqviewer of the Arabidopsis Information Resource (http://www.arabidopsis.org). Table modified from Yongqing Li.

gDNA/CDS position	**Col-0**	**Poly-morphism**	**Accession**	**Amino Acid Change (codon change)**	**Polymorphism name**
63/17	C	T	Tsu-1	P6L (CCT>CTT)	ossowski_1050507
66/20	T	G	Tsu-1	L7R (CTT>CGT)	ossowski_1050506
104/58	G	T	Tsu-1, Bur-0	V20L (GTT>TTG)	ossowski_1050504
106/60	T	G	Tsu-1, Bur-0	V20L (GTT>TTG)	ossowski_1050502
1273/795	G	A	pmr5 (Col-0)	W265*(TGG>TGA)	*pmr5* mutation
1565/992	T	C	Bur-0	I331S (TTG>TCG)	PERL1100882
1593/1020	T	A	Bur-0	N340K (AAT>AAA)	ossowski_1050482

Table 2.8. PMR5 signal peptide BLAST results of proteins with shared N-terminal sequences

Name	Sequence ID	Identity	Similarity	Gaps
hypothetical protein CRE_13971 [Caenorhabditis remanei]	ref|XP_003107519.1|	11/14(79%)	11/14(78%)	0/14(0%)
nickel ABC transporter, permease subunit NikB [Streptomyces viridochromogenes DSM 40736]	ref|ZP_07306636.1|	13/21(62%)	14/21(66%)	1/21(4%)
peptide ABC transporter [Streptomyces chartreusis NRRL 12338]	ref|ZP_09957701.1|	13/21(62%)	14/21(66%)	1/21(4%)
sn-glycerol-3-phosphate transport system permease [Ruegeria sp. TW15]	ref|ZP_08863475.1|	13/20(65%)	14/20(70%)	3/20(15%)
hypothetical protein CUS_6319 [Ruminococcus albus 8]	ref|ZP_08160471.1|	13/18(72%)	13/18(72%)	1/18(5%)
putative membrane protein [Helicobacter pylori R32b]	ref|ZP_16152684.1|	12/18(67%)	12/18(66%)	3/18(16%)
hypothetical protein HPHPH43_1131 [Helicobacter pylori Hp H-43]	ref|ZP_14946324.1|	12/18(67%)	12/18(66%)	3/18(16%)
conserved membrane hypothetical protein (Hemolysin/CBS domain) [Wolbachia pipientis wAlbB]	ref|ZP_09542635.1|	11/13(85%)	11/13(84%)	1/13(7%)
NAD(P) transhydrogenase subunit beta [Candidatus Pelagibacter sp. IMCC9063]	ref|YP_004357239.1|	7/10(70%)	7/10(70%)	1/10(10%)

Table 2.9. Phenotypes and genotypes of plant lines used in this study. Gene expression measured by qPCR analysis.

Stage / transgene	**Background**	**Fold Change versus Col-0**	**Growth Phenotype**	***G. cichoracearum* disease phenotype, 10dpi**
4-week-old rosette leaf	Col-0	1	Large	Susceptible
4-week-old rosette leaf	pmr5	-1.97	Small	Resistant
pPMR5:PMR5-Myc-His	pmr5	-1.23	Large	Susceptible
pPMR5:PMR5-mCherry-Myc-His	pmr5	1.06	Large	Susceptible
35S:PMR5-GFP	pmr5	166.54	Large	Susceptible
35S:PMR5-GFP / XT-mCherry	pmr5	69.79	Large*	Susceptible
pPMR5: PMR5-GFP A (homozygous)	pmr5	6.52	Large**	Partially susceptible
pPMR5-PMR5-GFP B (homozygous)	pmr5	-	Large**	Partially susceptible
pPMR5-PMR5-GFP C (homozygous)	pmr5	-	Large**	Partially susceptible
pPMR5-PMR5-GFP (A) / XT-mCherry	pmr5	-	Large*	Susceptible
4-day-old etiolated seedling	Col-0	1	Longer hypocotyl	-
4-day-old etiolated seedling	pmr5	-290.56	Shorter hypocotyl	-

* Phenotype is similar to 35S:XT-mCherry, which has slower growth, but eventually matures to wild-type size.
**Although the leaves are wild-type in size, they are flatter and rounder like *pmr5* leaves. See Figure 2.16c.

Table 2.10. MBP-PMR5-His binding affinity to commercially available polysaccharides. 100µg of polysaccharides was solubilized and spotted on nitrocellulose prior to binding with MBP-PMR5-His, LM5, LM6, or LM13. Cell wall antibodies (LM5, LM6, LM13) are used as controls for polysaccharide binding to nitrocellulose. MBP-PMR5-His = chemilluminescent detection of MBP-PMR5-His binding to polysaccharides. Acetic acid released after saponification of polysaccharides was used to test the acetylation of the polysaccharides. Acetic acid values are means +/- standard error (n=6). ND = not detected. This experiment was repeated twice with similar results.

	MBP-PMR5-His	**LM5 (galactan)**	**LM6 (arabinan)**	**LM13 (arabinan)**	**ng acetic acid / mg AIR**
Pectin (citrus)	116.8	53.3	75.2	16.5	ND
28% est. pectin (citrus)	127.0	32.5	88.0	16.5	ND
67% est. pectin (citrus)	89.1	46.7	106.2	16.4	ND
94% est. pectin (citrus)	124.5	26.9	16.6	16.5	ND
PGA (citrus)	127.0	115.8	83.1	16.7	3043+/-1242
RG (soybean)	19.2	83.7	127.0	25.5	ND
RG I (potato)	79.2	16.6	16.8	16.5	ND
Arabinan (sugar beet)	19.2	18.0	72.9	98.8	ND
Galactan (lupin)	24.0	125.8	39.4	16.6	ND
Arabinogalactan (larch)	49.5	16.7	17.8	16.6	ND
Arabinoxylan (wheat)	29.4	16.5	91.3	50.4	ND
Xyloglucan (tamarind)	18.0	18.5	42.9	40.5	ND

Appendix

Appendix 2.1. Sequence of the pPMR5:PMR5-mCherry-Myc-His construct with restriction enzyme sites (green), cleavage sites (orange), and purification tags (blue). PMR5 promoter is in lowercase black, and PMR5 coding sequence is in uppercase black.

EcoRI-HindIII-PMR5PROM-PMR5-XhoI-SacII-mCHERRY-SalI-FactorXa-MYC-Enterokinase-6xHis

GAATTCAAGCTTcctggtgatattgaatagaaatatagagggtacagtaggagagaggccatgagagtaaggatccctaacctggtgatattgatta
gtagtgcctttgatgctttacatgtgtaatataactgtctagagtcaatctataaataataagatgatagatacgaactgagaaacaagttcaaaga
catcgtgaccattcttggcaattgttcaagcctagagatgataaactaggcttctgatagtgactagagaatccatgaatcttagaaatggtcatag
cttcatacagtttttaactattcttaaattgttttacagggaaataaaaacacaagaagaaaggttgttgatcaagaaagaaaaccgtattgtaaag
ttttactcacgaagaaggtcaaaatgcatgaggttaacatgaagtatgaaccctccaaggttagagcatcctcagatactttgtctccaccacgagt
cctgttcagaatcttcaaacatcaaaggttgagatcttacgattaatgtgtgtataataatcttaagttgggaaacaacccaaatgtgttaatttaa
gaaaagaaaagaaaaaacgaaggaacaaatgcttacctctcttctgacacttgatatatatcattatttattgtatgaagttgccaagttggaaaag
aggaaacatatatgattaagcaaagtattatatgcctttgtgaattgttgtgatcaatagaaaaaagattcatttcaaatgtaattgctaccaataa
taggttgcgtttataaatctaactactaaccatgtgaacatgcagaagaagaaaagaagtccattaaatccttcacatctttagcaatgttgaaatt
tgaagtttatttaaatttatcatatgaccgaataatacaaattttgaaaactgtaaaatattaacacaagtaagaggacccacgtgaagacccatac
ccagttgcacagagacagacacacagatgaaaaatgaaaatctcaaaaaactttctttctttctaaagatatttctccaatctctcaattattttac
agcttcctttttttgttttccacgaaaaagcaaaagaATGGGTTCTCTTCTTCCTCTTCTTGGCATCTCAGTAGTCTCCGCCATTTTCTTTCTGGTTC
TTCAACAACCAGAACAATCTTCTTCAGCCATTATACTGAGCTTGAAGAAACGCCATGGAAGCTCCTCTGGTAGTAGTGGTAACCAGTACAGTTCAAG
CAGACCATCAGCTGGTTTCCAAGGGAACAGGAGCACGTGCTCTCTCTTCCTCGGCACGTGGGTTCGTGATAACTCTTATCCTCTCTATAAACCGGCG
GATTGTCCCGGCGTCGTTGAGCCTGAGTTCGATTGTCAGATGTACGGTCGTCCTGACTCTGACTACCTCAAGTATCGATGGCAACCTCAGAATTGCA
ATTTACCCACGTTCAATGGTGCTCAGTTTCTGTTGAAAATGAAGGGCAAAACCATAATGTTTGCGGGTGATTCATTGGGGAAGAATCAATGGGAGTC
TTTGATCTGCCTTATTGTTTCATCTGCACCGTCCACTCGGACAGAAATGACCAGAGGCTTGCCTCTCTCCACCTTCAGATTCTTGGATTATGGGATA
ACAATGTCATTTTACAAAGCTCCGTTCTTGGTGGACATAGATGCTGTTCAAGGCAAGCGTGTGTTGAAGCTGGATGAGATCTCTGGTAATGCCAATG
CTTGGCATGACGCTGATCTCCTCATCTTCAACACTGGTCACTGGTGGAGCCACACCGGATCTATGCAAGGATGGGACTTGATTCAATCAGGCAATTC
TTATTACCAAGACATGGACCGTTTTGTGGCAATGGAGAAAGCACTTCGTACTTGGGCGTATTGGGTCGAAACTCACGTTGATAGATCCCGAACACAA
GTCTTGTTCCTCTCCATTTCTCCAACACACGACAACCCGAGTGACTGGGCGGCATCATCGTCTTCAGGATCCAAGAACTGCTACGGAGAAACAGAAC
CGATCACAGGAACAGCTTATCCAGTGAGCTCCTACACAGATCAGCTAAGATCAGTGATTGTTGAAGTGCTTCACGGGATGCACAATCCGGCGTTTCT
TCTCGACATAACACTCCTCTCTTCCCTAAGAAAAGACGGTCATCCGTCAGTATACAGCGGCCTCATTAGCGGTTCACAAAGGTCTAGACCAGACCAG
TCTGCAGATTGTAGCCATTGGTGTTTGCCTGGTTTACCTGATACATGGAACCAGTTGTTGTATACGCTTCTCATCTATACTAGTCCGCGGatggtga
gcaagggcgaggaggataacatggccatcatcaaggagttcatgcgcttcaaggtgcacatggagggctccgtgaacggccacgagttcgagatcga
gggcgagggcgagggccgcccctacgagggcacccagaccgccaagctgaaggtgaccaagggtggccccctgcccttcgcctgggacatcctgtcc
cctcagttcatgtacggctccaaggcctacgtgaagcaccccgccgacatccccgactacttgaagctgtccttccccgagggcttcaagtgggagc
gcgtgatgaacttcgaggacggcggcgtggtgaccgtgacccaggactcctccctgcaggacggcgagttcatctacaaggtgaagctgcgcggcac
caacttcccctccgacggccccgtaatgcagaagaagaccatgggctgggaggcctcctccgagcggatgtaccccgaggacggcgccctgaagggc
gagatcaagcagaggctgaagctgaaggacggcggccactacgacgctgaggtcaagaccacctacaaggccaagaagcccgtgcagctgcccggcg
cctacaacgtcaacatcaagttggacatcacctcccacaacgaggactacaccatcgtggaacagtacgaacgcgccgagggccgccactccaccgg
cggcatggacgagctgtacaagGCTAGCatcgagggtaggGAACAAAAACTTATTTCTGAAGAAGATCTGgacgatgacgataagCACCATCACCAC
CATCACTAG

Appendix 2.2. PMR5 sequence submitted for TILLING service.

ctccgccattttctttctggttcttcaacaaccagaacaatcttcttcagccattatactgagcttgaagaaacgccatg
gaagctcctctggtagtagtggtaaccagtacagttcaagcagaccatcagctggtttccaagggaacaggagcacgtgc
tctctcttcctcggcacgtgggttcgtgataactcttatcctctctataaaccggcggattgtcccggcgtcgttgagcc
tgagttcgattgtcagatgtacggtcgtcctgactctgactacctcaagtatcgatggcaacctcagaattgcaatttac
ccacgtatgtacacatactcatcttcttcttctttctttttttgtcataaagttttctaattttcgtggttaaatctttga
gttttctggtaatagtgtatacctgtgtcgttattggtaatgaggttcgatttcgtcagaattttactgagctaagttgt
caaaatgtattcttttggcaaacccatttgaaagaattctactttaagatattacgactgctcaaaatcagagattctgt
ggttttagtgtttgatttctggtctttcacaaatggattaggttcaatggtgctcagtttctgttgaaaatgaagggcaa
aaccataatgtttgcgggtgattcattggggaagaatcaatgggagtctttgatctgccttattgtttcatctgcaccgt
ccactcggacagaaatgaccagaggcttgcctctctccaccttcagattcttggtaatgctttcttcttattcttcaatg
gctcacatcttgtttttcaggttcttctataagaaaactgttttttgatgtataggattatgggataacaatgtcatttt
acaaagctccgttcttggtggacatagatgctgttcaaggcaagcgtgtgttgaagctggatgagatctctggtaatgcc
aatgcttggcatgacgctgatctcctcatcttcaacactggtcactggtggagccacaccggatctatgcaagggtaagt
taccacacttccaatgacttgattttctagtgtgaaagtttctttatatatcttcttgtgaacacagatgggacttgatt
caatcaggcaattcttattaccaagacatggaccgttttgtggcaatggagaaagcacttcgtacttgggcgtattgggt
cgaaactcacgttgatagatcccgaacacaagtcttgttcctctccatttctccaacacacgacaagtaactcagcctct
cttgttatattggatcatattttctgatgtttttgaaatgaatgtcctgacaccatttgtatacattttgggattgatca
gcccgagtgactgggcggcatcatcgtcttcaggatccaagaactgctacggagaaacagaaccgatcacaggaacagct
tatccagtgagctcctacacagatcagctaagatcagtgattgttgaagtgcttcacgggatg

CHAPTER 3: Identifying potential *pmr5*-mediated disease resistance pathway partners

Introduction

Although it has been shown that PMR5 affects the acetylation of cell wall pectin, it is still unknown how PMR5 is involved in powdery mildew susceptibility. Since *pmr5*-mediated disease resistance works independently of the SA, JA, and ET pathways, it was hypothesized that there was another pathway associated with the cell wall changes in the mutant (Vogel et al., 2004). Alteration of the cell wall composition does not impact the penetration efficiency of the fungus, as the host mildew is able to successfully form haustoria at rates comparable to wild-type (Vogel et al., 2004). However, fungal hyphal growth is decreased and conidiation does not occur in the mutant, suggesting that there may be an internal plant-signaling network involved after fungal haustorial formation.

Two hypotheses were developed to understand *pmr5*-mediated disease resistance. The first hypothesis is that the *pmr5* mutant has an altered cell wall that is perceived as cell wall damage, constitutively activating the cell wall integrity (CWI)-signaling pathway and defense mechanisms. The second hypothesis is that the *pmr5* mutant is actively defending itself upon perception of the fungus, thus there would be induced gene expression soon after infection. This second hypothesis would resemble PAMP triggered immunity signaling (review of PTI, (Zipfel, 2009)). To test these two hypotheses and to identify potential pathway partners, ATH1 microarrays were used to monitor changes in expression trends between wild-type and *pmr5*.

The use of microarrays has been instrumental for large-scale mining of expression changes and identification of pathways (Orlando et al., 2009). Due to the widespread use of microarrays, several tools have been developed to integrate the vast amount of data available after each experiment (eFP browser, (Winter et al., 2007); Genevestigator, genevestigator.com). Several studies using microarrays to decipher powdery mildew resistance pathways have been done successfully (Fabro et al 2008; Chandran et al 2009; Chandran et al 2010). Thus, using microarrays to identify downstream pathway partners in the *pmr5* mutant seemed promising

Materials and Methods

Microarray sample preparation and experimental design

Uninfected tissue: Total RNA was extracted from three-week-old rosette leaves in biological triplicates using the RNeasy Plant Mini kit (Qiagen) with the on-column DNaseI treatment according to the manufacturer's protocol. Seeds were sown on potted soil and stratified for 2 nights at 4ºC before flats were transferred to a short day growth chamber. The plants were grown under short day conditions (12/12 h light/dark) with photosynthetically active radiation of 100 $\mu E\ m^{-2}\ s^{-1}$, 70% relative humidity, and 22ºC during the day and 20ºC during the night. Microarray hybridizations to Affymetrix ATH1 arrays and array scanning were performed by the Functional Genomics Laboratory (UC Berkeley). Raw microarray data for this experiment is described in NCBI Gene Expression Omnibus GSE39708.

Infected tissue: Total RNA was extracted from three-week-old rosette leaves in biological triplicates that were 5 dpi with *G. cichoracearum* using the RNeasy Plant Mini kit (Qiagen) with the on-column DNaseI treatment according to the manufacturer's protocol. Seeds were sown on potted soil and stratified for 2 nights at 4ºC before flats were transferred to a short day growth chamber. The plants were grown under short day conditions (12/12 h light/dark) with photosynthetically active radiation of 100 $\mu E\ m^{-2}\ s^{-1}$, 70% relative humidity, and 22ºC during the

day and 20ºC during the night. 3 weeks post stratification, rosette leaves were inoculated with *G. cichoracearum* and transferred to a growth chamber with 16 h light with photosynthetically active radiation of 100µE m^{-2} s^{-1}, 22ºC day and 20ºC night, and 75% relative humidity. Leaf tissue from biological triplicates containing leaves from 4-5 plants per pot was flash frozen in liquid nitrogen at 5 dpi. Powdery mildew disease symptoms on the remaining plants were assayed prior to isolating RNA. Microarray hybridizations to Affymetrix ATH1 arrays and array scanning were performed by the Functional Genomics Laboratory (UC Berkeley).

Expression analysis software
Expression values (log2) for three independent biological replicates per genotype were extracted using robust multiarray analysis using Partek Genomics Suite (http://www.partek.com) and CLC Genomics Workbench (http://www.clcbio.com/products/clc-genomics-workbench/). Data was subjected to quantile normalization and summarization by median polish. Relative log expression and normalized unscaled standard error box plots were used to confirm the uniform distribution of signal intensities across arrays and to assess reproducibility within replicates. Lists of differentially expressed genes were annotated and categorized with Mapman 3.5 (http://mapman.gabipd.org/web/guest/mapman, (Thimm et al., 2004)) and VirtualPlant 1.3 (http://virtualplant.bio.nyu.edu/cgi-bin/vpweb/, (Katari et al., 2010)).

qPCR verification of microarray data
qPCR was performed on RNA extracted from an independent experiment (separate but similar to microarray). Total RNA was extracted from three-week-old rosette leaves using the RNeasy Plant Mini kit (Qiagen) with the on-column DNaseI treatment according to the manufacturer's protocol. 1µg of RNA was used to synthesize cDNA using the ProtoScript M-MulV Taq RT-PCR kit (NEB), following the manufacturer's protocol. qPCR reactions were performed using SYBR GreenER qPCR SuperMix Universal (Invitrogen) on an Applied Biosystems Step One Plus Real Time-PCR machine. The amplification conditions were as follows: 50°C for 2 m, 95°C for 10 m; 40 cycles of 95°C for 15 s and 60°C for 60 s. Expression values were extracted using ΔΔCt method (Livak and Schmittgen, 2001), and normalized to that of the endogenous control Ubiquitin5 (UBQ5). For all genes, three technical replicates and four biological replicates were performed. The absence of primer-dimer formation was confirmed by performing a melting-curve and specificity of the primers was verified by performing National Center for Biotechnology Information primer BLAST searches.

Results

Gene expression trends support PMR5's role in cell wall modification.

A microarray experiment was done to examine gene expression in uninfected 3-week-old rosette leaves from wild-type (Col-0) and *pmr5*, as well as three other lines for suppressor analysis. Analysis on the suppressor lines in comparison to Col-0 and *pmr5* can be found in Chapter 4. For this section, only gene expression between Col-0 and *pmr5* are compared. A false discovery rate (FDR)-corrected p-value < 0.01 was used to sort differentially expressed genes between Col-0 and *pmr5* uninfected 3-week old rosette leaves. With this analysis, only two genes were identified that were differentially expressed in wild-type versus *pmr5*: At3g27050 (uncharacterized) and At1g70560 (TAA1, TRYPTOPHAN AMINOTRANSFERASE OF

ARABIDOPSIS 1) (Table 3.1). However, the TAA1 expression difference could not be replicated by qPCR analysis of similarly grown plants (data not shown).

It is likely that any transcriptional changes that would differentiate Col-0 from *pmr5* are subtle due to the plant's ability to adapt early on to important structural changes such as modification to the cell wall. To reveal any subtle transcriptional changes, 800 genes that passed a one-way ANOVA test with an unadjusted pval<0.05 and $\log_2$ fold changes >1 or <-1 were assembled to input into Mapman. An overview of the pathways reveals several interesting trends. Genes were sorted into BINs and using the Wilcoxon rank sum test, a list of BINs that were overrepresented was generated (Table 4.2).

The top two categories in the Mapman analysis are genes involved in cell wall processes and transcriptional regulation. The cell wall-related gene changes include processes of synthesis, degradation, and modification. This suggests that PMR5 may be directly involved in cell wall architecture, as several cell wall-related genes are differentially regulated in the mutant. In addition, many genes involved in transcriptional regulation were included in this set, including several WRKY transcription factors (WRKYs 11, 20, 22, 30, 33, and 53).

Gene expression changes in 5dpi leaves with *G. cichoracearum*

As the list of statistically significant differences in gene expression between uninfected wild-type and *pmr5* plants was limited, a second experiment was done using plants that were inoculated with *G. cichoracearum*. Five days post inoculation was chosen as the collection time point based on the finding that there was differential hyphal growth between wild-type and *pmr5* plants 5 days post inoculation (Vogel and Somerville, 2000; Vogel et al., 2004). *MIOX4* was the only hit that was found using FDR corrected p value < 0.05 (Table 4.3). qPCR confirms the difference in expression of *MIOX4*, where *MIOX4* is 285 times more induced in 5 dpi *pmr5* versus 5 dpi wild-type (Table 4.4). In uninfected tissue, *MIOX4* is 132 times more expressed in *pmr5* than in wild-type (Table 4.4). Infection resulted in a two-fold induction of *MIOX4* in wild-type, and a four-fold induction in *pmr5*. MIOX4 exists in a pathway for nucleotide sugar biosynthesis for cell wall polysaccharide (Kanter et al., 2005); however, no other genes in the pathway were differentially expressed as observed from the microarray data. Due to the limited number of genes generated with unadjusted p<0.05, there were no pathways highlighted in Mapman that gave a significant p-value based on the Wilcoxon rank sum test. An analysis of overrepresented *cis* elements from the list of 33 genes identified an enrichment of MYB2AT and CARGCW8GAT motifs (Table 4.5).

Comparison of uninfected versus infected tissue

Using Partek and CLC Genomics Workbench analysis software, several gene lists were generated based on pval<0.05. 33 genes were identified from the 5 dpi array experiment, and 244 genes shared between Partek and CLC were identified from the uninfected array experiment. Four genes were shared between the two groups (intersection, Virtual Plant, virtualplant.bio.nyu.edu) (Table 4.6). Comparing the two datasets, three of the four genes showed the same expression trends regardless of the pathogen treatment. This suggests that MIOX2, At1g13650, and At3g27050 expression changes are constitutive effects of the *pmr5* mutant. On the other hand, the gene expression change in ARR16 is an induced effect. When uninfected, *ARR16* expression is higher in Col-0, but after infection, *ARR16* expression is higher

in *pmr5* plants, suggesting an induction of *ARR16* expression in *pmr5* plants.

Discussion

To start to understand *pmr5*-mediated disease resistance, we analyzed expression data from uninfected and infected *pmr5* plants to determine whether *pmr5*-mediated resistance is a constitutive or induced effect. Few changes in expression were found when comparing uninfected wild-type and mutant plants. We relaxed the statistics to see if we could find trends, knowing that the list created would need to be verified by other means. The *pmr5* mutant had several cell wall related expression changes, which seems to be a theme of several altered disease resistance mutants (see introduction). These were expected based on the cell wall phenotypes we had characterized. In terms of potential defense pathways constitutively activated in uninfected plants, *pmr5* plants had upregulated expression in WRKY transcription factors and genes involved with secondary metabolism. Several WRKY transcription factors are induced with chitin and are associated with defense responses (Pandey and Somssich, 2009; Rushton et al., 2010). Glucosinolates have been shown to play a role in plant defense against insect herbivory (Grubb and Abel, 2006), and indolyl glucosinolates have been shown to be important for defense against microbial pathogens (Bednarek et al., 2009; Clay et al., 2009). Despite these trends, no clear pathway stood out that would represent a distinct CWI-signaling pathway.

One candidate that could be involved in *pmr5*-mediated disease resistance is *MIOX4* (*MYO-INOSITOL OXYGENASE 4*), a gene highly upregulated in the *pmr5* mutant compared to wild-type in both uninfected and infected rosette leaves. Interestingly, *MIOX4* is typically expressed in flowers and not in leaves. Inositol oxygenases are involved in a secondary pathway for the biosynthesis of nucleotide sugar precursors for cell wall polysaccharides, including pectin (Kanter et al., 2005). None of the other pathway players were differentially expressed, suggesting that this particular pathway is not involved, and that perhaps MIOX4 is recruited individually for *pmr5*-mediated powdery mildew disease resistance. MIOX2 was also upregulated in the *pmr5* mutant based on our microarray results, but has yet to be confirmed by qRT-PCR. MIOX2 has been shown to be induced when under low nutrient or low energy conditions (Alford et al., 2012), and its activity was found to have a positive correlation with cell wall uronic acid content in tomato (Cronje et al., 2012). The fact that two of four MIOX genes are represented in our small list of 33 differentially expressed genes between infected wild-type and *pmr5* plants is intriguing and worth investigating.

In a comparison of the uninfected and infected datasets, only ARR16 showed a differential trend in expression upon infection. ARR16 is a response regulator involved in cytokinin signaling (Kiba et al., 2002). Exogenous application of cytokinins (specifically, zeatin or zeatinriboside) was found to increase resistance of wheat against wheat powdery mildew in a dose dependent manner (Babosha, 2009). Cytokinins have been shown to intersect with salicylic acid signaling in immunity (Choi et al., 2011). However, we know that SA is not involved in *pmr5*-mediated disease resistance based on previous double mutant analysis (Vogel et al., 2004). Interestingly, Grosskinsky *et al*. found that cytokinins can work independent of SA signaling to increase phytoalexin synthesis and defense against *P. syringae* in tobacco (Grosskinsky et al., 2011). Cytokinins have also been shown to be important for cell cycle regulation (Dewitte et al., 2007). ARR16 is an interesting candidate and should be further investigated.

Recently, a separate analysis of our *pmr5* expression data led Chandran *et al.* to hypothesize that PMR5 may be taking part in cell cycle regulation and affecting powdery mildew

induced endoreduplication needed for enhanced metabolism to sustain fungal growth (Chandran et al., 2013). They found several cell cycle signatures based on an analysis of shared *cis* elements in the *pmr5* microarray dataset. Moreover, they found that the *pmr5* mutant also lacked induced ploidy after inoculation with the fungus, similar to the *myb3r4* transcription factor mutant, already implicated in cell cycle regulation (Chandran et al., 2013). When unphosphorylated, the MYB3R4 transcription factor is hypothesized to repress mitosis in the normal cell cycle, which is required for pathogen-induced endoreduplication (Chandran et al., 2010). They presented a model in which PMR5 works upstream of the MYB3R transcription factors that regulate the normal cell cycle. In the *pmr5* mutant, altered regulation of MYB3R transcription factors could affect the accumulation of unphosphorylated MYB3R4 needed to repress mitosis for pathogen-induced endoreduplication. Therefore, by affecting the cell cycle and inhibiting enhanced metabolic activity from powdery mildew-induced endoreduplication, Chandran *et al*. concluded that PMR5 is a susceptibility determinant for powdery mildew disease (Chandran et al., 2013).

The pathway between PMR5's role in the cell wall and its role in powdery mildew-induced endoreduplication is unknown. We obtained a few candidate partners that may be involved in *pmr5*-mediated disease resistance. Some of these genes have been previously characterized for their roles in pathogen defense, and include those that encode the WRKY transcription factors, ARR16 from the cytokinin signaling pathway, and genes involved with secondary metabolites. Other genes, like the myo-inositol oxygenases and those involved in cell cycle regulation, are less characterized for their roles in defense, and may be ideal candidates for investigating the hypothesis that PMR5 is involved in a CWI-sensing pathway. The most intriguing finding from these microarray experiments is that of PMR5's role in powdery mildew-induced endoreduplication. Exactly how PMR5's role in the cell wall is linked to endoreduplication is unknown. Other approaches will be needed to determine how these two phenomena are linked.

Tables

Table 3.1. Differentially expressed genes between uninfected Col-0 and *pmr5* 3-week-old rosette leaves based on false discovery rate (FDR)-corrected p-value<0.01.

Locus ID	**Gene name**	**ANOVA FDR p-value**	**Max fold change**	**Col-0 means**	***pmr5* means**	**P5S6 means**	***tbr1-1* means**	***tbr1-1/ pmr5* means**
At3g27050	Unknown	1.04E-4	-1.59	9.88	6.30	9.61	9.66	6.22
At1g70560	TAA1	8.39E-3	1.27	5.13	6.50	5.29	5.22	5.38

Table 3.2. Mapman 3.5 gene expression analysis of differentially expressed genes between uninfected Col-0 and *pmr5* 3-week-old rosette leaves based on unadjusted p-value<0.05. BH = Benjamini-Hochberg correction for false discovery rate

BIN	BIN name	elements	p-value	BH p-value
10	cell wall	26	0.000050	0.019404
27.3	RNA.regulation of transcription	68	0.000933	0.167171
27	RNA	80	0.001299	0.167171
16.5	secondary metabolism.sulfur-containing	3	0.004440	0.391486
10.2	cell wall.cellulose synthesis	5	0.006085	0.391486
10.2.1	cell wall.cellulose synthesis.cellulose synthase	5	0.006085	0.391486
26.12	misc.peroxidases	4	0.012745	0.702785
27.3.32	RNA.regulation of transcription.WRKY domain transcription factor family	5	0.015691	0.757098
33.1	development.storage proteins	2	0.022217	0.784519
16.5.1	secondary metabolism.sulfur-containing.glucosinolates	2	0.022658	0.784519
27.3.9	RNA.regulation of transcription.C2C2(Zn) GATA transcription factor family	2	0.027501	0.784519
27.3.22	RNA.regulation of transcription.HB,Homeobox transcription factor family	6	0.028369	0.784519
30.3	signalling.calcium	5	0.029193	0.784519
10.6.3	cell wall.degradation.pectate lyases and polygalacturonases	3	0.031028	0.784519
10.6	cell wall.degradation	3	0.031028	0.784519
10.7	cell wall.modification	6	0.037567	0.784519
27.3.25	RNA.regulation of transcription.MYB domain transcription factor family	9	0.045112	0.784519
30.2	signalling.receptor kinases	14	0.048986	0.784519

Table 3.3. Differentially expressed genes in *pmr5* compared to wild-type Col-0 (pval<0.01), five days post inoculation with *G. cichoracearum.* Negative fold change indicates up regulation in *pmr5*

Locus	Gene Title	Fold-Change of Col-0 versus pmr5
AT4G26260	MIOX4; inositol oxygenase	-21.8499
AT2G19800	MIOX2 (MYO-INOSITOL OXYGENASE 2); inositol oxygenase	-9.05823
AT4G19430	---	-6.34746
AT5G41080	glycerophosphoryl diester phosphodiesterase family	-5.02174
AT3G30775	ERD5 (EARLY RESPONSIVE TO DEHYDRATION 5); proline dehydrogenase	-4.58242
AT1G80130	Tetratricopeptide repeat (TPR)-like superfamily protein	-4.50762
AT2G44080	ARL (ARGOS-LIKE)	-3.54989
AT5G47130	Bax inhibitor-1 family / BI-1 family	-3.44951
AT2G44240	[Vitis vinifera] DUF239	-3.20812
AT1G32450	NRT1.5 (NITRATE TRANSPORTER 1.5); nitrate transmembrane transporter/ transporter; proton-dependent oligopeptide transport (POT) family protein	-3.20089
AT3G15720	glycoside hydrolase family 28 protein / polygalacturonase (pectinase) family protein	-3.11956
AT2G41210	PIP5K5 (PHOSPHATIDYLINOSITOL- 4-PHOSPHATE 5-KINASE 5); 1-phosphatidylinositol-4-phospha	-2.78543
AT1G10970	ZIP4 (ZINC TRANSPORTER 4 PRECURSOR); cation transmembrane transporter/ copper ion trans	-2.51531
AT1G25530	lysine and histidine specific transporter, putative	-2.42805
AT5G44210	ERF9 (ERF DOMAIN PROTEIN 9); DNA binding / transcription factor/ transcription repressor	-2.23305
AT2G40670	ARR16 (ARABIDOPSIS RESPONSE REGULATOR 16); transcription regulator/ two-component response regulator	-2.23081
AT5G28030	DES1, L-CYSTEINE DESULFHYDRASE 1; cysteine synthase, putative / O-acetylserine (thiol)-lyase, putative / O-acetylserine sulfhydrylase, putative	-2.18498
AT5G50335	---	-2.14722
AT2G38180	GDSL-motif lipase/hydrolase family protein	-2.08491
AT1G60960	IRT3; cation transmembrane transporter/ metal ion transmembrane transporter	-2.0744
AT4G21830, AT4G21840	MSRB8 methionine sulfoxide reductase domain-containing protein / SeIR domain-containing protein	2.00544
AT1G75900	family II extracellular lipase 3 (EXL3)	2.03255
AT1G04040	acid phosphatase class B family protein	2.12631
AT1G54040	ESP (EPITHIOSPECIFIER PROTEIN); enzyme regulator	2.20081
AT1G01120	KCS1 (3-KETOACYL-COA SYNTHASE 1); acyltransferase/ fatty acid elongase	2.39241
AT5G03120	---	2.41136
AT1G13650	similar to 18S pre-ribosomal assembly protein gar2-related	2.59043
AT5G58600	PMR5 (POWDERY MILDEW RESISTANT 5)	2.75921
AT1G76240	[Oryza sativa] DUF241	2.8888
AT5G24150	SQP1; squalene monooxygenase	3.84803
AT4G12490	protease inhibitor/seed storage/lipid transfer protein (LTP) family protein	4.48067
AT3G27050	---	16.996

Table 3.4. Fold change of *MIOX4* gene expression versus uninfected Col-0 as analyzed by qPCR. Values are means (n=3).

	Uninfected 3-week-old rosette leaves	**3-week-old rosette leaves 5 dpi with *G. cichoracearum***
Col-0	1.00	1.85
pmr5	132.73	529.89

Table 3.5. Overrepresented *cis* elements within gene list from Table 3.3 as analyzed by ATHENA with p-value<0.05

TF/motif	**promoters in subset (33)**		**promoters in genome (30067)**		**pval**
TATA-box	90%	30	75%	22707	0.023
CARGCW8GAT	78%	26	53%	16208	0.002
MYB2AT	42%	14	23%	7097	0.012

Table 3.6. Common genes between Col-0 and *pmr5*, uninfected and five days post inoculated with *G. cichoracearum,* with differentially expression and at least 2-fold change. Negative fold change indicates up regulation in *pmr5*

Locus	**Gene**	**Infected, fold change of Col-0 versus pmr5**	**Infected, pval**	**Uninfected, fold change of Col-0 versus pmr5**	**Uninfected, pval**	**Gene description**
At2g19800	MIOX2	-9.05823	0.001059	-2.60035	1.66E-05	MIOX2 (MYO-INOSITOL OXYGENASE 2); inositol oxygenase
At1g13650	?	2.59043	0.005153	2.14993	0.00216811	similar to 18S pre-ribosomal assembly protein gar2-related
At2g40670	ARR16	-2.23081	0.006105	1.71191	0.00100521	ARR16 (ARABIDOPSIS RESPONSE REGULATOR 16); transcription regulator/ two-component response regulator
At3g27050	?	16.996	0.000376	17.9585	5.27E-09	

CHAPTER 4: Suppressors of *pmr5*-mediated disease resistance

Introduction

To understand the mechanism behind *pmr5*-mediated disease resistance, a suppressor screen was done to isolate genetic suppressors that were susceptible to *G. cichoracearum* in the *pmr5* background (John Vogel, unpublished). Twenty suppressors were isolated, with leaf phenotypes ranging from *pmr5*-like to wild-type like, and growth phenotypes that included even smaller plants than *pmr5* (Fig. 4.1). The smaller stature of *pmr5* was attributed to a decrease in cell expansion (Vogel et al., 2004). As cell growth and expansion is largely influenced by cell wall constriction, it can be hypothesized that suppressors that are larger, like wild-type plants, likely affect the cell wall and could shed light on the role of PMR5 in the cell wall. Thus, two suppressors that looked wild-type-like were chosen for mapping: suppressor 6 (P5S6) and suppressor 20 (P5S20).

Materials and Methods

PCR-based mapping

P5S6 and P5S20 (Col-0) were crossed with Ler and left to self to obtain the F2 segregating populations. The F2 generation was screened for the *pmr5* background by genotyping using CAPS markers as in (Konieczny and Ausubel, 1993) and powdery mildew susceptibility to obtain the mapping population (1/16 of total plants). Individual segregants were pooled for bulk segregation analysis with PCR markers to narrow down mapping to a specific chromosome before finer mapping as in (Michelmore et al., 1991). Candidates in each suppressor were sequenced.

Microarray sample preparation and experimental design

Uninfected tissue: Total RNA was extracted from three-week-old rosette leaves in biological triplicates using the RNeasy Plant Mini kit (Qiagen) with the on-column DNaseI treatment according to the manufacturer's protocol. Seeds were sown on potted soil and stratified for 2 nights at 4ºC before flats were transferred to a short day growth chamber. The plants were grown under short day conditions (12/12 h light/dark) with photosynthetically active radiation of 100 $\mu E\ m^{-2}\ s^{-1}$, 70% relative humidity, and 22ºC during the day and 20ºC during the night. Microarray hybridizations to Affymetrix ATH1 arrays and array scanning were performed by the Functional Genomics Laboratory (UC Berkeley). Raw microarray data for this experiment is described in NCBI Gene Expression Omnibus GSE39708.

Expression analysis software

Expression values (log2) for three independent biological replicates per genotype were extracted using robust multiarray analysis using Partek Genomics Suite (http://www.partek.com) and CLC Genomics Workbench (http://www.clcbio.com/products/clc-genomics-workbench/). Data was subjected to quantile normalization and summarization by median polish. Relative log expression and normalized unscaled standard error box plots were used to confirm the uniform distribution of signal intensities across arrays and to assess reproducibility within replicates. Lists of differentially expressed genes were annotated and categorized with Mapman 3.5 (http://mapman.gabipd.org/web/guest/mapman, (Thimm et al., 2004)) and VirtualPlant 1.3 (http://virtualplant.bio.nyu.edu/cgi-bin/vpweb/, (Katari et al., 2010)).

Whole genome sequencing of P5S20

Genomic DNA was isolated from 5-day-old etiolated seedlings using the DNeasy Plant Mini kit (Qiagen) following the manufacturer's protocol. DNA was sent to the UC Davis Genome Center Core Services (http://www.genomecenter.ucdavis.edu/core-facilities/) for preparation of a 300bp paired end insert library and whole genome sequencing using Illumina Genome Analyzer II.

Results

P5S6 and P5S14 are mutant alleles of TBR

Identification of TBR as a suppressor of pmr5

With work by Frazier Phillips and a collaboration with Bradley Dotson from Chris Somerville's group, P5S6 was identified to have a mutation in *TBR1,* a gene encoding a member of the same protein family as PMR5. The suppressor mutation in P5S6 was rough mapped to the top arm of chromosome 5, in an area close to the locus of *TBR1* (Frazier Phillips, unpublished; Table 4.1). In parallel, a cross between *pmr5* and *tbr1-1* (single point mutation), and between *pmr5* and *tbr1-2* (T-DNA insertion) was made to understand the relationship between the two cloned TBL members (Bradley Dotson, unpublished). *pmr5* resistance to the native powdery mildew is suppressed when in a *tbr1-1* and *tbr1-2* background, indicating that the *TBR1* mutation is a suppressor of *pmr5* mediated resistance. The candidate gene *TBR1* was sequenced in P5S6 and a single nucleotide polymorphism (G1287A) was found that converted an early tryptophan in the DUF231 domain (pfam03005) to an early stop (W429*) (Fig. 4.2). This single nucleotide polymorphism is not found in the *TBR1* gene in *pmr5*. Based on early trichome birefringence screens of the *pmr5* suppressors, P5S6 and P5S14 were identified as potential *tbr1* mutant alleles (Bradley Dotson, unpublished). P5S14 also contains a single nucleotide polymorphism (G779A) in *TBR1* that converts G260D (Fig. 4.2).

To confirm that the *TBR1* gene corresponds to the suppressor 6 and suppressor 14 locus, several test crosses were made (Table 4.2). If P5S6 and P5S14 contain mutations in the *TBR1* gene, all of the F1 progeny from crosses with *pmr5/tbr1* lines should be susceptible to powdery mildew. If P5S6 and P5S14 are not allelic, the *TBR1* mutation should be complemented by a wild-type *TBR1* allele and the progeny should all be resistant to powdery mildew like *pmr5*. These lines have yet to be tested for disease resistance. A cross was also made between P5S6 x *tbr1-1*. 100% of the F1 had reduced trichome birefringence, indicating that P5S6 contains a mutation in *TBR1* (Bradley Dotson, unpublished) (Table 4.2). The F2 was harvested, but has yet to be tested for disease resistance.

To corroborate the genetic complementation efforts, several transgenic lines were generated to show molecular complementation with the *TBR1* gene (Table 4.3). It had previously been shown that a *p35S:TBR1-Myc-His-Flash* construct could complement *tbr1-1* and *tbr1-2*, but not *pmr5* (Bradley Dotson, unpublished). P5S6 and P5S14 were transformed with the same construct to determine whether it could complement the suppressors back to a *pmr5* phenotype. Nine individual BASTA resistant T1 plants containing the *p35S:TBR1* transgene in the P5S6 background were genotyped and found to all contain the transgene; however, all of them were susceptible (Table 4.3). Primers were designed at the 3' end of the transgene, and with BASTA resistance at the 5' end of the transgene, genotyping would have isolated the full transgene. It is possible that although these T1s have the transgene, they are not expressed due to silencing of the over expression construct.

A native promoter construct was generated to transform *tbr1-1,* as well as *tbr1-1/pmr5* (Frazier Philipps). Morphologically, *pTBR1:TBR1* complements *tbr1-1/pmr5*, as all of these plants look *pmr5*-like. However, *pTBR1:TBR1* does not complement P5S6 or P5S14 (Table 4.3). The T2 seed was collected for future genotyping and disease phenotyping.

Morphology and disease phenotyping of tbr1, P5S6, and P5S14

To confirm that the *tbr1* mutant is a suppressor of *pmr5*-mediated powdery mildew disease resistance, the disease phenotypes of the *tbr1* mutants were assayed after inoculation with *G. cichoracearum*. Eight days post inoculation, wild-type Col-0 showed signs of infection, whereas *pmr5* did not. The single mutants, *tbr1-1* and *tbr1-2*, as well as the original suppressors in the *pmr5* background, P5S6 and P5S14, were susceptible. *tbr1-1/pmr5* and *tbr1-2/pmr5* were also susceptible, confirming that *TBR1* is a suppressor of *pmr5*-mediated disease resistance (Fig. 4.3a).

The *tbr1* mutant is characterized by its reduced trichome birefringence (Bischoff et al., 2010). The *tbr1-1* allele seems to have a stronger effect than the *tbr1-2* allele, as the trichome birefringence phenotype was less apparent in the *tbr1-2* allele. Both P5S6 and P5S14 have reduced trichome birefringence like *tbr1-1*, indicating that both suppressor lines have mutations in *TBR1* (Fig. 4.3b). Similarly, the *tbr1-1/pmr5* mutant had *tbr1-1*-like trichome birefringence (Bradley Dotson, unpublished).

In addition to the its powdery mildew disease resistance phenotype, *pmr5* plants are about 20% smaller than wild-type (Vogel et al., 2004). This size difference is also seen at the seedling stage, including light-grown roots and dark grown hypocotyls. To characterize the suppression of *pmr5* by *tbr1*, plants were phenotyped and quantified based on seedling root growth, etiolated seedling hypocotyl elongation, rosette diameter, rosette leaf shape (length versus width), trichome birefringence, and powdery mildew disease symptoms (with Frazier Phillips and Brad Dotson, unpublished).

pmr5 has roughly 20% shorter roots than wild-type at five days post stratification, and this root phenotype is rescued in P5S6, but not P5S14. *tbr1-1* and *tbr1-2* also had shorter roots, similar to *pmr5*. *tbr1-1/pmr5* looked similar to P5S6, showing longer roots. However, *tbr1-2/pmr5* did not show the same rescuing effects as *tbr1-1/pmr5* (Fig. 4.3c). Five-day old etiolated *pmr5* seedlings had shorter hypocotyls than wild-type. The *tbr1* alleles did not show a hypocotyl phenotype. The suppressors and the *tbr1* double mutants all showed wild-type length hypocotyls. Thus, *tbr1* shows suppression of *pmr5*'s decreased hypocotyl length (Fig. 4.3d). The rosette diameters were measured to represent the smaller mature plants of *pmr5*. *tbr1-1* also has slightly smaller rosettes, whereas the T-DNA knockout allele *tbr1-2* does not. Consistent with the shorter roots of P5S14 seedlings, P5S14 also had much smaller rosettes. The *tbr1* double mutants all had wild-type rosette diameters (Fig. 4.3e). As *pmr5* leaves have rounder leaves, the ratio of the length versus width of each leaf blade was measured. Rounder leaves would have a length to width ratio closer to 1. Other than P5S14, which had rounder leaves than *pmr5*, all of the other lines showed wild-type length to width ratios (Fig. 4.3f)

Comparing gene expression across pmr5, tbr1, and P5S6

A microarray experiment including Col-0, *pmr5*, P5S6, *tbr1-1,*and *pmr5/tbr1-1* was done to compare transcripts among the mutant, the suppressor, and wild-type. Rosette leaves from 3-week-old plants were harvested for RNA and probed on ATH1 microarray chips in triplicate. Only four genes were extracted from an ANOVA analysis of genotype with FDR-corrected p-

value <0.1. When the FDR-corrected p-value was relaxed to <0.5 (genotype pval<0.5), 154 genes were extracted. When the data was grouped by phenotype, where *pmr5* is resistant, and all other genotypes are susceptible, a list of 26 genes was generated with FDR p-val <0.1 (phenotype pval<0.1). With stringent statistics (FDR p-val<0.01), 5 genes were extracted after ANOVA analysis by phenotype.

Since we could not obtain a robust list of genes, only trends could be inferred from the gene lists generated with weaker p-values. The gene lists, genotype pval<0.5 and phenotype pval<0.1, were intersected with Virtual Plant to find those common and shared between the two lists. This list represented the genes involved in *pmr5*-mediated disease resistance. When the genotype list was restricted to FDR-corrected p-val<0.2, only three of nine genes were annotated: TAA1, MIOX2, and MYB23 (Table 4.4). Inputting this list into Virtual Plant Biomaps did not yield any interesting or clear functional categories that were overrepresented.

T-tests between each genotype were used to create gene lists in CLC Genomics Workbench based on a p-value <0.05. Comparisons between P5S6 versus *pmr5* and *tbr1-1/pmr5* versus *pmr5* were made to represent the gene expression changes responsible for the suppression of *pmr5*. These gene lists were inputted into Mapman and tested with the Wilcoxon Rank Sum, which organized the genes into BIN categories and calculated p-values based on the overrepresentation of a particular BIN category over the others.

In comparing P5S6 with *pmr5*, the cell wall related gene expression changes in *pmr5* were missing, but new possibly defense related transcripts (ethylene, abscisic acid, phenylpropanoids) appeared. Lipid-related transcripts also appeared in this list (Table 4.5). An analysis of *tbr1-1/pmr5* compared to *pmr5* gene expression showed a mixture of changes in cell wall transcripts, defense related transcripts, and lipid metabolism (Table 4.6).

The lack of overlap was unexpected, based on the assumption that P5S6 and *tbr1-1/pmr5* shared mutations in both *TBR1* and *PMR5*. It is likely that there are background mutations in P5S6 to explain the difference in gene expression. Virtual Plant was used to intersect gene lists from Tables 18 and 19 to find overlapping genes and to remove any background. From a list of 2016 genes from P5S6 v *pmr5* and 1224 genes from *tbr1-1/pmr5* v *pmr5*, 326 genes overlapped. When the new list of 326 genes was submitted to Mapman, cell wall transcript changes seen in *pmr5* appeared, as well as lipid metabolism related transcripts (Table 4.7). To confirm the lipid metabolism trend, this gene list was also subjected to Virtual Plant. From 2094 genes from P5S6 v *pmr5* and 1266 genes from *tbr1-1/pmr5* v *pmr5*, 356 genes overlapped. This tool also pointed towards lipid metabolism based on a summary of GO terms (Table 4.8).

P5S20 and P5S3 contain splice site mutations in RWA2

P5S20 was mapped using PCR-based mapping techniques to the top arm of chromosome 3 close to the GAPC marker with a recombination frequency of 17% (Table 4.9). P5S20 was subjected to whole genome sequencing to identify all single nucleotide polymorphisms (SNPs) and insertions or deletions (indels). 3362 total homozygous genomic variants were found, with 292 variants on chromosome 3. The 292 homozygous variants on chromosome 3 were annotated using EnsemblPlants Variant Effect Predictor (http://plants.ensembl.org/tools.html). 55 nonsynonymous changes were found, including SNPs and indels that altered frameshift coding and splice sites, and introduced early stop codons (Table 4.10).

Interestingly, At3g05660 was a shared gene variant in P5S3 as well. At3g05660 encodes *RWA2 (REDUCE WALL ACETYLATION 2*). *RWA2* has been shown to be involved in acetylation

of cell wall polysaccharides (Manabe et al., 2011). Interestingly, *RWA2* was shown to act in the same pathway as *AXY4 (ALTERED XYLOGLUCAN 4)* (Gille et al., 2011), which is a TBL family member. P5S20 was crossed with P5S3 to test whether the mutations were allelic, and indeed the double mutant was still susceptible to powdery mildew even in the *pmr5* mutant background (Heidi Szemenyei, unpublished; Fig. 4.4). Thus, P5S20 and P5S3 are mutant alleles of *RWA2*, and *rwa2* is a suppressor of *pmr5*.

FTIR analysis of P5S6 and P5S20

Previously, *pmr5* cell walls were analyzed by FTIR, which led Vogel *et al*. to hypothesize that PMR5 may be involved in pectin biosynthesis or modification (Vogel et al., 2004). Cell walls isolated from wild-type and *pmr5* form distinct clusters by PCA (principle component analysis) (Vogel et al., 2004). To determine whether the wild-type like suppressors had reverted cell wall phenotypes, cell walls from P5S6 and P5S20 were prepared for analysis by FTIR spectroscopy. Both P5S6 and P5S20 form their own clusters separate from *pmr5* and wild-type, suggesting that the cell walls of the suppressors are not wild-type like and that other cell wall changes have occurred that compensate for the *pmr5* cell wall change to suppress the resistance phenotype (Fig. 4.5). Analysis of the PC eigenvectors responsible for the separation of Col and *pmr5* clusters did not reveal the same pectin spectral peaks (data not shown).

Other potential suppressors of PMR5

The suppressors that have been identified so far are directly related to the cell wall. Although suppressors were chosen that looked more wild-type to identify cell wall-related partners, many of the other suppressors that were isolated had morphological phenotypes more similar to *pmr5*. These suppressors are likely involved in signaling downstream of the cell wall phenotypes.

As more evidence has accumulated to support the role of PMR5 in pectin acetylation (this work), a mutation in *PMR5* is likely causing cell wall changes that could be recognized by the CWI-signaling pathway. There is likely a CWI-sensor that is recognizing the altered cell wall in the *pmr5* mutant, making CWI-sensor candidates good *pmr5* suppressor candidates as well. BAK1 may be a good sensor candidate since it has been shown to be nonspecific to several processes (Cyril Zipfel, personal communication). To test this, a genetic cross was made between *pmr5* and *bak1-5* and the F1 was allowed to self to form the segregating F2 population. To determine whether *bak1* is a suppressor of *pmr5*, plants with *pmr5*-like morphology and resistance should be genotyped to determine whether *bak1-5/bak1-5* plants can be found. If there are no *bak1-5/bak1-5 pmr5/pmr5* plants in this resistant population, then *bak1* is a suppressor of *pmr5*. The F2 seed is available for this genetic test.

Discussion

We hypothesized that the resistance phenotype of *pmr5* is dependent upon cell wall modification that is somehow altered in the suppressors. We identified four suppressors at two loci, both of which affect the plant cell wall. *tbr* mutants are characterized by their lack of trichome birefringence, due to an 80% reduction in cellulose abundance, as well as altered pectin composition (Bischoff et al., 2010). Identification of *tbr1* as a suppressor of *pmr5* corroborates

our findings that PMR5 is affecting pectin. *rwa2* mutants have a reduction in overall acetylation of cell wall polymers (Manabe et al., 2011). The decrease in acetylation in *pmr5* cell walls and the identification of *rwa2* as a suppressor of *pmr5* strongly suggests that PMR5 has a role in cell wall acetylation. Thus, identification of these cell wall mutants as suppressors of *pmr5* provide more evidence in PMR5's role in the acetylation of cell wall pectin, but how they suppress *pmr5*-mediated resistance is still unknown.

We began to characterize the suppression of *pmr5* by *tbr1*. *tbr1-1/pmr5* plants, as well as *tbr1-2/pmr5* plants are susceptible to the host mildew. Moreover, single point mutations in *TBR1* were found in two of the isolated *pmr5* suppressors, P5S6 and P5S14. We prepared several test crosses and transgenic lines for genetic and molecular complementation tests to determine whether a mutation in the *TBR* locus is the cause for *pmr5* suppression in P5S6 and P5S14, or whether there is an additional locus responsible for the suppression. We also began to characterize the morphological and growth phenotypes of the *TBR1* related lines, and show that P5S6 and *tbr1-1/pmr5* suppress the growth phenotypes associated with *pmr5*. P5S6 may be suppressing *pmr5* upstream of the pleiotropic morphological and growth phenotypes seen in the mutant plants. In contrast, P5S14 did not rescue the morphological phenotypes.

Gene expression analyses comparing transcripts from *pmr5* with P5S6 and *tbr1-1/pmr5* show that several cell wall-related transcripts are differentially expressed, and possibly genes involved in lipid metabolism. This is interesting because many lipases contain the GDSL motif, which is shared among all the TBL protein members. Lipases are esterases that catalyze lipids, components of the plant cuticle. Interestingly, both P5S6 and *tbr1* stained more strongly with toluidine blue, a dye used to test the permeability of the cuticle (Bradley Dotson, unpublished). This suggests that P5S6 and *tbr1* have more permeable cuticles, possibly due to the changes in lipid composition suggested by the altered lipid-related gene expression data. Although there are several cases of cuticle based defense (review, (Reina-Pinto and Yephremov, 2009)), none of the cuticular wax genes were differentially expressed. qPCR verification of these genes is still needed to confirm the changes seen in the microarray experiments.

There are still several *pmr5* suppressors that have yet to be identified. Analysis of suppressors without wild-type morphology should reveal more downstream players in *pmr5*-mediated disease resistance. Additionally, candidate players in the CWI pathway can also be tested for the suppression of *pmr5*, which may tell us more about *pmr5*-mediated disease resistance and its role in the CWI-signaling pathway.

Figures

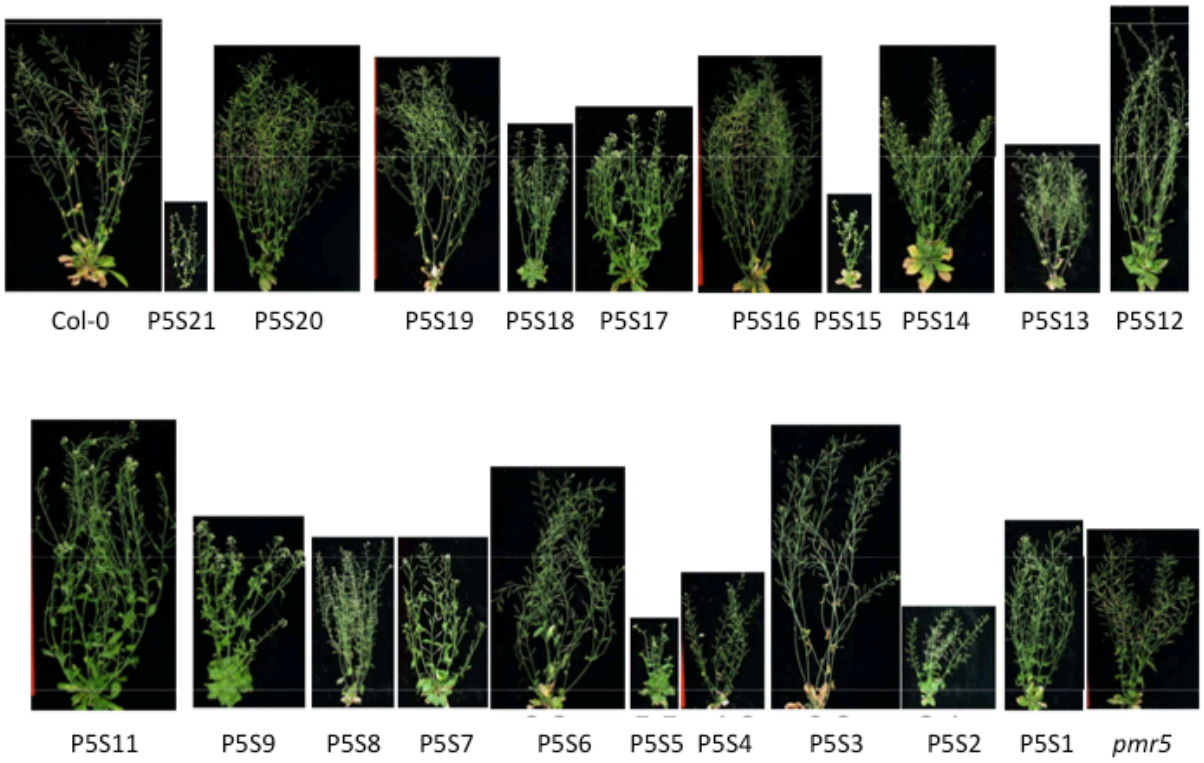

Figure 4.1. Growth phenotypes of the genetic suppressors of *pmr5*-mediated powdery mildew disease resistance. All *pmr5* suppressors are susceptible to *G. cichoracearum*. Figure modified from Bi Huei Hou.

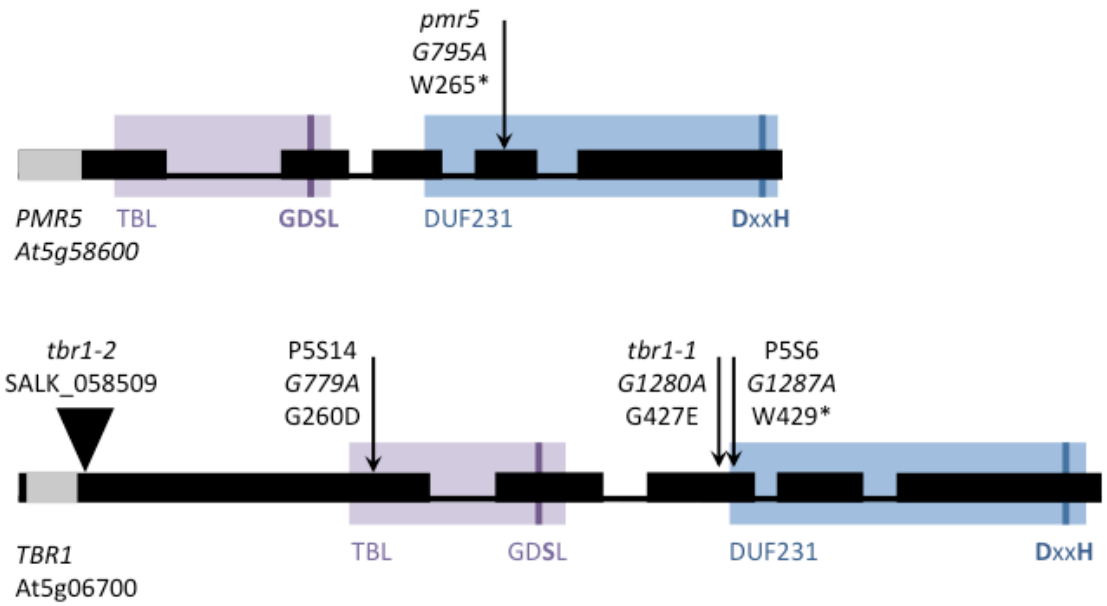

Figure 4.2. Gene diagram of *PMR5* and *TBR1* displaying nucleotide and amino acid changes in relevant mutants. Gray bars indicate hydrophobic regions. Purple (TBL domain) and light blue (DUF231, pfam03005) background bars indicate TBL family conserved regions. Dark purple (S from GDSL) and dark blue (DxxH in DUF231 domain) bars indicate putative catalytic residues.

A

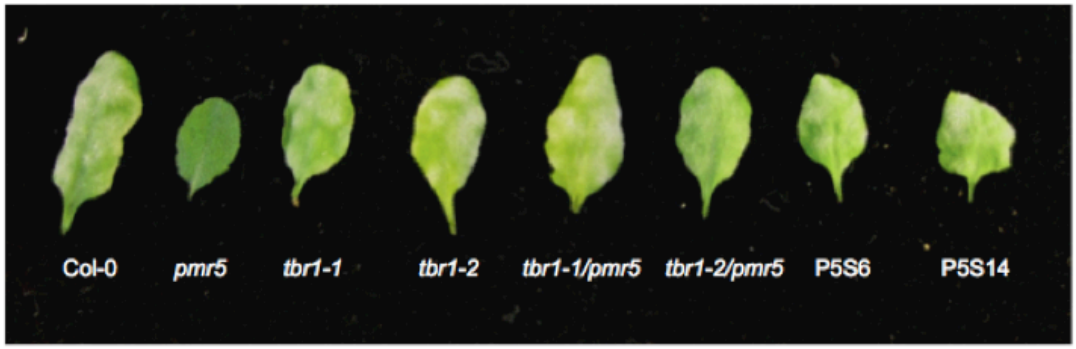

B

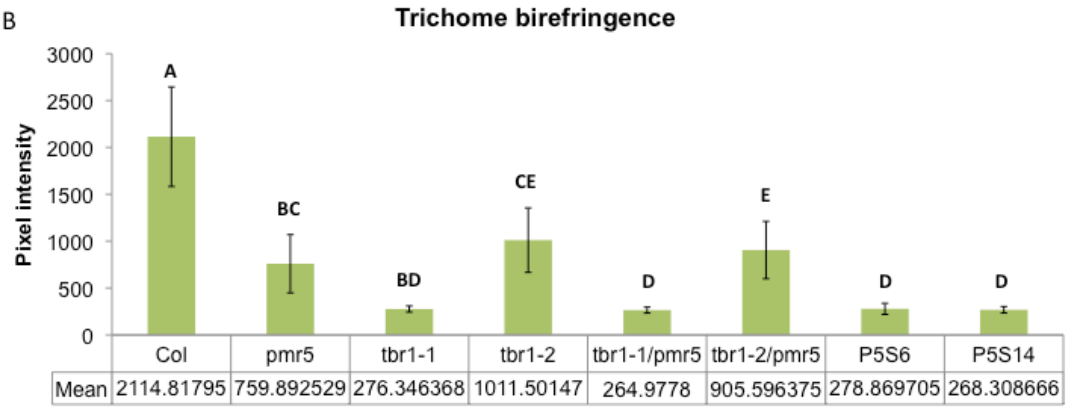

	Col	pmr5	tbr1-1	tbr1-2	tbr1-1/pmr5	tbr1-2/pmr5	P5S6	P5S14
Mean	2114.81795	759.892529	276.346368	1011.50147	264.9778	905.596375	278.869705	268.308666

C

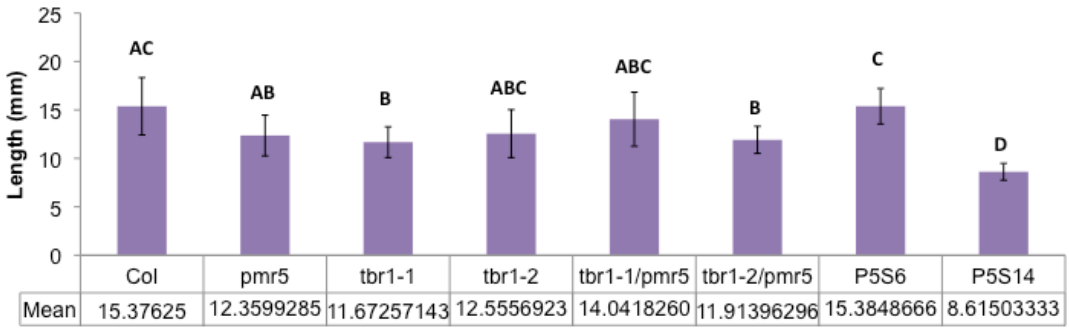

	Col	pmr5	tbr1-1	tbr1-2	tbr1-1/pmr5	tbr1-2/pmr5	P5S6	P5S14
Mean	15.37625	12.3599285	11.67257143	12.5556923	14.0418260	11.91396296	15.3848666	8.61503333

D

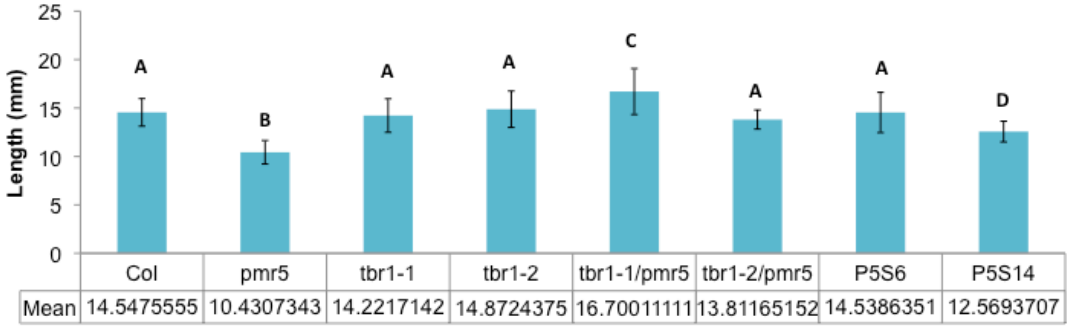

	Col	pmr5	tbr1-1	tbr1-2	tbr1-1/pmr5	tbr1-2/pmr5	P5S6	P5S14
Mean	14.5475555	10.4307343	14.2217142	14.8724375	16.70011111	13.81165152	14.5386351	12.5693707

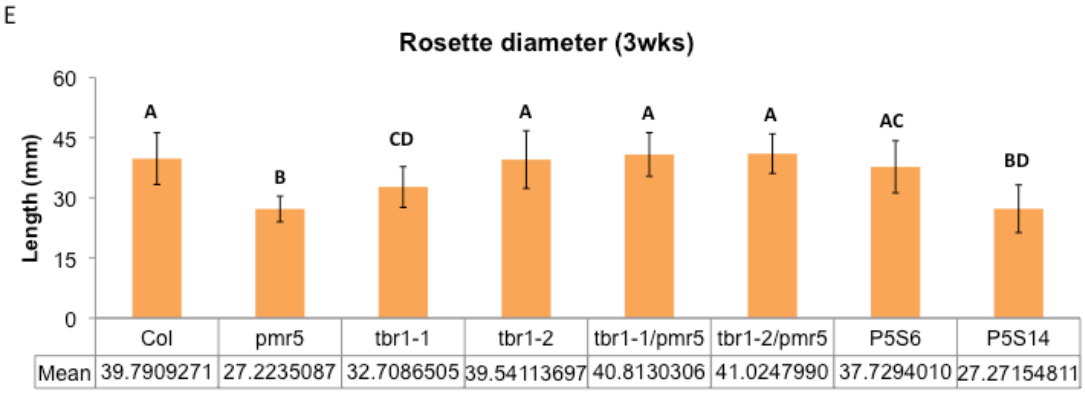

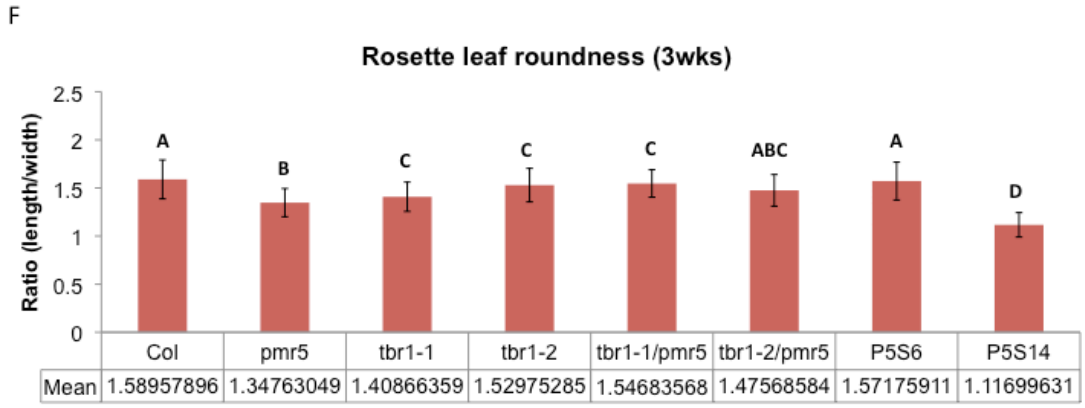

Figure 4.3. Morphological characterization of lines in this study. Data from Bradley Dotson (b), and Frazier Phillips (c-f).
(a) 3 week old plants were infected with *G. cichoracearum*, and representative leaves were collected and photographed 8dpi.
(b) Trichome birefringence was imaged using anti-phase polarlized light microscopy. The brightest frond in focus was used to calculate pixel intensity with ImageJ. Values shown are means +/- standard deviation (n>15). Statistical significance based on one way ANOVA on Ranks using Dunn's method ($p<0.05$)
(c) Root lengths after 5 days growth on 1/2 MS plates. Values shown are means +/- standard deviation (n>13). Statistical significance based on one way ANOVA on Ranks using Dunn's method ($p<0.05$)
(d) Hypocotyl lengths after 5 days etiolated growth on ½ MS plates. Values shown are means +/- standard deviation (n>68). Statistical significance based on one way ANOVA on Ranks using Dunn's method ($p<0.05$)
(e) Rosette diameter measured across the two largest leaves from 3-week-old rosettes. Values shown are means +/- standard deviation (n>10). Statistical significance based on one way ANOVA, Tukey test ($p<0.05$)
(f) Leaf roundness (length/width) of two oldest leaves from 3-week-old rosettes. Values shown are means +/- standard deviation (n>32). Statistical significance based on one way ANOVA on Ranks using Dunn's method ($p<0.05$)

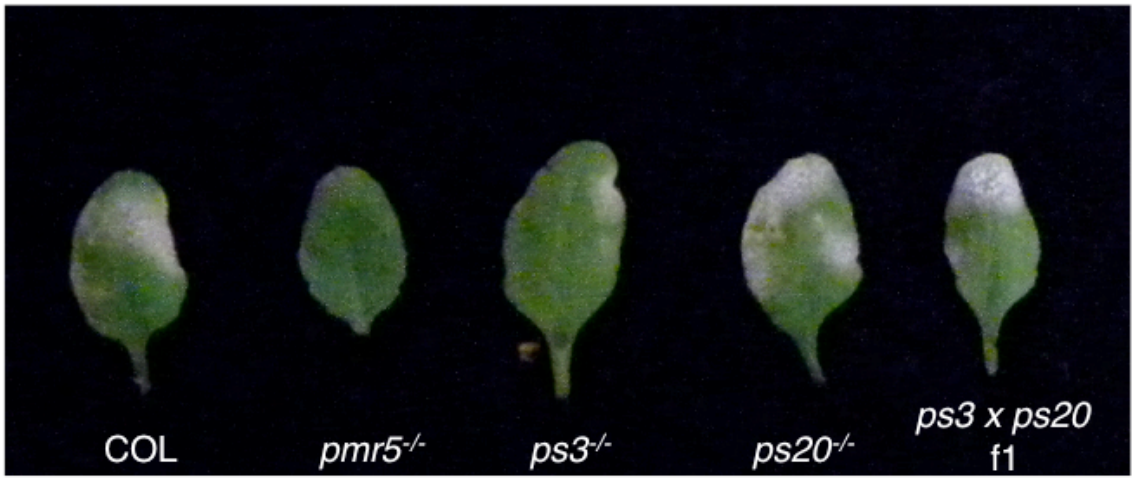

Figure 4.4. Allelism test between P5S20 (*ps20*) and P5S3 (*ps3*), both of which have splice site mutations in *RWA2*. A mutation in *RWA2* is responsible for suppression of *pmr5*-mediated disease resistance in P5S20 and P5S3. Figure from Heidi Szemenyei.

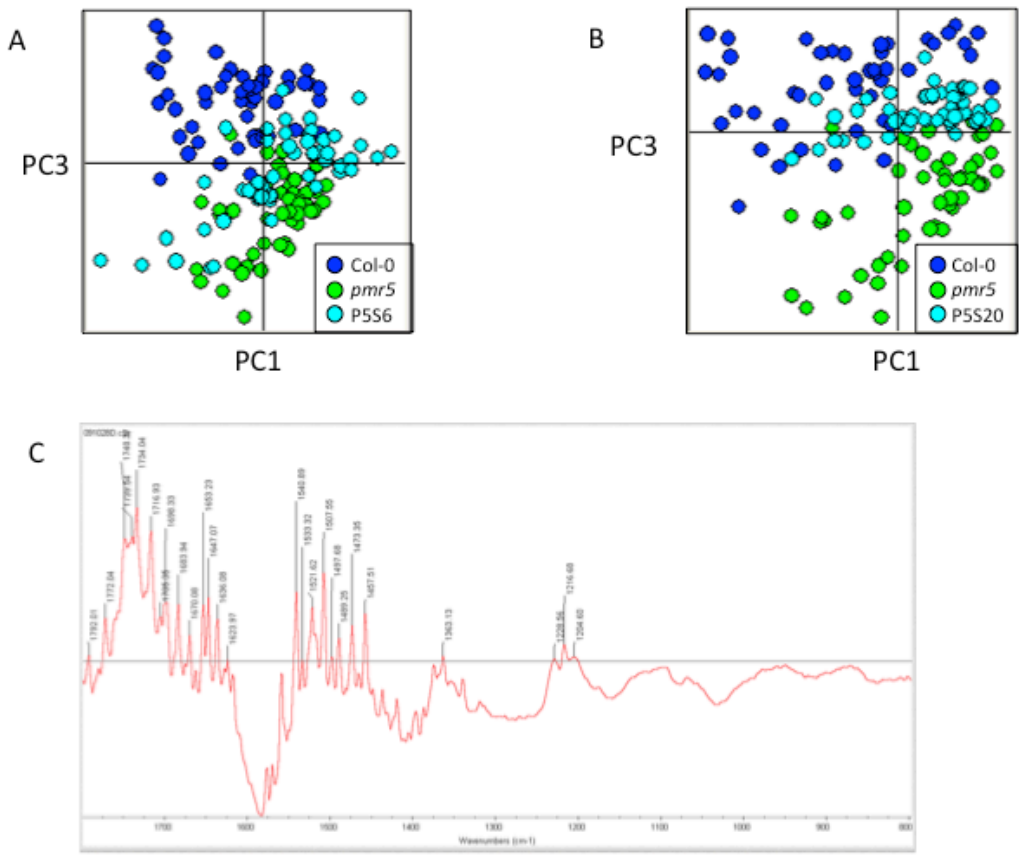

Figure 4.5. PCA analysis of FTIR spectra from cell walls isolated from 3-week-old rosette leaves. PCA biplot of FTIR spectral data showing separation of Col and pmr5 clusters, with suppressor clusters overlaid. Col-0, dark blue; *pmr5*, green; suppressor, light blue.
(a) P5S6 cell walls do not cluster with Col-0 or *pmr5* cell walls.
(b) P5S20 cell walls may cluster more with Col-0 than *pmr5*.
(c) PC3 eigenvector from b. accounting 14% of variance between Col-0 and P5S20 clusters versus *pmr5* cluster. Peaks were not assigned.

Tables

Table 4.1. P5S6 mapping data for the suppressor 6 locus at genetic locus ciw14 with a mapping population of 52 segregants, all in the *pmr5* mutant background

	ciw14
Recombinants, Ler	3
Mutants, Col	52
Heterozygotes	3
Recombination frequency	8.65%
Genetic distance from *TBR1*	8.65 cM

Table 4.2. Test crosses generated for genetic complementation of P5S6, P5S14, and *tbr1/pmr5*

Cross	**Expected Phenotype**	**Actual phenotype**
tbr1-1/pmr5 x P5S6	100% Susceptible in F1	Not tested
tbr1-1/pmr5 x P5S14	100% Susceptible in F1	Not tested
tbr1-2/pmr5 x P5S6	100% Susceptible in F1	Not tested
tbr1-2/pmr5 x P5S14	100% Susceptible in F1	Not tested
P5S6 x *tbr1-1*	100% reduced trichome birefringence in F1	100% reduced trichome birefringence in F1
P5S6 x *tbr1-1* selfed F2	100% susceptible in F2 (even with 25% homozygous *pmr5* background)	Not tested

Table 4.3. Transgenic lines generated for molecular complementation of P5S6 and P5S14 with *TBR1*. PM, powdery mildew.

Transgene	Background	Seed	Expected Phenotype	Actual phenotype
35S:TBR1-Myc-His-Flash	*tbr1-1*	T1	WT trichome birefringence	WT trichome birefringence
	tbr1-2	T1	WT trichome birefringence	WT trichome birefringence
	pmr5	T1	PM resistant (no complementation)	PM resistant
	P5S6	T1	PM resistant (complementation)	PM susceptible (silenced construct?)
	P5S14	T1	PM resistant (complementation)	PM susceptible (silenced construct?)
pTBR1:TBR1-Myc-His-Flash	*tbr1-1*	T1	WT trichome birefringence	Not tested
	tbr1-1/pmr5	T1	PM resistant (complementation)	*pmr5*-like morphology. Disease not tested
	P5S6	T1	PM resistant (complementation)	WT-like morphology. Disease not tested
	P5S14	T1	PM resistant (complementation)	WT-like morphology. Disease not tested

Table 4.4. Gene list intersected genotype pval<0.5 and phenotype pval<0.1, representing genes involved in *pmr5*-mediated disease resistance

Gene Symbol	AGI	Target	Unadjusted p-value
TAA1	AT1G70560	Tryptophan aminotransferase of Arabidopsis; SHADE AVOIDANCE 3, SAV3; WEAK ETHYLENE INSENSITIVE 8, WEI8; CYTOKININ INDUCED ROOT CURLING 1, CKRC1	8.92E-07
---	AT1G25530	Lysine and histidine specific transporter, putative similar to lysine and histi	3.35E-05
MIOX2	AT2G19800	myo-inositol oxygenase activity, oxidation-reduction process, syncytium formation	4.18E-05
---	AT1G32190	alpha/beta-Hydrolases superfamily protein, N-terminal protein myristoylation, hydrolase activity, metabolic process, plasma membrane	5.28E-05
---	AT2G22080	En/Spm-like transposon protein related to En/Spm transposon family of maize	7.18E-05
---	AT5G06330	harpin-induced protein-like, Late embryogenesis abundant (LEA) hydroxyproline-rich glycoprotein family	8.34E-05
MYB23	AT5G40330	myb-related protein, Encodes a MYB gene that, when overexpressed ectopically, can induce ectopic trichome formation.	9.31E-05
---	AT5G25460	putative protein hypothetical protein - Ricinus communis, EMBL:Z81012;supported	0.000173055
---	AT3G27180	S-adenosyl-L-methionine-dependent methyltransferases superfamily protein; FUNCTIONS IN: methyltransferase activity; chloroplast, methyltransferase activity, rRNA methylation	0.000180818
ACS4	AT2G22810	1-aminocyclopropane-1-carboxylate synthase (ACS4) identical to GB:U23481; suppor	0.000319852
---	AT2G22420	putative peroxidase, cytosol, heme binding, oxidation-reduction process, peroxidase activity, response to oxidative stress	0.000322753
---	AT1G11850	LOCATED IN: endomembrane system	0.0004318
---	AT3G02930	DUF827, LOCATED IN: chloroplast	0.000484866
---	AT2G33850	LOCATED IN: endomembrane system	0.000491643
---	AT5G54530	LOCATED IN: endomembrane system	0.000534921
---	AT1G19980	cytomatrix protein-related	0.000617152
ZPR1	AT2G45450	ZPR1, a small leucine zipper-containing protein that interacts with REV HD-ZIPIII and is involved in the establishment of leaf polarity.	0.0010476
---	AT2G36670	Eukaryotic aspartyl protease family protein; FUNCTIONS IN: aspartic-type endopeptidase activity; INVOLVED IN: proteolysis; LOCATED IN: endomembrane system	0.00145402
WSD1	AT5G37300	Encodes a bifunctional enzyme, wax ester synthase (WS) and diacylglycerol acyltransferase (DGAT). In vitro assay indicated a ratio of 10.9 between its WS and DGAT activities. Both mutant and in vivo expression/analysis in yeast studies indicated a role in wax biosynthesis	0.00150734
---	AT3G05600	alpha/beta-Hydrolases superfamily protein; putative epoxide hydrolase	0.00159243
---	AT3G31410	transposable element, DUF287	0.00163429
---	AT4G13710	putative pectate lyase A11 ; supported by cDNA: gi_15983435_gb_AF424592.1_AF424	0.00248272

Table 4.5. Mapman 3.5 gene expression analysis of differentially expressed genes between uninfected P5S6 and *pmr5* 3-week-old rosette leaves based on unadjusted p-value<0.05. BH = Benjamini-Hochberg correction for false discovery rate.

BIN	BIN name	elements	p-value	BH pval
27	RNA	210	0.00000	0.00000
27.3	RNA.regulation of transcription	174	0.00000	0.00000
34	transport	105	0.00000	0.00000
26.10	misc.cytochrome P450	21	0.00000	0.00058
16	secondary metabolism	47	0.00003	0.00341
28	DNA	70	0.00004	0.00341
28.1	DNA.synthesis/chromatin structure	59	0.00004	0.00341
26.9	misc.glutathione S transferases	10	0.00013	0.00987
26.2	misc.UDP glucosyl and glucoronyl transferases	11	0.00014	0.00987
17.5.2	hormone metabolism.ethylene.signal transduction	5	0.00020	0.01268
16.2	secondary metabolism.phenylpropanoids	11	0.00025	0.01470
20.1.7	stress.biotic.PR-proteins	18	0.00043	0.02331
17.1	hormone metabolism.abscisic acid	10	0.00127	0.06309
13	amino acid metabolism	27	0.00186	0.08589
11.9	lipid metabolism.lipid degradation	12	0.00212	0.09179
16.2.1	secondary metabolism.phenylpropanoids.lignin biosynthesis	7	0.00282	0.10221
27.3.40	RNA.regulation of transcription.Aux/IAA family	5	0.00282	0.10221
11	lipid metabolism	46	0.00284	0.10221
17	hormone metabolism	64	0.00401	0.13676
5	fermentation	7	0.00549	0.17784
26.21	misc.protease inhibitor/seed storage/lipid transfer protein (LTP) family	11	0.00646	0.19811
16.4.1	secondary metabolism.N misc.alkaloid-like	8	0.00727	0.19811
20.1	stress.biotic	38	0.00744	0.19811
16.4	secondary metabolism.N misc	9	0.00768	0.19811

Table 4.6. Mapman 3.5 gene expression analysis of differentially expressed genes between uninfected *tbr1-1/pmr5* and *pmr5* 3-week-old rosette leaves based on unadjusted p-value<0.05. BH = Benjamini-Hochberg correction for false discovery rate.

BIN	BIN name	elements	p-value	BH p-value
27.3.25	RNA.regulation of transcription.MYB domain TF family	5	0.00281	0.66904
27.3	RNA.regulation of transcription	113	0.00373	0.66904
26.21	misc.protease inhibitor/seed storage/lipid transfer protein (LTP) family	6	0.00582	0.66904
17.6.1	hormone metabolism.gibberelin.synthesis-degradation	4	0.00770	0.66904
30.2.17	signalling.receptor kinases.DUF 26	4	0.00946	0.66904
27.3.67	RNA.regulation of transcription.putative transcription regulator	8	0.00956	0.66904
10.2	cell wall.cellulose synthesis	6	0.01188	0.66904
10	cell wall	45	0.01301	0.66904
20.1.7	stress.biotic.PR-proteins	13	0.01842	0.66904
10.8.2	cell wall.pectin*esterases.acetyl esterase	3	0.01908	0.66904
26.10	misc.cytochrome P450	11	0.01961	0.66904
27.3.4	RNA.regulation of transcription.ARF, Auxin Response Factor family	3	0.02008	0.66904
17.3.1.1	hormone metabolism.brassinosteroid.synthesis-degradation.BRs	3	0.02141	0.66904
11.9	lipid metabolism.lipid degradation	8	0.02326	0.66904
27	RNA	134	0.02565	0.66904
26.12	misc.peroxidases	4	0.02758	0.66904
16.5	secondary metabolism.sulfur-containing	4	0.03187	0.66904
11.1	lipid metabolism.FA synthesis and FA elongation	9	0.03203	0.66904
16.2	secondary metabolism.phenylpropanoids	7	0.03261	0.66904
30.2.6	signalling.receptor kinases.leucine rich repeat VI	2	0.03623	0.66904
10.8	cell wall.pectin*esterases	8	0.03710	0.66904

Table 4.7. Mapman 3.5 gene expression analysis of 326 overlapping genes between P5S6 v *pmr5* and *tbr1-1/pmr5* v *pmr5*.

BIN	BIN Name	elements	p-value	BH pval
27.3	RNA.regulation of transcription	38	0.0001	0.0261
27	RNA	40	0.0002	0.0261
26.21	misc.protease inhibitor/seed storage/lipid transfer protein (LTP) family protein	3	0.0136	0.7394
27.3.25	RNA.regulation of transcription.MYB domain TF family	3	0.0140	0.7394
10.7	cell wall.modification	2	0.0540	0.7394
21.4	redox.glutaredoxins	2	0.0720	0.7394
11	lipid metabolism	10	0.0724	0.7394
10.6.3	cell wall.degradation.pectate lyases and polygalacturonases	3	0.0742	0.7394
10.6	cell wall.degradation	3	0.0742	0.7394
26.12	misc.peroxidases	2	0.0847	0.7394
11.9	lipid metabolism.lipid degradation	2	0.0875	0.7394
10.8	cell wall.pectin*esterases	1	0.0880	0.7394
10.8.2	cell wall.pectin*esterases.acetyl esterase	1	0.0880	0.7394
10.5.1	cell wall.cell wall proteins.AGPs	1	0.0900	0.7394

Table 4.8. Virtual Plant 2.1 gene expression analysis of 356 overlapping genes between P5S6 v *pmr5* and *tbr1-1/pmr5* v *pmr5*.

GO	Term	Observed Frequency	Expected Frequency	p-value
0006633	fatty acid biosynthetic process	10 out of 356 genes, 2.8%	122 out of 27870 genes, 0.4%	7.18E-06
0032787	monocarboxylic acid metabolic process	16 out of 356 genes, 4.5%	329 out of 27870 genes, 1.2%	9.34E-06
0006325	establishment and/or maintenance of chromatin architecture	11 out of 356 genes, 3.1%	165 out of 27870 genes, 0.6%	1.58E-05
0015985	energy coupled proton transport, down electrochemical gradient	6 out of 356 genes, 1.7%	46 out of 27870 genes, 0.2%	4.82E-05
0015986	ATP synthesis coupled proton transport	6 out of 356 genes, 1.7%	46 out of 27870 genes, 0.2%	4.82E-05
0006631	fatty acid metabolic process	11 out of 356 genes, 3.1%	189 out of 27870 genes, 0.7%	5.13E-05
0044255	cellular lipid metabolic process	17 out of 356 genes, 4.8%	439 out of 27870 genes, 1.6%	7.86E-05
0051276	chromosome organization and biogenesis	11 out of 356 genes, 3.1%	205 out of 27870 genes, 0.7%	0.000102
0006818	hydrogen transport	6 out of 356 genes, 1.7%	56 out of 27870 genes, 0.2%	0.000131
0015992	proton transport	6 out of 356 genes, 1.7%	56 out of 27870 genes, 0.2%	0.000131
0034220	transmembrane ion transport	6 out of 356 genes, 1.7%	57 out of 27870 genes, 0.2%	0.000143
0006334	nucleosome assembly	6 out of 356 genes, 1.7%	59 out of 27870 genes, 0.2%	0.00017
0006629	lipid metabolic process	22 out of 356 genes, 6.2%	709 out of 27870 genes, 2.5%	0.000172
0044271	nitrogen compound biosynthetic process	16 out of 356 genes, 4.5%	426 out of 27870 genes, 1.5%	0.000177
0006950	response to stress	46 out of 356 genes, 12.9%	2058 out of 27870 genes, 7.4%	0.000191

Table 4.9. P5S20 mapping of the suppressor 20 locus using PCR-based markers on chromosome 3 with mapping population of 59 segregants, all in the *pmr5* mutant background

	nga172	**GAPC**	**MNSOD**	**nga162**
	7cM 786296	**8cM 1081292**	**14cM 3418106**	**4608277**
Col	36	47	35	37
Ler	9	8	8	9
Het	14	4	13	12
Total	118	118	112	116
Recombination frequency	0.271	0.169	0.258	0.258

Table 4.10. Nonsynonymous changes on chromosome 3 from whole genome sequencing of P5S20 as annotated by EnsemblPlants Variant Effect Predictor

Uploaded Variation	Gene, Transcript	Consequence	cDNA	Protein	Amino acid change
3_325230-325229_-/GG	AT3G01961.1	FRAMESHIFT_CODING	49-50	17	-
3_2040104_C/T	AT3G06550.1	ESSENTIAL_SPLICE_SITE	-	-	-
3_2040104_C/T	AT3G06550.2	ESSENTIAL_SPLICE_SITE	-	-	-
3_2040104_C/T	AT3G06550.3	ESSENTIAL_SPLICE_SITE	-	-	-
3_2436714_C/T	AT3G07630.1	NON_SYNONYMOUS_CODING	782	257	A/V
3_2436714_C/T	AT3G07630.2	NON_SYNONYMOUS_CODING	782	257	A/V
3_2900291-2900290_-/A	AT3G09410.1	SPLICE_SITE	-	-	-
3_2900291-2900290_-/A	AT3G09410.3	SPLICE_SITE	-	-	-
3_2909816_C/T	AT3G09450.1	STOP_GAINED	2053	685	Q/*
3_3007742_C/G	AT3G09800.1	NON_SYNONYMOUS_CODING	197	11	K/N
3_3174371_C/T	AT3G10270.1	NON_SYNONYMOUS_CODING	2062	678	A/T
3_3281866_C/T	AT3G10525.1	NON_SYNONYMOUS_CODING	167	33	D/N
3_3552436_C/T	AT3G11330.1	NON_SYNONYMOUS_CODING	1462	465	G/E
3_3681871_C/T	AT3G11670.1	NON_SYNONYMOUS_CODING	1791	576	M/I
3_3681871_C/T	AT3G11670.2	NON_SYNONYMOUS_CODING	1779	576	M/I
3_4163727_C/T	AT3G13010.1	NON_SYNONYMOUS_CODING	1007	336	S/N
3_4228123_C/T	AT3G13150.1	NON_SYNONYMOUS_CODING	1529	503	R/Q
3_4684721_G/T	AT3G14120.1	NON_SYNONYMOUS_CODING	3141	987	E/D
3_4684721_G/T	AT3G14120.2	NON_SYNONYMOUS_CODING	3069	963	E/D
3_4684721_G/T	AT3G14120.3	NON_SYNONYMOUS_CODING	3132	984	E/D
3_4690351-4690350_-/G	AT3G14140.1	FRAMESHIFT_CODING	1368-1369	456-457	-
3_4738946_C/T	AT3G14230.1	NON_SYNONYMOUS_CODING	191	19	V/I
3_4738946_C/T	AT3G14230.2	NON_SYNONYMOUS_CODING	196	19	V/I
3_4738946_C/T	AT3G14230.3	NON_SYNONYMOUS_CODING	191	19	V/I
3_4885275_A/C	AT3G14550.1	NON_SYNONYMOUS_CODING	599	188	F/V
3_5018831_C/T	AT3G14920.1	NON_SYNONYMOUS_CODING	557	186	T/I
3_5094945_C/T	AT3G15120.1	NON_SYNONYMOUS_CODING	538	180	E/K
3_5244925_C/T	AT3G15510.1	NON_SYNONYMOUS_CODING	1169	328	S/F
3_5920892_C/T	AT3G17340.1	NON_SYNONYMOUS_CODING	3156	1029	A/T
3_5920892_C/T	AT3G17340.2	NON_SYNONYMOUS_CODING	3176	1032	A/T
3_5979979_C/T	AT3G17470.1	NON_SYNONYMOUS_CODING	146	38	P/S
3_6051541_C/T	AT3G17700.1	NON_SYNONYMOUS_CODING	1813	552	A/V
3_6417775_C/T	AT3G18650.1	NON_SYNONYMOUS_CODING	730	244	D/N
3_6429434_G/A	AT3G18680.1	NON_SYNONYMOUS_CODING	1064	312	G/R
3_6497573_C/T	AT3G18840.2	NON_SYNONYMOUS_CODING	1376	459	T/I
3_6629024_C/T	AT3G19170.1	NON_SYNONYMOUS_CODING	1683	508	M/I
3_6629024_C/T	AT3G19170.2	NON_SYNONYMOUS_CODING	1585	497	M/I
3_6813981_C/T	AT3G19610.1	NON_SYNONYMOUS_CODING	739	227	S/N

3_6939545_C/T	AT3G19940.1	NON_SYNONYMOUS_CODING	1115	372	A/V
3_8054378_C/T	AT3G22790.1	NON_SYNONYMOUS_CODING	3652	1144	A/T
3_8776934_G/A	AT3G24230.1	NON_SYNONYMOUS_CODING	1085	355	G/E
3_9099944_G/A	AT3G24900.1	NON_SYNONYMOUS_CODING	1894	632	R/W
3_9178053_G/A	AT3G25200.1	NON_SYNONYMOUS_CODING	292	98	E/K
3_9521941_C/T	AT3G26050.1	NON_SYNONYMOUS_CODING	160	12	S/L
3_9585007_C/T	AT3G26190.1	NON_SYNONYMOUS_CODING	103	26	G/E
3_9639792_C/T	AT3G26300.1	NON_SYNONYMOUS_CODING	910	304	D/N
3_9779221_C/T	AT3G26610.1	NON_SYNONYMOUS_CODING	880	272	T/I
3_10394159_C/T	AT3G27980.1	NON_SYNONYMOUS_CODING	256	86	L/F
3_10625036_C/T	AT3G28380.1	NON_SYNONYMOUS_CODING	2429	810	G/D
3_10795221_C/T	AT3G28760.1	SPLICE_SITE	-	-	-
3_10795221_C/T	AT3G28760.2	SPLICE_SITE	-	-	-
3_10832250_C/T	AT3G28830.1	NON_SYNONYMOUS_CODING	997	311	A/V
3_10849326_C/T	AT3G28850.1	NON_SYNONYMOUS_CODING	658	220	P/S
3_13368899_C/A	AT3G32410.1	NON_SYNONYMOUS_CODING	235	79	A/S
3_14680336-14680335_-/G	AT3G42560.1	FRAMESHIFT_CODING	71-72	24	-

CHAPTER 5: A hypothetical model for *pmr5*-mediated disease resistance

We now know that PMR5 affects pectin acetylation. This is based on our work showing that *pmr5* has less acetylation in its cell walls, is suppressed by a mutation in *RWA2*, and exists in a protein family with the putative xyloglucan acetyltransferase, AXY4. Since *pmr5* cell walls have less acetylation, it is also likely that PMR5 is an acetyltransferase, but enzyme activity has yet to be shown. Further characterization of the *pmr5* mutant cell wall has shown changes in rhamnogalacturonan I side chains, but based on the lack of binding of PMR5 to rhamnogalacturonan and its side chains, we believe the cell wall phenotype we see is due to secondary effects. In contrast, PMR5 protein can specifically bind pectin, polygalacturonic acid, and oligogalacturonic acid, leading us to believe that PMR5 is acetylating homogalacturonan. Based on the identification of *tbr* and *rwa2* as suppressors of *pmr5*-mediated disease resistance, it seems that the specific pectin acetylation profile that is generated in the *pmr5* mutant is an important component in understanding *pmr5*-mediated disease resistance.

Microarray analysis of gene expression in the *pmr5* mutant revealed cell cycle-related gene changes that correlated with a lack of pathogen-induced endoreduplication (Chandran et al., 2013). As *pmr5*-mediated disease resistance is specific to powdery mildews and not to other pathogens (Vogel et al., 2004), inhibition of powdery mildew-induced endoreduplication could explain the specificity of *pmr5*-mediated resistance. Interestingly, host ploidy is affected in surrounding mesophyll cells and not in epidermal cells, where fungal penetration occurs. Similarly, PMR5-GFP was found to be more abundant in root cortical cells than in root epidermal cells as detected by microscopy methods. Although PMR5-GFP could not be detected in leaf epidermal or mesophyll cells due to high background autofluorescence, PMR5's higher expression in cells underlying the epidermal layer may be relevant to its role in inhibiting pathogen-induced endoreduplication in leaf mesophyll cells.

Using the acetylated pectin fragment as the signal, we can create a model that factors our hypothesis that PMR5 exists in a CWI-signaling pathway with pathogen-induced endoreduplication (Fig. 5.1). In the *pmr5* mutant, the lack of acetylation early in cell wall biogenesis causes the plant to respond by altering its cell wall, which we see as secondary effects when we analyze the cell wall. Fragments of the altered cell wall that are generated during normal growth and expansion or during fungal penetration may be acting as elicitors or signals for the CWI pathway. These elicitors may be important in signaling to regulate cell cycle processes and powdery mildew induced-endoreduplication. Mutations in *TBR1* and *RWA2* may be suppressing *pmr5*-mediated disease resistance early in the pathway by altering the cell wall in such a way that the fragments are no longer recognized as damage. It would be interesting to see whether these suppressors rescue the ploidy phenotype, which would suggest that powdery mildew-induced endoreduplication is indeed the endpoint response of this pathway.

Plants have likely evolved a CWI pathway to integrate multiple metabolic signals about its status before cell growth and expansion. It seems that pectin composition is particularly important based on our work identifying PMR5 as a putative pectin acetyltransferase. More work is needed to dissect the players connecting the putative CWI signal generated in the *pmr5* mutant to the end result of inhibition of powdery mildew-induced endoreduplication.

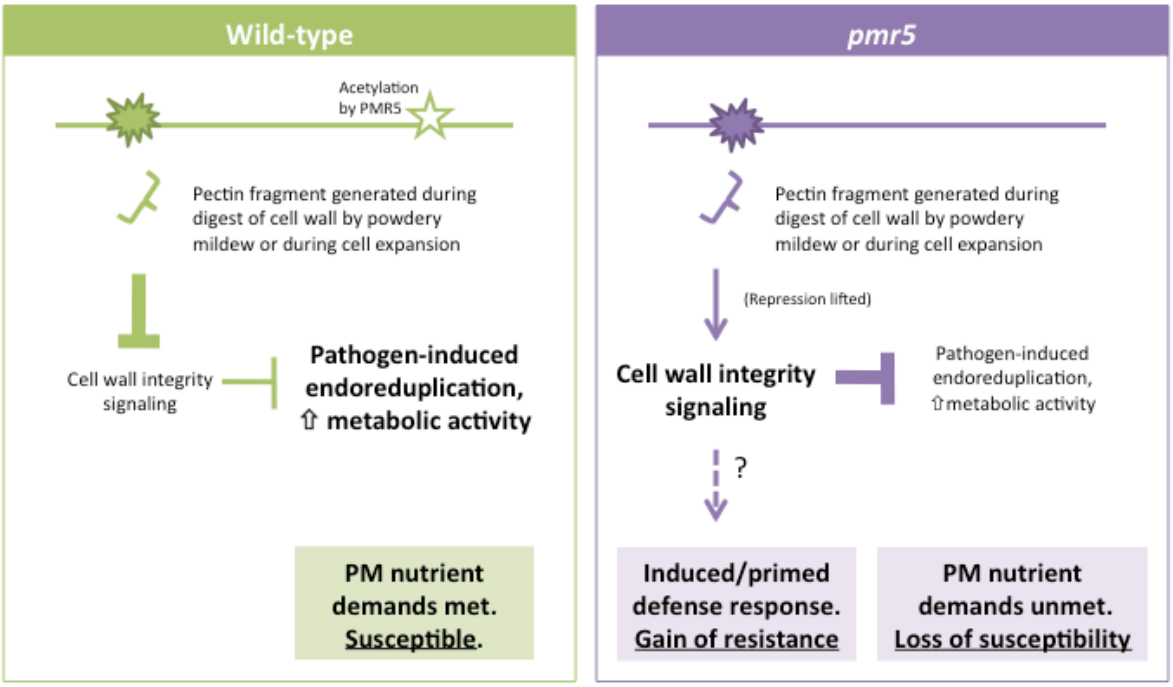

Figure 5.1. Hypothetical model of *pmr5*-mediated disease resistance. PMR5 functions as a homogalacturonan acetyltransferase. In the *pmr5* mutant, compensating changes result in alterations in the cell wall (e.g., RGI side chain composition) and cell wall integrity-signaling that inhibit pathogen induced endoreduplication necessary for powdery mildew growth and reproduction. The suppressors, *tbr1* and *rwa2*, alter the cell wall to restore repression of cell wall integrity-signaling as in wild-type.

References Cited

Adam L, Somerville SC (1996) Genetic characterization of five powdery mildew disease resistance loci in *Arabidopsis thaliana*. Plant Journal **9:** 341-356

Akoh CC, Lee GC, Liaw YC, Huang TH, Shaw JF (2004) GDSL family of serine esterases/lipases. Progress in Lipid Research **43:** 534-552

Alford SR, Rangarajan P, Williams P, Gillaspy GE (2012) myo-Inositol Oxygenase is Required for Responses to Low Energy Conditions in *Arabidopsis thaliana*. Frontiers in Plant Science **3:** 69

Alonso JM, Stepanova AN, Leisse TJ, Kim CJ, Chen H, Shinn P, Stevenson DK, Zimmerman J, Barajas P, Cheuk R, Gadrinab C, Heller C, Jeske A, Koesema E, Meyers CC, Parker H, Prednis L, Ansari Y, Choy N, Deen H, Geralt M, Hazari N, Hom E, Karnes M, Mulholland C, Ndubaku R, Schmidt I, Guzman P, Aguilar-Henonin L, Schmid M, Weigel D, Carter DE, Marchand T, Risseeuw E, Brogden D, Zeko A, Crosby WL, Berry CC, Ecker JR (2003) Genome-wide insertional mutagenesis of *Arabidopsis thaliana*. Science **301:** 653-657

Altschul SF, Madden TL, Schaffer AA, Zhang J, Zhang Z, Miller W, Lipman DJ (1997) Gapped BLAST and PSI-BLAST: a new generation of protein database search programs. Nucleic Acids Research **25:** 3389-3402

Anantharaman V, Aravind L (2010) Novel eukaryotic enzymes modifying cell-surface biopolymers. Biology Direct **5:** 1

Anderson CT, Carroll A, Akhmetova L, Somerville C (2010) Real-time imaging of cellulose reorientation during cell wall expansion in Arabidopsis roots. Plant physiology **152:** 787-796

Ausubel FM, Katagiri F, Mindrinos M, Glazebrook J (1995) Use of Arabidopsis thaliana defense-related mutants to dissect the plant response to pathogens. Proceedings of the National Academy of Sciences of the United States of America **92:** 4189-4196

Aziz A, Gauthier A, Bezier A, Poinssot B, Joubert JM, Pugin A, Heyraud A, Baillieul F (2007) Elicitor and resistance-inducing activities of beta-1,4 cellodextrins in grapevine, comparison with beta-1,3 glucans and alpha-1,4 oligogalacturonides. Journal of Experimental Botany **58:** 1463-1472

Aziz A, Heyraud A, Lambert B (2004) Oligogalacturonide signal transduction, induction of defense-related responses and protection of grapevine against *Botrytis cinerea*. Planta **218:** 767-774

Babosha AV (2009) Regulation of resistance and susceptibility in wheat-powdery mildew pathosystem with exogenous cytokinins. Journal of Plant Physiology **166:** 1892-1903

Bai L, Zhang G, Zhou Y, Zhang Z, Wang W, Du Y, Wu Z, Song CP (2009) Plasma membrane-associated proline-rich extensin-like receptor kinase 4, a novel regulator of Ca2+ signalling, is required for abscisic acid responses in Arabidopsis thaliana. Plant Journal **60:** 314-327

Bauer S, Vasu P, Persson S, Mort AJ, Somerville CR (2006) Development and application of a suite of polysaccharide-degrading enzymes for analyzing plant cell walls. Proceedings of the National Academy of Sciences of the United States of America **103:** 11417-11422

Bednarek P (2012) Chemical warfare or modulators of defence responses - the function of secondary metabolites in plant immunity. Current Opinion in Plant Biology **15:** 407-414

Bednarek P, Pislewska-Bednarek M, Svatos A, Schneider B, Doubsky J, Mansurova M, Humphry M, Consonni C, Panstruga R, Sanchez-Vallet A, Molina A, Schulze-Lefert P (2009) A glucosinolate metabolism pathway in living plant cells mediates broad-spectrum antifungal defense. Science **323:** 101-106

Benatti MR, Penning BW, Carpita NC, McCann MC (2012) We are good to grow: dynamic integration of cell wall architecture with the machinery of growth. Frontiers in Plant Science **3:** 187

Bendtsen JD, Nielsen H, von Heijne G, Brunak S (2004) Improved prediction of signal peptides: SignalP 3.0. Journal of Molecular Biology **340:** 783-795

Bestwick CS, Brown IR, Bennett MH, Mansfield JW (1997) Localization of hydrogen peroxide accumulation during the hypersensitive reaction of lettuce cells to Pseudomonas syringae pv phaseolicola. The Plant cell **9:** 209-221

Bhat RA, Miklis M, Schmelzer E, Schulze-Lefert P, Panstruga R (2005) Recruitment and interaction dynamics of plant penetration resistance components in a plasma membrane microdomain. Proceedings of the National Academy of Sciences of the United States of America **102:** 3135-3140

Bhuiyan NH, Selvaraj G, Wei Y, King J (2008) Gene expression profiling and silencing reveal that monolignol biosynthesis plays a critical role in penetration defence in wheat against powdery mildew invasion. Journal of Experimental Botany

Bischoff V, Cookson SJ, Wu S, Scheible WR (2009) Thaxtomin A affects CESA-complex density, expression of cell wall genes, cell wall composition, and causes ectopic lignification in Arabidopsis thaliana seedlings. Journal of Experimental Botany **60:** 955-965

Bischoff V, Nita S, Neumetzler L, Schindelasch D, Urbain A, Eshed R, Persson S, Delmer D, Scheible WR (2010) *TRICHOME BIREFRINGENCE* and its homolog *AT5G01360* encode plant-specific DUF231 proteins required for cellulose biosynthesis in Arabidopsis. Plant Physiology **153:** 590-602

Bischoff V, Selbig J, Scheible WR (2010) Involvement of TBL/DUF231 proteins into cell wall biology. Plant Signaling & Behavior **5:** 1057-1059

Bohlenius H, Morch SM, Godfrey D, Nielsen ME, Thordal-Christensen H (2010) The multivesicular body-localized GTPase ARFA1b/1c is important for callose deposition and ROR2 syntaxin-dependent preinvasive basal defense in barley. Plant Cell **22:** 3831-3844

Boisson-Dernier A, Kessler SA, Grossniklaus U (2011) The walls have ears: the role of plant CrRLK1Ls in sensing and transducing extracellular signals. Journal of Experimental Botany **62:** 1581-1591

Boller T, Felix G (2009) A renaissance of elicitors: perception of microbe-associated molecular patterns and danger signals by pattern-recognition receptors. Annual Review of Plant Biology **60:** 379-406

Bouwmeester K, de Sain M, Weide R, Gouget A, Klamer S, Canut H, Govers F (2011) The lectin receptor kinase LecRK-I.9 is a novel *Phytophthora* resistance component and a potential host target for a RXLR effector. PLoS Pathogens **7:** e1001327

Bouwmeester K, Govers F (2009) Arabidopsis L-type lectin receptor kinases: phylogeny, classification, and expression profiles. Journal of Experimental Botany **60:** 4383-4396

Brady SM, Orlando DA, Lee JY, Wang JY, Koch J, Dinneny JR, Mace D, Ohler U, Benfey PN (2007) A high-resolution root spatiotemporal map reveals dominant expression patterns. Science **318:** 801-806

Broekaert WF, J VANP, Leyns F, Joos H, Peumans WJ (1989) A Chitin-Binding Lectin from Stinging Nettle Rhizomes with Antifungal Properties. Science **245:** 1100-1102

Brutus A, Sicilia F, Macone A, Cervone F, De Lorenzo G (2010) A domain swap approach reveals a role of the plant wall-associated kinase 1 (WAK1) as a receptor of oligogalacturonides. Proceedings of the National Academy of Sciences of the United States of America **107:** 9452-9457

Burch-Smith TM, Schiff M, Liu Y, Dinesh-Kumar SP (2006) Efficient virus-induced gene silencing in Arabidopsis. Plant Physiology **142:** 21-27

Cabrera JC, Boland A, Messiaen J, Cambier P, Van Cutsem P (2008) Egg box conformation of oligogalacturonides: the time-dependent stabilization of the elicitor-active conformation increases its biological activity. Glycobiology **18:** 473-482

Caffall KH, Mohnen D (2009) The structure, function, and biosynthesis of plant cell wall pectic polysaccharides. Carbohydrate Research **344:** 1879-1900

Cannon MC, Terneus K, Hall Q, Tan L, Wang Y, Wegenhart BL, Chen L, Lamport DT, Chen Y, Kieliszewski MJ (2008) Self-assembly of the plant cell wall requires an extensin scaffold. Proceedings of the National Academy of Sciences of the United States of America **105:** 2226-2231

Canut H, Carrasco A, Galaud JP, Cassan C, Bouyssou H, Vita N, Ferrara P, Pont-Lezica R (1998) High affinity RGD-binding sites at the plasma membrane of *Arabidopsis thaliana* links the cell wall. Plant Journal **16:** 63-71

Casson S, Spencer M, Walker K, Lindsey K (2005) Laser capture microdissection for the analysis of gene expression during embryogenesis of Arabidopsis. Plant Journal **42:** 111-123

Chandran D, Inada N, Hather G, Kleindt CK, Wildermuth MC (2010) Laser microdissection of Arabidopsis cells at the powdery mildew infection site reveals site-specific processes and regulators. Proceedings of the National Academy of Sciences of the United States of America **107:** 460-465

Chandran D, Rickert JC, Cherk C, Dotson BR, Wildermuth MC (2013) Host ploidy underlying the fungal feeding site is a determinant of powdery mildew growth and reproduction. Molecular Plant-Microbe Interactions

Chaouch S, Queval G, Noctor G (2012) AtRbohF is a crucial modulator of defence-associated metabolism and a key actor in the interplay between intracellular oxidative stress and pathogenesis responses in Arabidopsis. Plant Journal **69:** 613-627

Charkowski AO, Alfano JR, Preston G, Yuan J, He SY, Collmer A (1998) The *Pseudomonas syringae* pv. *tomato* HrpW protein has domains similar to harpins and pectate lyases and can elicit the plant hypersensitive response and bind to pectate. Journal of Bacteriology **180:** 5211-5217

Choi J, Choi D, Lee S, Ryu CM, Hwang I (2011) Cytokinins and plant immunity: old foes or new friends? Trends in Plant Science **16:** 388-394

Clay NK, Adio AM, Denoux C, Jander G, Ausubel FM (2009) Glucosinolate metabolites required for an Arabidopsis innate immune response. Science **323:** 95-101

Clough SJ, Bent AF (1998) Floral dip: a simplified method for *Agrobacterium*-mediated transformation of *Arabidopsis thaliana*. Plant Journal **16:** 735-743

Collins NC, Thordal-Christensen H, Lipka V, Bau S, Kombrink E, Qiu JL, Huckelhoven R, Stein M, Freialdenhoven A, Somerville SC, Schulze-Lefert P (2003) SNARE-protein-mediated disease resistance at the plant cell wall. Nature **425:** 973-977

Consonni C, Humphry ME, Hartmann HA, Livaja M, Durner J, Westphal L, Vogel J, Lipka V, Kemmerling B, Schulze-Lefert P, Somerville SC, Panstruga R (2006) Conserved requirement for a plant host cell protein in powdery mildew pathogenesis. Nature Genetics **38:** 716-720

Coppinger P, Repetti PP, Day B, Dahlbeck D, Mehlert A, Staskawicz BJ (2004) Overexpression of the plasma membrane-localized NDR1 protein results in enhanced bacterial disease resistance in Arabidopsis thaliana. Plant Journal **40:** 225-237

Cosgrove DJ (2005) Growth of the plant cell wall. Nature Reviews Molecular Cell Biology **6:** 850-861

Cronje C, George GM, Fernie AR, Bekker J, Kossmann J, Bauer R (2012) Manipulation of L-ascorbic acid biosynthesis pathways in *Solanum lycopersicum*: elevated GDP-mannose pyrophosphorylase activity enhances L-ascorbate levels in red fruit. Planta **235:** 553-564

Daudi A, Cheng Z, O'Brien JA, Mammarella N, Khan S, Ausubel FM, Bolwell GP (2012) The apoplastic oxidative burst peroxidase in Arabidopsis is a major component of pattern-triggered immunity. Plant Cell **24:** 275-287

Day B, Dahlbeck D, Staskawicz BJ (2006) NDR1 interaction with RIN4 mediates the differential activation of multiple disease resistance pathways in Arabidopsis. Plant Cell **18:** 2782-2791

Decreux A, Messiaen J (2005) Wall-associated kinase WAK1 interacts with cell wall pectins in a calcium-induced conformation. Plant Cell Physiology **46:** 268-278

Delgado-Cerezo M, Sanchez-Rodriguez C, Escudero V, Miedes E, Fernandez PV, Jorda L, Hernandez-Blanco C, Sanchez-Vallet A, Bednarek P, Schulze-Lefert P, Somerville S, Estevez JM, Persson S, Molina A (2012) Arabidopsis heterotrimeric G-protein regulates cell wall defense and resistance to necrotrophic fungi. Molecular Plant **5:** 98-114

Denness L, McKenna JF, Segonzac C, Wormit A, Madhou P, Bennett M, Mansfield J, Zipfel C, Hamann T (2011) Cell wall damage-induced lignin biosynthesis is regulated by a reactive oxygen species- and jasmonic acid-dependent process in Arabidopsis. Plant Physiology **156:** 1364-1374

Dewitte W, Scofield S, Alcasabas AA, Maughan SC, Menges M, Braun N, Collins C, Nieuwland J, Prinsen E, Sundaresan V, Murray JA (2007) Arabidopsis CYCD3 D-type cyclins link cell proliferation and endocycles and are rate-limiting for cytokinin responses. Proceedings of the National Academy of Sciences of the United States of America **104:** 14537-14542

Dick-Perez M, Zhang Y, Hayes J, Salazar A, Zabotina OA, Hong M (2011) Structure and interactions of plant cell-wall polysaccharides by two- and three-dimensional magic-angle-spinning solid-state NMR. Biochemistry **50:** 989-1000

Diener AC, Ausubel FM (2005) *RESISTANCE TO FUSARIUM OXYSPORUM 1,* a dominant Arabidopsis disease-resistance gene, is not race specific. Genetics **171:** 305-321

Dong X, Hong Z, Chatterjee J, Kim S, Verma DP (2008) Expression of callose synthase genes and its connection with *Npr1* signaling pathway during pathogen infection. Planta **229:** 87-98

Drakakaki G, van de Ven W, Pan S, Miao Y, Wang J, Keinath NF, Weatherly B, Jiang L, Schumacher K, Hicks G, Raikhel N (2012) Isolation and proteomic analysis of the SYP61 compartment reveal its role in exocytic trafficking in Arabidopsis. Cell Research **22:** 413-424

Duan Q, Kita D, Li C, Cheung AY, Wu HM (2010) FERONIA receptor-like kinase regulates RHO GTPase signaling of root hair development. Proceedings of the National Academy of Sciences of the United States of America **107:** 17821-17826

Edwards K, Johnstone C, Thompson C (1991) A simple and rapid method for the preparation of plant genomic DNA for PCR analysis. Nucleic acids research **19:** 1349

Ellis C, Karafyllidis I, Turner JG (2002) Constitutive activation of jasmonate signaling in an Arabidopsis mutant correlates with enhanced resistance to *Erysiphe cichoracearum, Pseudomonas syringae,* and *Myzus persicae*. Molecular Plant-Microbe Interactions **15:** 1025-1030

Ellis C, Karafyllidis I, Wasternack C, Turner JG (2002) The Arabidopsis mutant *cev1* links cell wall signaling to jasmonate and ethylene responses. Plant Cell **14:** 1557-1566

Emanuelsson O, Nielsen H, Brunak S, von Heijne G (2000) Predicting subcellular localization of proteins based on their N-terminal amino acid sequence. Journal of Molecular Biology **300:** 1005-1016

Enrique R, Siciliano F, Favaro MA, Gerhardt N, Roeschlin R, Rigano L, Sendin L, Castagnaro A, Vojnov A, Marano MR (2011) Novel demonstration of RNAi in citrus reveals importance of citrus callose synthase in defence against *Xanthomonas citri* subsp. *citri*. Plant Biotechnology Journal **9:** 394-407

Favery B, Chelysheva LA, Lebris M, Jammes F, Marmagne A, De Almeida-Engler J, Lecomte P, Vaury C, Arkowitz RA, Abad P (2004) Arabidopsis formin AtFH6 is a plasma membrane-associated protein upregulated in giant cells induced by parasitic nematodes. Plant Cell **16:** 2529-2540

Field B, Jordan F, Osbourn A (2006) First encounters--deployment of defence-related natural products by plants. New Phytologist **172:** 193-207

Gaulin E, Drame N, Lafitte C, Torto-Alalibo T, Martinez Y, Ameline-Torregrosa C, Khatib M, Mazarguil H, Villalba-Mateos F, Kamoun S, Mazars C, Dumas B, Bottin A, Esquerre-Tugaye M-T, Rickauer M (2006) Cellulose Binding Domains of a *Phytophthora* Cell Wall Protein Are Novel Pathogen-Associated Molecular Patterns. Plant Cell **18:** 1766-1777

Gheysen G, Mitchum MG (2011) How nematodes manipulate plant development pathways for infection. Current Opinion in Plant Biology **14:** 415-421

Gierlinger N, Sapei L, Paris O (2008) Insights into the chemical composition of *Equisetum hyemale* by high resolution Raman imaging. Planta **227:** 969-980

Gille S, de Souza A, Xiong G, Benz M, Cheng K, Schultink A, Reca IB, Pauly M (2011) O-acetylation of Arabidopsis hemicellulose xyloglucan requires AXY4 or AXY4L, proteins with a TBL and DUF231 domain. Plant Cell **23:** 4041-4053

Gouget A, Senchou V, Govers F, Sanson A, Barre A, Rouge P, Pont-Lezica R, Canut H (2006) Lectin receptor kinases participate in protein-protein interactions to mediate plasma membrane-cell wall adhesions in Arabidopsis. Plant Physiology **140:** 81-90

Grosskinsky DK, Naseem M, Abdelmohsen UR, Plickert N, Engelke T, Griebel T, Zeier J, Novak O, Strnad M, Pfeifhofer H, van der Graaff E, Simon U, Roitsch T (2011) Cytokinins mediate resistance against Pseudomonas syringae in tobacco through

increased antimicrobial phytoalexin synthesis independent of salicylic acid signaling. Plant Physiology **157:** 815-830

Grubb CD, Abel S (2006) Glucosinolate metabolism and its control. Trends in Plant Science **11:** 89-100

Gunl M, Kraemer F, Pauly M (2011) Oligosaccharide mass profiling (OLIMP) of cell wall polysaccharides by MALDI-TOF/MS. Methods in Molecular Biology **715:** 43-54

Guo H, Li L, Ye H, Yu X, Algreen A, Yin Y (2009) Three related receptor-like kinases are required for optimal cell elongation in Arabidopsis thaliana. Proceedings of the National Academy of Sciences of the United States of America **106:** 7648-7653

Haffani YZ, Silva-Gagliardi NF, Sewter SK, Grace Aldea M, Zhao Z, Nakhamchik A, Cameron RK, Goring DR (2006) Altered Expression of PERK Receptor Kinases in *Arabidopsis* Leads to Changes in Growth and Floral Organ Formation. Plant Signaling & Behavior **1:** 251-260

Hamann T (2012) Plant cell wall integrity maintenance as an essential component of biotic stress response mechanisms. Frontiers in Plant Science **3:** 77

Hamann T, Bennett M, Mansfield J, Somerville C (2009) Identification of cell-wall stress as a hexose-dependent and osmosensitive regulator of plant responses. Plant Journal **57:** 1015-1026

Hamann T, Denness L (2011) Cell wall integrity maintenance in plants: lessons to be learned from yeast? Plant Signaling & Behavior **6:** 1706-1709

Han S, Kim D (2006) AtRTPrimer: database for Arabidopsis genome-wide homogeneous and specific RT-PCR primer-pairs. BMC Bioinformatics **7:** 179

Hardham AR, Jones DA, Takemoto D (2007) Cytoskeleton and cell wall function in penetration resistance. Current Opinion in Plant Biology **10:** 342-348

Haswell ES, Peyronnet R, Barbier-Brygoo H, Meyerowitz EM, Frachisse JM (2008) Two MscS homologs provide mechanosensitive channel activities in the Arabidopsis root. Current Biology **18:** 730-734

He ZH, Fujiki M, Kohorn BD (1996) A cell wall-associated, receptor-like protein kinase. Journal of Biological Chemistry **271:** 19789-19793

He ZH, He D, Kohorn BD (1998) Requirement for the induced expression of a cell wall associated receptor kinase for survival during the pathogen response. Plant Journal **14:** 55-63

Heazlewood JL, Tonti-Filippini J, Verboom RE, Millar AH (2005) Combining experimental and predicted datasets for determination of the subcellular location of proteins in Arabidopsis. Plant Physiology **139:** 598-609

Hematy K, Cherk C, Somerville S (2009) Host-pathogen warfare at the plant cell wall. Current Opinion in Plant Biology **12:** 406-413

Hematy K, Hofte H (2008) Novel receptor kinases involved in growth regulation. Current Opinion in Plant Biology **11:** 321-328

Hematy K, Sado PE, Van Tuinen A, Rochange S, Desnos T, Balzergue S, Pelletier S, Renou JP, Hofte H (2007) A receptor-like kinase mediates the response of Arabidopsis cells to the inhibition of cellulose synthesis. Current Biology **17:** 922-931

Hernandez-Blanco C, Feng DX, Hu J, Sanchez-Vallet A, Deslandes L, Llorente F, Berrocal-Lobo M, Keller H, Barlet X, Sanchez-Rodriguez C, Anderson LK, Somerville S, Marco Y, Molina A (2007) Impairment of cellulose synthases required for Arabidopsis secondary cell wall formation enhances disease resistance. Plant Cell **19:** 890-903

Hewezi T, Howe P, Maier TR, Hussey RS, Mitchum MG, Davis EL, Baum TJ (2008) Cellulose Binding Protein from the Parasitic Nematode *Heterodera schachtii* Interacts with Arabidopsis Pectin Methylesterase: Cooperative Cell Wall Modification during Parasitism. Plant Cell**:** tpc.108.063065

Huckelhoven R (2007) Cell wall-associated mechanisms of disease resistance and susceptibility. Annual Review Phytopathology **45:** 101-127

Humphrey TV, Bonetta DT, Goring DR (2007) Sentinels at the wall: cell wall receptors and sensors. New Phytologist **176:** 7-21

Janbon G, Himmelreich U, Moyrand F, Improvisi L, Dromer F (2001) Cas1p is a membrane protein necessary for the O-acetylation of the *Cryptococcus neoformans* capsular polysaccharide. Molecular Microbiology **42:** 453-467

Julenius K, Molgaard A, Gupta R, Brunak S (2005) Prediction, conservation analysis, and structural characterization of mammalian mucin-type O-glycosylation sites. Glycobiology **15:** 153-164

Kadler KE, Hill A, Canty-Laird EG (2008) Collagen fibrillogenesis: fibronectin, integrins, and minor collagens as organizers and nucleators. Current Opinion in Cell Biology **20:** 495-501

Kall L, Krogh A, Sonnhammer EL (2004) A combined transmembrane topology and signal peptide prediction method. Journal of Molecular Biology **338:** 1027-1036

Kamper J, Kahmann R, Bolker M, Ma LJ, Brefort T, Saville BJ, Banuett F, Kronstad JW, Gold SE, Muller O, Perlin MH, Wosten HA, de Vries R, Ruiz-Herrera J, Reynaga-Pena CG, Snetselaar K, McCann M, Perez-Martin J, Feldbrugge M, Basse CW, Steinberg G, Ibeas JI, Holloman W, Guzman P, Farman M, Stajich JE, Sentandreu R, Gonzalez-Prieto JM, Kennell JC, Molina L, Schirawski J, Mendoza-Mendoza A, Greilinger D, Munch K, Rossel N, Scherer M, Vranes M, Ladendorf O, Vincon V, Fuchs U, Sandrock B, Meng S, Ho EC, Cahill MJ, Boyce KJ, Klose J, Klosterman SJ, Deelstra HJ, Ortiz-Castellanos L, Li W, Sanchez-Alonso P, Schreier PH, Hauser-Hahn I, Vaupel M, Koopmann E, Friedrich G, Voss H, Schluter T, Margolis J, Platt D, Swimmer C, Gnirke A, Chen F, Vysotskaia V, Mannhaupt G, Guldener U, Munsterkotter M, Haase D, Oesterheld M, Mewes HW, Mauceli EW, DeCaprio D, Wade CM, Butler J, Young S, Jaffe DB, Calvo S, Nusbaum C, Galagan J, Birren BW (2006) Insights from the genome of the biotrophic fungal plant pathogen *Ustilago maydis*. Nature **444:** 97-101

Kanter U, Usadel B, Guerineau F, Li Y, Pauly M, Tenhaken R (2005) The inositol oxygenase gene family of Arabidopsis is involved in the biosynthesis of nucleotide sugar precursors for cell-wall matrix polysaccharides. Planta **221:** 243-254

Kanzaki H, Saitoh H, Takahashi Y, Berberich T, Ito A, Kamoun S, Terauchi R (2008) NbLRK1, a lectin-like receptor kinase protein of *Nicotiana benthamiana*, interacts with *Phytophthora infestans* INF1 elicitin and mediates INF1-induced cell death. Planta **228:** 977-987

Katari MS, Nowicki SD, Aceituno FF, Nero D, Kelfer J, Thompson LP, Cabello JM, Davidson RS, Goldberg AP, Shasha DE, Coruzzi GM, Gutierrez RA (2010) VirtualPlant: a software platform to support systems biology research. Plant Physiology **152:** 500-515

Kelley LA, Sternberg MJ (2009) Protein structure prediction on the Web: a case study using the Phyre server. Nature Protocols **4:** 363-371

Kessler SA, Shimosato-Asano H, Keinath NF, Wuest SE, Ingram G, Panstruga R, Grossniklaus U (2010) Conserved molecular components for pollen tube reception and fungal invasion. Science **330:** 968-971

Kiba T, Yamada H, Mizuno T (2002) Characterization of the ARR15 and ARR16 response regulators with special reference to the cytokinin signaling pathway mediated by the AHK4 histidine kinase in roots of Arabidopsis thaliana. Plant & Cell Physiology **43:** 1059-1066

Kilian J, Whitehead D, Horak J, Wanke D, Weinl S, Batistic O, D'Angelo C, Bornberg-Bauer E, Kudla J, Harter K (2007) The AtGenExpress global stress expression data set: protocols, evaluation and model data analysis of UV-B light, drought and cold stress responses. Plant Journal **50:** 347-363

Knepper C, Savory EA, Day B (2011) Arabidopsis NDR1 is an integrin-like protein with a role in fluid loss and plasma membrane-cell wall adhesion. Plant Physiology **156:** 286-300

Knox JP (1997) The use of antibodies to study the architecture and developmental regulation of plant cell walls. International Review of Cytology **171:** 79-120

Ko JH, Kim JH, Jayanty SS, Howe GA, Han KH (2006) Loss of function of COBRA, a determinant of oriented cell expansion, invokes cellular defence responses in *Arabidopsis thaliana*. Journal of Experimental Botany **57:** 2923-2936

Koh S, Andre A, Edwards H, Ehrhardt D, Somerville S (2005) Arabidopsis thaliana subcellular responses to compatible *Erysiphe cichoracearum* infections. Plant Journal **44:** 516-529

Koh S, Somerville S (2006) Show and tell: cell biology of pathogen invasion. Current Opinion in Plant Biology **9:** 406-413

Kohorn BD, Johansen S, Shishido A, Todorova T, Martinez R, Defeo E, Obregon P (2009) Pectin activation of MAP kinase and gene expression is WAK2 dependent. Plant Journal **60:** 974-982

Kohorn BD, Kobayashi M, Johansen S, Riese J, Huang LF, Koch K, Fu S, Dotson A, Byers N (2006) An Arabidopsis cell wall-associated kinase required for invertase activity and cell growth. Plant Journal **46:** 307-316

Kohorn BD, Kohorn SL (2012) The cell wall-associated kinases, WAKs, as pectin receptors. Frontiers in Plant Science **3:** 88

Kohorn BD, Kohorn SL, Todorova T, Baptiste G, Stansky K, McCullough M (2012) A dominant allele of Arabidopsis pectin-binding wall-associated kinase induces a stress response suppressed by MPK6 but not MPK3 mutations. Molecular Plant **5:** 841-851

Kong Y, Zhou G, Yin Y, Xu Y, Pattathil S, Hahn MG (2011) Molecular analysis of a family of Arabidopsis genes related to galacturonosyltransferases. Plant Physiology **155:** 1791-1805

Konieczny A, Ausubel FM (1993) A procedure for mapping Arabidopsis mutations using co-dominant ecotype-specific PCR-based markers. Plant Journal **4:** 403-410

Krishnamurthy N, Brown DP, Kirshner D, Sjolander K (2006) PhyloFacts: an online structural phylogenomic encyclopedia for protein functional and structural classification. Genome Biology **7:** R83

Laemmli UK (1970) Cleavage of structural proteins during the assembly of the head of bacteriophage T4. Nature **227:** 680-685

Laluk K, Mengiste T (2010) Necrotroph attacks on plants: wanton destruction or covert extortion? The Arabidopsis book / American Society of Plant Biologists **8:** e0136

Lefebvre V, Fortabat MN, Ducamp A, North HM, Maia-Grondard A, Trouverie J, Boursiac Y, Mouille G, Durand-Tardif M (2011) *ESKIMO1* disruption in Arabidopsis alters vascular tissue and impairs water transport. PloS One **6:** e16645

Levin DE (2005) Cell wall integrity signaling in *Saccharomyces cerevisiae*. Microbiology and Molecular Biology Reviews **69:** 262-291

Levin DE (2011) Regulation of cell wall biogenesis in *Saccharomyces cerevisiae*: the cell wall integrity signaling pathway. Genetics **189:** 1145-1175

Liepman AH, Wightman R, Geshi N, Turner SR, Scheller HV (2010) Arabidopsis - a powerful model system for plant cell wall research. The Plant journal : for cell and molecular biology **61:** 1107-1121

Liepman AH, Wilkerson CG, Keegstra K (2005) Expression of cellulose synthase-like (*Csl*) genes in insect cells reveals that *CslA* family members encode mannan synthases. Proceedings of the National Academy of Sciences of the United States of America **102:** 2221-2226

Lipka U, Fuchs R, Lipka V (2008) Arabidopsis non-host resistance to powdery mildews. Current Opinion in Plant Biology **11:** 404-411

Lipka V, Dittgen J, Bednarek P, Bhat R, Wiermer M, Stein M, Landtag J, Brandt W, Rosahl S, Scheel D, Llorente F, Molina A, Parker J, Somerville S, Schulze-Lefert P (2005) Pre- and postinvasion defenses both contribute to nonhost resistance in Arabidopsis. Science **310:** 1180-1183

Livak KJ, Schmittgen TD (2001) Analysis of relative gene expression data using real-time quantitative PCR and the 2(-Delta Delta C(T)) Method. Methods **25:** 402-408

Llorente F, Alonso-Blanco C, Sanchez-Rodriguez C, Jorda L, Molina A (2005) ERECTA receptor-like kinase and heterotrimeric G protein from Arabidopsis are required for resistance to the necrotrophic fungus *Plectosphaerella cucumerina*. Plant Journal **43:** 165-180

Loria R, Bignell DR, Moll S, Huguet-Tapia JC, Joshi MV, Johnson EG, Seipke RF, Gibson DM (2008) Thaxtomin biosynthesis: the path to plant pathogenicity in the genus *Streptomyces*. Antonie Van Leeuwenhoek **94:** 3-10

Macquet A, Ralet MC, Kronenberger J, Marion-Poll A, North HM (2007) In situ, chemical and macromolecular study of the composition of *Arabidopsis thaliana* seed coat mucilage. Plant & Cell Physiology **48:** 984-999

Manabe Y, Nafisi M, Verhertbruggen Y, Orfila C, Gille S, Rautengarten C, Cherk C, Marcus SE, Somerville S, Pauly M, Knox JP, Sakuragi Y, Scheller HV (2011) Loss-of-function mutation of *REDUCED WALL ACETYLATION2* in Arabidopsis leads to reduced cell wall acetylation and increased resistance to Botrytis cinerea. Plant Physiology **155:** 1068-1078

Martiniere A, Gayral P, Hawes C, Runions J (2011) Building bridges: formin1 of Arabidopsis forms a connection between the cell wall and the actin cytoskeleton. Plant Journal **66:** 354-365

McCallum CM, Comai L, Greene EA, Henikoff S (2000) Targeting induced local lesions IN genomes (TILLING) for plant functional genomics. Plant Physiology **123:** 439-442

Mellersh DG, Heath MC (2001) Plasma membrane-cell wall adhesion is required for expression of plant defense responses during fungal penetration. Plant Cell **13:** 413-424

Melton LD, Smith BG (2001) Isolation of Plant Cell Walls and Fractionation of Cell Wall Polysaccharides. Current Protocols in Food Analytical Chemistry **Unit E3.1:** E3.1.1-E3.1.23

Michelmore RW, Paran I, Kesseli RV (1991) Identification of markers linked to disease-resistance genes by bulked segregant analysis: a rapid method to detect markers in specific genomic regions by using segregating populations. Proceedings of the National Academy of Sciences of the United States of America **88:** 9828-9832

Misas-Villamil JC, van der Hoorn RAL (2008) Enzyme-inhibitor interactions at the plant-pathogen interface. Current Opinion in Plant Biology **11:** 380-388

Mohnen D (2008) Pectin structure and biosynthesis. Current Opinion in Plant Biology **11:** 266-277

Moscatiello R, Mariani P, Sanders D, Maathuis FJ (2006) Transcriptional analysis of calcium-dependent and calcium-independent signalling pathways induced by oligogalacturonides. Journal of Experimental Botany **57:** 2847-2865

Nakagawa T, Kurose T, Hino T, Tanaka K, Kawamukai M, Niwa Y, Toyooka K, Matsuoka K, Jinbo T, Kimura T (2007) Development of series of gateway binary vectors, pGWBs, for realizing efficient construction of fusion genes for plant transformation. Journal of bioscience and bioengineering **104:** 34-41

Nakagawa Y, Katagiri T, Shinozaki K, Qi Z, Tatsumi H, Furuichi T, Kishigami A, Sokabe M, Kojima I, Sato S, Kato T, Tabata S, Iida K, Terashima A, Nakano M, Ikeda M, Yamanaka T, Iida H (2007) Arabidopsis plasma membrane protein crucial for Ca2+ influx and touch sensing in roots. Proceedings of the National Academy of Sciences of the United States of America **104:** 3639-3644

Nakai K, Horton P (1999) PSORT: a program for detecting sorting signals in proteins and predicting their subcellular localization. Trends in Biochemical Sciences **24:** 34-36

Nakamura A, Furuta H, Maeda H, Nagamatsu Y, Yoshimoto A (2001) Analysis of structural components and molecular construction of soybean soluble polysaccharides by stepwise enzymatic degradation. Bioscience, Biotechnology, and Biochemistry **65:** 2249-2258

Nakhamchik A, Zhao Z, Provart NJ, Shiu SH, Keatley SK, Cameron RK, Goring DR (2004) A comprehensive expression analysis of the Arabidopsis proline-rich extensin-like receptor kinase gene family using bioinformatic and experimental approaches. Plant & Cell Physiology **45:** 1875-1881

Nicaise V, Roux M, Zipfel C (2009) Recent advances in PAMP-triggered immunity against bacteria: pattern recognition receptors watch over and raise the alarm. Plant Physiology **150:** 1638-1647

Nishimura MT, Stein M, Hou B-H, Vogel JP, Edwards H, Somerville SC (2003) Loss of a Callose Synthase Results in Salicylic Acid-Dependent Disease Resistance. Science **301:** 969-972

Nomura K, Debroy S, Lee YH, Pumplin N, Jones J, He SY (2006) A bacterial virulence protein suppresses host innate immunity to cause plant disease. Science **313:** 220-223

Nuhse TS (2012) Cell wall integrity signaling and innate immunity in plants. Frontiers in Plant Science **3:** 280

O'Brien JA, Daudi A, Butt VS, Bolwell GP (2012) Reactive oxygen species and their role in plant defence and cell wall metabolism. Planta **236:** 765-779

O'Brien JA, Daudi A, Finch P, Butt VS, Whitelegge JP, Souda P, Ausubel FM, Bolwell GP (2012) A peroxidase-dependent apoplastic oxidative burst in cultured Arabidopsis cells functions in MAMP-elicited defense. Plant Physiology **158:** 2013-2027

O'Connor TR, Dyreson C, Wyrick JJ (2005) Athena: a resource for rapid visualization and systematic analysis of Arabidopsis promoter sequences. Bioinformatics **21:** 4411-4413

Obro J, Harholt J, Scheller HV, Orfila C (2004) Rhamnogalacturonan I in *Solanum tuberosum* tubers contains complex arabinogalactan structures. Phytochemistry **65:** 1429-1438

Orlando DA, Brady SM, Koch JD, Dinneny JR, Benfey PN (2009) Manipulating large-scale Arabidopsis microarray expression data: identifying dominant expression patterns and biological process enrichment. Methods in Molecular Biology **553:** 57-77

Osorio S, Castillejo C, Quesada MA, Medina-Escobar N, Brownsey GJ, Suau R, Heredia A, Botella MA, Valpuesta V (2008) Partial demethylation of oligogalacturonides by pectin methyl esterase 1 is required for eliciting defence responses in wild strawberry (*Fragaria vesca*). Plant Journal **54:** 43-55

Pandey SP, Somssich IE (2009) The role of WRKY transcription factors in plant immunity. Plant Physiology **150:** 1648-1655

Panstruga R (2003) Establishing compatibility between plants and obligate biotrophic pathogens. Current Opinion in Plant Biology **6:** 320-326

Parsons HT, Drakakaki G, Heazlewood JL (2012) Proteomic dissection of the Arabidopsis Golgi and trans-Golgi network. Frontiers in Plant Science **3:** 298

Pauly M, Scheller HV (2000) O-Acetylation of plant cell wall polysaccharides: identification and partial characterization of a rhamnogalacturonan O-acetyl-transferase from potato suspension-cultured cells. Planta **210:** 659-667

Persson S, Wei H, Milne J, Page GP, Somerville CR (2005) Identification of genes required for cellulose synthesis by regression analysis of public microarray data sets. Proceedings of the National Academy of Sciences of the United States of America **102:** 8633-8638

Peumans WJ, Van Damme EJ (1995) Lectins as plant defense proteins. Plant Physiology **109:** 347-352

Plotnikova JM, Rahme LG, Ausubel FM (2000) Pathogenesis of the human opportunistic pathogen *Pseudomonas aeruginosa* PA14 in Arabidopsis. Plant Physiology **124:** 1766-1774

Poraty-Gavra L, Zimmermann P, Haigis S, Bednarek P, Hazak O, Rogovoy Stelmakh O, Sadot E, Schulze-Lefert P, Gruissem W, Yalovsky S (2013) The Arabidopsis ROP GTPase AtROP6 functions in developmental and pathogen response pathways. Plant Physiology **161:** 1172-1188

Pryor SW, Nahar N (2010) Deficiency of cellulase activity measurements for enzyme evaluation. Applied biochemistry and biotechnology **162:** 1737-1750

Qin L, Kudla U, Roze EHA, Goverse A, Popeijus H, Nieuwland J, Overmars H, Jones JT, Schots A, Smant G, Bakker J, Helder J (2004) Plant degradation: A nematode expansin acting on plants. Nature **427:** 30-30

Randoux B, Renard-Merlier D, Mulard G, Rossard S, Duyme F, Sanssene J, Courtois J, Durand R, Reignault P (2010) Distinct defenses induced in wheat against powdery mildew by acetylated and nonacetylated oligogalacturonides. Phytopathology **100:** 1352-1363

Reina-Pinto JJ, Yephremov A (2009) Surface lipids and plant defenses. Plant physiology and biochemistry : PPB / Societe francaise de physiologie vegetale **47:** 540-549

Ringli C (2010) Monitoring the outside: cell wall-sensing mechanisms. Plant Physiology **153:** 1445-1452

Ritzenthaler C, Nebenfuhr A, Movafeghi A, Stussi-Garaud C, Behnia L, Pimpl P, Staehelin LA, Robinson DG (2002) Reevaluation of the effects of brefeldin A on plant cells using tobacco Bright Yellow 2 cells expressing Golgi-targeted green fluorescent protein and COPI antisera. Plant Cell **14:** 237-261

Ron M, Avni A (2004) The receptor for the fungal elicitor ethylene-inducing xylanase is a member of a resistance-like gene family in tomato. Plant Cell **16:** 1604-1615

Roux M, Schwessinger B, Albrecht C, Chinchilla D, Jones A, Holton N, Malinovsky FG, Tor M, de Vries S, Zipfel C (2011) The Arabidopsis leucine-rich repeat receptor-like kinases BAK1/SERK3 and BKK1/SERK4 are required for innate immunity to hemibiotrophic and biotrophic pathogens. Plant Cell **23:** 2440-2455

Rushton PJ, Somssich IE, Ringler P, Shen QJ (2010) WRKY transcription factors. Trends in Plant Science **15:** 247-258

Sanchez-Rodriguez C, Estevez JM, Llorente F, Hernandez-Blanco C, Jorda L, Pagan I, Berrocal M, Marco Y, Somerville S, Molina A (2009) The ERECTA Receptor-Like Kinase Regulates Cell Wall-Mediated Resistance to Pathogens in *Arabidopsis thaliana*. Molecular Plant-Microbe Interactions **22:** 953-963

Sanchez-Rodriguez C, Rubio-Somoza I, Sibout R, Persson S (2010) Phytohormones and the cell wall in Arabidopsis during seedling growth. Trends in Plant Science **15:** 291-301

Schmid M, Davison TS, Henz SR, Pape UJ, Demar M, Vingron M, Scholkopf B, Weigel D, Lohmann JU (2005) A gene expression map of *Arabidopsis thaliana* development. Nature Genetics **37:** 501-506

Schmidt M, Schwartzberg AM, Carroll A, Chaibang A, Adams PD, Schuck PJ (2010) Raman imaging of cell wall polymers in *Arabidopsis thaliana*. Biochemical and Biophysical Research Communications **395:** 521-523

Seifert GJ, Blaukopf C (2010) Irritable walls: the plant extracellular matrix and signaling. Plant Physiology **153:** 467-478

Senchou V, Weide R, Carrasco A, Bouyssou H, Pont-Lezica R, Govers F, Canut H (2004) High affinity recognition of a *Phytophthora* protein by *Arabidopsis* via an RGD motif. Cellular and Molecular Life Sciences **61:** 502-509

Shiu SH, Bleecker AB (2001) Plant receptor-like kinase gene family: diversity, function, and signaling. Science Signaling STKE **2001:** RE22

Somerville C, Bauer S, Brininstool G, Facette M, Hamann T, Milne J, Osborne E, Paredez A, Persson S, Raab T, Vorwerk S, Youngs H (2004) Toward a systems approach to understanding plant cell walls. Science **306:** 2206-2211

Sorek N, Poraty L, Sternberg H, Bar E, Lewinsohn E, Yalovsky S (2007) Activation status-coupled transient S acylation determines membrane partitioning of a plant Rho-related GTPase. Molecular and Cellular Biology **27:** 2144-2154

Sorek N, Segev O, Gutman O, Bar E, Richter S, Poraty L, Hirsch JA, Henis YI, Lewinsohn E, Jurgens G, Yalovsky S (2010) An S-acylation switch of conserved G domain cysteines is required for polarity signaling by ROP GTPases. Current Biology **20:** 914-920

Stein M, Dittgen J, Sanchez-Rodriguez C, Hou BH, Molina A, Schulze-Lefert P, Lipka V, Somerville S (2006) Arabidopsis PEN3/PDR8, an ATP binding cassette transporter,

contributes to nonhost resistance to inappropriate pathogens that enter by direct penetration. Plant Cell **18:** 731-746

Tedman-Jones JD, Lei R, Jay F, Fabro G, Li X, Reiter WD, Brearley C, Jones JD (2008) Characterization of Arabidopsis *mur3* mutations that result in constitutive activation of defence in petioles, but not leaves. Plant Journal **56:** 691-703

Temple BR, Jones AM (2007) The plant heterotrimeric G-protein complex. Annual Review of Plant Biology **58:** 249-266

Thimm O, Blasing O, Gibon Y, Nagel A, Meyer S, Kruger P, Selbig J, Muller LA, Rhee SY, Stitt M (2004) MAPMAN: a user-driven tool to display genomics data sets onto diagrams of metabolic pathways and other biological processes. Plant Journal **37:** 914-939

Torres MA, Dangl JL, Jones JD (2002) *Arabidopsis* gp91phox homologues *AtrbohD* and *AtrbohF* are required for accumulation of reactive oxygen intermediates in the plant defense response. Proceedings of the National Academy of Sciences of the United States of America **99:** 517-522

Toth IK, Birch PR (2005) Rotting softly and stealthily. Current Opinion in Plant Biology **8:** 424-429

Tronchet M, Balague C, Kroj T, Jouanin L, Roby D (2010) Cinnamyl alcohol dehydrogenases-C and D, key enzymes in lignin biosynthesis, play an essential role in disease resistance in Arabidopsis. Molecular Plant Pathology **11:** 83-92

Tsang DL, Edmond C, Harrington JL, Nuhse TS (2011) Cell wall integrity controls root elongation via a general 1-aminocyclopropane-1-carboxylic acid-dependent, ethylene-independent pathway. Plant Physiology **156:** 596-604

Underwood W (2012) The plant cell wall: a dynamic barrier against pathogen invasion. Frontiers in Plant Science **3:** 85

Underwood W, Somerville SC (2008) Focal accumulation of defences at sites of fungal pathogen attack. Journal of Experimental Botany **59:** 3501-3508

Vanholme R, Demedts B, Morreel K, Ralph J, Boerjan W (2010) Lignin biosynthesis and structure. Plant Physiology **153:** 895-905

Vega-Sanchez ME, Verhertbruggen Y, Christensen U, Chen X, Sharma V, Varanasi P, Jobling SA, Talbot M, White RG, Joo M, Singh S, Auer M, Scheller HV, Ronald PC (2012) Loss of *Cellulose synthase-like F6* function affects mixed-linkage glucan deposition, cell wall mechanical properties, and defense responses in vegetative tissues of rice. Plant Physiology **159:** 56-69

Verhertbruggen Y, Marcus SE, Haeger A, Verhoef R, Schols HA, McCleary BV, McKee L, Gilbert HJ, Knox JP (2009) Developmental complexity of arabinan polysaccharides and their processing in plant cell walls. Plant Journal **59:** 413-425

Verica JA, Chae L, Tong H, Ingmire P, He ZH (2003) Tissue-specific and developmentally regulated expression of a cluster of tandemly arrayed cell wall-associated kinase-like kinase genes in Arabidopsis. Plant Physiology **133:** 1732-1746

Vissenberg K, Martinez-Vilchez IM, Verbelen JP, Miller JG, Fry SC (2000) In vivo colocalization of xyloglucan endotransglycosylase activity and its donor substrate in the elongation zone of Arabidopsis roots. Plant Cell **12:** 1229-1237

Vogel J, Somerville S (2000) Isolation and characterization of powdery mildew-resistant Arabidopsis mutants. Proceedings of the National Academy of Sciences of the United States of America **97:** 1897-1902

Vogel JP, Raab TK, Schiff C, Somerville SC (2002) PMR6, a Pectate Lyase-Like Gene Required for Powdery Mildew Susceptibility in Arabidopsis. Plant Cell **14:** 2095-2106
Vogel JP, Raab TK, Somerville CR, Somerville SC (2004) Mutations in *PMR5* result in powdery mildew resistance and altered cell wall composition. Plant Journal **40:** 968-978
Wagner TA, Kohorn BD (2001) Wall-associated kinases are expressed throughout plant development and are required for cell expansion. Plant Cell **13:** 303-318
Wei GS, A.H. (2006) Extensin over-expression in Arabidopsis limits pathogen invasiveness. Molecular Plant Pathology **7:** 579-592
Western TL, Skinner DJ, Haughn GW (2000) Differentiation of mucilage secretory cells of the Arabidopsis seed coat. Plant Physiology **122:** 345-356
Wieczorek K, Hofmann J, Blochl A, Szakasits D, Bohlmann H, Grundler FM (2008) Arabidopsis endo-1,4-beta-glucanases are involved in the formation of root syncytia induced by *Heterodera schachtii*. Plant Journal **53:** 336-351
Wildermuth MC (2010) Modulation of host nuclear ploidy: a common plant biotroph mechanism. Current Opinion in Plant Biology **13:** 449-458
Willats WG, McCartney L, Knox JP (2001) In-situ analysis of pectic polysaccharides in seed mucilage and at the root surface of *Arabidopsis thaliana*. Planta **213:** 37-44
Winter D, Vinegar B, Nahal H, Ammar R, Wilson GV, Provart NJ (2007) An "Electronic Fluorescent Pictograph" browser for exploring and analyzing large-scale biological data sets. PloS One **2:** e718
Wolf S, Hematy K, Hofte H (2012) Growth control and cell wall signaling in plants. Annual Review of Plant Biology **63:** 381-407
Wolf S, Mravec J, Greiner S, Mouille G, Hofte H (2012) Plant cell wall homeostasis is mediated by brassinosteroid feedback signaling. Current Biology **22:** 1732-1737
Xiang T, Zong N, Zou Y, Wu Y, Zhang J, Xing W, Li Y, Tang X, Zhu L, Chai J, Zhou JM (2008) *Pseudomonas syringae* effector AvrPto blocks innate immunity by targeting receptor kinases. Current Biology **18:** 74-80
Xin Z, Wang A, Yang G, Gao P, Zheng ZL (2009) The Arabidopsis A4 subfamily of lectin receptor kinases negatively regulates abscisic acid response in seed germination. Plant Physiology **149:** 434-444
Xu H, Mendgen K (1997) Targeted cell wall degradation at the penetration site of cowpea rust basidiosporelings. Molecular Plant-Microbe Interactions **10:** 87-94
Xu SL, Rahman A, Baskin TI, Kieber JJ (2008) Two leucine-rich repeat receptor kinases mediate signaling, linking cell wall biosynthesis and ACC synthase in Arabidopsis. Plant Cell **20:** 3065-3079
Yamanaka T, Nakagawa Y, Mori K, Nakano M, Imamura T, Kataoka H, Terashima A, Iida K, Kojima I, Katagiri T, Shinozaki K, Iida H (2010) MCA1 and MCA2 that mediate Ca2+ uptake have distinct and overlapping roles in Arabidopsis. Plant Physiology **152:** 1284-1296
Yapo BM (2011) Pectic substances: From simple pectic polysaccharides to complex pectins: A new hypothetical model. Carbohydrate Polymers **86:** 373-385
Zeyen R, Bushnell W (1979) Papilla response of barley epidermal cells caused by *Erysiphe graminis*: rate and method of deposition determined by microcinematography and transmission electron microscopy. Canadian Journal of Botany **57:** 898-913

Zhu Y, Nam J, Carpita NC, Matthysse AG, Gelvin SB (2003) Agrobacterium-mediated root transformation is inhibited by mutation of an Arabidopsis cellulose synthase-like gene. Plant Physiology **133:** 1000-1010

Zipfel C (2009) Early molecular events in PAMP-triggered immunity. Current Opinion in Plant Biology **12:** 414-420